Dynamics and Nonlinear Phenomena in Continuous Cultivations of Saccharomyces Cerevisiae

Lei, Frede; Jørgensen, Sten Bay

Publication date:
2001

Document Version
Publisher's PDF, also known as Version of record

Dynamics and nonlinear phenomena in continuous cultivations of *Saccharomyces cerevisiae*

Frede Lei

11th June 2001

Department of Chemical Engineering
Technical University of Denmark

Preface

This thesis presents the results of my Ph.D study carried out from Marts 1998 to May 2001 at the Computer Aided Process Engineering Center (CAPEC), Department of Chemical Engineering at the Technical University of Denmark in association with the Center for Process Biotechnology, BioCentrum-DTU, Technical University of Denmark. The study was financed through a grant from the Technical University of Denmark, while equipment and running costs associated with the experimental part were financed by the Center of Process Biotechnology.

I would like to thank my supervisor, Professor Sten Bay Jørgensen, for the opportunity to carry out this Ph.D study within CAPEC. I am very grateful for the scientific freedom and fruitful discussions he offered throughout the study. I would also like to express me sincere gratitude to my co-supervisor Associate Professor Lisbeth Olsson for introducing me to the experimental aspect of biotechnology as well as for valuable discussions regarding yeast physiology.

A special thanks goes to Professor Urs von Stockar, EPFL, Switzerland for letting me work in his lab for 3 month period from October to December 2000. In this regard, I am very grateful to Christoph Herwig both for making my stay as convenient as possible and for interesting discussions. Thanks also goes to Martin, Chris and everyone else in the LGCB group for making me fell very welcome.

Also thanks to technicians Martin Nielsen, Tina Johansen, Jette Mortensen, Kianoush Hansen and Vibeke Fagerberg for providing help in the lab.

A number colleagues from CAPEC and CPB have contributed with scientific and social input through my study. I would like to acknowledge the contributions from Morten Skov Hansen during the last experimental phase. Also thanks to Christoffer Bro and Kasper Møller for discussions on yeast metabolism and experimental set-ups. Also thanks to Kurt Creutzburg, Lars Gregersen, Teresa Zangirolami, John Bagterp, Dennis Bonné, Niels Rode Kristensen for interesting discussions in the office.

Finally, a sincere thanks to my family and friends for excellent support throughout this study and to Jette for an immense understanding and patience during the many weekends and nights I had to run experiments.

May, 2001

Frede Lei

Contents

Appendices

Summary

Physiological and modelling aspects of aerobic continuous cultivations of *Saccharomyces cerevisiae* were investigated in this work. The main focus was directed towards operation of a continuous cultivation at maximal biomass productivity and the possible existence of multiple steady-states for a range of dilution rates were investigated.

The starting point of the investigations was a biochemically structured model describing glucose limited, aerobic growth of *S. cerevisiae*. For glucose feed concentrations above 15 g/l, the model predicted that multiple steady-states exist in a range of dilution rates just below the critical dilution rate, D_{crit}. Moreover, the model predicted that the dilution rate interval where multiple steady-states exist will increase with an increasing glucose feed concentration.

The hypothesis of multiple steady-states were investigated by operating a continuous cultivation of *S. cerevisiae* as a productostat, i.e. the dilution rate was manipulated based on an on-line measurement relating to the state of the cultivation. Three different controller types were investigated through model simulations of the biochemically structured model: An incremental PI controller, a PI controller with a nonlinear error term and a LQ controller. Two different measurements, the respiratory quotient and the ethanol concentration, were used as controller input. Based on the model simulations, it was decided to apply the PI controller with a nonlinear error term using ethanol as measurement in the experimental investigations of multiple steady-states.

In continuous cultivation experiments with *S. cerevisiae* CEN.PK113-7D, oxido-reductive steady-states were obtained at dilution rates up to 0.09 h^{-1} below D_{crit} by operating the cultivation as a productostat. Thus, it was shown that at least two steady-states (an oxidative and an oxido-reductive) can be obtained for a range of dilution rate just below D_{crit}, thus multiple steady-states do exist. The existence of multiple steady-states were attributed to two distinct physiological effects occurring when growth changed from oxidative to oxido-reductive: i) A decrease in the efficiency of ATP production and utilisation and ii) Repression of the respiratory system. Both these effects could be interpreted as product inhibition of growth which, from a modelling point of view, was a key factor for obtaining multiple steady-states in a mathematical model of *S. cerevisiae*.

However, it was further found that oxido-reductive steady-states determined in a continuous culture are not uniquely defined by the dilution rate (in a chemostat) or the ethanol setpoint (in a productostat), but also is a function of the history of the culture. The oxido-reductive steady-

states were found to be strongly dependent on the degree of repression of the respiratory system. Depending on how the cultivation was operated, different degrees of repression could be obtained at a given dilution rate (or ethanol setpoint). Consequently, the oxido-reductive steady-states obtained below D_{crit} in the productostat could not be achieved through a D shift-down from an oxido-reductive steady-state in a chemostat, since a D shift-down led to a derepression of the respiratory system.

Two other aspects of continuous *S. cerevisiae* cultures, not directly associated with the multiple steady-state phenomenon, were also studied in this work. Biomass estimation and acetate production.

Two biomass estimation methods were investigated: A commercial probe measuring optical density (Wedgewood 653) and a software sensor estimating the dry weight biomass concentration based on the alkali addition rate. The optical density measurement could not describe the dry weight biomass concentration quantitatively in neither batch nor continuous cultivations. In contrast, the software sensor, which was based on a mass balance over the proton production in the medium, was able to estimate the dry weight biomass concentration within 5% during transient experiments in aerobic batch and continuous cultivations of *Saccharomyces cerevisiae* CEN.PK113-7D when the production of organic acids were negligible. Inclusion of off-line acetate measurements was able to further improve the alkali based biomass estimate.

Acetate production in *S. cerevisiae* was studied during aerobic growth on glucose through dynamic experiments in continuous cultivations. The amount of acetate formed during a dilution rate shift-up was dependent on the initial dilution rate before the shift-up; a shift-up from a low dilution rate (D=0.085 to 0.31 h^{-1}), yielded the largest acetate accumulation (1.0 g/l). The maximal acetate production rate was observed approximately 1 h after the dilution rate was increased. The dynamics of acetate production was shown neither to be controlled by the enzyme activities of acetaldehyde dehydrogenase (ACDH) and acetyl-CoA synthetase (ACS), nor acetaldehyde inhibition of ACDH. Instead, it was proposed that the mitochondrial NAD^+ concentration is involved in the regulation of the acetate production during an increase in dilution rate.

Dansk resumé

Fysiologiske og modelleringsmæssige aspekter af aerobe kontinuære gæringer med *Saccharomyces cerevisiae* er blevet undersøgt. Det primære formål med arbejdet har været at studere hvordan en kontinuær gæring opfører sig når den køres ved maksimal biomasse produktivitet og om multiple stationære tilstande forefindes for visse fortyndingshastigheder.

Udgangspunktet for undersøgelserne har været en biokemisk strukturer model af den aerobe *S. cerevisiae* metabolisme. Modelsimuleringer viste at multiple stationære tilstande eksisterer i et interval af fortyndingshastigheder beliggende under den kritiske fortyndingshastighed, D_{crit}, når fødekoncentrationen af glukose er højere end 15 g/l.

Eksistensen af multiple stationære tilstande blev undersøgt ved at kontrollere fortyndingshastigheden af en kontinuært gæring ud fra en måling der relaterer til væksten af gæringen, d.v.s i en produktostat. Tre forskellige regulator typer blev undersøgt vha. modelsimuleringer af den biokemiske strukturede model: En inkremental PI regulator, en PI regulator med et ulineært fejlled og en LQ regulator. RQ eller ethanol koncentrationen blev brugt som målinger til regulatorerne. Udfra simuleringerne blev ethanol målingen og PI regulatoren med det ulineære fejlled valgt til at skulle implementeres i det experimentelle set-up for at videre undersøge om multiple stationære tilstande eksisterer.

Kontinuærte gæringer med *S. cerevisiae* CEN.PK113-7D i en produktostat resulterede i oxido-reduktive staionære tilstande ved fortyndingshastigder der lå 0.09 h^{-1} lavere D_{crit}. Dermed blev det vist at der eksisterer mindst to forskellige stationære tilstande for den samme fortyndingshastighed i en region af fortyndingshastigheder beliggende lidt under D_{crit}. To fysiologiske effekter, som sker når væksten ændres fra at være oxidativ til oxido-reduktiv blev observeret og kan knyttes sammen med eksistensen af multiple stationære tilstande: i) Effektiviteten af ATP produktionen og ATP forbruget daler og ii) Det respiratoriske system bliver represseret. Begge disse effekter kan fortolkes som produktinhibering af væksten, hvilket, fra et modelleringssynspunkt, kan forklare hvorfor multiple stationære tilstande findes.

Det var også vist at en oxido-reduktiv stationær tilstand ikke er unik defineret udfra fortyndingshastigheden (i en kemostat) eller udfra ethanol setpunktet (i en produktostat), men også er en funktion af hvordan gæringen er forløbet før den stationære tilstand blev opnået. Det blev observet at en oxido-reduktiv stationære tilstand varierer meget afhængigt af hvor represseret the respiratoriske system er. Da repressionen af det respiratoriske system afhænger af hvorledes gæringen bliver kørt (kemostat eller produktostat) var det kun muligt at opnå oxido-reduktive stationære til-

stande ved fortyndingshastigheder lavere end D_{crit} når gæringen blev kørt som en produktostat. Når fortyndingshastigheden blev sat ned fra en oxido-reduktiv stationær tilstand resulterede det i en derepression af det respiratoriske system. Derfor kunne der ikke opnås en oxido-reduktiv stationær tilstand ved en fortyndingshastighed lavere end D_{crit} i en kemostat.

I dette Ph.D arbejde er der også blevet studeret to andre emner som ikke er direkte relateret til multiple stationære tilstande, nemlig biomasse estimering af og acetate produktion i *S. cerevisiae*.

To forskellige biomasse estimeringsmetoder blev undersøgt: En kommerciel optisk densitet måler (Wedgewood 653) og en software baseret sensor som beregner biomasse tørvægten udfra baseforbruget. Den optiske optiske densitet måler kunne hverken beskrive forløbet af biomasse (tørvægt) koncentrationen under en batch eller en kontinuært gæring. Derimod klarede software sensoren, som beregner biomassekoncentrationen udfra en massebalance over protondannelsen i gæringsmediet, sig udemærket. Software sensoren kunne estimerere biomasse (tørvægt) koncentrationen med en maksimal fejl på 5 % under både batch og kontinuære gæringer med *S. cerevisiae* så længe produktionen af organiske syrer var neglicibelt.

Produktionen af acetate i *S. cerevisiae* blev studeret under aerobe forhold ved vækst på glucose vha. dynamiske eksperimenter på kontinuærte gæringer. Mængden af produceret acetate efter at fortyndingshastigheden blev øget var afhængig af den oprindelige fortyndingshastighed. Mest acetate blev observeret når fortyndingshastigheden blev øget fra en lav fortyndingshastighed. Det blev vist at acetate produktionen ikke er kontrolleret af acetaldehyd dehydrogenase (ACDH) eller acetyl-coA synthetase (AcS) enzyme aktiviteterne og ej heller acetaldehyde inhibering af ACDH. Istedet ser det ud til at den mitokondrielle koncentration af NAD^+ spiller en vigtig rolle i kontrollen af den observerede acetate produktion.

1

General introduction

1.1 Background

Today, a significant number of pharmaceuticals and enzymes are being produced by genetically engineered microorganisms. During cultivation of these microorganisms an important goal is to maximise the productivity of the desired product in order to minimise production costs. However, maximising the productivity of a fermentation process leads to exploitation of nonlinear behaviour, which potentially can trigger undesirable effects such as instability or oscillatory behaviour and consequently decreasing productivity. In order to avoid these behaviours and operate safely near the maximal productivity, a mathematical understanding of the nonlinear process behaviour is necessary. However, in biochemical engineering science the effects of nonlinear phenomena on process operation have received only little attention, although e.g. operational difficulties around the maximal biomass productivity in continuous cultivations of *S. cerevisiae* have been reported (Rieger *et al.*, 1983). This fact might be attributed to the lack of reliable mathematical models of biochemical systems required for analysis of nonlinear phenomena.

In this thesis, aerobic glucose limited continuous cultivations of *S. cerevisiae* were investigated in order to study nonlinear phenomena in a biochemical system. *S. cerevisiae* is probably the single most important microorganism to mankind due to its historic role in bread and ethanol production. *S. cerevisiae* also holds a pivotal position in science where studies of *S. cerevisiae* have been used in the elucidation of the basic biochemical and metabolic processes in living cells. More recently, due to the GRAS (Generally Regarded As Safe) status of *S. cerevisiae*, genetical engineering has been widely applied on the microorganism for heterologous protein production. Today, *S. cerevisiae* is also used as a model system for studying general aspects of eukaryotic cells. The versatile nature of *S. cerevisiae* can be illustrated by listing some of its many application areas: Beverage products (beer, wine, sake), baker's yeast for bread production, heterologous protein production (human insulin, human α-interferon, hepatitis B surface antigen), biotransformations, flavour components, single cell protein (SCP) for feedstock enrichment, bioethanol, glycerol, invertase, glucoamylase and food additives (Burden and Eveleigh, 1990).

1.2 Motivation and aims

It has been speculated that the operational difficulties observed near the maximal biomass productivity in aerobic glucose limited continuous cultivations of *S. cerevisiae* arise due to a nonlinear phenomenon (a so-called fold bifurcation) leading to multiple steady-states (Axelsson *et al.*, 1992; Jørgensen *et al.*, 1992). Although some experimental evidence of multiple steady-states in continuous cultures of *S. cerevisiae* has been presented a thorough investigation of this phenomenon remains. Furthermore, the modelled physiological mechanisms in mathematical models, predicting multiple steady-states, have not been validated experimentally .

It is the primary aim of this thesis to experimentally and theoretically investigate the existence of multiple steady-states in aerobic continuous cultivations of *S. cerevisiae*. The physiological mechanisms causing multiple steady-states will received special attention in order to develop an understanding of the dynamic behaviour around maximal biomass productivity.

The starting point of the presented work was a biochemically structured model of *S. cerevisiae* (Lei *et al.*, 2001), also described in chapter 3. Since the model exhibits multiple steady-states, it was used to design experiments which could verify the existence of multiple steady-states and validate the modelled mechanism leading to multiple steady-states.

Traditionally, a continuous cultivation is operated as a chemostat, i.e. the dilution rate is fixed. If multiple steady-states exist in a continuous cultivation at least one of the steady-states will be unstable in a chemostat. However, in a productostat where the dilution rate of the continuous cultivation is manipulated based on a measurement related to the state of the cells all multiple states can be stabilised. The possibilities and drawbacks of using a productostat for operation of continuous cultivations is therefore investigated in this work with respect to operation a the maximal biomass productivity.

In this thesis, two additional aspects not directly related to the existence of multiple steady-states were also studied. Biomass estimation and acetate production in *S. cerevisiae*. The latter topic was addressed since it was observed during this study that the yeast model (Lei *et al.*, 2001) could not explain the dynamics of acetate production. Biomass estimation was addressed since off-line, dry weight biomass measurements are rather time consuming to perform and frequent sampling of the biomass concentration was needed during transient experiments to calculated specific reaction rates.

1.3 Outline of thesis

Chapter 2 contains an introduction to the concepts dealt with in this thesis. First, a brief overview of the physiology of *S. cerevisiae* during aerobic conditions is presented and the Crabtree effect is given special attention. Subsequently, mathematical modelling of *S. cerevisiae* is discussed and and finally, an introduction to bifurcation analysis, a tool for investigating nonlinear models, is given. It is illustrated how nonlinear phenomena such as multiple steady-states and sustained oscillations in continuous cultivations of *S. cerevisiae* can be explained in terms of bifurcation points.

Chapter 3 presents a biochemically structured model for aerobic growth of *S. cerevisiae* on glucose and ethanol. The model structure, which is based on experimental observations by Postma *et al.* (1989) and originally was developed by Rotbøll (1992), contains two overflow metabolisms. Overflow occurs at the pyruvate branchpoint leading to acetate excretion, and at acetaldehyde resulting in ethanol formation. A bifurcation analysis is carried out on the model by varying the dilution rate and inlet feed concentration. The model predicts that multiple steady-states exist for certain dilution rates within an interval below the critical dilution rate. The model is validated on batch, chemostat and fed-batch experiments.

In **chapter 4**, operation of a continuous cultivation as a productostat is discussed. In a productostat, the dilution rate is manipulated through a dilution rate controller based on a measurement which relates to the state of the cell metabolism. The model presented in chapter 3 is used for experimental design of productostat experiments and the choice of a measurement for productostat operation is discussed. Experimental results for productostat operation of *S. cerevisiae* using ethanol as measurement are compared with computer simulations of the previously described model.

In **chapter 5** an experimental investigation of multiple steady-states around the critical dilution rate in continuous cultivations is conducted. Experimental data show that it is possible to obtain oxido-reductive steady-states in a productostat at dilution rates below the critical dilution rate, thus verifying that multiple steady-states exist. Physiological events such as glucose repression as well as energetic aspects of the cell metabolism are related to the existence of multiple steady-states.

Two biomass estimation methods are presented and compared in **chapter 6**. A commercial optical density probe and a software sensor estimating the dry weight biomass concentration from the alkali addition rate. The performance of the two methods are evaluated on *S. cerevisiae* through transient conditions in continuous and batch cultivations.

Chapter 7 deals with dynamics of the repression and derepression of the respiratory system in *S. cerevisiae*. The capacity of the respiratory system is studied during transient conditions in a chemostat and a productostat. The relation between the glucose uptake rate, the glycolytic flux and the

repression of the respiratory system is investigated. The dependence of an obtained oxido-reductive steady-state is shown to be strongly dependent on the history of the culture which renders the investigation of multiple steady-states more complex.

In **chapter 8**, acetate production by *S. cerevisiae* during growth on glucose is addressed. Dynamic responses upon changes in the feed rate are evaluated in terms of metabolic fluxes and enzyme activities. A hypothesis for the regulation of acetate formation following an increase in the feed rate is presented.

Chapter 9 contains the overall conclusions for the presented work along with a discussion of possible future work in the fields addressed in the thesis.

Chapters 3 to 8 were written in article format containing separate abstracts, conclusions and bibliographies to rationalise the process of publishing in scientific journals.

Appendices

In **appendix A**, a methodology for estimating parameters in structured kinetics models using regularisation is presented. The methodology is applied on the model presented in chapter 3.

Appendix B contains a description of the Matlab routines developed for converting raw process data into reconciled reaction rates and calculating metabolic fluxes.

In **appendix C** an overview of conducted experiments are shown along with steady-state data for all steady-states obtained in continuous cultivations.

References

Axelsson, J.; Münch, T. and Sonnleitner, B. (1992). Multiple steady-states in continuous cultivation of yeast. *IFAC Modelling and Control of Biotechnical Processes, Colorado, USA*, **10**, 383–386.

Burden, D. and Eveleigh, D. (1990). *Yeast - diverse substrates and products*. Springer-Verlag, Berlin. In Spencer, J.F. and Spencer, D.M. (ed.): Yeast technology.

Jørgensen, S.; Møller, H. and Andersen, M. (1992). Adaptive control of continuous yeast fermentation. *Proc. 9th Int. Biotechnol. Symposium*, pages 364–369.

Lei, F.; Rotbøll, M. and Jørgensen, S. (2001). A biochemically structured model for *Saccharomyces cerevisiae*. *Accepted for publication in J. Biotechnol.*.

Postma, E.; Verduyn, C.; Scheffers, A. and van Dijken, J. (1989). Enzymic analysis of the Crabtree effect in glucose-limited chemostat cultures of *Saccharomyces cerevisiae*. *Appl. Env. Microbiol.*, **55**, 468–477.

Rieger, M.; Käppeli, O. and Fiechter, A. (1983). The role of a limited respiration in the complete oxidation of glucose by *Saccharomyces cerevisiae*. *J. Gen. Microbiol.*, **129**, 653–661.

Rotbøll, M. (1992). *Udvikling af model for kontinert gæring*. Master's thesis, Department of Chemical Engineering, Technical University of Denmark.

2

Introductory concepts

The purpose of this chapter is to introduce readers with a chemical engineering background to the physiology of *S. cerevisiae*. A basic introduction to the biochemical pathways in *S. cerevisiae* is presented along with more detailed discussions of the Crabtree effect and the pyruvate metabolism. For readers with a biochemical background an introduction to bifurcation analysis is given. Furthermore, a short discussion of modelling of microorganisms is included.

2.1 Physiology of *Saccharomyces cerevisiae*

In this section, a brief overview of the main metabolic pathways which are active in *S. cerevisiae* during aerobic growth on glucose are given. Subsequently, the pyruvate dehydrogenase bypass and the Crabtree effect are treated in more detail where more aspects of acetate and ethanol production are discussed.

2.1.1 Metabolism of *S. cerevisiae*

During growth on sugars, the cellular metabolism can be divided into two interacting parts: Catabolism and anabolism. In the catabolism, sugars are taken up and catabolised into low weight precursor metabolites with simultaneous production of energy (ATP) and redox (NADPH) equivalents. The precursor metabolites are subsequently used as building blocks in the anabolism for synthesis of cell material such as macromolecules, DNA, RNA, proteins, lipids and carbohydrohydrates. Biosynthesis of building blocks and the further polymerisation of building blocks leading to macromolecules also require ATP and NADPH (figure 2.1).

2.1.2 Sugar uptake and phosphorylation

In *S. cerevisiae* sugars are taken up through facilitated diffusion where carrier molecules (hexose transporters) embedded in the cytoplasmic membrane facilitate the sugar influx. Kinetic analysis of the glucose uptake system has suggested the existence of a high affinity (K_M=1-2 mM) and low affinity (K_M=20-50 mM) transport system (Bisson and Fraenkel, 1983) for glucose uptake. However, from genetic data no less than 20 hexose trans-

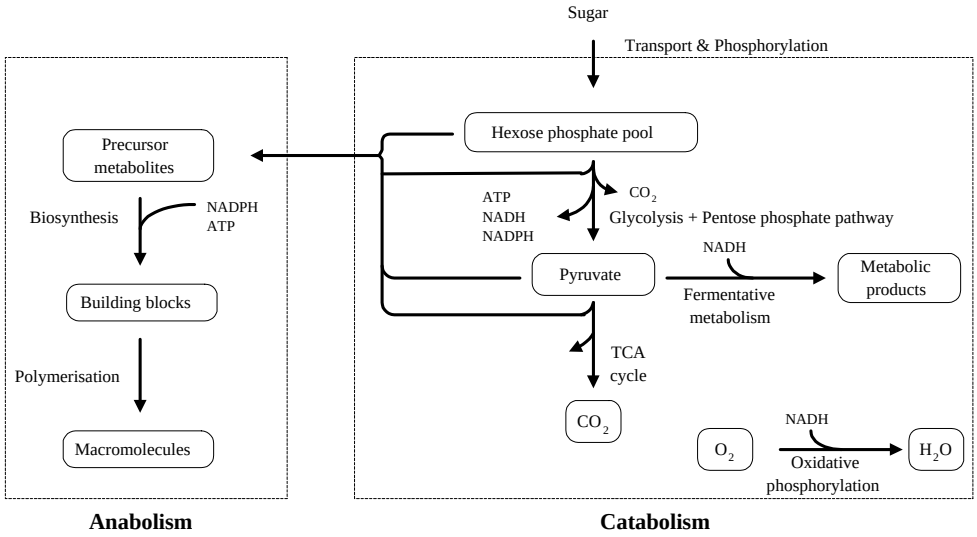

Figure 2.1. Overview of cell metabolism from sugars. In the catabolism, sugars are taken up and phosphorylated whereafter the hexose phosphates undergo glycolytic reactions whereby they either are converted to pyruvate or used in the synthesis of carbohydrates. Pyruvate can be oxidised in the TCA cycle or converted to metabolic products via the fermentative pathway. NADH produced in the catabolic reactions are either oxidised to NAD^+ in the oxidative phosphorylation or in the fermentative pathways. Intermediates from the catabolic pathways serve as precursor metabolites in the anabolic pathways where ATP and NADPH also are consumed. Adapted from Stephanopoulos *et al.* (1998).

port genes (*HXT*) have been identified (Kruckeberg, 1996) and it now appears as if each individual transporter protein have a distinct affinity for glucose (Ciriacy and Reifenberger, 1997).

Phosphorylation of intracellular glucose to glucose-6-phosphate proceeds through one of three isoenzymes with different substrate specificity: Hexokinase PI (encoded by *HXK1*), hexokinase PII (*HXK2*) or glucokinase (*GLK1*). Whereas the hexokinases can phosphorylate both glucose, fructose and mannose, glucokinase only accepts glucose and mannose as substrate (Entian, 1997). Hexokinase PII has been identified as a key protein in glucose repression where it has been suggested that it is the presence rather than the phosphorylation activity of hexokinase PII, which modulates glucose repression (Entian, 1997).

2.1.3 Catabolic pathways

The glycolysis is the sum of all pathways by which glucose-6-phosphate is converted into pyruvate. Two of the major pathways (EMP and PP pathway) are shown in figure 2.2. The overall reaction scheme for the

glycolysis is:

$$\text{Glucose} + 2\,\text{ADP} + 2\,\text{P}_i + 2\,\text{NAD}^+ \longrightarrow 2\,\text{Pyruvate} + 2\,\text{ATP} + 2\,\text{NADH} \qquad (2.1)$$

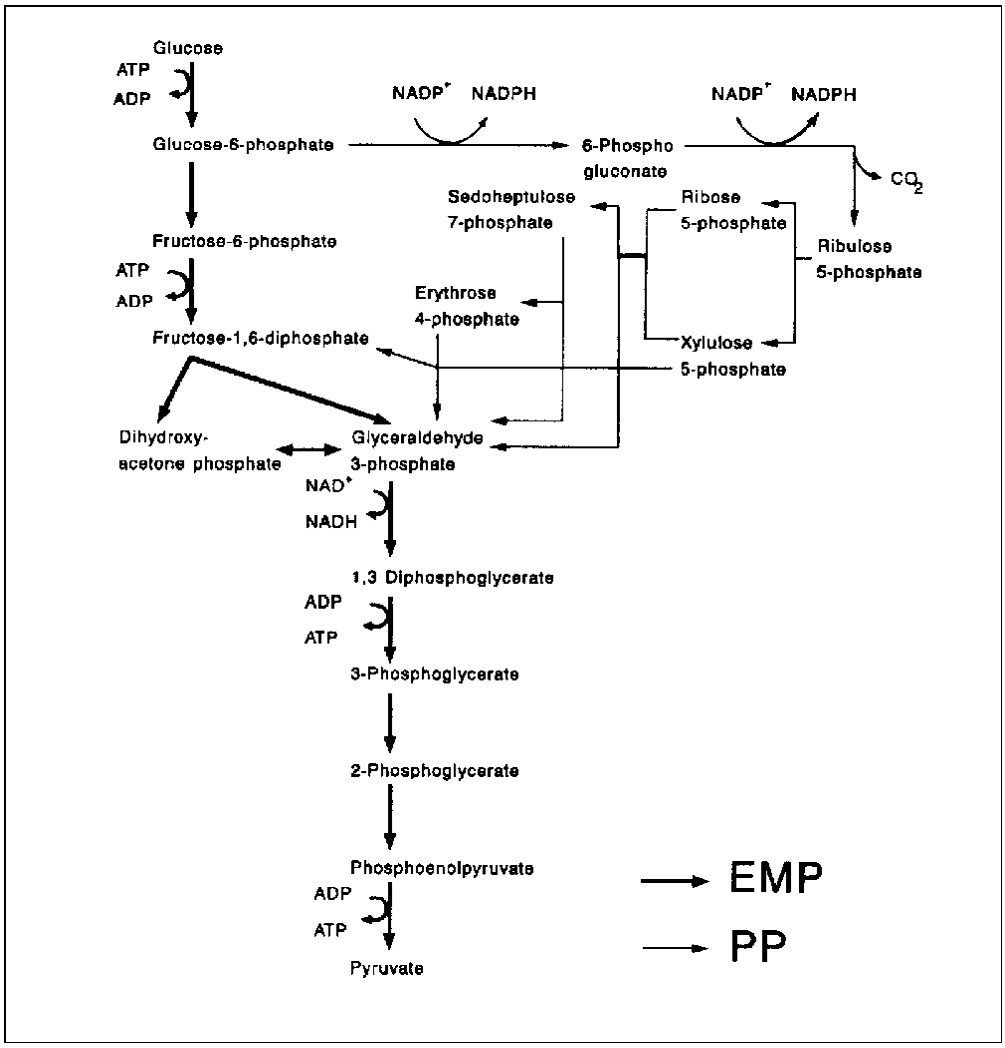

Figure 2.2. The EMP and PP pathways. Taken from Nielsen and Villadsen (1994).

The control of the fluxes through the EMP pathways is primarily placed at the phosphofructokinase reaction (fructose-6-phosphate to fructose-1,6-diphosphate), whereas the control through the PP pathway mainly occurs at its initial reaction from glucose-6-phosphate to 6-phosphogluconate (Zubay, 1988). The end product of the glycolysis, pyruvate, can either be dissimilated in the TCA cycle or in the fermentative pathway (to ethanol, figure 2.3).

During aerobic conditions, at low glycolytic fluxes, pyruvate is only dissimilated through the TCA cycle resulting in production of carbon dioxide

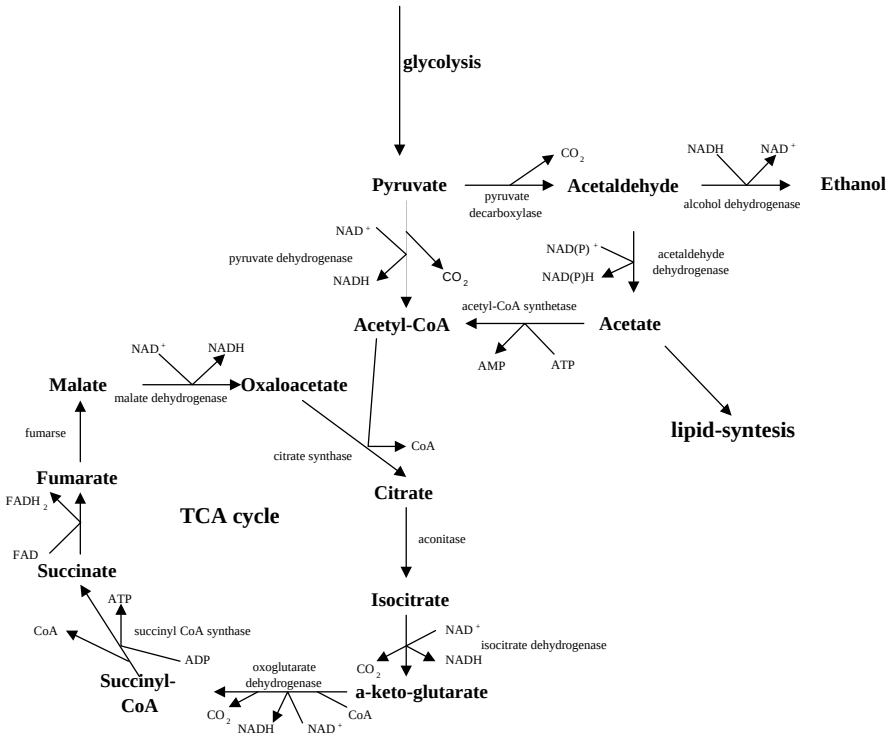

Figure 2.3. Pyruvate metabolism and TCA cycle. The conversion of pyruvate to acetyl-CoA can proceed in two ways. Either through pyruvate dehydrogenase (PDH) or through the concerted action of pyruvate decarboxylase, acetaldehyde dehydrogenase and acetyl-CoA synthetase. The latter pathway is also referred to as the PDH-bypass.

and redox equivalents:

$$\text{Pyruvate} + \text{GDP} + \text{FAD} + 4\,\text{NAD}^+ \longrightarrow 3\,\text{CO}_2 + \text{GTP} + \text{FADH}_2 + 4\,\text{NADH} \quad (2.2)$$

The redox equivalents produced in the glycolysis and the TCA cycle need to be reoxidised to maintain the redox balance. During aerobic conditions, the co-factors $FADH_2$ and NADH are reoxidised by transport of electrons from the co-factors to oxygen in a process referred to as oxidative phosphorylation. The stoichiometry for the oxidative phosphorylation is given by:

$$\text{NADH} + 3\,\text{ADP} + \tfrac{1}{2}\,\text{O}_2 \longrightarrow \text{NAD}^+ + 3\,\text{ATP} \quad (2.3)$$

$$\text{FADH}_2 + 2\,\text{ADP} + \tfrac{1}{2}\,\text{O}_2 \longrightarrow \text{FAD} + 2\,\text{ATP} \quad (2.4)$$

The different stoichiometry for NADH and $FADH_2$ is caused by the fact that $FADH_2$ enters the electron transport chain at a later stage than NADH. The number of moles of ATP formed for each oxygen atom consumed during oxidative phosphorylation is usually referred to as the P/O ratio. According to equations (2.3-2.4) it can be seen that the theoretical

P/O ratio will be between 2 and 3 depending on the ratio between $FADH_2$ and NADH reoxidation. In *S. cerevisiae*, NADH produced in the cytosol cannot pass the inner mitochondrial membrane where the oxidative phosphorylation takes place and therefore reoxidation of cytosolic NADH is coupled to reduction of mitochondrial FAD to $FADH_2$. Thus, the theoretical P/O ratio for reoxidation of cytosolic NADH is 2. However, due to incomplete coupling between the oxidation and phosphorylation processes, the operational P/O ratio is significantly lower than the theoretical ratio. Experimental P/O ratios of 0.95 and 1.2 have been reported for *S. cerevisiae* (Verduyn, 1992; van Gulik and Heijnen, 1995).

In *S. cerevisiae*, cytosolic NADH can also be reoxidised in the fermentative pathway from pyruvate to ethanol via acetaldehyde (2.5 + 2.6):

$$\text{Pyruvate} \longrightarrow CO_2 + \text{Acetaldehyde} \tag{2.5}$$

$$\text{Acetaldehyde} + \text{NADH} \longrightarrow \text{Ethanol} + \text{NAD}^+ \tag{2.6}$$

During aerobic conditions, *S. cerevisiae* can grow on ethanol and reaction (2.6) runs in the direction of acetaldehyde. Acetaldehyde is converted, via acetate, to acetyl-CoA:

$$\text{Acetaldehyde} + \text{NAD(P)}^+ \longrightarrow \text{Acetate} + \text{NAD(P)H} \tag{2.7}$$

$$\text{Acetate} + \text{ATP} \longrightarrow \text{Acetyl-CoA} + \text{AMP} + 2\,P_i \tag{2.8}$$

Acetyl-CoA can be used for generating ATP in the oxidative phosphorylation but can also be transformed to oxaloacetate in the TCA cycle and enter the gluconeogenetic pathway for producing C6 compounds. The gluconeogenetic pathway runs from oxaloacetate to glucose-6-phosphate, however, two steps are not catalysed by the same enzymes as used in the glycolysis: The first step from oxaloacetate to phosphoenolpyruvate is catalysed by phosphoenolpyruvate kinase and since phosphofructokinase catalyses an irreversible step in the glycolysis it is replaced by fructose-1,6-diphosphatase for converting 1,6-diphosphate to fructose-6-phosphate in the gluconeogenetic pathway.

S. cerevisiae is also capable of producing glycerol. Dihydroxy acetone phosphate (DHAP) from the glycolysis is converted into glycerol-3-phosphate and further to glycerol. During anaerobic conditions, where oxidative phosphorylation does not occur, glycerol production is used for reoxidising NADH produced during formation of precursers for biosynthesis. The overall reaction from glucose to glycerol can be written as:

$$\begin{aligned}\text{Glucose} + 2\,\text{ATP} + 2\,\text{NADH} \longrightarrow \\ 2\,\text{Glycerol} + 2\,\text{ADP} + 2\,P_i + 2\,\text{NAD}^+\end{aligned} \tag{2.9}$$

2.1.4 PDH bypass

The first step in oxidative dissimilation of pyruvate is conversion to acetyl-CoA which is an intermediate of the TCA cycle. This conversion can

proceed in two ways: Either directly via pyruvate dehydrogenase complex (PDH) a large mitochondrially located enzyme complex or through the concerted action of pyruvate decarboxylase (PDC), acetaldehyde dehydrogenase (ACDH) and acetyl-CoA synthetase (ACS). The latter pathway is also denoted the PDH-bypass and acetyl-CoA is formed from pyruvate via acetaldehyde and acetate (figure 2.3). The compartmentation of the reactions involved in the conversion from pyruvate to acetyl-CoA is illustrated in figure 2.4.

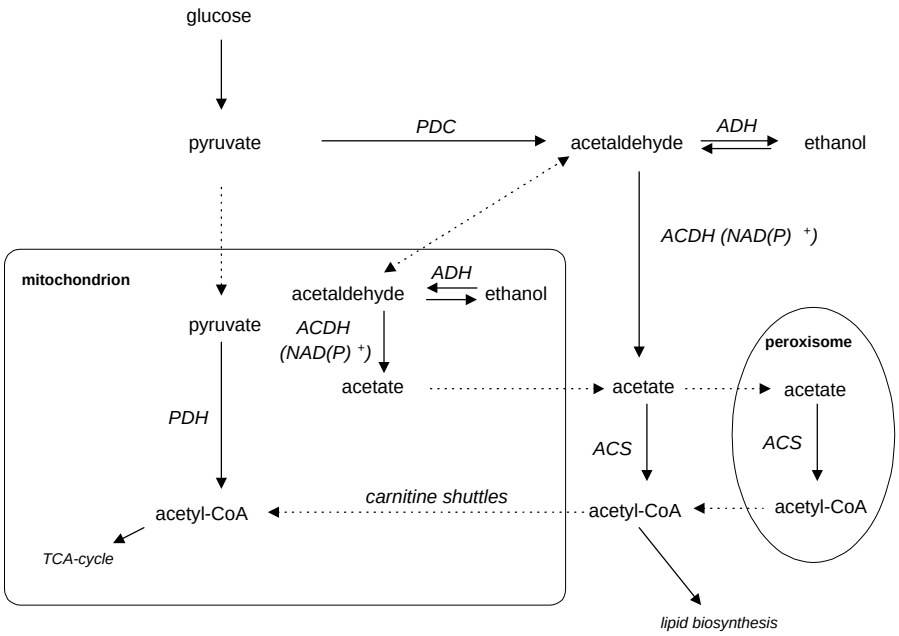

Figure 2.4. Schematic representation of the compartmentation of the enzymes involved in the pyruvate metabolism: PDH (pyruvate dehydrogenase), PDC (pyruvate decarboxylase), ADH (alcohol dehydrogenase), ACDH (acetaldehyde dehydrogenase), and ACS (acetyl-CoA synthetase).

Whereas pyruvate, acetaldehyde, acetate and ethanol can pass the mitochondrial membranes, acetyl-CoA cannot diffuse freely between the cytosol and mitochondria. Instead, cytosolic acetyl-CoA can be transported into the mitochondria via the carnitine shuttle, which catalyses the transfer of acetyl groups between carnitine and CoA, both in the mitochondrial matrix and the cytosol (Steensma, 1997). Transport of acetyl-CoA from the mitochondria to the cytosol, however, does not seem possible. Flikweert *et al.* (1996) has observed that mutants lacking PDC activity could not grow on defined glucose media, however when acetate was added to the medium, growth was restored. Their results showed that cytosolic acetyl-CoA, which is used in the lipid synthesis and formed through the

PDH bypass, cannot be supplied by transport of mitochondrial acetyl-CoA to the cytosol, suggesting that the carnitine shuttle only can operate in one direction.

For the first step in the PDH bypass, six PDC genes have been described in literature. *PDC1*, *PDC5*, and *PDC6*, have been found to encode for structural genes whereas the gene products from *PDC2*, *PDC3*, and *PDC4*, are believed to be involved in the control of the expression of the structural genes (Hohmann, 1997). The PDC reaction is taking place in the cytosol (van Urk *et al.*, 1989).

Five genes have been identified encoding for ACDH enzymes but unfortunately the nomenclature used in literature for designating each of the five genes has not been consistent. However, recently Navarro-Avino *et al.* (1999) have proposed a standard nomenclature. Details regarding each gene encoding for ACDH are given in table 2.1. Both cytosolic and a mitochondrial enzyme activity have been assayed from *S. cerevisiae*. The cytosolic isoenzyme is Mg^{2+}-activated and $NADP^+$-specific, whereas the K^+-stimulated mitochondrial enzyme has a higher affinity for NAD^+, but also accepts $NADP^+$ (Jacobson and Bernofsky, 1974). It has been proposed that the cytosolic $NADP^+$-dependent enzyme (encoded by *ALD6* (Meaden *et al.*, 1997)) is responsible for conversion of acetaldehyde to acetate during growth on glucose since the mitochondrial ACDH is more than 99% repressed during growth on glucose (Jacobson and Bernofsky, 1974). *ALD4* has been found to encode for K^+activated NAD(P)-dependent ACDH and is essential for growth on ethanol (Tessier *et al.*, 1998).

The last step in the PDH bypass is the conversion of acetate to acetyl-CoA mediated by ACS. Two structural genes encoding ACS, *ACS1* and *ACS2* have been described. Both genes are extramitochondrial and located in the cytosol (*ACS2*) and in the peroxisomal membrane (*ACS1*) (de Jong-Gubbels, 1998, chap.6). The transcription of *ACS1* is repressed by glucose (at concentrations above 100 mg/l) and to a lesser extent by ethanol (van den Berg *et al.*, 1996). Furthermore, its gene product, Acs1p, is subject to glucose catabolite inactivation (de Jong-Gubbels *et al.*, 1997). *ACS2*, on the other hand, is expressed constitutively and an *acs*2Δ mutant could not grow at high glucose concentrations in batch experiments (van den Berg *et al.*, 1996).

2.1.5 Anabolism

Cellular growth requires biosynthesis of building blocks such as amino acids, lipids, nucleotides, polysaccharides and amino sugars. At least 11 precursor metabolites are required in the biosynthesis of the approximately 75-100 building blocks. The precursors, listed in table 2.2, are withdrawn from various stages in the glycolysis, PP pathway and TCA cycle. Macromolecules constituting cellular biomass are subsequently synthesised from the building blocks through polymerisation and they can

Table 2.1. Genes encoding for acetaldehyde dehydrogenase and their functions.

Gene	Co-factor	Localisation	Comments
ALD2	NAD^+	cytosol	Stress induced enzyme which transcription is glucose repressed (Navarro-Avino *et al.*, 1999).
ALD3	NAD^+	cytosol	Similar to *ALD2* (Navarro-Avino *et al.*, 1999).
ALD4	$NAD(P)^+$	mitochondria	K^+-activated enzyme mainly active during growth on ethanol (Tessier *et al.*, 1998). The gene is referred to as *ALD7* in Tessier *et al.* (1998).
ALD5	$NAD(P)^+$	mitochondria	Encodes for a minor form of NAD(P) ACDH which might be involved in the biosynthesis of electron transport chain components (Kurita and Nishida, 1999).
ALD6	$NADP^+$	cytosol	Mg^{2+}- activated enzyme which plays an important role in the control of acetate production during growth on glucose, although it is not solely responsible for production of cytosolic acetyl-CoA (Meaden *et al.*, 1997).

be grouped into six categories: 1) RNA, 2) DNA, 3) proteins, 4) carbohydrates, 5) aminocarbohydrates, and 6) lipids (Stephanopoulos *et al.*, 1998).

Table 2.2. Overview of precursor metabolites used in biosynthesis.

Precursor	Building blocks	Pathway
Fructose-6-phosphate	UDP-NAG, UDP-NAM[a]	glycolysis
Glucose-6-phosphate	Polysaccharides	glycolysis
Glyceraldehyde-3-phosphate	UDP-glucose[b]	glycolysis
Phosphoenolpyruvate	Amino acids	glycolysis
3-phosphoglycerate	Amino acids, nucleotides	glycolysis
Pyruvate	Amino acids	glycolysis
Erythrose-4-phosphate	Amino acids, nucletides	PP pathway
Ribose-5-phosphate	Amino acids, nucleotides	PP pathway
Acetyl-CoA	Amino acids, lipids	TCA cycle
α-ketoglutarate	Amino acids	TCA cycle
Oxaloacetate	Amino acids, nucleotides	TCA cycle

[a] UDP-NAG and UDP-NAM are used in synthesis of peptidoglycan, which forms the cell wall in bacteria.

[b] UDP-glucose is used for synthesis of storage carbohydrates.

2.1.6 Regulation of carbon metabolism

S. cerevisiae is a flexible microorganism which can utilise a large number of different carbon sources, however with different efficiency. To avoid superfluous energy expenditure during growth, the catabolic and anabolic pathways are regulated through a complex regulatory network.

The control of a flux through an enzyme catalysed pathway can occur on two levels. Either the control can work directly on the enzyme activity (inhibition/activation) or it can alter the net protein synthesis of the enzyme (repression/induction). The most direct regulation of the enzyme activity occurs by activation/deactivation of the enzyme through covalent modifications. Phosphorylation of the enzyme may also modulate its activity, however most often the enzyme activity is changed gradually through association of the enzyme with another molecule, e.g. the reagent or product from the reaction catalysed by the enzyme. Control of the net synthesis rate, also referred to as regulation of gene expression, can be modulated in several ways on the levels of DNA transcription and mRNA translation. Frequently, the gene expression is regulated at the level of DNA transcription, which makes sense as there is no need to transcribe a gene if the gene product (the enzyme) is not needed in the cell. However, the stability of mRNA and proteins as well as of the translation process from mRNA to protein are also subjected to regulation.

2.1.7 Crabtree effect

The production of ethanol during aerobic conditions was first observed in cancer cells by Crabtree (1929) and it therefore referred to as the Crabtree effect (de Deken, 1966). The Crabtree effect has further been split up into a short-term and a long-term effect.

The short-term Crabtree effect has been defined as *the occurrence of instantaneous aerobic alcoholic fermentation after a transition of sugar-limited cultures to sugar excess* (Petrik *et al.*, 1983) and it can be observed when a glucose pulse is added to an oxidative continuous culture at steady-state. Immediately after the pulse, the glucose uptake rate and subsequently the glycolytic flux increases. However, due to a limitation in the dissimilation of pyruvate through the TCA cycle and oxidative phosphorylation, overflow occurs at the pyruvate node leading to acetate and ethanol formation. When the glucose pulse has been consumed, acetate and ethanol are reconsumed and the cultivation will return to oxidative growth. Frandsen (1993) has observed that acetate was excreted 1 min after a glucose pulse whereas ethanol was first observed 2 min later. That acetaldehyde preferentially is converted to acetate is also indicated by the affinity constants (K_m) for acetaldehyde dehydrogenase (reaction 2.7) and alcohol dehydrogenase (reaction 2.6). The K_m for acetaldehyde dehydrogenase is 100 times smaller than the K_m value for alcohol dehydrogenase Postma *et al.* (1989).

Whereas the short-term effect results in transient ethanol formation, the long-term effect results in permanent ethanol formation. The long-term Crabtree effect has been defined as *aerobic alcoholic fermentation irrespectively of the mode of cultivation (sugar limitation or sugar excess)* (Pronk *et al.*, 1994) and can be observed in glucose limited continuous cultivations of *S. cerevisiae*. At low glycolytic fluxes, all pyruvate is dissimilated through the TCA cycle and the oxidative phosphorylation. However, when the glycolytic flux is increased above a certain critical value, ethanol formation is observed. The growth of *S. cerevisiae* is referred to as oxidative (or respiratory) when only carbon dioxide and biomass are formed and as oxido-reductive (or respiro-fermentative) when ethanol formation occurs. When *S. cerevisiae* is grown at steady-state in a continuous cultivation, the overflow at the pyruvate branchpoint occurs at a critical dilution rate, also denoted D_{crit}.

General for both Crabtree effects are the limitation in the conversion of pyruvate through the TCA cycle and the oxidative phosphorylation, i.e. the respiratory system. The cause for this limitation was originally thought to be caused by glucose repression since repression of components of the respiratory chain and of several enzymes in the tricarboxylic acid cycle has been observed during oxido-reductive growth (Polakis *et al.*, 1965; Beck and von Meyenburg, 1968). Furthermore, steady-state chemostat data of a glucose limited *S. cerevisiae* cultivation has showed that the specific oxygen uptake rate decreased above the critical dilution rate, also

suggesting repression of the respiratory system (Meyenburg, 1969).

However, the experimental results obtained by Meyenburg (1969) have been contested by Barford and Hall (1979) and Rieger *et al.* (1983) who did not observe a decrease in the specific oxygen uptake rate above the D_{crit} but instead found a constant specific oxygen uptake rate. Barford *et al.* (1981) have proposed that repression of the respiration only is a transient phenomenon and that no repression takes place in adapted cells growing 30-200 generations at oxido-reductive conditions. In their evaluation of the work of Meyenburg (1969), Rieger *et al.* (1983) showed that the original medium used by Meyenburg contained nutritional limitations which could account for the observed decrease in the specific oxygen uptake rate above D_{crit}.

The observations of a constant specific oxygen uptake rate above D_{crit} has led to formulation of the bottleneck hypothesis (Sonnleitner and Käppeli, 1986), which states that ethanol production is a consequence of a limited capacity in the respiratory system. Furthermore, the hypothesis states that the respiratory capacity is constant during oxido-reductive growth corresponding to a constant q_{O_2} above D_{crit} in a continuous cultivation.

Although not included in the hypothesis from Sonnleitner and Käppeli (1986), repression of enzymes involved in the respiratory system does occur during oxido-reductive growth in *S. cerevisiae* (Petrik *et al.*, 1983). However, since the repression of the respiratory system could not be observed experimentally as a decline in q_{O_2} at oxido-reductive steady-states in the studies from Barford and Hall (1979); Rieger *et al.* (1983), Alexander and Jeffries (1990) proposed that two respiratory systems exist in *S. cerevisiae*. When the normal cytochrome containing respiratory system is repressed, an alternative, less efficient (with a lower P/O ratio), respiratory system will be present along with the normal one, resulting in a constant q_{O_2}. Although the authors have presented an outline of how to identify such an alternative respiration system, so far no experimental evidence of the existence of an alternative respiratory system in *S. cerevisiae* has been reported.

Experimental results from Verduyn *et al.* (1992) have shown that by adding benzoate to the feed medium, a higher respiratory activity could be obtained compared with the maximal activity observed when no benzoate was added. At a dilution rate of 0.1 h^{-1}, a specific oxygen uptake rate of 19.5 mmol/g/h was observed during growth on a mixture of glucose and benzoate, whereas the maximal q_{O_2} obtained during growth on glucose was 12 mmol/g/h. The results showed that the maximal respiratory capacity at steady-state for a given dilution rate is not constant in *S. cerevisiae* but decreases for steady-states at higher dilution rates and thus is in contrast to the bottleneck hypothesis proposed by Sonnleitner and Käppeli (1986). It has been suggested that it is the specific glucose flux which determines the degree of repression of the respiratory system and thereby the maximal

obtainable q_{O_2} (Verduyn *et al.*, 1992).

The findings by Verduyn *et al.* (1992) nicely elucidates the relation between repression of the respiratory system and a limited oxidative capacity with respect to the Crabtree effect: Ethanol formation occurs due to a limited capacity of the respiratory system as proposed by Sonnleitner and Käppeli (1986) and the capacity of the respiratory system is subject to glucose repression. It should therefore be possible to increase D_{crit} by alleviating the repression of the respiratory system. Indeed, it was shown by Blom (2001) that through overproduction of Hap4p, a positive transcriptional regulator of genes involved in respiratory metabolism, D_{crit} could be increased by 10 % relative to the isogenic wild type.

The results presented in this thesis (mainly chapter 5 and 7) show that glucose repression is very pronounced during oxido-reductive growth for the cultivated strain (CEN.PK113-7D). However, the studies by Rieger *et al.* (1983); Barford and Hall (1979) suggest that glucose repression of the respiratory system is much less pronounced in their *S. cerevisiae* strain (ATCC 32167). Therefore the regulation of glucose repression varies even between different *S. cerevisiae* strains.

2.2 Mathematical modelling of microorganisms

2.2.1 Purpose of modelling

First engineering principles modelling of microbial growth is an important and powerful tool in bioreaction engineering. By combining experimental work with mathematical modelling it is possible to provide meaningful interpretation of the experimental results exposing new aspects of microbial physiology. Simulations of a mathematical model can be used for designing new focussed experiments to reveal further aspects of cell physiology or for optimising e.g. the feed rate in a continuous or fed-batch cultivation in order to obtain maximal productivity.

Due to the complexity of microbial systems, it is virtually impossible to mathematically describe all events taking place in a cell. Thus, a series of assumptions are required when setting up a mathematical model. It is therefore crucial to define the purpose of a model before developing the model equations since this will be reflected in the model structure. A model which is intended for describing the physiology and kinetics of a series of metabolic reactions, e.g. the glycolysis, will probably be more detailed than a model developed for the sole purpose of predicting the conversion of substrate into a product during well-specified conditions.

2.2.2 Classification of models

During the last four decades numerous microbial kinetic models describing microbial growth have been presented. The simplest kind of microbial models have unstructured biomass and use Monod growth kinetics. Despite the simplicity, these models include the most fundamental features of microbial growth such as: The rate of biomass production is proportional to the biomass concentration and the existence of an upper limit for the growth rate. The characteristic of the unstructured models are no recognition of any internal structure of the cell nor the morphology of the cell culture. During conditions where the internal cell composition does not change, i.e. balanced growth conditions, the unstructured models are quite satisfactory. When the internal structure or the morphology of the cell influence the observed kinetics, the unstructured model generally fails. Unstructured models are able to give a fairly good description of steady-state data in a chemostat, but do usually fail to describe transient behaviour.

To improve the obvious limitations of unstructured models, structured models containing compartments have been developed. A compartment can describe the activity of a certain pool of enzymes responsible for a metabolic pathway or active biomass. The latter models are called structured biomass models. By including compartments, regulation of the synthesis rate of enzymes (repression/induction) can be modelled whereas unstructured models only can modulate the regulation of a flux through a given reaction or pathway (inhibition/activation).

A model is said to be biochemically structured if branch point metabolites are included, i.e. an unstructured biochemical model only contains substrates, biomass and metabolic products. If set-up properly, structured models should be able to predict the outcome of experiments carried out at new environmental conditions such as dilution rate shift-up in continuous cultures or lag phases during diauxic growth. The model presented in chapter 3 is both biochemically and biomass structured.

Segregated models, which can be either structured or unstructured, are used for describing changes within a cell population (segregated) or changes of the cell structure (morphological structured). In segregated models, different cell populations are modelled, e.g. daughter and mother cells for describing synchronised growth of a continuous *S. cerevisiae* cultivation (Hjortsø and Nielsen, 1994). In a morphological structured model, the cell population is assumed to be homogenous, however the cell is divided up into different regions with different metabolisms which interact through so-called metamorphosis reactions. A comprehensive review of modelling of microbial growth is given in Nielsen and Villadsen (1992).

2.2.3 Parameter estimation

When the model structure of a kinetic model has been set-up, model parameters (mainly kinetic parameters) need to be determined. Most often parameter estimation in simple unstructured models is carried out by either determining one parameter at a time from a specific experiment or by calculating all parameters simultaneously using a least square or maximum likelihood criterion. However, for more complex models, parameter estimation is not a straight forward procedure and a more structured methodology is required (see Appendix A). The parameter estimation problem also imposes a constraint for setting up the model structure since sufficient data should be available in order to perform a robust identification of each parameter in the model. Thus, for each term included in a model, the improvement of the model should be compared to the risk of obtaining insensitive model parameters.

2.3 Bifurcation analysis

Mathematical models based on Monod kinetics are inherently dynamic nonlinear systems. Depending on the nature of the kinetic expressions and operating conditions such systems can exhibit multiple steady-states, sustained oscillations and even chaotic behaviour. These phenomena which usually are undesirable from a production point of view can be identified from a bifurcation analysis. The term *bifurcation* is used to indicate a qualitative change in the solutions of a model system as a control parameter (bifurcation parameter) is varied across a critical value, a so-called bifurcation point (Andersen, 2000). In the following, a brief introduction to bifurcation analysis is presented and two examples of bifurcations which might occur in continuous cultivations of *S. cerevisiae* as the dilution rate is varied are discussed. For a more thorough mathematical description of bifurcation theory, the text book by Nayfeh and Balachandran (1995) can be recommended.

In the bifurcation analysis, a system consisting of first order differential equations is considered:

$$\frac{dx}{dt} = f(x, t; \phi) \quad x \in \mathbb{R}^n \quad \phi \in \mathbb{R}^m \tag{2.10}$$

where x is a vector of state variables and ϕ a parameter vector for the system. A bifurcation analysis is conducted on a linear system, thus the model system is linearised around a stationary point (x_0,ϕ_0):

$$\frac{dx}{dt} \approx A_{x_0,\phi_0} x \tag{2.11}$$

where the elements in A (Jacobian matrix) are defined as $A_{ij} = \frac{\partial f_i}{\partial x_j}$. The eigenvalues of A evaluated at (x_0,ϕ_0) reflect the dynamics and stability of

the operating point. By calculating A for varying values of ϕ, the dynamics and stability of a nonlinear system can be evaluated in a series of operating points. From linear theory it is known that a process is stable if the real part of all eigenvalues of A is negative. In that case, the dominating time constant for the system can be approximated by $-1/\lambda_{min}$, where λ_{min} is the smallest eigenvalue. A bifurcation occurs when one or more eigenvalues cross the imaginary axis, i.e. becomes positive, as ϕ is varied.

When a single parameter is varied from a stationary solution, two different bifurcation types can occur: 1) A fold bifurcation and 2) a Hopf bifurcation. Such a bifurcation is also referred to as a codimension 1 bifurcation (Andersen, 2000) and might e.g. occur when the dilution rate is varied in a continuous cultivation.

Fold bifurcation A fold bifurcation (also referred to as a saddle-node bifurcation) occurs when a single non-complex eigenvalue crosses the imaginary axis as a parameter is varied. The fold bifurcation results in multiple steady-states since two static solutions arise, which have different stability.

Hopf bifurcation A Hopf bifurcation occurs when two complex conjugate eigenvalues cross the imaginary axis as a parameter is varied. At a Hopf bifurcation a periodic solution arises from a static solution. The static solution does not disappear but changes stability. Thus, if a Hopf bifurcation occurs as a parameter is varied from a stable steady-state, sustained oscillations can be observed (supercritical Hopf bifurcation).

An example of a co-dimension 1 bifurcation is observed in the steady-state solution to a mathematical model describing aerobic growth of *S. cerevisiae* in a continuous cultivation (Lei *et al.*, 2001). The one-parameter bifurcation diagram (figure 2.5A) shows two fold bifurcations at D=0.345 and 0.38 h^{-1} resulting in a region of dilution rates with three stationary solutions. Since a fold bifurcation results in two new steady-states with different stability only two of the three steady-states are stable. In the region of multiple steady-states, one eigenvalue of the Jacobian is larger than zero. A two-parameter, or a co-dimension 2, bifurcation diagram can be obtained by following the fold bifurcation points as a second parameter is varied. In figure 2.5B, the fold bifurcation points are followed as the inlet glucose concentration (S_f) is varied. It can be observed that when S_f decreases below 15 g/l the two fold bifurcation curves collide and no fold bifurcations are found for S_f values below 15 g/l. At this point one stable steady-state was turned into three steady-states, which also is referred to as a static cusp bifurcation. This bifurcation is a codimension 2 bifurcation which means that two parameters need to be varied in order for this bifurcation to occur (not described above) as opposed to the codimension 1 bifurcation where only one parameter needs to be varied (Andersen, 2000).

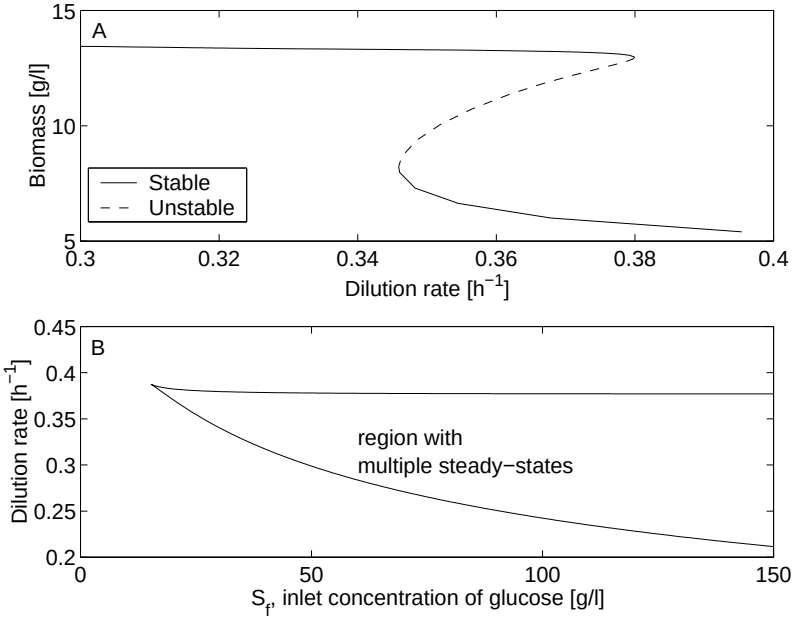

Figure 2.5. One and two-parameter bifurcation diagram for a yeast model. A) The one-parameter bifurcation diagram shows that the model predicts that two fold bifurcations, at D=0.345 h^{-1} and D=0.38 h^{-1}, occur in a continuous cultivation of *S. cerevisiae* . The fold bifurcations give rise to three steady-states between the two bifurcation points, whereof one is unstable. B) The figure presents a two-parameter bifurcation diagram of the dilution rate versus the inlet concentration of glucose (S_f). The curve indicates where fold bifurcations occur. Where the two curves collide a static cusp bifurcation occurs.

When the dilution rate is varied from a stable steady-state in a continuous bioreactor and two complex conjugate eigenvalues crosses the imaginary axis, a Hopf bifucation occurs leading to sustained oscillations. Sustained oscillations in continuous cultivations of *S. cerevisiae* due to cell cycle events have been observed experimentally as the dilution rate was increased from a stable oxidative steady-state (Meyenburg, 1969; Münch *et al.*, 1992). At first sight the occurrence of sustained oscillations might be assumed to be due to a Hopf bifurcation. However, since a Hopf bifurcation from a stable steady-state implies that the stability of the steady-state changes, it should not be possible to experimentally obtain a steady-state at a dilution rate where sustained oscillations also are observed. However, since a stable steady-state and oscillatory state have been reported at the same operating conditions (Chen *et al.*, 1990), it has been concluded that the sustained oscillations observed by Meyenburg (1969); Chen *et al.* (1990); Münch *et al.* (1992) cannot be due to a codimension 1 Hopf bifurcation (Zhang *et al.*, 2000). Instead, sustained oscillations must arise from a more complex bifurcation.

References

Alexander, M. and Jeffries, T. (1990). Respiratory efficiency and metabolite partitioning as regulatory phenomena in yeasts. *Enzyme Microb. Technol.*, **12**, 2–19.

Andersen, B. (2000). *Nonlinear dynamics of catalytic ammonia reactors*. Ph.D. thesis, KT, Technical University of Denmark.

Barford, J. and Hall, R. (1979). An examination of the Crabtree effect in *Saccharomyces cerevisiae*: The role of respiratory adaptation. *J. Gen. Microbiol.*, **114**, 267–275.

Barford, J.; Jeffery, P. and Hall, R. (1981). The Crabtree effect in *Saccharomyces cerevisiae* - primary control mechanism of transient? *Adv. Biotechnol.*, **1**, 255–260.

Beck, C. and von Meyenburg, H. (1968). Enzyme pattern and aerobic growth of *Saccharomyces cerevisiae* under various degrees of glucose limitation. *J. Bacteriol.*, **96**, 479–486.

Bisson, L. and Fraenkel, D. (1983). Involvement of kinase in glucose and fructose uptake by *Saccharomyces cerevisiae*. *Proc. Natl. Acad. Sci.*, **80**, 1730–1734.

Blom, J. (2001). Redirection of the respiro-fermentative flux distribution in continuous cultures of *Saccharomyces cerevisiae* by overexpression of the transcription factor Hap4p. Personal communication.

Chen, C.; McDonald, K. and Bisson, L. (1990). Oscillatory behaviour of *Saccharomyces cerevisiae* in continuous culture: I. effects of pH and nitrogen levels. *Biotechnol. Bioeng.*, **36**, 19–27.

Ciriacy, M. and Reifenberger, E. (1997). *Hexose transport*, chapter 3, pages 45–65. Technomic Publishing Company, Inc. In Zimmermann, F.K. and Entian, K.D (ed.): Yeast sugar metabolism.

Crabtree, H. (1929). Observations on the carbohydrate metabolism of tumours. *Biochem. J.*, **21**, 536–545.

de Deken, R. (1966). The Crabtree effect: A regulatory system in yeast. *J. Gen. Microbiol.*, **44**, 149.

de Jong-Gubbels, P. (1998). *Metabolic fluxes at the interface of glycolysis and TCA cycle in Saccharomyces cerevisiae*. Ph.D. thesis, Kluyver Laboratory of Biotechnology, Delft University of Technology.

de Jong-Gubbels, P.; van den Berg, M. and Steensma, H. (1997). The *Saccharomyces cerevisiae* acetyl-coenzyme A synthetase encoded by the *ACS1* gene, but not the *ACS2*-encoded isoenzyme, is subject to glucose catabolite inactivation. *FEMS Microbiol. Lett.*, **153**, 75–81.

Entian, K.-D. (1997). *Sugar phosphorylation in yeast*, chapter 4, pages 67–79. Technomic Publishing Company, Inc. In Zimmermann, F.K. and Entian, K.D (ed.): Yeast sugar metabolism.

Flikweert, M.; van der Zanden, L.; Janssen, W.; Steensma, H.; van Dijken, J. and Pronk, J. (1996). Pyruvate decarboxylase: An indispensable enzyme for growth of *Saccharomyces cerevisiae on glucose*. *Yeast*, **12**, 247–257.

Frandsen, S. (1993). *Dynamics of Saccharomyces cerevisiae in continuous culture*. Ph.D. thesis, IBT, Technical University of Denmark.

Hjortsø, M. and Nielsen, J. (1994). A conceptual model of autonomous oscillations in microbial cultures. *Chem. Eng. Sci.*, **49**, 1083–1095.

Hohmann, S. (1997). *Pyruvate decarboxylases*, chapter 11, pages 187–211. Technomic Publishing Company, Inc. In Zimmermann, F.K. and Entian, K.D (ed.): Yeast sugar metabolism.

Jacobson, M. and Bernofsky, C. (1974). Mitochondrial acetaldehyde dehydrogenase from *Saccharomyces cerevisiae*. *Biochim. et Biophys.*, **350**, 277–291.

Kruckeberg, A. (1996). The hexose transporter family of *Saccharomyces cerevisiae*. *Arch. Microbiol.*, **166**, 283–292.

Kurita, O. and Nishida, Y. (1999). Involvement of mitochondrial aldehyde dehydrogenase ALD5 in maintenance of the mitochondrial electron transport chain in Saccharomyces cerevisiae. *FEMS Microbiology Letters*, **181**(2), 281–288.

Lei, F.; Rotbøll, M. and Jørgensen, S. (2001). A biochemically structured model for *Saccharomyces cerevisiae*. *Accepted for publication in J. Biotechnol.*.

Meaden, P.; Dickinson, F.; Mifsud, A.; Tessier, W.; Westwater, J.; Bussey, H. and Midgley, M. (1997). The *ALD6* gene of *Saccharomyces cerevisiae* encodes a cytosolic, Mg^{2+}-activated acetaldehyde dehydrogenase. *Yeast*, **13**, 1319–1327.

Meyenburg, K. v. (1969). *Katabolit-Repression und der Sprossungszyklus von Saccharomyces cerevisiae*. Ph.D. thesis, ETH Zürich.

Münch, T.; Sonnleitner, B. and Fiechter, A. (1992). The decisive role of the *Saccharomyces cerevisiae* cell cycle behaviour for dynamic growth characterization. *J. Biotechnol.*, **22**, 329–352.

Navarro-Avino, J. P.; Prasad, R.; Miralles, V. J.; Benito, R. M. and Serrano, R. (1999). A Proposal for Nomenclature of Aldehyde Dehydrogenases in Saccharomyces cerevisiae and Characterization of the Stress-inducible ALD2 and ALD3 Genes. *Yeast*, **15**(10A), 829–842.

Nayfeh, A. and Balachandran, B. (1995). *Applied nonlinear dynamics*. John Wiley & Sons, New York.

Nielsen, J. and Villadsen, J. (1992). Modelling of microbial kinetics. *Chem. Eng. Sci.*, **47**, 4225–4270.

Nielsen, J. and Villadsen, J. (1994). *Bioreaction Engineering Principles*. Plenum Press.

Petrik, M.; Käppeli, O. and Fiechter, A. (1983). An expanded concept for the glucose effect in the yeast *Saccharomyces uvarum*: involvement of short-term and long-term regulation. *J. Gen. Microgiol.*, **129**, 43–49.

Polakis, E.; Bartley, W. and Meek, J. (1965). Changes in the activities of respiratory enzymes during the aerobic growth on yeast on different carbon sources. *Biochemical J.*, **97**, 298–302.

Postma, E.; Verduyn, C.; Scheffers, A. and van Dijken, J. (1989). Enzymic analysis of the Crabtree effect in glucose-limited chemostat cultures of *Saccharomyces cerevisiae*. *Appl. Env. Microbiol.*, **55**, 468–477.

Pronk, J.; Wenzel, T.; Luttik, M.; Klassen, C.; Scheffers, W.; Steensma, H. and van Dijken, J. (1994). Energetic aspects of glucose metabolism in a pyruvate-dehydrogenase-negative mutant of *Saccharomyces cerevisiae*. *Microbiology*, **140**, 601–610.

Rieger, M.; Käppeli, O. and Fiechter, A. (1983). The role of a limited respiration in the complete oxidation of glucose by *Saccharomyces cerevisiae*. *J. Gen. Microbiol.*, **129**, 653–661.

Sonnleitner, B. and Käppeli, O. (1986). Growth of *Saccharomyces cerevisiae* is controlled by its limited respiratory capacity: Formulation and verification of a hypothesis. *Biotechnol. Bioeng.*, **28**, 927–937.

Steensma, H. (1997). *From pyruvate to acetyl-Coenzyme A and oxaloacetate*, chapter 18, pages 339–357. Technomic Publishing Company, Inc. In Zimmermann, F.K. and Entian, K.D (ed.): Yeast sugar metabolism.

Stephanopoulos, G.; Nielsen, J. and Aristodou, A. (1998). *Metabolic Engineering*. Academic Press, London.

Tessier, W. D.; Meaden, P. G.; Dickinson, F. M. and Midgley, M. (1998). Identification and disruption of the gene encoding the K/sup +/-activated acetaldehyde dehydrogenase of Saccharomyces cerevisiae. *FEMS Microbiology Letters*, **164**(1), 29–34.

van den Berg, M. A.; de Jong-Gubbels, P.; Kortland, C.; van Dijken, J.; Pronk, J. and Steensma, H. (1996). The two acetyl-coenzyme A synthetases of *Saccharomyces cerevisiae* differ with respect to kinetic properties and transcriptional regulation. *J. Biol. Chem.*, **271**, 28953–28953.

van Gulik, W. and Heijnen, J. (1995). A metabolic network stoichiometry analysis of microbial growth and product formation. *Biotechnol. Bioeng.*, **48**, 681–698.

van Urk, H.; Schipper, D.; Breedveld, G.; Mak, P.; Scheffers, W. and van Dijken, J. (1989). Localization and kinetics of pyruvate-metabolizing enzymes in relation to aerobic alcoholic fermentation in *Saccharomyces cerevisiae* CBS8066 and *Candida utilis* CBS 621. *Biochim. et Biophys, Acta*, **992**, 78–86.

Verduyn, C. (1992). *Energetic aspects of metabolic fluxes in yeasts*. Ph.D. thesis, Department of Biochemical Engineering, Delft University of Technology.

Verduyn, C.; Postma, E.; Scheffers, W. and van Dijken, J. (1992). Effect of benzoic acid on metabolic fluxes in yeasts: A continuous culture study on the regulation of respiration and alcoholic fermentation. *Yeast*, **8**, 501–517.

Zhang, Y.; Zhu, G.-Y.; Zamamiri, A.; Henson, M. and Hjortso, M. (2000). Bifurcation analysis and control of yeast cultures in continuous bioreactors. *Proceedings of the 2000 American Control Conference. ACC (IEEE Cat. No.00CH36334)*, pages 1742–6 vol.3.

Zubay, G. (1988). *Biochemistry*. Macmillan, second edition.

3

A biochemically structured model for *Saccharomyces cerevisiae*

A biochemically structured model for the aerobic growth of Saccharomyces cerevisiae *on glucose and ethanol is presented. The model focusses on the pyruvate and acetaldehyde branch points where overflow metabolism occurs when the growth changes from oxidative to oxido-reductive. The model is designed to describe the onset of aerobic alcoholic fermentation during steady-state as well as under dynamical conditions, by triggering an increase in the glycolytic flux using a key signalling component which is assumed closely related to acetaldehyde.*

An investigation of the modelled process dynamics in a continuous cultivation revealed multiple steady-states in a region of dilution rates around the transition between oxidative and oxido-reductive growth. A bifurcation analysis using the two external variables: The dilution rate, D, and the inlet concentration of glucose, S_f, as parameters, showed that a fold bifurcation occurs close to the critical dilution rate resulting in multiple steady-states. The region of dilution rates within which multiple steady-states may occur depends strongly on the substrate feed concentration: Consequently a single steady-state may prevail at low feed concentrations whereas multiple steady-states may occur over a relatively wide range of dilution rates at higher feed concentrations.

3.1 Introduction

Today a huge amount of fermentation data are accessible and every day a lot of data are still being added hereto. As new fast on-line measurement techniques are developed the complexity of the fermentation data is growing and the need for methods and tools for data analysis is obvious, not only in academic research, but also in industry where a minimum of time is spent on data analysis and a lot of potentially profitable information is inevitably lost. First engineering principles modelling is a potentially important and powerful tool in bioreaction engineering. By combining

experimental work with mathematical modelling it is possible to provide meaningful interpretation of the experimental results exposing new aspects of microbial physiology. The model can then be used for designing new more focussed experiments.

3.1.1 Physiology of *Saccharomyces cerevisiae*

In a glucose limited continuous cultivation *S. cerevisiae* exhibits two distinct growth regimes under aerobic conditions. At low dilution rates, the growth is purely oxidative and biomass and carbon dioxide are produced as main products. When the dilution rate is increased above a certain value, the critical dilution rate (D_{crit}), the growth changes to oxido-reductive growth and significant amounts of ethanol is formed. This phenomenon has usually been referred to as the Crabtree effect (Crabtree, 1929; de Deken, 1966; Fiecther *et al.*, 1994): The occurrence of alcoholic fermentation in spite of aerobic conditions (van Dijken and Scheffers, 1986), and has been thought to be caused by glucose repression of components of the respiratory chain (Beck and von Meyenburg, 1968) and several enzymes in the tricarboxylic acid cycle (Polakis *et al.*, 1965). Sonnleitner and Käppeli (1986) has proposed that the onset of alcoholic fermentation is caused by a limitation in the respiratory capacity, however it has been found that addition of propionate to the media in a glucose limited culture results in an increase in the oxygen uptake rate (Postma *et al.*, 1989) suggesting that a limiting respiratory capacity is not solely responsible for the onset of the aerobic fermentation. Still the exact mechanism for the shift in metabolism remains to be resolved.

Much focus has been directed towards the pyruvate branch point (figure 3.1) in the research for a mechanistic explanation for what causes aerobic alcoholic fermentation (Postma *et al.*, 1989; Pronk *et al.*, 1996; van Urk *et al.*, 1989). Respiratory metabolism of pyruvate can proceed in two ways: At low glycolytic fluxes pyruvate is mainly oxidised to acetyl-CoA by the pyruvate dehydrogenase complex. However, the pyruvate dehydrogenase bypass represents an alternative pathway where the concerted action of pyruvate decarboxylase, acetaldehyde dehydrogenase and acetyl-CoA synthetase also result in production of acetyl-CoA from pyruvate. At low glycolytic flux only a small amount of pyruvate is directed through the bypass (since cytosolic acetyl-CoA is needed as precursor in the lipid synthesis (Flikweert *et al.*, 1996)), however the bypass can also be used for respiratory metabolism of pyruvate if pyruvate dehydrogenase is inactivated (Pronk *et al.*, 1994). Postma *et al.* (1989) has proposed that alcoholic fermentation is a consequence of saturation of the pyruvate dehydrogenase bypass.

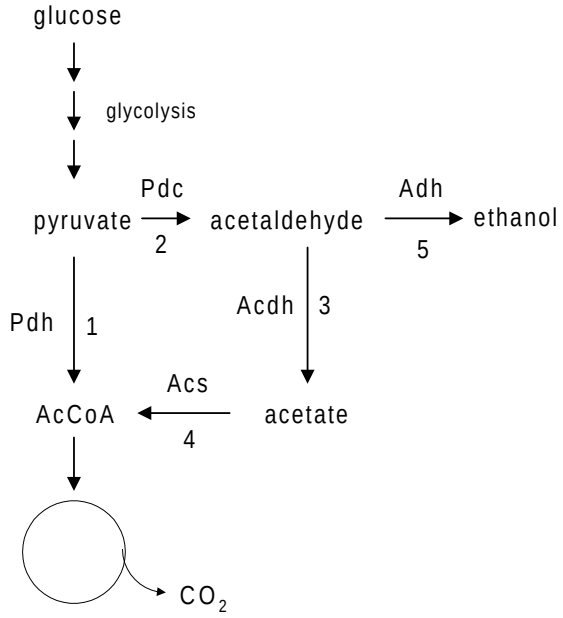

Figure 3.1. Alternative routes of pyruvate metabolism in *S. cerevisiae*. Numbers refer to the enzyme which catalyzes the corresponding reaction. 1: Pyruvate dehydrogenase complex (Pdh). 2: Pyruvate decarboxylase (Pdc). 3: Acetaldehyde dehydrogenase (Acdh). 4: Acetyl-CoA synthetase (Acs). 5: Alcohol dehydrogenase (Adh). The anaplerotic pathway from pyruvate to oxaloacetate is not included in the figure.

3.1.2 Contents of paper

In this paper a mathematical model is proposed describing the aerobic growth of *S. cerevisiae* on glucose or ethanol limited medium. The model is tested on steady-state experiments in glucose limited continuous cultures, batch experiments and dynamic experiments in chemostats such as glucose pulses or shift-up in the dilution rate (hence short and long-term Crabtree effect) to validate its performance during steady-state and dynamic conditions.

The formulation of the yeast model is based on experimental observations of the pyruvate metabolism around the critical dilution rate (de Jong-Gubbels, 1998; Flikweert *et al.*, 1997; Postma *et al.*, 1989; Pronk *et al.*, 1996), where pyruvate and acetaldehyde are important branch points. The model has some similarities with the biomass structured model of Nielsen and Villadsen (1992), but provides a new interpretation of the shift in yeast metabolism based on overflow metabolisms at the pyruvate and acetaldehyde nodes.

Most yeast models in literature following Sonnleitner and Käppeli (1986) comprises the bottleneck concept, which usually is modelled as an on/off switch. In this work a primary objective was to more closely reveal the possible underlying biochemical changes related to the pathway shift at

the pyruvate node. A secondary objective was upon this basis to develop a continuous model formulation which is amenable for analysis and for optimisation.

This paper also aims to exploit the possibilities and expose the challenges in developing a structured model for describing dynamic conditions. It is well-known that models based on Monod kinetics are able to describe balanced growth conditions well, however it has been disputed that Monod kinetics is not suited for modelling transient phenomena. The model presented here will be calibrated and validated on dynamic data in order to evaluate the model performance during different dynamic conditions. Finally, the steady-state model performance around the pathway shift is analysed for various substrate concentrations using bifurcation analysis to more closely investigate the phenomenon of multiple steady-states.

The model is intended for production optimisation both for batch as well as continuous cultures and the model can be used as a starting point for developing more specific models which can describe e.g. growth on multiple sugar substrates, oscillations in glycolysis or heterologous protein production.

3.2 Modelling and Theoretical Aspects

The model proposed in this paper is a two compartment biochemically structured model describing aerobic growth of *S. cerevisiae* under ideal fermentation conditions. The model is illustrated in figure 3.2 and the model structure was based on the following main assumptions:

1) Glucose is metabolised via two pathways: A catabolic pathway resembling the glycolysis leading to pyruvate (r_1) and an anabolic pathway which leads to the formation of biomass (r_7).

2) At low glycolytic fluxes pyruvate is converted via pyruvate dehydrogenase and the tricarboxylic acid (TCA) cycle to CO_2 (r_2).

3) When the glycolytic flux exceeds a critical value, the respiratory dissimilation of pyruvate via pyruvate dehydrogenase is saturated and acetaldehyde is formed (r_3).

4) Acetaldehyde is preferably converted into acetate (r_4) however saturation of acetaldehyde dehydrogenase (Acdh) results in ethanol production (r_6).

5) If no glucose is present in the medium the cell is able to utilise ethanol as substrate. Ethanol is converted via acetaldehyde to acetate, which can be used in the catabolic pathway leading to CO_2 (r_6+r_4+r_5) or the anabolic pathway (r_8).

6) The biomass produced from glucose or acetate is pooled into an active compartment resembling all parts of the cell which are directly growth associated. Furthermore an acetaldehyde dehydrogenase compartment was modelled to account for the varying enzymatic capacity of the two acetaldehyde dehydrogenase isoenzymes. Moreover degradation of both

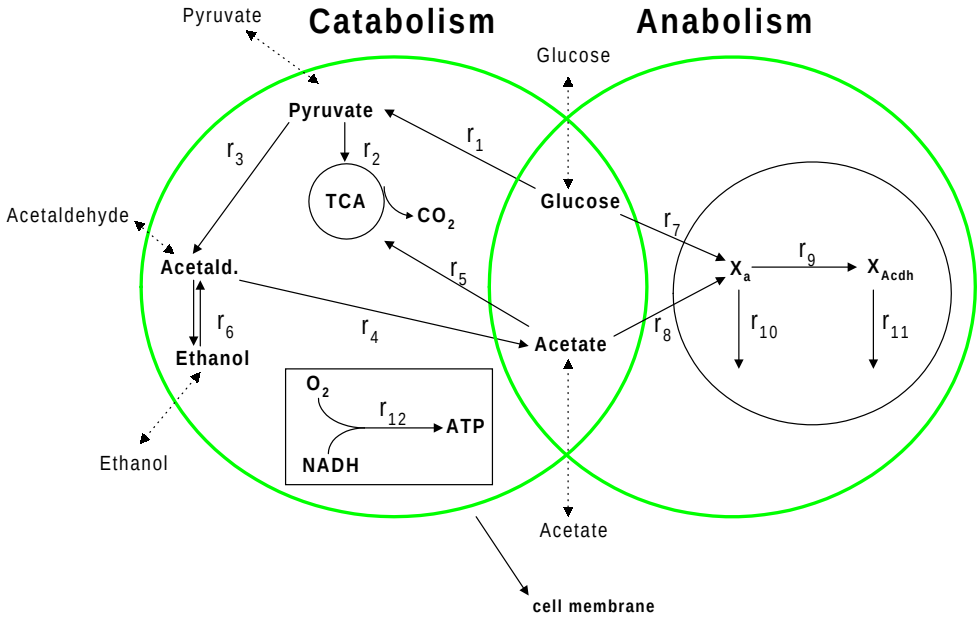

Figure 3.2. The metabolic and biomass structured model. The model reactions can be divided into catabolic and anabolic reactions as indicated by the two circles. Glucose and acetate participate in both catabolic and anabolic reactions.

compartments was included ($r_{10} + r_{11}$).

The overflow metabolism at pyruvate and acetaldehyde branch points can further be supported by enzyme affinity measurements for the reactions in the pyruvate metabolism shown in table 3.1.

3.2.1 Assumptions

In this paper the biotic subsystem of the microorganisms is in focus which implies a definition of an ideal abiotic subsystem. The assumptions for

Table 3.1. Apparent substrate affinity constants, K_M, and maximal reaction rates, v_{max}. The *in-vitro* enzyme activities were used as an indication of the maximal reaction rate. Data are from Postma *et al.* (1989) unless stated.

Enzyme	Substrate	K_M [mM]	v_{max} [U/mg]
Pyruvate dehydrogenase	Pyruvate	0.13-0.65[a]	0.16[a]
Pyruvate decarboxylase	Pyruvate	6	0.5
Acetaldehyde dehydrogenase	Acetaldehyde	0.006	0.1
Alcohol dehydrogenase	Acetaldehyde	0.61	4
Acetyl-CoA synthetase	Acetate	0.17	0.08

[a] from Kresze and Ronft (1981)

a perfect abiotic subsystem are stated in table 3.2 and can be fulfilled by applying a high performance bioreactor using a well-defined medium with the necessary growth components in excess. In addition, seven biotic assumptions were made in order to restrict the level of complexity in the model (see table 3.2). All modelled reactions are shown in figure 3.2 and their stoichiometry is listed in table 3.3.

Table 3.2. Abiotic and biotic model assumptions.

Abiotic model assumptions:		
AA1	:	Reactors are perfectly mixed.
AA2	:	Growth is only limited by glucose and ethanol.
AA3	:	Reactors are perfectly controlled with respect to dissolved oxygen, temperature, pH, N-source and other necessary growth components.
AA4	:	Evaporation and stripping of metabolites can be neglected.
Biotic model assumptions:		
BA1	:	Population of yeast cells is homogeneous.
BA2	:	Material within the cell is uniformly distributed.
BA3	:	Intermediate enzyme complexes and intermediate metabolites not modelled are in steady-state.
BA4	:	Stoichiometric coefficients are constant during all operating conditions.
BA5	:	The composition formula for the biomass ($CH_{1.61}O_{0.52}N_{0.15}$, 8% ash) is independent of fermentation conditions.
BA6	:	The intracellular metabolite concentrations can be algebraically decoupled from the extracellular concentrations.
BA7	:	The glucose uptake system can be modelled by two Michaelis-Menten expressions.

3.2.2 Reactions

All reactions in the model shown in table 3.5 were modelled based on Michaelis-Menten kinetics with respect to a given substrate and with a first order dependency on the active biomass pool X_a. X_a is defined as the active cell material used in the various growth processes as proposed by Nielsen and Villadsen (1994)(see table 3.4). Based on physiological knowledge of *S. cerevisiae* most rate expressions have been extended and in the following any deviations from the general Michaelis-Menten expression will be commented.

Table 3.3. The stoichiometry in [C-mole/C-mole] for reactions (r_1)-(r_{12}). The stoichiometric coefficients have been found in biochemical textbooks (Roels, 1983; Stryer, 1995) and by assuming constant biomass composition, hence the coefficients were calculated from C-mole and redox balances.

(r_1)	S_{glu}	$\rightarrow$	S_{pyr} + 0.33 NADH
(r_2)	S_{pyr}	$\rightarrow$	CO_2 + 1.67 NADH
(r_3)	S_{pyr}	$\rightarrow$	0.67 $S_{acetald}$ + 0.33 CO_2
(r_4)	$S_{acetald}$	$\rightarrow$	$S_{acetate}$ + 0.5 NADH
(r_5)	$S_{acetate}$	$\rightarrow$	CO_2 + 2 NADH
(r_6)	$S_{acetald}$ + 0.5 NADH	$\rightarrow$	S_{EtOH}
(r_7)	S_{glu}	$\rightarrow$	0.913 X_a + 0.087 CO_2+ 0.119 NADH
(r_8)	$S_{acetate}$	$\rightarrow$	0.778 X_a + 0.222 CO_2+ 0.401 NADH
(r_9)	X_a	$\rightarrow$	X_{Acdh}
(r_{10})	X_a	$\rightarrow$	degradation
(r_{11})	X_{Acdh}	$\rightarrow$	degradation
(r_{12})	NADH + 0.5 O_2	$\rightarrow$	ATP production

The first catabolic reaction in the model (r_1) is a lumped reaction describing the glucose uptake system and the glycolytic pathway. It has now been generally accepted that a flux through a metabolic pathway usually is controlled by more than one specific reaction (Stephanopoulos *et al.*, 1998). r_1 was therefore modelled by the use of an empirical rate description.

For the uptake of glucose into the cell a low affinity and a high affinity system have been identified, however several other uptake systems exist (Reifenberger *et al.*, 1995). Here it was assumed that the uptake system can be modelled as two single Michaelis-Menten expressions (Benthin *et al.*, 1992). The rate expression for the glycolysis further contains a term that is activated by acetaldehyde and therefore only active during oxidoreductive growth. The activation is empirical but can be interpreted as a consequence of the saturation of the oxidative catabolism (Sonnleitner and Käppeli, 1986). To produce energy for growth at higher growth rates it is necessary for the cell to produce energy by using the fermentative pathway, hence ethanol is formed. This pathway is less energy efficient and consequently it demands a larger specific flow through the glycolysis. In the model acetaldehyde was used as a signal metabolite for this activation of the fermentative pathway due to experimental observations by Postma *et al.* (1989) of acetaldehyde accumulation above the critical dilution rate in chemostats.

Respiratory metabolism of pyruvate can proceed through two routes in the model: Pyruvate dehydrogenase complex converts pyruvate to acetyl-CoA which then enters the TCA-cycle (r_2) or the pyruvate dehydrogenase

bypass can be used to produce acetyl-CoA (r_3+r_4+r_5). A glucose inhibition term is included in the rate description of (r_2) to account for glucose repression of the respiration (Alexander and Jeffries, 1990).

Pyruvate decarboxylase has been found to exhibit cooperativity with respect to pyruvate Pronk *et al.* (1996). The rate description of (r_3) was therefore based on the Hill equation (Stephanopoulos *et al.*, 1998) to include the effect of cooperativity. Since pyruvate decarboxylase enzyme is a tetramer (Pronk *et al.*, 1996) a fourth order dependency on pyruvate was used in the Hill equation.

Two reactions are modelled for the conversion of acetaldehyde. Acetaldehyde is either converted by alcohol dehydrogenase to form ethanol or by acetaldehyde dehydrogenase to acetate. The latter reaction (r_4) was modelled with a first order dependency on the concentration of acetaldehyde dehydrogenase. The concentration of acetaldehyde dehydrogenase in the cell was assumed to be proportional with the cell compartment, X_{Acdh}, (representing the measured activity/g-protein) multiplied by the active cell compartment X_a (proportional to the protein content of the cell). It was assumed that only NADH is formed as cofactor in this reaction although both a NADH- and a NADPH-dependent form of acetaldehyde dehydrogenase exist.

The formation of ethanol from acetaldehyde (r_6) is reversible and the equilibrium is controlled by the redox-balance along with the concentrations of acetaldehyde and ethanol (Barman, 1969). Since no redox-balance was included in the model a reversible enzymatic rate description was set up in the acetaldehyde and ethanol concentration including a first order dependency on the active compartment(X_a).

Acetate is part of the pyruvate dehydrogenase bypass and r_5 describes the respiration of acetate. The rate expression was set up with two terms corresponding to the two genes encoding for acetyl-CoA synthetase, *ACS1* and *ACS2* (van den Berg *et al.*, 1996). Only the first term (corresponding to the reaction catalysed by the enzyme Acs2p) is active during all growth conditions provided acetate is present, and accounts for the amount of acetate which is converted to acetyl-CoA via the pyruvate dehydrogenase bypass. The second term in (r_5) resembles the reaction catalysed by Acs1p which is repressed by glucosevan den Berg and Steensma (1995) and therefore only active at low glucose concentrations.

Biomass is formed from glucose which is converted into active cellular material in compartment X_a by reaction (r_7).

Biomass, X_a, can also be formed from acetate in reaction (r_8), which resembles the anabolic pathways which are repressed by glucose (e.g gluconeogenesis Stryer (1995)). The reaction rate of anabolic conversion of acetate therefore contains a glucose inhibition term to ensure that these anabolic pathways are repressed during growth on glucose. The rate expression for (r_8) is similar to the second term in (r_5) since it is assumed that the inhibition of both reactions occurs at approximately the same

Table 3.4. Definitions of symbols and units for the model presented in this paper.

Symbol		Definition	Unit
S_{glu}	:	Intracellular glucose concentration	[C-mole/l]
s_{glu}	:	Extracellular glucose concentration	[g/l]
S_{pyr}	:	Intracellular pyruvate concentration	[C-mole/l]
s_{pyr}	:	Extracellular pyruvate concentration	[g/l]
$S_{acetald}$	:	Intracellular acetald concentration	[C-mole/l]
$s_{acetald}$	:	Extracellular acetaldehyde concentration	[g/l]
$S_{acetate}$	:	Intracellular acetate concentration	[C-mole/l]
$s_{acetate}$	:	Extracellular acetate concentration	[g/l]
S_{EtOH}	:	Intracellular ethanol concentration	[C-mole/l]
s_{EtOH}	:	Extracellular ethanol concentration	[g/l]
x	:	Biomass concentration (dry weight).	[g/l]
X_a	:	Active cell material comprising the protein synthesis system apparatus (RNA, ribosomes), various anabolic and catabolic enzymes, transport enzymes, precursors and active metabolites.	[g-X_a/g-bio]
X_{Acdh}	:	Acetaldehyde dehydrogenase proportional to the measured activity (activity/g-protein)	[g-X_{Acdh}/g-bio]
q_{O_2}	:	Specific oxygen uptake rate	[mmole/g/h]
q_{CO_2}	:	Specific carbon dioxide evolution rate	[mmole/g/h]

glucose concentration; hence the number of model parameters is reduced.

The acetaldehyde dehydrogenase compartment is formed from the active components in the cell material, X_a, through reaction (r_9). A stoichiometry of one to one was assumed. The rate equation (r_9) was set up empirically to follow the experimental *in-vitro* activity measurements found by Postma *et al.* (1989). The first two terms include a glucose repression term since a decrease in activity has been observed with increasing glucose concentration. An additional Monod term was included to ensure a small constitutive synthesis of the compartment at high glucose concentrations.

The degradation rate of the active compartment, r_{10}, was assumed to depend on whether glucose or ethanol is present in the medium, therefore the reaction rate for the degradation of X_a consists of two terms describing first order decay of the compartment. Monod kinetics is used to activate each of the two decay terms when ethanol or glucose are present by choosing very low affinity constants (K_{10} and K_{10e}) such that the Monod term acts as a continuous on/off switch. This leads to an apparent contradiction in the model since r_{10}=0 when both the glucose and ethanol concentrations are zero, thus the model is only valid if either the ethanol or glucose

concentration is nonzero.

The degradation of acetaldehyde dehydrogenase compartment, r_{11}, was modelled with a first order decay.

The oxidative phosphorylation, r_{12}, was not modelled with a kinetic expression since it was assumed that all NADH produced is converted into ATP instantaneously. Since the dynamics of gas transport from the head space and into the cell, and vice visa, is much faster than the effects of the metabolism modelled, the specific gas turnover rates, q_{O_2} and q_{CO_2} can be calculated directly from the kinetic expressions (table 3.6).

Table 3.5. Rate expressions for model reactions.

$$
\begin{aligned}
r_1 &= k_{1l}\frac{s_{glu}}{s_{glu}+K_{1l}}\cdot X_a \;+\; k_{1h}\frac{s_{glu}}{s_{glu}+K_{1h}}\cdot X_a \\
&\qquad + k_{1e}\frac{s_{glu}}{s_{glu}\cdot(K_{1i}\cdot s_{acetald}+1)+K_{1e}}\cdot s_{acetald}\cdot X_a \\
r_2 &= k_2\frac{s_{pyr}}{s_{pyr}+K_2}\cdot\frac{1}{K_{2i}\cdot s_{glu}+1}\cdot X_a \\
r_3 &= k_3\frac{s_{pyr}^4}{s_{pyr}^4+K_3}\cdot X_a \\
r_4 &= k_4\frac{s_{acetald}}{s_{acetald}+K_4}\cdot X_a\cdot X_{Acdh} \\
r_5 &= k_5\frac{s_{acetate}}{s_{acetate}+K_5}\cdot X_a + k_{5e}\frac{s_{acetate}}{s_{acetate}+K_{5e}}\cdot\frac{1}{1+K_{5i}\cdot s_{glu}}\cdot X_a \\
r_6 &= k_6\frac{s_{acetald}-k_{6r}\cdot s_{EtOH}}{s_{acetald}+K_6+K_{6e}\cdot s_{EtOH}}\cdot X_a \\
r_7 &= k_7\frac{s_{glu}}{s_{glu}+K_7}\cdot X_a \\
r_8 &= k_8\frac{s_{acetate}}{s_{acetate}+K_{5e}}\cdot\frac{1}{1+K_{5i}\cdot s_{glu}}\cdot X_a \\
r_9 &= \left(k_9\frac{s_{glu}}{s_{glu}+K_9}+k_{9e}\frac{s_{EtOH}}{s_{EtOH}+K_{9e}}\right)\cdot\frac{1}{K_{9i}\cdot s_{glu}+1}\cdot X_a \\
&\qquad + k_{9c}\frac{s_{glu}}{s_{glu}+K_9}\cdot X_a \\
r_{10} &= k_{10}\frac{s_{glu}}{s_{glu}+K_{10}}\cdot X_a + k_{10e}\frac{s_{EtOH}}{s_{EtOH}+K_{10e}}\cdot X_a \\
r_{11} &= k_{11}\cdot X_{Acdh}
\end{aligned}
$$

Table 3.6. Mass balances in the yeast model.

$$\frac{\mathrm{d}s_{glu}}{\mathrm{dt}} = \text{-}(r_1 + r_7) \cdot x + (S_f - s_{glu}) \cdot \mathrm{D}$$

$$\frac{\mathrm{d}s_{pyr}}{\mathrm{dt}} = (0.978\, r_1 - r_2 - r_3) \cdot x - s_{pyr} \cdot \mathrm{D}$$

$$\frac{\mathrm{d}s_{acetald}}{\mathrm{dt}} = (0.5\, r_3 - r_4 - r_6) \cdot x - s_{acetald} \cdot \mathrm{D}$$

$$\frac{\mathrm{d}s_{acetate}}{\mathrm{dt}} = (1.363\, r_4 - r_5 - r_8) \cdot x - s_{acetate} \cdot \mathrm{D}$$

$$\frac{\mathrm{d}s_{EtOH}}{\mathrm{dt}} = 1.045\, r_6 \cdot x - s_{EtOH} \cdot \mathrm{D}$$

$$\frac{\mathrm{d}x}{\mathrm{dt}} = (0.732\, r_7 + 0.619\, r_8 - \mathrm{D}) \cdot x$$

$$\frac{\mathrm{d}X_a}{\mathrm{dt}} = 0.732\, r_7 + 0.619\, r_8 - r_9 - r_{10} - (0.732\, r_7 + 0.619\, r_8) \cdot X_a$$

$$\frac{\mathrm{d}X_{Acdh}}{\mathrm{dt}} = r_9 - r_{11} - (0.732\, r_7 + 0.619\, r_8) \cdot X_{Acdh}$$

$$q_{O_2} = \frac{1000}{32} \cdot (0.178\, r_1 + 0.908\, r_2 + 0.363\, r_4 + 1.066\, r_5 - 0.363\, r_6 + 0.063\, r_7 + 0.214\, r_8)$$

$$q_{O_2} = \frac{1000}{44.01} \cdot (1.499\, r_2 + 0.5\, r_3 + 1.466\, r_5 + 0.127\, r_7 + 0.325\, r_8)$$

$D = 0$ for batch reactors

$D = \frac{1}{V}\frac{\mathrm{d}V}{\mathrm{d}t}$ for fed-batch

D is constant for chemostats

Table 3.7. Kinetic parameter values for the model. Parameter units are given in the list of symbols.

Parameter	Value	Parameter	Value	Parameter	Value
k_{1h}	0.584	k_4	4.80	K_7	0.0101
K_{1h}	0.0116	K_4	$2.64 \cdot 10^{-4}$	k_8	0.589
k_{1l}	1.43	k_5	0.0104	k_9	0.008
K_{1l}	0.94	K_5	0.0102	K_9	$1.0 \cdot 10^{-6}$
k_{1e}	47.1	k_{5e}	0.775	k_{9e}	0.0751
K_{1e}	0.12	K_{5e}	0.10	K_{9e}	13
K_{1i}	14.2	K_{5i}	440	K_{9i}	25
k_2	0.501	k_6	2.82	k_{9c}	$3.99 \cdot 10^{-3}$
K_2	$2.0 \cdot 10^{-5}$	K_6	0.034	k_{10}	0.392
K_{2i}	0.101	k_{6r}	0.0125	K_{10}	$2.3 \cdot 10^{-3}$
k_3	5.81	K_{6e}	0.057	k_{10e}	$3.39 \cdot 10^{-3}$
K_3	$5.0 \cdot 10^{-7}$	k_7	1.203	K_{10e}	$1.8 \cdot 10^{-3}$
				k_{11}	0.02

3.3 Results and Discussion

It was a main objective in this work to investigate the validity of the proposed model during various operation modes for the modelled components and timescales. Steady-state data as well as various kinds of dynamic experiments were used for this purpose.

The model parameters were estimated using a combination of steady-state and dynamic data to limit the number of insensitive model parameters during the estimation, whereas the model validation was carried out on dynamic data only.

The estimation of parameters in kinetic models can be rather cumbersome due to the strong correlation between the rate and affinity constants in Monod type expressions. In a compartment structured model as the one presented here, the challenge is even greater due to the very different time scales between the dynamics of the compartments and metabolites. A five step approach for parameter estimation and validation in such models was developed as a part of this work (Lei and Jørgensen, 2001, App. A). The kinetic parameters are given in table 3.7.

The behaviour of the model was first studied on data used for parameter estimation. Subsequently the model was validated on different experimental data. The study was purely theoretical and all experimental data were obtained from literature from various authors. Consequently, the fermentation conditions might differ, however the three contributors of experimental data, (Frandsen, 1993; Pham *et al.*, 1998; Postma *et al.*, 1989) all used the same medium and cultivation conditions. All experimental data

were obtained from cultures of *S. cerevisiae* CBS 8066.

3.3.1 Estimation data

3.3.1.1 Steady-state simulation

The steady-state chemostat simulation in figure 3.3 shows that the model is capable of describing the shift in metabolism from purely oxidative to oxido-reductive growth for glucose, ethanol and biomass occurring at the critical dilution rate (D_{crit}). The gas turnover rates are also well described but the model is not able to mimic the peak for specific oxygen uptake rate, q_{O_2}, close to D_{crit} (attributed to the presence of weak acids in the medium by Postma *et al.* (1989)) since this effect not has been included in the model.

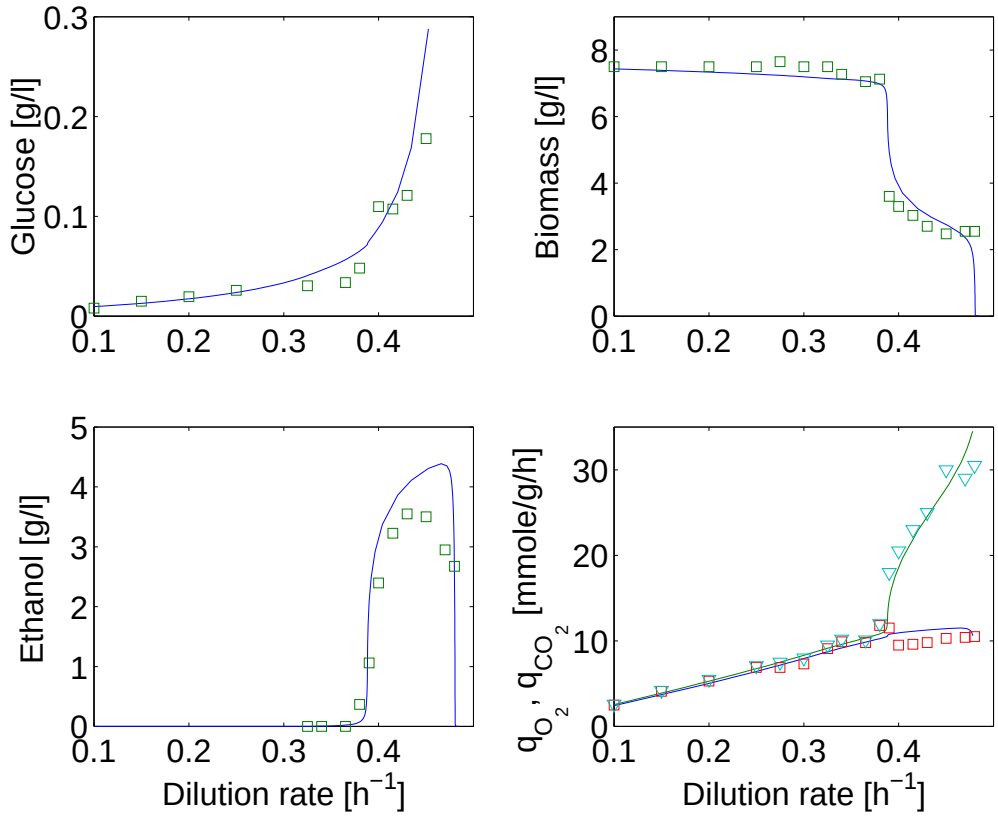

Figure 3.3. Steady-state chemostat simulations using an inlet glucose concentration of 15 g/l are shown as full lines. Experimental data are from Postma *et al.* (1989) and are presented with (□) for glucose, biomass, ethanol and q_{O_2}, whereas the specific carbon dioxide evolution rate, q_{CO_2}, data are indicated with (▽).

The model describes two overflow metabolisms: 1) Pyruvate branch-point: At a dilution rate around D=0.30 h^{-1} the maximal capacity of pyruvate dehydrogenase is reached and the pyruvate dehydrogenase by-pass is activated. Since, at this high D-value, the flux through pyruvate

decarboxylase (Pdc, reaction r_3) is greater than the flux through acetyl-CoA synthetase (Acs, reaction r_5) acetate accumulates. This can be seen on the acetate profile in figure 3.4. 2) Acetaldehyde branchpoint: At D=0.38 h^{-1} the maximal capacity of acetaldehyde dehydrogenase (Acdh, reaction r_4) is reached hence ethanol is formed. This dilution rate corresponds to the *second* overflow metabolism in the current model. It is usually referred to as the critical dilution rate (D_{crit}=0.38 h^{-1}). Washout ($D_{washout}$) occurs at D=0.48 h^{-1}.

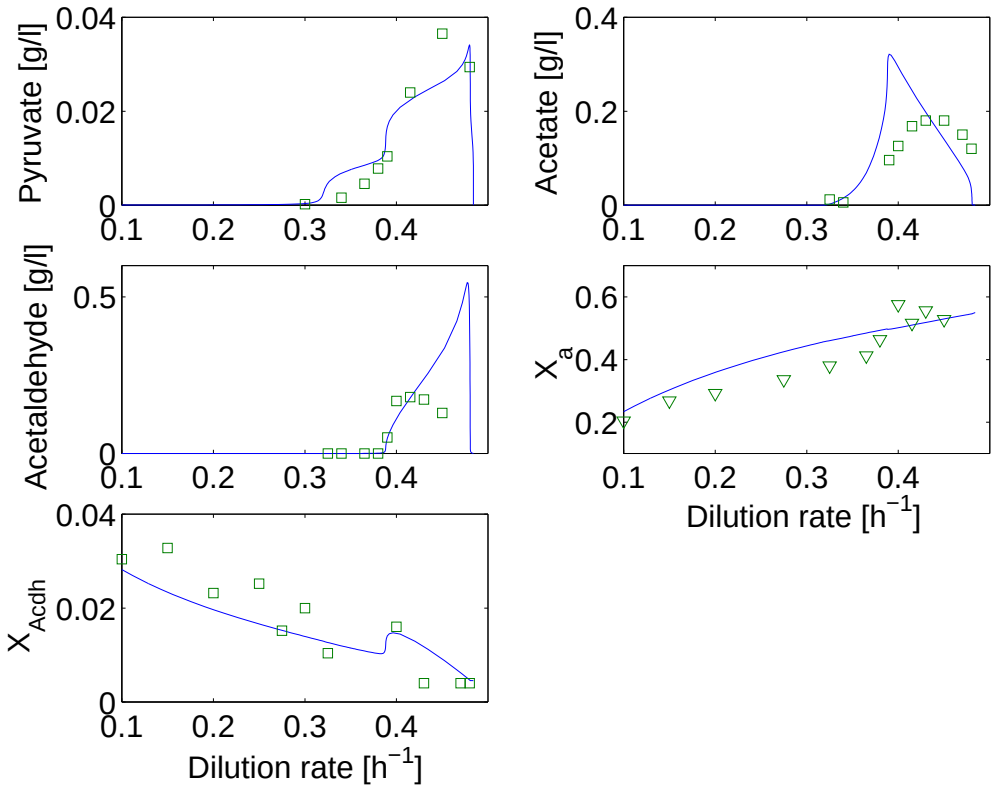

Figure 3.4. Steady-state model simulations of pyruvate, acetate, acetaldehyde, X_a and X_{Acdh}. Experimental data for pyruvate, acetate and acetaldehyde (□) are from Postma *et al.* (1989). Measurements of intracellular level of RNA (▽) from Frandsen (1993) are used for comparison with for X_a where the RNA measurements (given as [% g intra. RNA/g cell]) were scaled with a factor of 0.04 [g X_a/% g intra. RNA]. The measurements of specific enzyme activity for acetaldehyde dehydrogenase (NAD$^+$-dependent) (□) from Postma *et al.* were used for comparison for X_{Acdh} with a scaling factor of 0.001 [g X_a mg pro/g cell/U].

The steady-state profiles for pyruvate, acetaldehyde, acetate and ethanol agree fairly well with experimental data, although the maximum peaks for the simulated concentration profiles are located at a different dilution rate than the experimental data. In the model the acetate concentration decreases for D>D_{crit} whereas experimental data show an increase until D=0.45 h^{-1}. The decrease in acetate concentration in the model is caused

by a decrease in size of the X_{Acdh} compartment above D_{crit}. Hence the flux through r_4 drops and the capacity of r_5 becomes greater than r_4 to give a consumption of acetate. According to experimental data (Postma *et al.*, 1989), the specific activity of acetyl-CoA synthetase also decreases above D_{crit} leading to a lower capacity of r_5. However, since this enzyme was not included in the model the discrepancy in the acetate description is explainable.

For pyruvate, acetaldehyde and ethanol the simulated maximum values are located very close to $D_{washout}$=0.48 h^{-1} whereas the experimental peaks for these compounds and acetate is observed at a dilution rate of 0.45 h^{-1}. The simulated acetaldehyde profile can be improved by including the enzyme alcohol dehydrogenase in the model. Experimental data from Postma *et al.* (1989) show that the specific activity of the enzyme increases above D_{crit}. If included in the model this would lead to a greater conversion of acetaldehyde to ethanol and the concentration of acetaldehyde would increase less drastically above D_{crit}.

However, inclusion of compartments describing the activity of acetyl-CoA synthetase and alcohol dehydrogenase in the model would require at least 8 new intracellular parameters to be estimated and since the availability of literature data for enzyme activities during various operation modes is limited this extension of the model was not pursued.

The simulated concentration of the active compartment shows approximate proportionality between active cell compartment, X_a, and the cellular content of RNA. Moreover, the enzyme compartment for acetaldehyde dehydrogenase seems to fit the experimental data (Postma *et al.*, 1989). The specific activity of Acdh is decreasing with increasing dilution rate and decreases approximately threefold from low dilution rate (0.10 h^{-1}) until the critical dilution rate. The decrease in specific activity is one of the controlling factors responsible for the accumulation of acetaldehyde in the model due to the saturation of Acdh (reaction r_4) and thus ethanol formation.

3.3.1.2 Batch simulation

The model provides a fairly good description of the glucose and ethanol profiles during the batch fermentation shown in figure 3.5. However neither biomass nor gas flow measurements were available for direct comparison.

The model shows a qualitatively reasonable behaviour for pyruvate and acetate. During the first exponential growth phase where glucose is in excess, the cells cannot utilise all glucose oxidatively, consequently ethanol is formed. Furthermore, excretion of pyruvate and acetate occurs. Before ethanol is being utilised the accumulated amounts of pyruvate and acetate are consumed. During growth on ethanol acetate is excreted again. The qualitative trends are well captured by the model, however the level of acetate does not fit quantitatively.

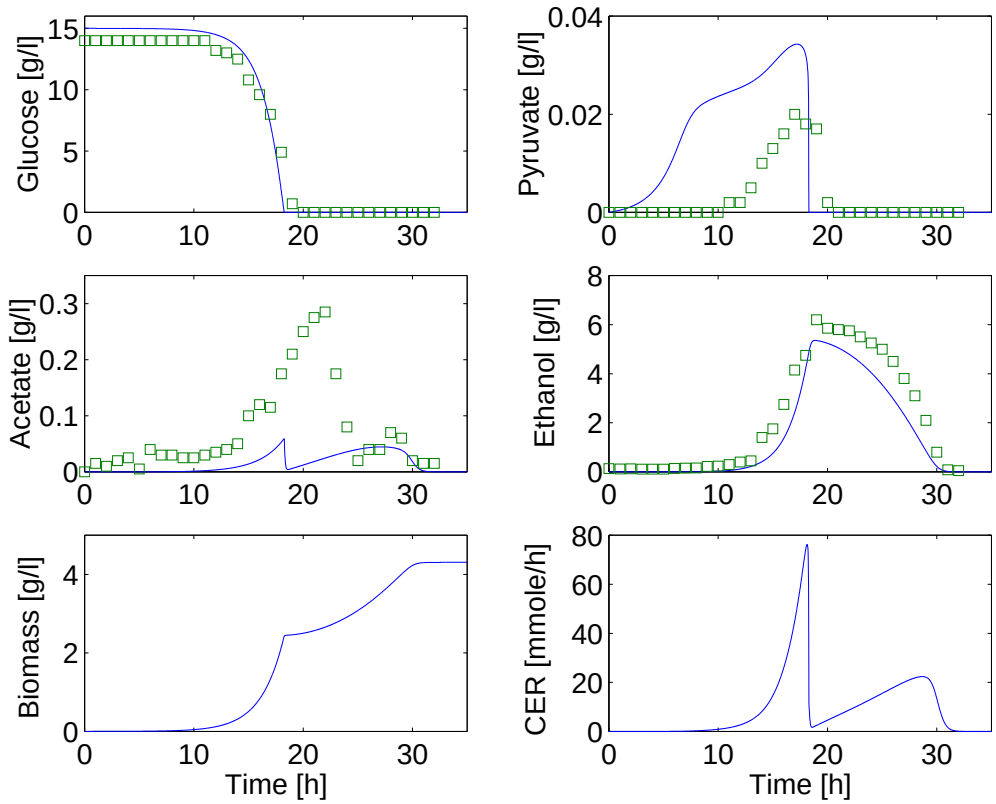

Figure 3.5. Batch simulations of the model using an initial glucose concentration of 15 g/l. The experimental data are from Frandsen (1993).

According to the model, pyruvate and acetate are consumed almost instantly when glucose is depleted, however experimental data show that the consumption time for pyruvate and acetate is approximately one and three hours, respectively. Hence the batch experiment shows that the structure of the model is unable to describe the sequential growth on pyruvate and acetate, but only on glucose and ethanol.

The batch simulations are extremely sensitive towards initial conditions which in the current case are not known for biomass and the intracellular compartments. For the simulations showed here the initial conditions for biomass(x), X_a and X_{Acdh} are set to 0.002 g/l, 0.1 and 0.0075, respectively.

3.3.1.3 Dilution rate shift-up simulation

To examine the ability of the model to describe dynamic phenomena, glucose pulse addition and dilution rate shift-up experiments were simulated.

During dilution rate shift-up experiments, as opposed to glucose pulses, the physiological steady-state of the cell changes. Glucose pulse experiments can be described quite well by unstructured models since the duration is less than one hour where it can be assumed that the enzyme levels (i.e the compartment concentrations) are unchanged. However, during a shift-up experiment the cells have to adapt to new conditions and the

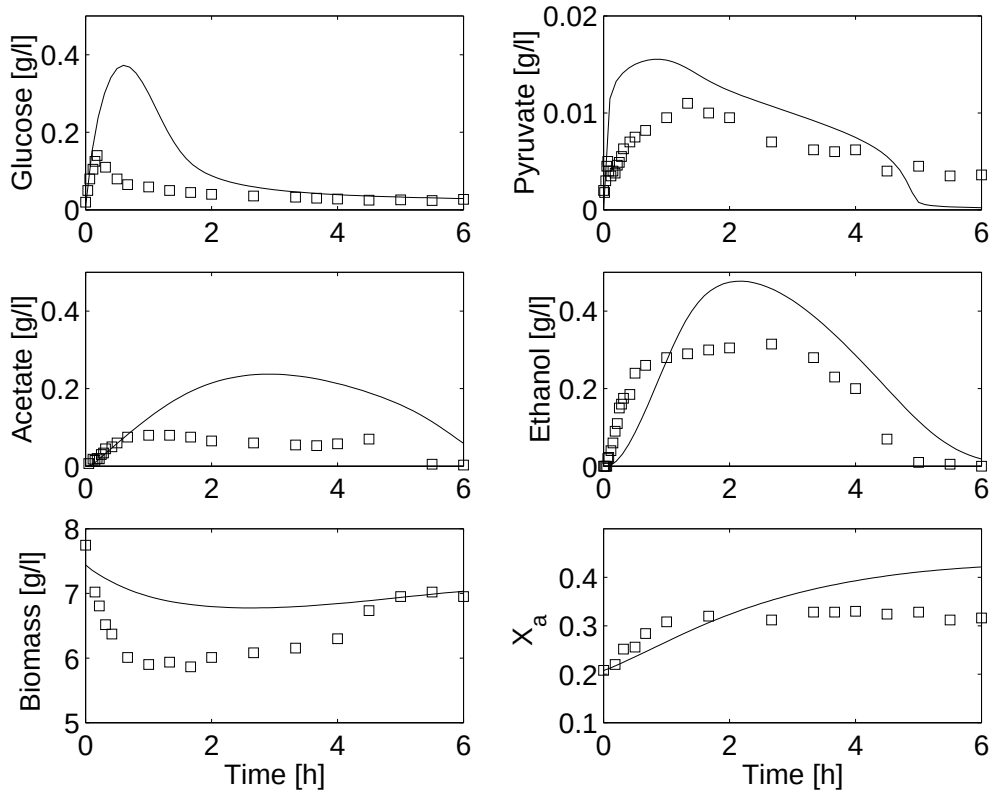

Figure 3.6. Dilution rate shift-up of a continuous culture from D=0.08 h^{-1} to 0.265 h^{-1}. The model is able to capture the dynamics of ethanol formation and consumption quite well. Furthermore an undershoot in the biomass concentration was observed experimentally and in the simulations. Experimental data are from Frandsen (1993) and the data were used for estimation of kinetic parameters. The initial conditions at the shift-up were not known and in the simulations the initial conditions were assumed to be the steady-state values for D=0.08 h^{-1}.

dynamics of such experiments have a much longer duration than a glucose pulse. This adaption also implies that a model capturing the during a shift-up needs to be more complex than a model for glucose pulse experiments. Duboc *et al.* (1998) and Sonnleitner and Hahnemann (1994) have modelled first order expressions to unstructured growth models in order to account for the changes occurring in the anabolic (Duboc *et al.* (1998)) and catabolic (Duboc *et al.* (1998); Sonnleitner and Hahnemann (1994)) machinery during a shift-up in dilution rate; in the latter case such a modification was necessary in order to model ethanol excretion at dilution rates less than D_{crit}.

The dilution rate shift-up experiment (figure 3.6) shows a discrepancy between the modelled and experimental glucose profile. Even though two uptake systems are used for modelling the consumption of glucose, a too large accumulation of glucose occurs. The ethanol and pyruvate profiles are described well by the model, whereas too much acetate is predicted.

The biomass and X_a profiles show correct qualitative trends during the shift-up, but the model does not capture all the details of the biomass and X_a profiles.

3.3.2 Validation data

3.3.2.1 Fed-batch simulation

A fed-batch cultivation was simulated for model validation (figure 3.7). The experimental work has been performed by Pham *et al.* (1998) and consisted of an exponential feeding phase followed by a constant feeding phase. The simulations reveal two problems in the model structure when describing a fed-batch cultivation. The maximal ethanol level is too low (1 g/l instead of 3 g/l) whereas the maximal q_{CO_2} level is too high. This indicates that the distribution of fluxes at the pyruvate and acetaldehyde branch points are not correctly modelled for the fed-batch case since too much carbon is directed into the TCA cycle. Furthermore, the simulated q_{O_2} seems to differ qualitatively from the experimental data.

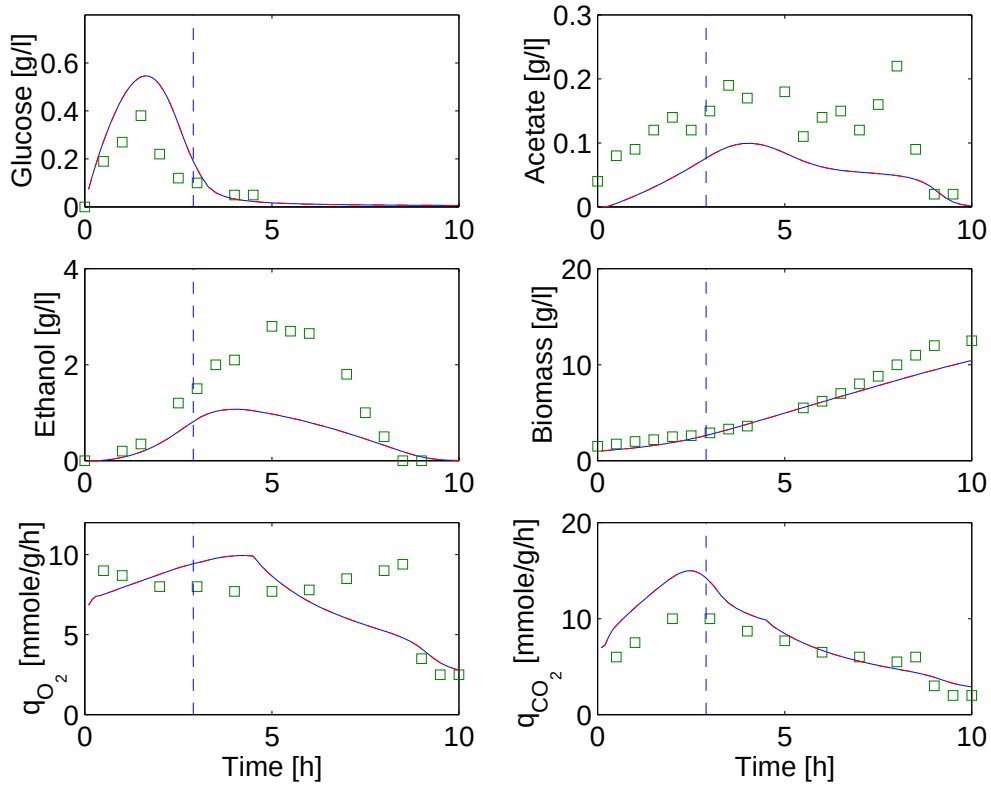

Figure 3.7. Fed-batch simulations of the model. The feed rate was increased exponentially until approximately three hours (indicated by the dotted line), whereafter it was kept constant. Experimental data are taken from Pham *et al.* (1998).

3.3.2.2 Glucose pulse simulation

Experimental data of a glucose pulse experiment (Frandsen, 1993) was used for validation of the short-term dynamics of the model. The experimental data in figure 3.8 show a delay in the production of acetate and ethanol following addition of glucose whereas the pyruvate concentration increases instantaneously. The delays are approximately 1-2 minutes for acetate and 3 minutes for ethanol. The model was able to describe these delays quite well even though the model shows a too large accumulation of pyruvate. A possible physiological explanation of the delays in the acetate and ethanol responses can be given by considering the pathways around the pyruvate metabolism. The large glucose pulse provides an increasing glycolytic flux and respiration of pyruvate via pyruvate dehydrogenase (Pdh) is saturated thus the pyruvate decarboxylase bypass (see figure 3.1) is activated. Since pyruvate decarboxylase (Pdc) has a lower substrate affinity than Pdh (see table 3.1) the pyruvate concentration increases. The flux through the Pdc-bypass leads to a (delayed) increase in the acetate concentration, and ethanol is formed after a further delay when the acetaldehyde dehydrogenase (Acdh) is saturated.

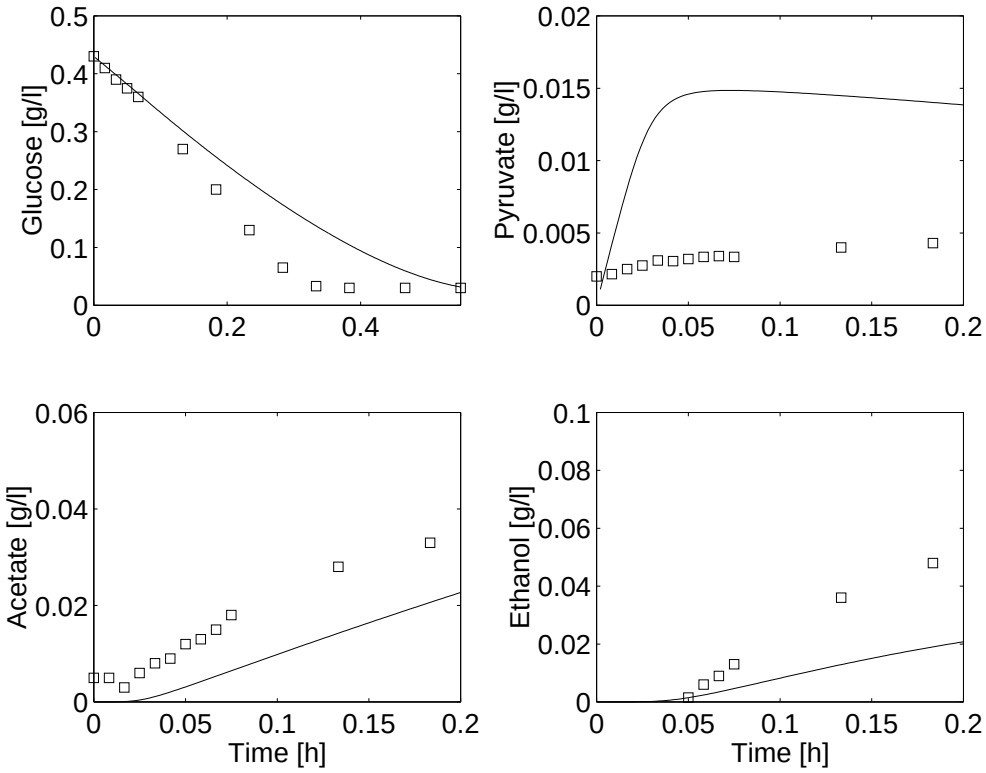

Figure 3.8. A glucose pulse was added at time=0. The dilution rate was kept constant at D=0.25 h^{-1} and the inlet concentration of glucose was 5 g/l. The short-term Crabtree effect can be observed as ethanol is produced at a dilution rate below D_{crit}. Notice the different time spans for glucose and the other three metabolites. The experimental data are from Frandsen (1993).

The discrepancies for acetate and pyruvate are qualitatively similar to what was observed for the batch simulation. The simulated pyruvate concentration is significantly higher than what is experimentally observed whereas the simulated acetate level is lower than the experimental data.

3.3.2.3 Dilution rate shift-up simulation

The dynamics around D_{crit} was validated using a dilution rate shift-up experiment performed in the region around D_{crit}. The experiment showed that the dynamics of a continuous cultivation becomes much slower close to D_{crit} (figure 3.9) where more than 25 residence times are needed before ethanol and biomass reach a new steady-state at D=0.39 h^{-1}. The dynamics of the model might seem much slower than what is seen in the experimental data but this is caused by the large sensitivity close to D_{crit}. To illustrate this point a simulation of the shift-up experiment to D=0.40 h^{-1} instead of D=0.39 h^{-1} is shown as well in figure 3.9.

3.3.3 Model performance

The structure of the model presented in this paper was set up based on observations primarily from glucose limited continuous cultivations. It is therefore not surprising that the model was able to describe the chemostat behaviour quite nicely. However, the dynamic simulations of batch, fed-batch and dilution rate shift-up experiments showed that the model structure indeed has its limitations.

The batch experiment revealed that the acetate profile as well as the sequential growth on pyruvate, acetate and ethanol after glucose depletion cannot be described properly by the model. To obtain a better description of the sequential growth a further compartmentation of the model is needed by including the synthesis of the enzymes which metabolise pyruvate and acetate. Still, this work suggests that including detailed information regarding enzyme kinetics is not sufficient for explaining the role of acetate during dynamic conditions. Thus, modelling of redox balances and energetic aspects would probably improve the model performance with respect to acetate prediction.

Model simulations of dilution rate shift-up experiments and a fed-batch cultivation further illustrated the limitations of the model for describing different dynamic operation modes using the same model structure and parameters.

3.3.4 Multiple steady-states

Indications of multiple steady-state for *S. cerevisiae* in a continuous culture has been observed experimentally by Axelsson *et al.* (1992) and Jørgensen *et al.* (1992) by dilution rate shift-up/down and ethanolostat experiments, respectively. However, these works has been performed on a

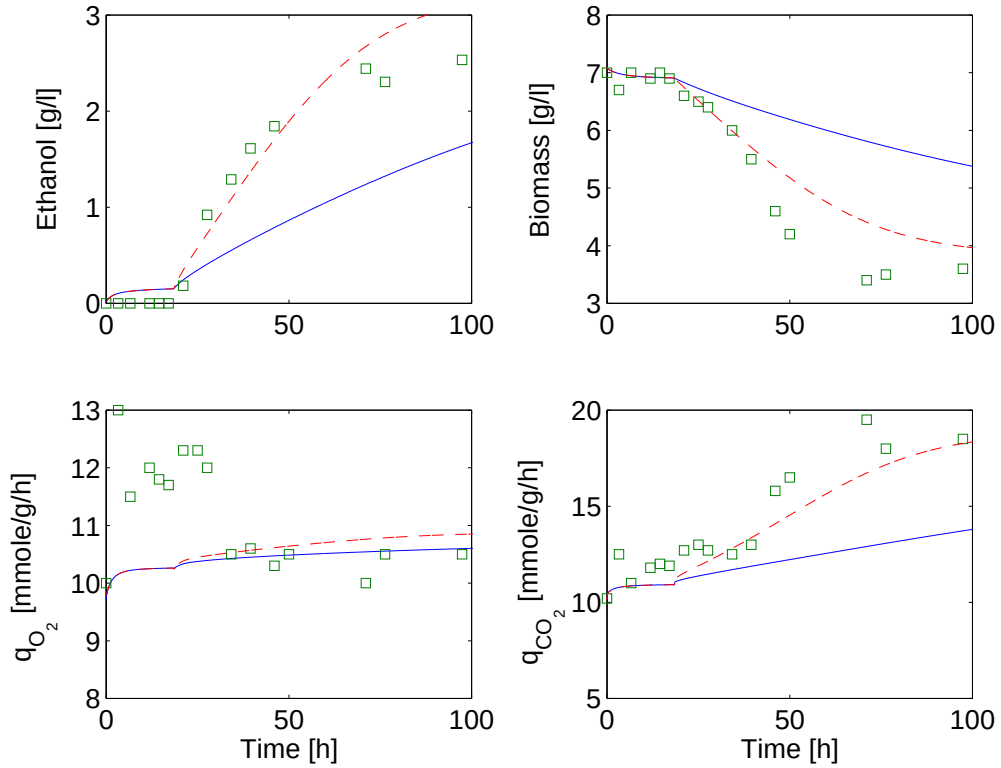

Figure 3.9. Dilution rate shift-up experiment near the critical dilution rate. At time 0 h, the dilution rate was shifted from 0.36 to 0.38 h^{-1}. At time=18.5 h the dilution rate was shifted further to 0.39 h^{-1}. Experimental data was taken from Postma *et al.* (1989). The full line is a model simulation of the same experiment whereas the dotted line is a simulation of an experiment where the second shift is from 0.38 to 0.40 h^{-1}. This illustrates how sensitive the system is near D_{crit}. The high level for q_{O_2} during the first 20 h in the experimental data was attributed to the uncoupling effect (Postma *et al.*, 1989). This effect is not included in the model, hence the discrepancies for q_{O_2}.

different strain than the one modelled in this paper and sufficient experimental data for comparison with the proposed model is unfortunately not available.

From a mathematical point of view multiple steady-states may arise when a bifurcation occurs as a parameter (in this case the dilution rate) is varied (Nayfeh and Balachandran, 1995). A continuation program CONT (Kubicek and Schreiber, 1997) was used for investigating the model for various kinds of bifurcations as well as finding unstable steady-state solutions. The program provides a numerical solution (steady-state and dynamical) and can follow a steady-state solution as one or two model parameters are varied.

Model simulations of a chemostat revealed multiple steady-states in a narrow region below and up to D_{crit} at an inlet substrate concentration of 30 g/l glucose (figure 3.10A).

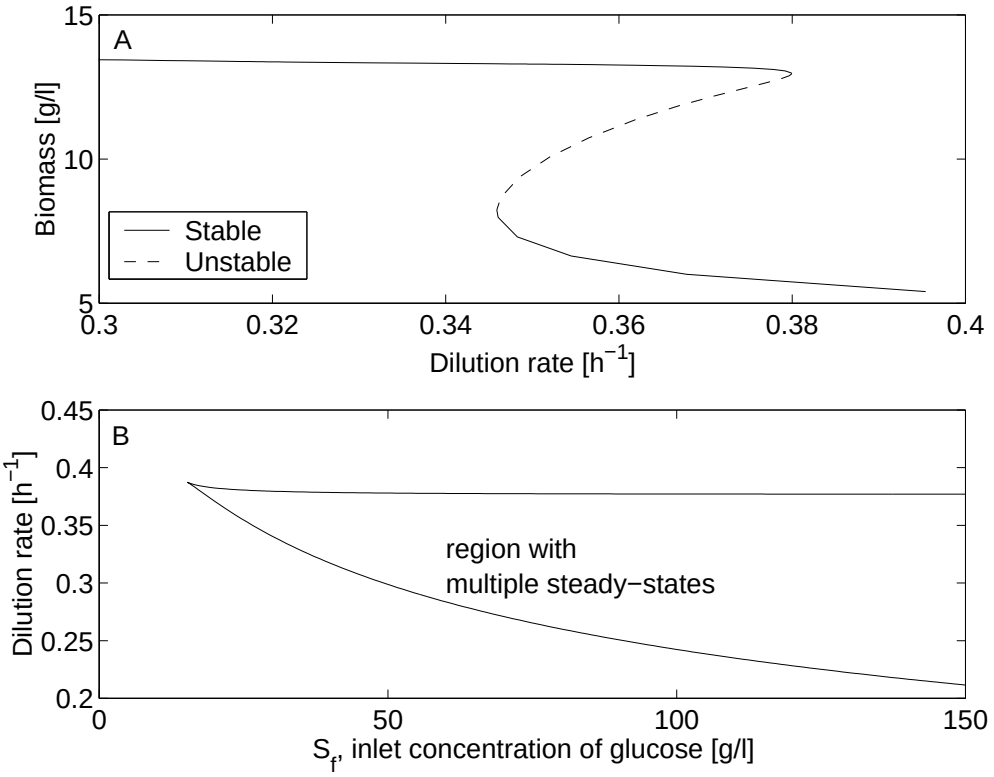

Figure 3.10. Bifurcation diagram for the model. A) This figure is a simulation of biomass concentration as a function of the dilution rate at an inlet substrate concentration of 30 g/l glucose. Multiple steady-states are present in a region close to the critical dilution rate, i.e. for dilution rates between the two fold bifurcation points. B) The figure presents a two-parameter bifurcation diagram of the dilution rate versus the inlet concentration of glucose (S_f). The curve indicates where the fold bifurcations occur. Thus the vertical distance between the two curves depict the width of the region where multiple steady-states are present. Note that this region vanishes for $S_f < 16$ g/l.

In the two parameter bifurcation diagram in figure 3.10B, the solution of interest is the static solution where the fermentation is marginally stable, i.e. possesses an eigenvalue on the imaginary axis. The loci for these solutions is plotted in figure 3.10B where it can be seen that the region of multiple steady-states increases as the inlet glucose of concentration, S_f, increases. Furthermore, it can be seen that multiplicity is not an inherent feature of the model, but depends on the operating conditions. E.g. for the obtained set of kinetic parameters multiple steady-states are not present below a S_f of 16 g/l glucose. This observation provides a possible explanation why multiple steady-states only seldom is reported experimentally since most yeast fermentations carried out in lab scale use small inlet concentrations of glucose. Since multiple steady-states in chemostat cultivations are more likely to be observed at high inlet

concentrations of glucose the multiple steady-state phenomenon indeed has industrial relevance as most fermentations in industry are carried out at high S_f-concentrations in order to obtain a high biomass concentration.

During the bifurcation analysis no Hopf-bifurcation was found which implies that the model does not exhibit sustained oscillatory behaviour in the investigated region of D and S_f.

Xiu *et al.* (1998) investigated a simple model system describing a general overflow metabolism of a microorganism in continuous cultivations with respect to stability and multiplicity. It was found that the combined effects of excess product formation and product inhibition of the specific growth rate are necessary for the model to exhibit two stable non-trivial steady-states. However, for the model to show a profile similar to the biomass concentration in figure 3.10A, a term describing excess substrate uptake at the overflow branch point is required.

The proposed model of *S. cerevisiae* does fulfil the requirements of excess product formation, excess substrate uptake and product inhibition when the growth changes from oxidative to oxido-reductive, which argues for the existence of multiplicity:

- Excess product formation occurs when ethanol (and acetaldehyde) are formed due to overflow at the acetaldehyde branch point.
- Excess substrate uptake is observed at oxido-reductive growth (and modelled as the activation of the third term in r_1 by acetaldehyde).
- Product inhibition of the specific growth rate (r_7+r_8) is not modelled directly. However, for a given steady-state, an increase in the acetaldehyde concentration will increase r_1 and thereby cause the distribution of carbon flux between anabolism (r_7+r_8) and catabolism (r_1) to be shifted towards catabolism, hence the specific growth rate is indirectly inhibited by acetaldehyde.

Although the current model has a more complex structure than the model investigated by Xiu *et al.* (1998) the above statements provide an understanding of what features are required in order for the model to exhibit multiplicity and why the proposed model exhibits multiplicity.

To explain why the region of multiple steady-states increases with S_f the structure of the excess uptake term (the third term in r_1) is considered in two cases:

- **From low D to high D:** Consider what happens when D is increased from below to above D_{crit}. The excess term is activated when a sufficient amount of acetaldehyde has accumulated. From figure 3.11 it can be seen that the D value corresponding to formation of acetaldehyde is approximately constant for all S_f values. This results in a nearly horizontal upper curve in figure 3.10B.

- **From high D to low D:** Consider a dilution rate above D_{crit}. As D is decreased the acetaldehyde concentration drops. However, the concentration of acetaldehyde for a certain D-value also depends on S_f (the larger S_f, the larger acetaldehyde concentration - see figure 3.11). For a given oxido-reductive state within the multiplicity region the dilution rate (and acetaldehyde concentration) have to be decreased sufficiently to turn off the excess uptake term in r_1. The excess term will therefore be turned off at different dilution rates depending on S_f. This behaviour is clearly seen on the lower curve in figure 3.10B.

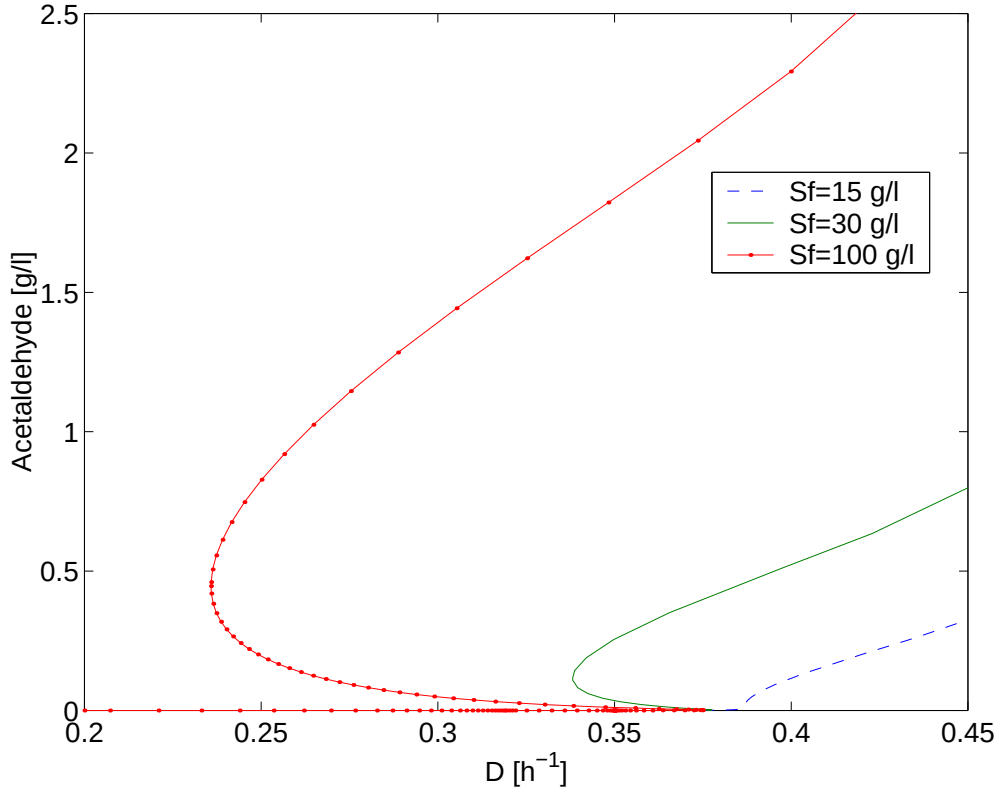

Figure 3.11. Model predictions of acetaldehyde concentration as a function of the dilution rate calculated at three different feed concentrations of glucose (15 g/l, 30 g/l and 100 g/l). In all cases, acetaldehyde is formed at D=0.38 h^{-1} when increasing D from an oxidative state, whereas acetaldehyde formation stops at lower D values for higher feed concentrations.

In the current model acetaldehyde is the trigger which activates the excess uptake of glucose, the product inhibition and the excess product formation, hence causes multiplicity. However, if multiple steady-states were the only aim for the model, the multiplicity could also have been modelled using ethanol as activating compound. Axelsson *et al.* (1992) has extended the bottleneck model with an ethanol inhibition term on the oxidative consumption of glucose to model multiple steady-states. For

their model, the multiplicity region also increases with feed concentration which is caused by the ethanol concentration depending on S_f. Hence the general explanation to why the multiplicity region increases with the feed concentration is *the fact that the concentration of the compound that triggers the multiplicity varies for a given D with S_f.*

3.4 Conclusions

In this paper a biochemically structured model which describes the aerobic growth of *S. cerevisiae* near pathway shifts connected to glucose overflow metabolism was been presented. As opposed to the bottleneck model proposed by Sonnleitner and Käppeli (1986), the new model operates with two bottlenecks, a limitation in the oxidative catabolism and a limitation in the pyruvate dehydrogenase bypass (conversion of acetaldehyde to acetate). The new model uses acetaldehyde as signalling compound to enhanced the glucose uptake rate and the glycolytic flux. This use of a signalling compound makes it possible to represent the new model in a continuous differentiable form as opposed to the bottleneck model and makes the model directly amenable for analysis and for optimisation.

One objective of this work was to investigate the opportunities and challenges of a moderately complicated structured model based on Monod-type kinetics when applied for simulations of various fermentation modes. It was concluded that steady-state chemostat data are described well by the model, furthermore, by structuring the biomass the model is able to describe dynamic effects such as ethanol formation during glucose pulses and dilution rate shift-up.

However, and not surprisingly, not all dynamic phenomena are captured by the model. The discrepancies in pyruvate and acetate concentrations between the batch simulations and experimental data are due to limitations in the model structure. A more quantitatively correct description of the acetate and pyruvate concentrations would require a further structuring of the model to better account for the internal changes in the cells when shifting between substrates. Such a structuring should take global control mechanisms imposed by redox equivalents and energetic constraints into account and not only enzyme kinetics.

Since the validation of the yeast model was based on literature data verification of all model results could not be accomplished. However, the model is appropriate for nonlinear analysis and design of new experiments which can be use to reveal new aspects of yeast physiology. More measurements during dynamic conditions of intracellular enzymes in the pyruvate metabolism could provide valuable information regarding the intracellular model structure. Especially the activity of acetaldehyde dehydrogenases during different growth conditions should be investigated further since it is the key enzyme in the model.

Nonlinear analysis of the model dynamics revealed multiplicity around

D_{crit}, a phenomenon which previously has been indicated experimentally, however only a very limited amount of convincing data exists in the vicinity of D_{crit} to experimentally verify the existence of multiple steady-states. Such measurements are necessary if the steady-state solution of the model should be validated further and closed loop experiments (e.g. control of the dilution rate using an ethanol related measurement) are required in order to stabilise the unstable steady-states and provide reproducible data in the region of dilution rates near D_{crit}. Closed loop experiments are currently being conducted in the investigation of multiple steady-states in continuous cultivations of *S. cerevisiae*.

An explanation for the occurrence and for the features of multiple steady-states were given based on the model structure. Product inhibition of the specific growth rate is a key factor to the occurrence of multiplicity. The multiplicity region will increase with S_f if the concentration of this compound depends on the feed concentration. Even if acetaldehyde is *not* the trigger for multiple steady-states as proposed in the current model the dependency of such a trigger on the feed concentration should be addressed in further investigations of multiple steady-states.

The proposed model is by no means meant to mirror the complete yeast physiology and since relatively few metabolites are included the model cannot be expected to describe many of the regulatory functions in the cell. However the model can be used for describing dynamical trends of many measurable metabolites and gas flows in yeast cultivations related to glucose overflow metabolism. Thus the model can be employed for simulations in the design phase for developing control strategies for optimising continuous and fed-batch cultivations.

The kinetic modelling approach used in this work obviously has its limitations. The number of kinetic parameters increases significantly with the number of metabolites included in the model. This high number of parameters limits the possibilities for developing detailed models describing whole metabolic networks. However, kinetic models are required if the model has to be used for control design or for investigations of the nonlinear dynamics of the process.

List of symbols

CER	carbon dioxide evolution rate [mmole CO_2/h]
D	dilution rate [h^{-1}]
D_{crit}	critical dilution rate in chemostat (onset of alcoholic fermentation) [h^{-1}]
$D_{washout}$	dilution rate in chemostat at which washout occurs [h^{-1}]
k_i	rate constant for reaction i [g substrate /g X_a/h]
K_i	affinity constant for reaction i [g-substrate/l]
K_{ji}	inhibition constant for reaction j [l/g-substrate]
K_M	affinity constant [g-substrate/l]
OUR	oxygen uptake rate [mmole O_2/h]
q_{O_2}	specific oxygen uptake rate [mmole O_2/g bio/h]
q_{CO_2}	specific oxygen uptake rate [mmole CO_2/g bio/h]
q_{glu}	glucose uptake rate [g glu/h]
r_i	reaction rate for reaction i [h^{-1}]
s_i	extracellular concentration of component i [g/l]
S_f	inlet concentration of glucose in chemostat [g/l]
S_i	intracellular concentration of component i
U	specific enzyme activity [g enzyme · mg protein/g bio]
v_{max}	rate constant [h^{-1}]
V	volume [l]
x	biomass concentration [g/l]
X_i	Intracellular concentration of compartment i [no unit, between 0 and 1]

References

Alexander, M. and Jeffries, T. (1990). Respiratory efficiency and metabolite partitioning as regulatory phenomena in yeasts. *Enzyme Microb. Technol.*, **12**, 2–19.

Axelsson, J.; Münch, T. and Sonnleitner, B. (1992). Multiple steady-states in continuous cultivation of yeast. *IFAC Modelling and Control of Biotechnical Processes, Colorado, USA*, **10**, 383–386.

Barman, T. (1969). *Enzyme Handbook vol.1*. Springer-Verlag Heidelberg New York.

Beck, C. and von Meyenburg, H. (1968). Enzyme pattern and aerobic growth of *Saccharomyces cerevisiae* under various degrees of glucose limitation. *J. Bacteriol.*, **96**, 479–486.

Benthin, S.; Nielsen, J. and Villadsen, J. (1992). Anomeric specificity of glucose uptake systems in *Lactococcus cremoris*, *Escherichia coli* and *Saccharomyces cerevisiae*: Mechanism, kinetics and implications. *Biotechnol. Bioeng.*, **40**, 137–146.

Crabtree, H. (1929). Observations on the carbohydrate metabolism of tumours. *Biochem. J.*, **21**, 536–545.

de Deken, R. (1966). The Crabtree effect: A regulatory system in yeast. *J. Gen. Microbiol.*, **44**, 149.

de Jong-Gubbels, P. (1998). *Metabolic fluxes at the interface of glycolysis and TCA cycle in Saccharomyces cerevisiae*. Ph.D. thesis, Kluyver Laboratory of Biotechnology, Delft University of Technology.

Duboc, P.; Stockar, U. v. and Villadsen, J. (1998). Simple generic model for dynamic experiments with *Saccharomyces cerevisiae* in continuous culture: Decoupling between anabolism and catabolism. *Biotechnol. Bioeng.*, **60**, 180–189.

Fiecther, A.; Fuhrmann, G. and Käppeli, O. (1994). Regulation of glucose metabolism in growing yeast cells. *Adv. Microb. Physiol.*, **36**, 145–180.

Flikweert, M.; van der Zanden, L.; Janssen, W.; Steensma, H.; van Dijken, J. and Pronk, J. (1996). Pyruvate decarboxylase: An indispensable enzyme for growth of *Saccharomyces cerevisiae on glucose*. *Yeast*, **12**, 247–257.

Flikweert, M.; van Dijken, J. and Pronk, J. (1997). Metabolic responses of pyruvate decarboxylase-negative *Saccharomyces cerevisiae* to glucose excess. *Appl Environ Microbiol*, **63**, 3399–3404.

Frandsen, S. (1993). *Dynamics of Saccharomyces cerevisiae in continuous culture*. Ph.D. thesis, IBT, Technical University of Denmark.

Jørgensen, S.; Møller, H. and Andersen, M. (1992). Adaptive control of continuous yeast fermentation. *Proc. 9th Int. Biotechnol. Symposium*, pages 364–369.

Kresze, G.-B. and Ronft, H. (1981). Pyruvate dehydrogenase complex from baker's yeast. I. Purification and some kinetic and regulatory properties. *Eur. J. Biochem.*, **119**, 573–579.

Kubicek, M. and Schreiber, I. (1997). Computational analysis of nonlinear dynamical systems. *Zeitschrift für Angewandte Mathematik und Mechanik*, **77**, S603–4.

Lei, F. and Jørgensen, S. (2001). Estimation of kinetic parameters in a structured yeast model using regularisation. *Accepted for publication in J. Biotechnol.*.

Nayfeh, A. and Balachandran, B. (1995). *Applied nonlinear dynamics*. John Wiley & Sons, New York.

Nielsen, J. and Villadsen, J. (1992). Modelling of microbial kinetics. *Chem. Eng. Sci.*, **47**, 4225–4270.

Nielsen, J. and Villadsen, J. (1994). *Bioreaction Engineering Principles*. Plenum Press.

Pham, H.; Larsson, G. and Enfors, S.-O. (1998). Growth and energy metabolism in aerobic fed-batch cultures of *Saccharomyces cerevisiae*: Simulation and model verification. *Biotechnol. Bioeng.*, **60**, 474–482.

Polakis, E.; Bartley, W. and Meek, J. (1965). Changes in the activities of respiratory enzymes during the aerobic growth on yeast on different carbon sources. *Biochemical J.*, **97**, 298–302.

Postma, E.; Verduyn, C.; Scheffers, A. and van Dijken, J. (1989). Enzymic analysis of the Crabtree effect in glucose-limited chemostat cultures of *Saccharomyces cerevisiae*. *Appl. Env. Microbiol.*, **55**, 468–477.

Pronk, J.; Wenzel, T.; Luttik, M.; Klassen, C.; Scheffers, W.; Steensma, H. and van Dijken, J. (1994). Energetic aspects of glucose metabolism in a pyruvate-dehydrogenase-negative mutant of *Saccharomyces cerevisiae*. *Microbiology*, **140**, 601–610.

Pronk, J.; Steensma, H. and van Dijken, J. (1996). Pyruvate metabolism in *Saccharomyces cerevisiae*. *Yeast*, **12**, 1607–1633.

Reifenberger, E.; Freidel, K. and Ciriacy, M. (1995). Identification of novel *HXT* genes in *Saccharomyces cerevisiae* reveals the impact of individual hexose transporters on glycolytic flux. *Mol. Microbiol.*, **16**, 157–167.

Roels, J. (1983). *Energetics and kinetics in biotechnology*. Elsevier Biomedical Press.

Sonnleitner, B. and Hahnemann, U. (1994). Dynamics of the respiratory bottleneck of Saccharomyces cerevisiae. *J. Biotechnol.*, **38**, 63–79.

Sonnleitner, B. and Käppeli, O. (1986). Growth of *Saccharomyces cerevisiae* is controlled by its limited respiratory capacity: Formulation and verification of a hypothesis. *Biotechnol. Bioeng.*, **28**, 927–937.

Stephanopoulos, G.; Nielsen, J. and Aristodou, A. (1998). *Metabolic Engineering*. Academic Press, London.

Stryer, L. (1995). *Biochemistry 4th edition*. W.H. Freeman and Company, New York.

van den Berg and Steensma, H. (1995). ACS2, a *Saccharomyces cerevisiae* gene encoding acetyl-CoA, essential for growth on glucose. *Eur. J. Biochem.*, **231**, 704–713.

van den Berg, M. A.; de Jong-Gubbels, P.; Kortland, C.; van Dijken, J.; Pronk, J. and Steensma, H. (1996). The two acetyl-coenzyme A synthetases of *Saccharomyces cerevisiae* differ with respect to kinetic properties and transcriptional regulation. *J. Biol. Chem.*, **271**, 28953–28953.

van Dijken, J. and Scheffers, W. (1986). Redox balances in the metabolism of sugars by yeasts. *FEMS Microbiol. Rev.*, **32**, 199–224.

van Urk, H.; Schipper, D.; Breedveld, G.; Mak, P.; Scheffers, W. and van Dijken, J. (1989). Localization and kinetics of pyruvate-metabolizing enzymes in relation to aerobic alcoholic fermentation in *Saccharomyces cerevisiae* CBS8066 and *Candida utilis* CBS 621. *Biochim. et Biophys, Acta*, **992**, 78–86.

Xiu, Z.; Zeng, A. and Deckwer, W.-D. (1998). Multiplicity and stability analysis of microorganisms in continuous culture: Effects of metabolic overflow and growth inhibition. *Biotechnol. Bioeng.*, **57**, 251–261.

4

Setpoint tracking of oxido-reductive steady-states in continuous cultivations of *S.cerevisiae*

Oxido-reductive steady-states were obtained in aerobic, glucose limited continuous cultivations of Saccharomyces cerevisiae *by manipulating the dilution rate based on ethanol related signals. The selection of measurement and control structure was based on model investigations of a structured yeast model. Three different controllers were evaluated through model simulations: A incremental PI controller, a PI controller with a nonlinear error term and a LQ controller. It was found that the ethanol measurement was superior to the RQ measurement when tracking oxido-reductive steady-states at low ethanol concentrations, whereas both measurement could be used at higher ethanol concentrations. Setpoint tracking of ethanol concentrations was performed experimentally using the PI controller with a nonlinear error term. Experimental oxido-reductive steady-states in the interval from 0.1 to 6 g/l ethanol were obtained by manipulating the dilution rate based on the ethanol concentration. However, it was not possible to obtain experimental oxido-reductive steady-states at higher ethanol concentrations by stepwise increasing the ethanol setpoint. Instead, pseudo steady-states were obtained in this region by using an accelero-productostat, where the ethanol setpoint was increased as a ramp.*

4.1 Introduction

During glucose limited aerobic continuous cultivations of *Saccharomyces cerevisiae* it is, in contrast to batch cultivations, possible to obtain oxidative growth where glucose is converted into biomass and carbon dioxide. Oxidative growth of *S. cerevisiae* is preferable during production of baker's yeast and heterologous protein production where the desired product concentration is related to the biomass concentration. However, when the dilution rate in a continuous cultivation is increased above a certain

limit, D_{crit}, ethanol formation occurs and the biomass yield decreases. The growth of *S. cerevisiae* above D_{crit} is referred to as oxido-reductive growth.

In continuous cultivations, the maximal productivity of biomass ($D \cdot x$) is reached near D_{crit}, however due to a drastic decrease in the biomass productivity above D_{crit}, operation at the dilution rate corresponding to maximal biomass productivity is not straight forward in a chemostat. A small disturbance might trigger the formation of large amounts of ethanol and consequently a decrease in productivity. Therefore many studies have focussed on how to manipulate the dilution rate in order to control continuous cultivations of *S. cerevisiae* near D_{crit} based on on-line measurements relating to the states of the culture.

Meyer and Beyeler (1984) has combined respiratory quotient (RQ), carbon evolution rate (CER) and culture fluorescence measurements in a PID controller in a control scheme for manipulating the dilution rate in order to operate at the maximal biomass productivity. The fluorescence measurement was used in a feed forward manner to indicate the onset of glucose repression during transient conditions. Axelsson (1988) has applied a semiconductor gas sensor (Figaro) to control the ethanol concentration in continuous cultivations of *S. cerevisiae* using a PID controller. The ethanol concentration was shifted between different levels (0.4 to 0.8 g/l) to investigate the dynamics of ethanol production and consumption. Andersen *et al.* (1997) has found that the Figaro ethanol sensor was superior to a culture fluorescence measurement with respect to disturbance rejection in continuous cultivations operated near D_{crit} since the fluorescence measurement was insensitive during oxido-reductive growth. The Figaro ethanol sensor has also been used by Andersen *et al.* (1997) where setpoint tracking of the ethanol concentration was attempted to investigate the process dynamics in closed loop operation at various ethanol concentrations. An adaptive dilution rate controller based on a 3rd order ARX-model with a 3 min delay (sample time: 1 min) was used. The dilution controller showed good tracking performance at low ethanol concentrations (from 0.05 g/l to 1.8 g/l), however it failed at higher ethanol concentrations (the gain of the process was estimated to zero due to a fixed model order). The application of feedback control of the dilution rate during start-up of a continuous cultivation has been illustrated by Møller and Jørgensen (1997), again using the ethanol related signal from the Figaro sensor. Two model based controllers from Andersen *et al.* (1997) have been applied: A model based (IMC) PI controller with fixed parameters and an adaptive linear quadratic controller. The latter controller was found to be superior to the PI controller. Duboc *et al.* (1998) has used calorimetric measurements for controlling the increase in the dilution rate to avoid ethanol formation during an increase in the feed rate. The heat evolution rate was sensitive to the metabolic switch between oxidative and oxido-reductive growth, and thus provided an fast estimate of the metabolic state of the

cultivation. A nonlinear proportional control law was applied to increase the dilution rate in order to avoid saturation of the oxidative capacity.

Previous investigations of a mathematical model describing aerobic growth of *S. cerevisiae* in continuous cultivations have revealed multiple steady-state in a region around D_{crit} (Lei *et al.*, 2001). The model predicted that three steady-states exist in the multiplicity region below D_{crit} whereof two are stable and should be obtainable in open loop (figure 4.1). If multiple steady-states do exist, at least one of the steady-states will be unstable and at least one eigenvalue in the linearised model will be greater than zero, Nayfeh and Balachandran (1995). Such a steady-state cannot be reached in a traditional chemostat since it is unstable and thus a small perturbation when operating at the unstable steady-state will cause the process to move to a new (and stable) steady state at the same dilution rate. Instead, the unstable steady-state can be obtained by specifying e.g. the ethanol concentration and using feedback control of the dilution rate. This operation mode has also been referred to as a productostat (Andersen *et al.*, 1997).

The purpose of this work was to investigate oxido-reductive steady-states in continuous cultivations of *S. cerevisiae* using feedback control of the dilution rate. If multiple steady-states exist, as predicted by the Lei *et al.* (2001) model, it should be possible to obtain oxido-reductive steady-states at dilution rates lower than D_{crit}.

In this work, possible measurements which could be applied for feedback control of the dilution rate during oxido-reductive growth were evaluated. Furthermore, the performance of three dilution rate controllers; an incremental PI-controller, a PI-controller with a nonlinear error term, and a linear quadratic (LQ) controller, were investigated through model simulations of setpoint changes in the ethanol concentration. Finally, ethanol setpoint tracking experiments in continuous cultivations of *S. cerevisiae* were simulated using the yeast model proposed by Lei *et al.* (2001) to evaluate the model performance during oxido-reductive growth.

4.1.1 Measurement selection

Four different measurements were considered for performing feedback control of the dilution rate in the oxido-reductive region: Biomass, ethanol, RQ and the heat evolution rate. Steady-state values for these measurements predicted by the yeast model (Lei *et al.*, 2001) are shown in figure 4.1. From the simulations, it is evident that the heat evolution rate is not an appropriate measurement since the same heat evolution rate can be obtained for two different dilution rates around D_{crit}. The biomass concentration should not be used as measurement due to the very slow dynamics of cell growth and due to the lack of an appropriate on-line biomass sensor.

The remaining measurement options, ethanol and RQ, have both been

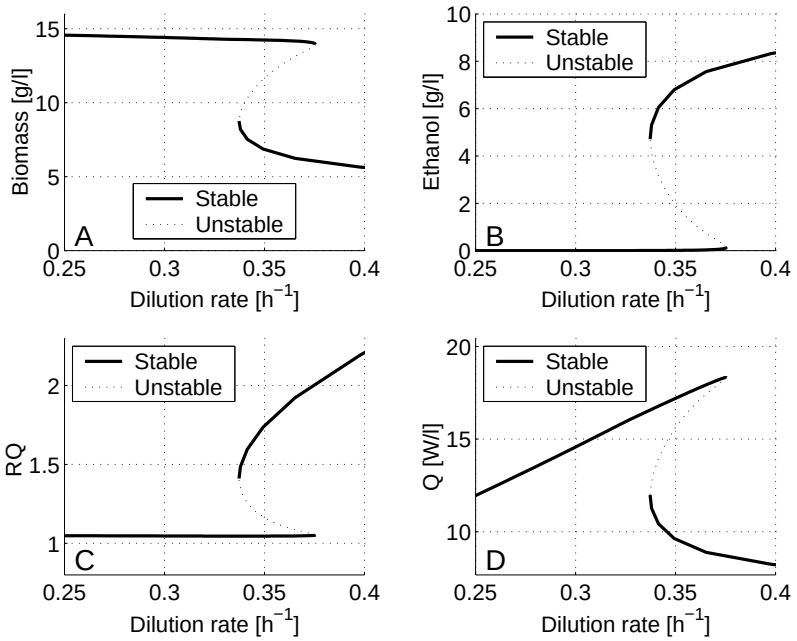

Figure 4.1. Steady-state model predictions of A: biomass, B: ethanol, C: respiratory quotient (RQ) and D: heat evolution (Q) around D_{crit} for a feed concentration of 30 g/l glucose (Lei *et al.*, 2001). The heat evolution was calculated by assuming proportionality between heat evolution and oxygen uptake (Duboc *et al.*, 1998). The simulations show that three steady-states exist in a dilution rate region around D_{crit}. The full curves indicate a stable steady-state whereas the dashed curve represents an unstable steady-state. The unstable steady-state solutions can only be realised using closed loop control of the dilution rate.

applied in previous studies around D_{crit} (as discussed above) and are both available in the applied fermentation system. Whereas the ethanol measurement is indicative of a concentration in the reactor, RQ reflects a reaction rate. Consequently, it might seem more advantageous to use the RQ measurement since it reflects the current flux distribution between oxidative and fermentative catabolism, whereas the ethanol concentration *per se* does not provide information about the flux distribution in the cell. On the other hand, according to figure 4.1, the range of the RQ measurement corresponding to the unstable steady-states (1.05 to 1.41) is much smaller than the ethanol range (0.1 to 4.7 g/l). Accounting for the noise on the two measurements points to that ethanol could be the preferred alternative.

4.1.2 Dilution rate controllers

The performance of dilution rate controllers based on RQ as well as ethanol measurement were evaluated during simulations of three different dilution rate controllers: An incremental PI controller, a PI controller

with a nonlinear error term and a LQ controller.

4.1.2.1 Incremental PI controller

The incremental PI controller used was taken from Andersen (1990). In the control algorithm, the new actuator value is calculated based on the previous actuator value, hence no reference actuator value is used. This implementation further eliminates the possibility of wind-up during actuator saturation.

The controller was implemented in discrete time by approximating $\Delta D(t) = \frac{dD}{dt} \cdot T_s$:

$$\Delta D(t) = K_c \cdot (e(t) - e(t - T_s)) + K_c/T_i \cdot e(t) \tag{4.1}$$
$$D(t) = D(t - T_s) + \Delta D(t) \tag{4.2}$$

$$D(t) = D_{max} \quad \text{if} \quad D(t) > D(t)_{max} \tag{4.3}$$
$$D(t) = D_{min} \quad \text{if} \quad D(t) < D(t)_{min} \tag{4.4}$$
$$e(t) = y_{ref} - y(t), \tag{4.5}$$

where $y(t)$ represent the measured variable and y_{ref} is the current setpoint.

4.1.2.2 PI controller with nonlinear error term

The nonlinear PI controller applied in this study was originally developed as a proportional controller by Creutzburg (2001) for chemostat operation at the maximal biomass productivity. Since the process behaviour is very nonlinear around D_{crit}, it might be expected that conventional linear controllers will not be able keep the process at the optimal operation point. Instead the nonlinear P controller was proposed by Creutzburg (2001) based on the notion that the controller should have a higher gain in the vicinity of the setpoint and a lower gain further away from the desired setpoint.

The dilution rate, D, was calculated as

$$e(t) = 2\frac{y_{ref}^{\beta p_c}}{y_{ref}^{\beta p_c} + y^{p_c}(t)} - 1, \tag{4.6}$$

$$D(t) = K_c\, e(t) + \frac{K_c}{T_i} \int_0^t \left(2\frac{y_{ref}^{p_c}}{y_{ref}^{p_c} + y^{p_c}(\tau)} - 1 \right) d\tau, \tag{4.7}$$

where the exponent p_c is used to change the degree of nonlinearity in the controller. The β parameter was included in the proportional error calculation to reduce the overshoot in the response during a setpoint change which was observed in preliminary simulations. The effect of the β parameter can be illustrated by calculating the linearised closed loop transfer

function for the process. In the continuous time domain, the controller looks like

$$D(t) = K_c \left(2\frac{y_{ref}^{\beta p_c}}{y_{ref}^{\beta p_c} + y^{p_c}(t)} - 1 + \frac{1}{T_i}\int_0^t (2\frac{y_{ref}^{p_c}}{y_{ref}^{p_c} + y^{p_c}(t)} - 1)d\tau \right). \quad (4.8)$$

A linearisation of the controller around the operating point (D_0,y_0) yields

$$\overline{D}(t) = \frac{K_c p_c}{2y_0} \left(\frac{4y_0^{(\beta-1)p_c}}{(y_0^{(\beta-1)p_c}+1)^2}(\beta\overline{y}_{ref} - \overline{y}(t)) + \frac{1}{T_i}\int_0^t (\overline{y}_{ref} - \overline{y}(\tau))d\tau \right), \quad (4.9)$$

where a bar denotes deviation variables. By Laplace transforming the controller equation and considering a linear process, $Y(s) = G_p(s)U(s)$, the closed loop transfer function from the setpoint to the measurement can found as

$$Y(s) = \frac{G_p(s)\frac{K_c p_c}{2y_0}\left(\frac{4\beta y_0^{(\beta-1)p_c}}{(y_0^{(\beta-1)p_c}+1)^2} + \frac{1}{sT_i}\right)}{1 + G_p(s)\frac{K_c p_c}{2y_0}\left(1 + \frac{1}{sT_i}\right)} Y_{ref}(s). \quad (4.10)$$

Hence, the controller imposes a zero in the transfer function at

$$s_z = -\frac{(y_0^{(\beta-1)p_c}+1)^2}{4T_i\beta y_0^{(\beta-1)p_c}}. \quad (4.11)$$

Thus introduction of β gives a handle to pull the controller zero present for $\beta = 1$ (s_z=$1/T_i$) further away from the imaginary axis by choosing a β value in the interval from $]0;1[$ and thereby decreasing a possible overshoot.

The nonlinear PI controller was implemented with a variable reference setpoint, D_{ref}, in order to enable tracking of the desired setpoints without off-set. This implementation was necessary since the operation points (D_0,y_0) corresponding to the desired steady-states were not known.

$$e_1(t) = 2\frac{y_{ref}^{\beta p_c}}{y_{ref}^{\beta p_c} + y^{p_c}(t)} - 1 \quad (4.12)$$

$$e_2(t) = 2\frac{y_{ref}^{p_c}}{y_{ref}^{p_c} + y^{p_c}(t)} - 1 \quad (4.13)$$

$$D(t) = D_{ref}(t) + K_c \cdot e_1(t) \quad (4.14)$$

$$D_{ref}(t + T_s) = D_{ref}(t) + \frac{K_c}{T_i} \cdot T_s \cdot e_2(t). \quad (4.15)$$

4.1.2.3 LQ controller

A linear quadratic (LQ) controller was also used for setpoint tracking of the ethanol concentration. The LQ objective function used was

$$J_N = \sum_{i=1}^{N} (y^T(t+i)Q_y y(t+i) + \Delta u^T(t+i)Q_u, \Delta u(t+i) \quad (4.16)$$

where the weighting matrices Q_y and Q_u are positive scalars, since a SISO system is considered. The incremental control term ensures off-set elimination. The model was reformulated in a state-space representation as in Andersen *et al.* (1997), and the control gain was calculated off-line for each operating point.

4.2 Materials and methods

4.2.1 Strain and medium

The yeast *S. cerevisiae* CEN.PK113-7D was cultivated in an aerobic continuous culture. The substrate (glucose) concentration was 30 g/l and a defined minimal medium was used (Lei, 2001, chap.5).

4.2.2 Preparation of inoculum

S. cerevisiae strain CEN.PK113-7D was stored at -80°C in glycerol and cultures from -80°C was plated onto YPD agar plates and incubated at 30°C. After three days, a single culture was transferred to a shake-flask containing mineral medium (Lei, 2001, chap.5), at an initial pH of 6.5 and containing 1% (w/v) glucose. Cells, growing exponentially on glucose, were used as inoculum for the fermenter.

4.2.3 Equipment and analytical methods

The equipment and analytical methods have been described in Lei (2001, chap.5).

4.2.4 Measurements for control

The carbon dioxide evolution rate (CER) and oxygen uptake rate (OUR) were calculated according to van Urk *et al.* (1988). RQ was calculated as CER/OUR.

Two ethanol related measurements were available by measuring the outlet gas: A reducing gas sensor (Figaro, Hammer electronic, Elsinore, Denmark) measuring the content of reducing gases the CHx signal from a Bruel & Kjær Innova Industrial Emissions Monitor 1311 measuring the total content of CHx. The Figaro sensor is most sensitive and was therefore used at low ethanol setpoints where a linear correlation between the sensor reading and the ethanol concentration was found. The CHx measurement was applied for control when the ethanol setpoint was increased above 0.6 g/l. The Figaro and CHx signals were correlated to the extracellular ethanol concentration by the following relations: Figaro: $EtOH[g/l] = (Fig[V] - 0.21)/13.97$ and CHx: $EtOH[g/l] = 1.40 \cdot (CHx[V] + 0.01)$. These correlations were found valid in the range 0.5-10 V for the Figaro

sensor and in the range 0.5-4.5 V for the CHx sensor, respectively (figure 4.2).

4.2.5 Cultivation conditions

The data presented in this paper were obtained from two independent continuous cultivations. Both cultivations (C7 and C8) were carried out using set-up 1, where the fermenter was operated as a productostat using either the Figaro or CHx signal as measurement. The presented experiments are summarised in table 4.1.

Table 4.1. Overview of the conducted experiments. The table states for each experiment, the corresponding cultivation and the number of the figure in which the experiment is presented.

Experiment	Cultivation	Figure
Start-up and tracking	C7	4.12
EtOH: 4.9 → 0.1 g/l	C8	4.13
EtOH: 4.9 → 7.8 g/l	C7	4.14
EtOH ramp: 4.9 → 9.0 g/l	C8	4.15

4.3 Results

This section is structured into two main parts. First, the yeast model proposed by Lei *et al.* (2001) was investigated with respect to control design, control performance and process dynamics. In the second part,

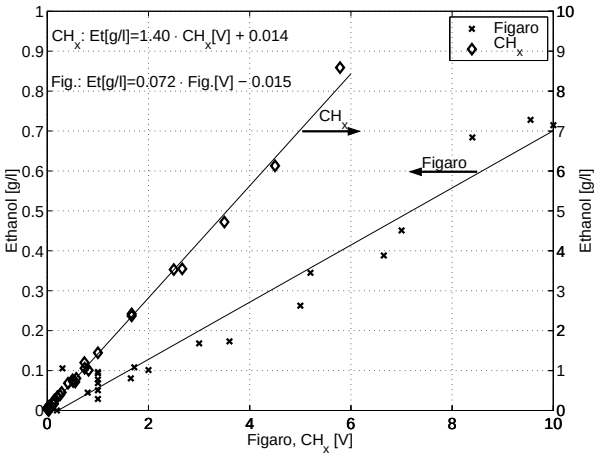

Figure 4.2. Relationship between the on-line ethanol related signals, Figaro and CH_x, and the ethanol concentration in the fermenter.

setpoint tracking experiments are presented and compared with model simulations.

4.3.1 Selection of controller measurement

The performance of the two PI controllers with respect to using RQ or ethanol (Figaro or CHx signals) as measurement was evaluated through model simulations in order to select the most appropriate measurement.

4.3.1.1 Simulation scenario

The simulated scenario used for evaluation of the dilution rate controllers (table 4.2), started with a batch cultivation on 30 g/l glucose. When glucose was depleted, continuous operation with a glucose feed of 30 g/l was initiated using feedback control of the dilution rate. The initial setpoint (RQ=1.055, Figaro=1.0 V) corresponds to a very low ethanol concentration (0.05 g/l). When a steady-state was reached at this setpoint (80 h), two steady-states at higher ethanol (or RQ) values were tracked, whereafter it was simulated that the cultivation was returned to the steady-state at 0.05 g/l ethanol. In the simulations, the ethanol concentration was converted to Figaro and CHx signals through the correlations stated in section 4.2.4 and it was the Figaro or CHx signal which entered the dilution rate controller.

Table 4.2. Simulation scenario for comparing RQ and ethanol as measurement for the dilution rate controller. The setpoint for the RQ or ethanol measurement is stated along with the ethanol concentration at each setpoint.

Time	RQ	Ethanol	Ethanol	Action
0 h				Inoculation of fermenter. Batch phase.
20 h	1.055	F[a]=1.0 V	0.05 g/l	Initiation of continuous phase and dilution rate controller.
80 h	1.29	C[b]=2.5 V	3.5 g/l	Setpoint increase.
140 h	1.64	C=4.5 V	6.31 g/l	Setpoint increase.
200 h	1.055	F=1.0 V	0.05 g/l	Setpoint decrease.
260 h				End of experiment.

a: Figaro sensor

b: CHx signal from gas analyser.

To render the model simulations more realistic, noise on the measurements (RQ, CHx and Figaro) were included in the simulations. The standard deviation of the measurement noise was obtained from experimental data (figures 4.3-4.4). For the RQ measurement, it was decided to use a

constant relative error (0.3%) in the simulations, since the standard deviation at higher RQ values was found to be larger than at low RQ values. For the ethanol related signals, constant standard deviations were used in the simulations (0.02 V for Figaro , 0.01 V for CHx). The measurement range for both sensors was 0–10 V. With respect to the actuator (D), perfect control of the dilution rate was assumed.

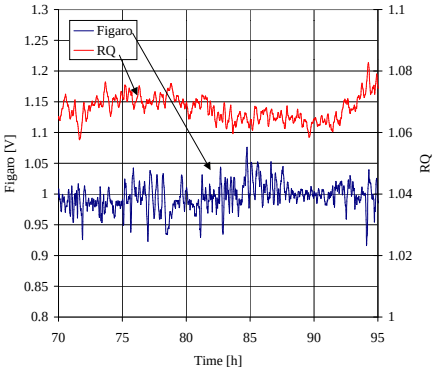

Figure 4.3. Experimental data of RQ and the Figaro sensor obtained during closed loop operation at D=0.31 h^{-1} (0.05 g/l ethanol). The standard deviation was 0.02 V for the Figaro sensor and 0.0031 for RQ.

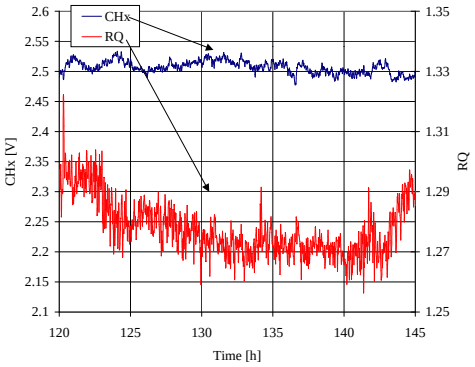

Figure 4.4. Experimental data of RQ and the CHx sensor obtained during closed loop operation at D=0.30 h^{-1} (3.6 g/l ethanol). The standard deviation was 0.01 V for the Figaro sensor and 0.0039 for RQ.

No measurement delay was applied since the effect of a realistic delay (3 min) was found to be negligible in preliminary simulations. Furthermore, it was found that the performance of the controllers did not vary significantly whether the sample time was 2 min or 10 min. A sample time of 10 min was therefore used throughout the simulations to decrease the computer simulation time. Simulation parameters are given in table 4.3.

4.3.1.2 Simulation results

In the simulations of the scenario described in table 4.2, the dilution rate controllers were initiated when continuous operation began at 20 h. The lower limit of the actuator was set to 0.1 h^{-1}, thus the dilution rate was kept at 0.1 h^{-1} until the controlled measurement dropped below its setpoint value. From the simulations, it is evident that both PI controllers using the RQ measurement were not able to track the desired setpoint at RQ=1.055, corresponding to an ethanol concentration of 0.05 g/l (figures 4.5-4.6). The controller failure was due to the nonlinear behaviour

Table 4.3. Parameters used during simulation of the dilution rate controllers. The upper limit of D (D_{max}) corresponded to the maximal pump speed in the experimental set-up, while a lower limit of D (D_{min}) was used to assure continuous feed of glucose.

Parameter	Value
Figaro (std)	0.02 V
CHx (std)	0.02 V
RQ (std)	0.3% (relative)
Measurement delay	0 min
D_{max}	0.5 h^{-1}
D_{min}	0.1 h^{-1}

of the RQ signal around the onset of ethanol production. During oxidative growth the model predicts a RQ=1.045 for all dilution rates in the oxidative region, thus the difference between the RQ setpoint and RQ during oxidative growth on glucose resulted in a very slow integration of the off-set. Hence the dilution rate did not reach a steady-state during the simulated interval. Both PI controller were, however, able to track the RQ setpoints at RQ=1.29 and RQ=1.64. The nonlinear PI controller showed slightly better performance during tracking of RQ=1.29, due to the incorporation of the β parameter which decreased the overshoot. In contrast, during tracking of RQ=1.64, the nonlinear PI controller exhibited fast oscillations immediately after the setpoint change, probably caused by a higher gain used in the nonlinear controller compared to the incremental PI controller. When the RQ setpoint was decreased back to 1.055 from 1.64, both controllers still were not able to track the setpoint, although the corresponding dilution rates were significantly higher than during tracking of the same setpoint immediately after the batch phase.

Table 4.4. Parameters for each of the two dilution rate controllers used during simulation with ethanol or RQ as measurement. The same controller parameters were used for both measurements and are stated for each of the four setpoints.

	Incremental PI	Nonlinear PI
K_c	$\{0.03^1; 0.1^2; 0.1^2; 0.03^4\}$	$\{0.05; 0.23; 0.3; 0.05\}$
T_i	$\{1; 2; 2; 1\}$	$\{2; 4; 4; 2\}$
β	–	$\{1; 0.65; 0.85; 1\}$
p	–	$\{3; 3; 3; 3\}$

1: Figaro=1.0 V (RQ=1.055), 2: CHx=2.5 V (RQ=1.29).

3: CHx=4.5 V (RQ=1.64), 4: Figaro=1.0 V (RQ=1.055).

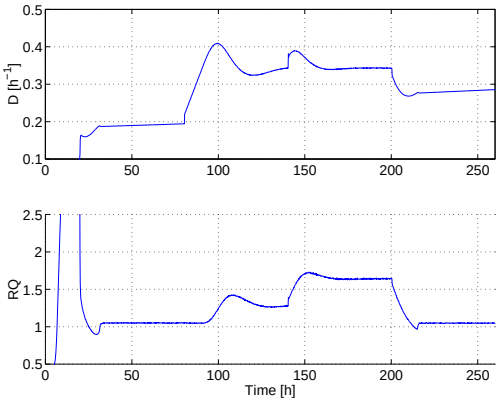

Figure 4.5. Simulation of start-up and setpoint tracking in a continuous *S. cerevisiae* cultivation using the incremental PI controller and RQ as measurement. Controller parameters are given in tables 4.3-4.4.

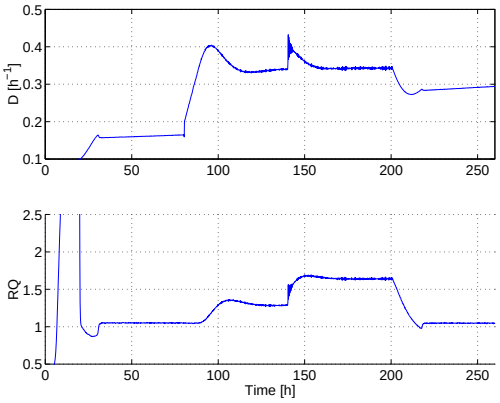

Figure 4.6. Simulation of start-up and setpoint tracking in a continuous *S. cerevisiae* cultivation using the PI controller with a nonlinear error term and RQ as measurement. Controller parameters are given in tables 4.3-4.4.

When the ethanol related measurements (Figaro and CHx) were used as input to the dilution rate controllers, both PI controllers were able to track all setpoints (figures 4.7-4.8). As observed when using RQ as measurement, the nonlinear controller showed slightly better performance during tracking of the two setpoints at high ethanol concentration compared to the incremental PI controller.

For the nonlinear PI controller, a β-value less than one was used during tracking of the two setpoints at CHx=2.5 V and CHx=4.5 V. As a consequence of $\beta \neq 1$, the controller output $D \neq D_{ref}$ according to equations (4.12-4.15). Since the effect of the β parameter is to reduce the overshoot, β was set back to 1 when a steady-state level was reached to avoid $D \neq D_{ref}$ when a new setpoint change was made. This change did not affect the controller output provided that D_{ref} was set equal to D simultaneously with setting β=1.

The model simulations of the experimental scenario clearly showed that the ethanol measurement should be preferred for tracking of setpoints at low ethanol concentrations since the ethanol measurement is much more sensitive than the RQ measurement in this region. At higher ethanol concentrations both measurements could be applied. It was therefore decided to apply the two ethanol related measurements for setpoint tracking of oxido-reductive steady-states in the following experiments.

4.3.2 Performance of a LQ controller

Model simulations using the two PI controllers confirmed that setpoint tracking of oxido-reductive steady-states can be achieved with relatively

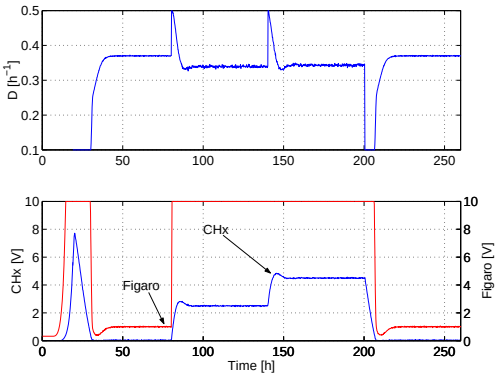

Figure 4.7. Simulation of start-up and set-point tracking in a continuous *S. cerevisiae* cultivation using the incremental PI controller with ethanol as measurement. Controller parameters are given in tables 4.3-4.4.

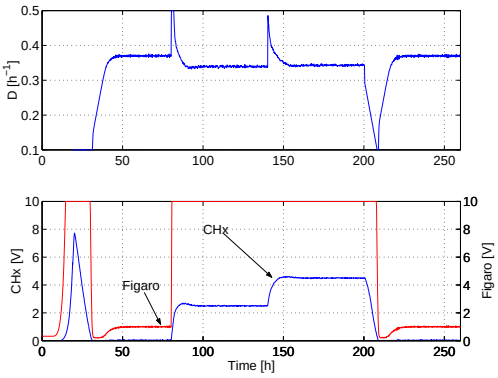

Figure 4.8. Simulation of start-up and set-point tracking in a continuous *S. cerevisiae* cultivation using the PI controller with a nonlinear error term and ethanol as measurement. Controller parameters are given in tables 4.3-4.4.

simple controllers. However, it was necessary to change the control parameters with the operating point and the tuning of the parameters were carried out through model simulations. A less empirical procedure for selecting control parameters were obtained using a LQ controller, where the control parameters were calculated from a linearised model in the operating point based on user defined weighting of the state and actuator movements.

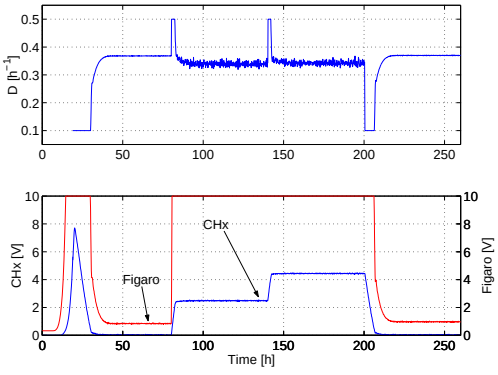

Figure 4.9. Simulation of start-up and set-point tracking in a continuous *S. cerevisiae* cultivation using a LQ controller with ethanol as measurement. LQ controller parameters are stated in table 4.5.

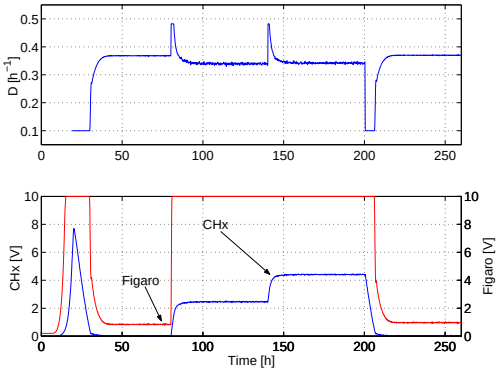

Figure 4.10. Same simulation scenario as in figure 4.9, however actuator movements were penalised more during tracking of CHx=2.5 V and 4.5 V.

The performance of a LQ controller using ethanol as measurement was tested on the simulation scenario (figures 4.9-4.10). The LQ controllers

showed better performance than the two PI-controllers with respect to tracking the desired setpoints. During tracking of the setpoint at a low ethanol concentration (Figaro=1.0 V), the ethanol signal did not drop below its setpoint as observed for the PI controllers resulting in a shorter response time for the LQ controller. The tuning of the LQ controller is illustrated in figures 4.9-4.10. In figure 4.9, deviations between the ethanol measurement and setpoint were penalised heavily compared to actuator movements, thus a quite noisy dilution rate signal was obtained at the two steady-states at high ethanol concentrations. Since the purpose of performing setpoint tracking in this work was to obtain oxido-reductive steady-states, it was important to have a low standard deviation of the dilution rate signal. The actuator movements were therefore penalised more during tuning of the LQ controller in figure 4.10. Consequently, a less noisy dilution rate signal was obtained on the expense of a slightly longer response time of the ethanol signal.

Table 4.5. Parameters for the LQ controller used during simulation of the scenario stated in table 4.2 with ethanol as measurement.

	Figure 4.9	Figure 4.10
Q_y	{1; 1; 1; 1}	{1; 1; 1; 1}
Q_u	{1; 10; 10; 1}	{1; 100; 100; 1}

4.3.3 Model investigations - dynamics and RHP zeros

In order to obtain a better understanding of the control problem during setpoint tracking, the model was linearised in selected operating points where poles and zeros of the open loop transfer function between the dilution rate and the measurements (RQ or ethanol) were calculated. The time constants of the process can then be calculated as

$$\tau_j = 1/|p_j|, \tag{4.17}$$

where p_j are the poles of the transfer function. The largest time constant, corresponding to the numerically smallest pole, is also the dominating time constant for the process. It could be observed that the dynamics of the yeast metabolism is rather fast at low ethanol concentrations, actually proportional to $1/D$ during oxidative growth (Axelsson *et al.*, 1992), whereas slower dynamics can be observed at higher ethanol concentrations (table 4.6). The bold time constants were calculated from unstable steady-states, where the corresponding pole in the transfer function is positive.

The zeros of the transfer functions between the dilution rate and either RQ or ethanol were also calculated for a series of oxido-reductive steady-states. From table 4.7, it can be seen that a zero in the right half plane

Table 4.6. Time constants [h] determined from a linearised version of the Lei *et al.* (2001) yeast model. Time constants were calculated from the poles of the system.

Et=0.05	Et=0.10	Et=0.40	Et=2.0	Et=4.0	Et=6.0	Et=8.0
0.002	0.002	0.002	0.002	0.001	0.001	0.002
0.005	0.005	0.005	0.01+0.01i	0.02+0.0i	0.0169	0.040
0.027	0.027	0.022	0.01−0.01i	0.02−0.0i	0.0659	0.152
0.664	1.297	1.6+0.4i	1.9+0.6i	2.1+0.7i	2.17+0.65i	2.0+0.5i
1.6+0.4i	1.407	1.6−0.4i	1.9−0.6i	2.1−0.7i	2.17−0.65i	2.0−0.5i
1.6−0.4i	2.639	2.661	2.831	2.930	2.899	2.596
2.579	2.800	2.724	2.854	2.930	2.905	2.606
2.670	6.051	**8.139**	**15.19**	**55.31**	26.007	5.959

The bold numbers indicate that the time constant was calculated from a positive pole (unstable system). The time constants do not increase monotonous with the ethanol concentration since infinite time constant are found at the bifurcation points at 0.15 and 4.6 g/l ethanol. Et is the ethanol setpoint [g/l].

Table 4.7. Zeros [h^{-1}] in the right hand plane for the Lei *et al.* (2001) yeast model for ethanol and RQ as measurement.

	Et=0.05	Et=0.10	Et=0.40	Et=2.0	Et=4.0	Et=6.0	Et=8.0
Ethanol	626	479	256	91.7	35.2	11.7	2.44
RQ	392	460	547	621	525	326	95.6

(RHP) is present for all investigated oxido-reductive steady-states. For the ethanol measurement, the RHP zero decreases as the ethanol concentration increases. This might lead to a performance limitation of the dilution rate controller at high ethanol concentrations since a real RHP-zero (z) imposes poor performance on a SISO system at frequencies higher than $z/2$ (Skogestad and Postlehwaite, 1996). It was seen that in the case where Et=8 g/l, the bandwidth is limited to $\omega_c = z/2 = 1.22$ h^{-1} (table 4.7). Thus, the dynamics of the controller in this operation point should not be faster than $1/\omega_c$=0.82 h. For the RQ measurement, the RHP zero does not impose any operational problems.

4.3.3.1 Chemostat versus productostat

The slow dynamics of the yeast model in the oxido-reductive region observed in table 4.6 would result in long response times when dilution rate shift-ups or downs are made to an oxido-reductive steady-state. Long response times can, however, be avoided by using feedback control of the

dilution rate, also referred to as closed loop operation. By operating a continuous cultivation in closed loop, the poles of the process transfer function can be moved resulting in a faster response. Furthermore, closed loop operation can stabilise unstable steady-states.

To illustrate the advantage of operating a continuous cultivation as a productostat, a jump from oxidative growth at D=0.30 h^{-1} to oxido-reductive growth at 0.4 h^{-1} was simulated in a chemostat and in a productostat where the dilution rate was controlled by the ethanol measurement (figure 4.11). The simulations were carried out using a feed concentration of glucose of 15 g/l. At this feed concentration the model does not exhibit multiple steady-states (Lei *et al.*, 2001), thus no unstable steady-states are present and all ethanol concentrations can be achieved during traditional chemostat operation.

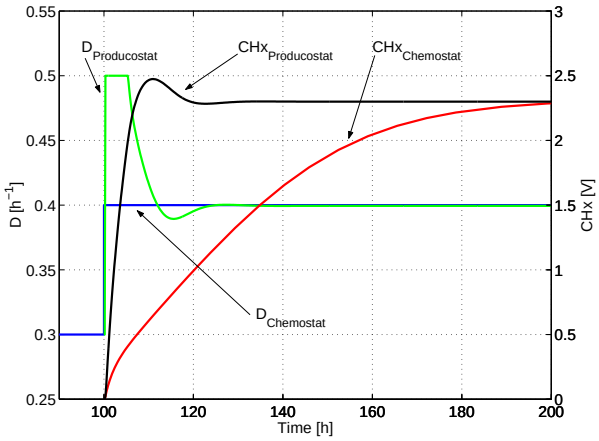

Figure 4.11. Simulation of a continuous cultivation. At time 100 h, the culture was shifted from oxidative growth at D=0.30 h^{-1} to oxido-reductive growth at D=0.4 h^{-1}. A dilution rate shift-up performed in a chemostat is compared with a productostat, where the ethanol setpoint was increased to 3.23 g/l (CHx=2.3 V) at 100 h.

From figure 4.11, the superiority of the productostat over the chemostat with respect to tracking ethanol concentrations can be observed. The steady-state ethanol concentration (CHx signal) was reached after 20 h through closed loop operation, whereas more than 100 h was used in a chemostat.

4.3.4 Comparison between experiments and simulations

In the following section, experimental data obtained through closed loop control of the dilution rate in continuous cultivations of *S. cerevisiae* are compared with model simulations of the yeast model proposed by Lei *et al.* (2001). Since the experiments were carried out with a different yeast strain (CEN.PK113-7D) than the strain used for parameter estimation in the

yeast model (CBS8066, Lei and Jørgensen (2001)), some discrepancies between the experimental data and model simulations were unavoidable, e.g. D_{crit}=0.37 h^{-1} in the model while D_{crit}=0.31 h^{-1} was found experimentally. However, the purpose of the comparison was mainly to evaluate the structure of the yeast model to pinpoint any model deficiencies in describing dynamic behaviour within the oxido-reductive region. Furthermore, the possibility of tracking oxido-reductive steady-states at the desired ethanol concentration using closed loop control of the dilution rate was discussed. For a more thorough interpretation of the results with respect to the existence of multiple steady-states and other physiological phenomena, the reader is referred to Lei (2001, chap.5+7).

4.3.4.1 Start-up of a continuous cultivation

All continuous cultivations were initiated following a batch cultivation on glucose. When glucose was exhausted (monitored from the CO_2 signal) continuous operation was started and the dilution rate controller was turned on. An example of start-up of a continuous cultivation and tracking of three ethanol setpoints are presented in figure 4.12. The first setpoint of the dilution rate controller was Figaro=1.0 V, corresponding to an ethanol concentration of approximately 0.1 g/l whereafter steady-states corresponding to CHx=2.5 V (3.6 g/l ethanol) and CHx=3.5 V (4.9 g/l) were tracked.

Table 4.8. Settings for the dilution rate controller applied experimentally and in the model simulations shown in figure 4.12.

Setpoint	Figaro=1.0 V	CHx=2.5 V	CHx=3.5 V
Time	23-101 h	101-173 h	173-220 h
K_c	0.05	0.23	0.30
T_i	2 h	4 h	4 h
β	1	0.60	0.85
p	3	3	3
$T_{s,exp.}$	1 min	1 min	1 min
$T_{s,sim.}$	10 min	10 min	10 min
$\lvert\Delta D_{max,exp.}\rvert$	0.002 h^{-1}	0.002 h^{-1}	0.002 h^{-1}
$\lvert\Delta D_{max,sim.}\rvert$	0.02 h^{-1}	0.02 h^{-1}	0.02 h^{-1}

A comparison between model simulation and experimental data of the ethanol consumption following the batch phase (23-40 h) reveals that the ethanol concentration initially decreased much faster in the simulation than experimentally observed (figure 4.12B) due to a shorter lag phase. The decrease in the CHx signal at low ethanol concentrations (30 h in simulation, 40 h in experiment) shows, however, that the maximal ethanol consumption rate was larger in the experiment than in model simulations.

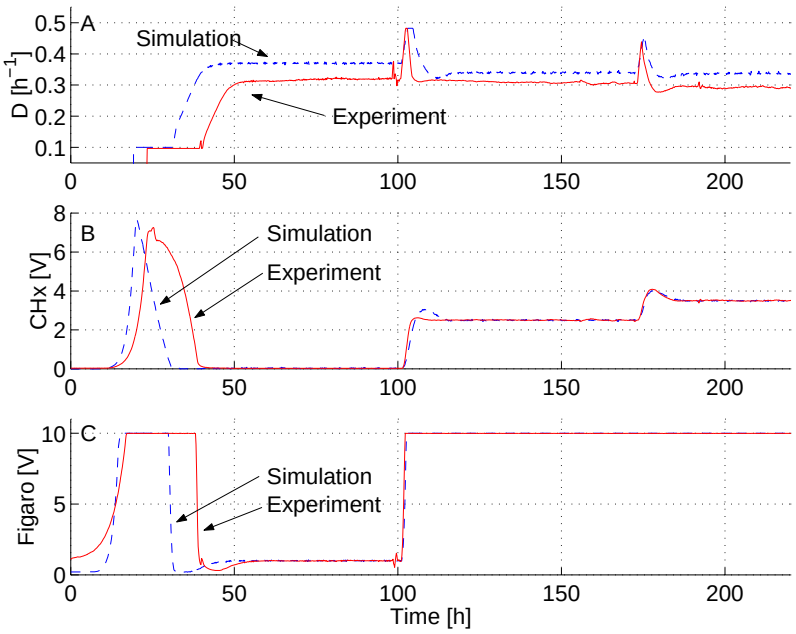

Figure 4.12. Experimental data compared with model simulation of start-up and setpoint tracking of three ethanol concentrations. The dilution rate (A), the CHx signal (B), and the Figaro signal (C) are shown. The Figaro signal was saturated (10 V) during most of the batch phase and after 101 h. The controller settings are stated in table 4.8.

Thus, the data suggests that the model does not describe the diauxic shift properly, despite the structured nature of the yeast model. On the other hand, simulation and experimental data of setpoint tracking of the three setpoints showed very similar profiles. The dynamics of the controlled ethanol signal was almost identical for tracking the first and third setpoint, whereas the experimental data for tracking CHx=2.5 V showed a smaller overshoot than expected from the model simulation.

4.3.4.2 Decrease in ethanol setpoint

A decrease in ethanol setpoint from 4.9 to 0.1 g/l is shown in figure 4.13. Following the setpoint decrease, the controller decreased D to its lower limit as quickly as possible, only constrained by the limit of $|\Delta D_{min}|$ which is the maximally allowed decrease in D during one sample time. A comparison between model simulations and experimental data (figure 4.13B) shows, similarly to figure 4.12B, that the ethanol concentration decreased faster in the experiment than in the simulation at low ethanol concentrations.

The response of D during tracking of the ethanol setpoint at 0.1 g/l was qualitatively different between experimental data and the model simulation (figure 4.13A). In the experiment, D made an overshoot at 433 h whereafter it decreased, whereas no overshoot was observed in the simu-

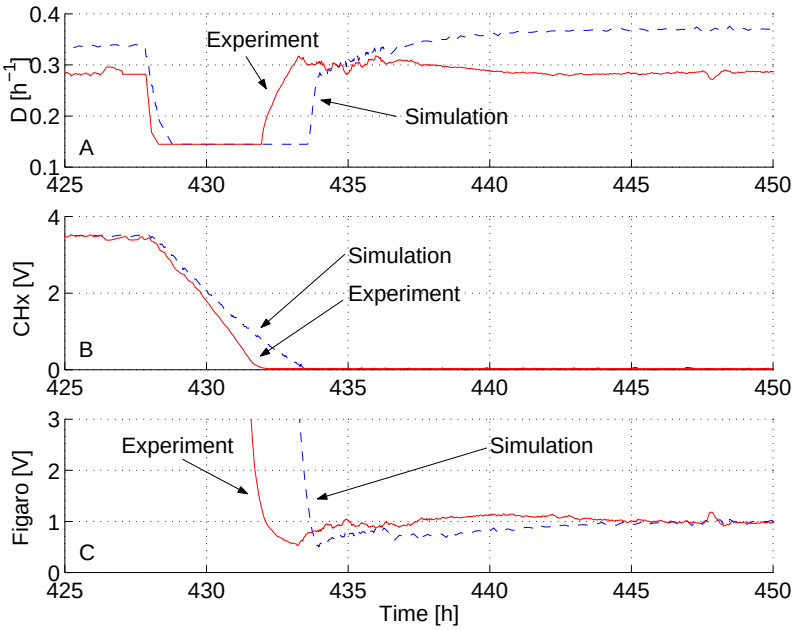

Figure 4.13. Experimental data compared with model simulation of a decrease in the ethanol setpoint from 4.9 to 0.1 g/l. The dilution rate (A), the CHx signal (B), and the Figaro signal (C) are shown. The controller settings are stated in table 4.9.

lations. Even when the controller gain in the simulations was kept at 0.1 from 428 to 450 h, instead of being decreased to 0.05, no overshoot was observed (results not shown).

4.3.4.3 Increase in ethanol setpoint

For the first two experiments shown, model simulations and experimental data agreed fairly well, however during a shift-up in ethanol setpoint from 4.9 to 7.8 g/l (figure 4.14), a severe discrepancy between model simulations and experimental data was observed. It could be observed that the ethanol concentration (CHx signal) only increased during the first 3 h after the setpoint change, whereafter it began to decrease even though the dilution rate was kept above 0.4 h^{-1} (figure 4.14C). This behaviour was not expected from the model simulations where the desired ethanol setpoint was tracked smoothly. According to the simulations, q_{O_2} should have increased slightly, however in the experiments q_{O_2} decreased drastically (figure 4.14B) which lead to a washout-like scenario with glucose accumulation in the fermenter and decreasing biomass concentration (figure 4.14D).

4.3.4.4 Accelero-productostat

An approximation to the oxido-reductive steady-states at ethanol concentrations above 6 g/l were obtained by operating a continuous cultivation as an accelero-productostat. By continuously but slowly increasing the

Table 4.9. Settings for the dilution rate controller applied experimentally and in simulations in figure 4.13.

Setpoint	CHx=3.5 V	Figaro=1.0 V	Figaro=1.0 V
Time	390-428 h	428-436 h	436-450 h
K_c	0.3	0.1	0.05
T_i	4 h	1 h	2 h
β	1	1	1 h
p	3	3	3
$T_{s,exp.}$	1 min	1 min	1 min
$T_{s,sim.}$	10 min	2 min	10 min
$\lvert\Delta D_{max,exp.}\rvert$	0.002 h^{-1}	0.01 h^{-1}	0.01 h^{-1}
$\lvert\Delta D_{max,sim.}\rvert$	0.02 h^{-1}	0.1 h^{-1}	0.1 h^{-1}

K_c was decreased to 0.05 at 436 h to reduce the standard deviation of the dilution rate.

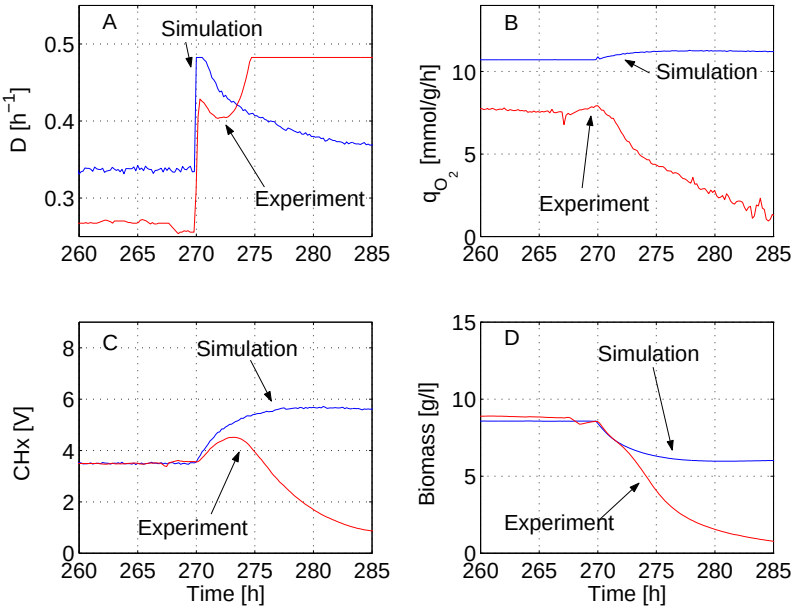

Figure 4.14. Experimental data compared with model simulation of an increase in the ethanol setpoint from 4.9 to 7.8 g/l (CHx=3.5 to 5.5 V). The dilution rate (A), the specific oxygen uptake rate (B), the CHx signal (C), and the biomass concentration (D) are shown. The controller settings are stated in table 4.10.

Table 4.10. Settings for the dilution rate controller applied experimentally and in simulations in figure 4.14.

Setpoint	CHx=3.5 V	CHx=5.5 V
Time	260-270 h	270-285 h
K_c	0.3	0.3
T_i	4 h	4 h
β	0.85	0.85
p	3	3
$T_{s,exp.}$	1 min	1 min
$T_{s,sim.}$	10 min	10 min
$\lvert\Delta D_{max,exp.}\rvert$	0.02 h^{-1}	0.02 h^{-1}
$\lvert\Delta D_{max,sim.}\rvert$	0.2 h^{-1}	0.2 h^{-1}

CHx setpoint from CHx=3.5 V to 6 V over a period of 90 h, the dilution rate controller was able to track the desired setpoints (figure 4.15). From figure 4.15C, it can be seen that the CHx setpoint was followed nicely by the controller both in the experiment and simulation. As observed during the increase in the ethanol setpoint from 3.5 to 5.5 V (figure 4.14B), the experimental q_{O_2} was much lower than in the model simulation (figure 4.15B). The deviation between the simulated and experimentally determined biomass concentration was a consequence of the CHx sensor not being linear above 4.5 V (figure 4.15D). Thus, the experimental CHx signal corresponded to a higher ethanol concentration than used in the simulation. As a result, the experimental biomass concentration was lower than the simulated biomass concentration.

Table 4.11. Settings for the dilution rate controller applied experimentally and in simulations in figure 4.15.

Setpoint	CHx=3.5 V	CHx=3.5-6.0 V (ramp)
Time	670-680 h	680-770 h
K_c	0.2	0.2
T_i	2 h	2 h
β	1	1
p	3	3
$T_{s,exp.}$	1 min	1 min
$T_{s,sim.}$	10 min	10 min
$\lvert\Delta D_{max,exp.}\rvert$	0.02 h^{-1}	0.02 h^{-1}
$\lvert\Delta D_{max,sim.}\rvert$	0.2 h^{-1}	0.2 h^{-1}

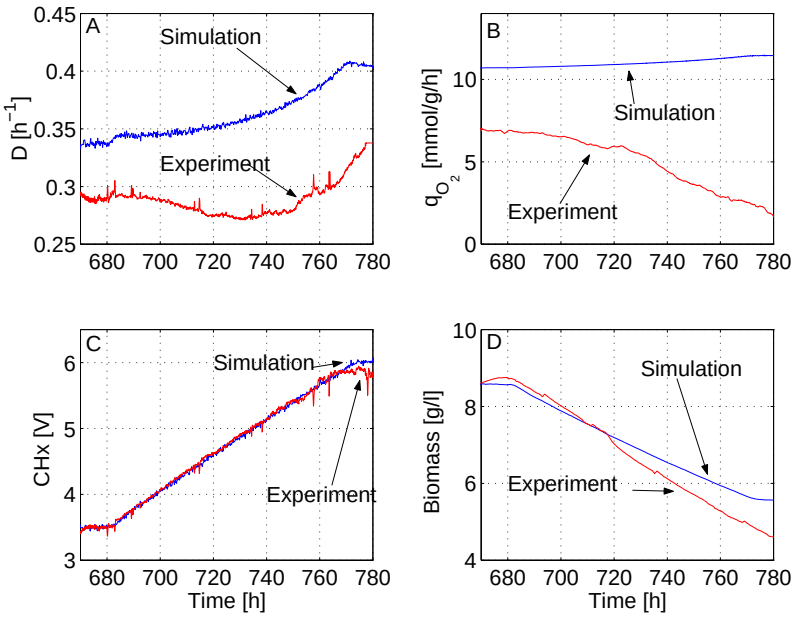

Figure 4.15. Experimental data compared with model simulation of an accelero-productostat were the ethanol setpoint was increased as a ramp from 3.5 V to 6.0 V over 90 h (from 4.9 to 9 g/l ethanol). The dilution rate (A), the specific oxygen uptake rate (B), the CHx signal (C), and the biomass concentration (D) are shown. The controller settings are stated in table 4.11.

4.3.5 Robustness of on-line measurements

4.3.5.1 CHx signal

During the experiments, it was observed that the CHx signal was sensitive towards sampling when the CHx reading was larger than 2.0 V. When a sample was taken, either directly from the fermenter or from the fermenter outlet (by redirecting the outlet flow into a test tube), a drop in the CHx signal was observed. Since the CHx signal is a measure of the CHx content in the off-gas, it is related to the ethanol content in the headspace of the fermenter. Apparently, sampling caused the pressure in the fermenter to increase and thereby the mole fraction of ethanol (related to CHx) to decrease. Unfortunately, there was no control of the pressure installed on the fermenter to compensate for this undesired effect. Consequently, frequent sampling during transient conditions when the CHx signal was used for control of the dilution rate resulted in very noisy CHx and D signals.

4.3.5.2 Figaro sensor

The Figaro sensor was found to work satisfactory and was not influenced by sampling. However, due to the large sensitivity of the sensor and the small region of ethanol concentrations which could be measured with the

sensor, the off-line determined ethanol concentrations, corresponding to a Figaro signal of 1.0 V, varied between 30-90 mg/l due to uncertainties with respect to sampling.

4.3.5.3 RQ measurement

The RQ measurement was calculated from the carbon evolution rate and oxygen uptake rate and was therefore sensitive towards calibration of the gas analyser. However, by operating with a large biomass concentration (10-15 g/l) and an airflow of 1.5 vvm, high gas turnover rates were obtained and the noise on the RQ measurements thereby minimised. However, when the specific oxygen uptake rate decreased significantly as observed in figure 4.14, the RQ measurement became more noisy.

4.4 Discussion

The purpose of designing a dilution rate controller in this work was to be able to obtain oxido-reductive steady-states at a desired ethanol concentration, or RQ value to investigate the possible existence of multiple steady-states. If multiple steady-states, as predicted by the yeast model proposed by Lei *et al.* (2001), exist, unstable steady-states will be present close to D_{crit}. Since these unstable steady-states cannot be achieved in a chemostat, it is necessary to operate the continuous cultivation by manipulating the dilution rate based on a measurement, a productostat.

In the proceeding discussion, the selection of ethanol as measurement for the dilution rate controller and the performance of the tested dilution rate controllers will be evaluated. Finally, the performance of the Lei *et al.* (2001) model during dynamic oxido-reductive conditions is treated.

4.4.1 Selection of measurement for dilution rate controller

From the presented results, it was clear that the ethanol concentration is to be preferred as input for the dilution rate controller compared with the RQ measurement when tracking low ethanol concentrations. The Figaro sensor was very sensitive at low ethanol concentrations enabling tracking of an oxido-reductive steady-state with an ethanol concentration of only 0.05 g/l, whereas the RQ at this steady-state was practically identical to RQ at oxidative growth resulting in failure of the RQ dilution rate controller ((figures 4.5-4.6)).

At higher ethanol concentrations (up to 6.3 g/l), model simulations showed that both the RQ and ethanol (CHx) measurement could be applied as input for the dilution rate controller, whereas RQ should be chosen for tracking even higher ethanol concentrations since performance limitations were imposed when ethanol was used as measurement due to a RHP

zero approaching zero.

The choice between ethanol and RQ as measurement is also a choice between using a concentration or a reaction rate related measurement. Control of a continuous cultivation based on reaction rates has been proposed by Meyer and Beyeler (1984) for operating a continuous cultivation at maximal biomass productivity. They found that using the RQ measurement was not sufficient for this purpose and included the carbon evolution rate (CER) as input to the dilution rate controller as well. Still, their results were not convincing; the corresponding dilution rate during closed loop operation was significantly lower than D_{crit} found from steady-state experiments. Another disadvantage of their control design was that the CER setpoint which was a function of the feed concentration. Thus, the controller setpoint varied with the substrate feed concentration. Still, RQ provides a rough measure of the current flux distribution inside the cells and the dynamics of RQ is therefore faster than the dynamics of the ethanol concentration; thus sudden disturbances due to changes in the feed rate or concentration will be more pronounced in the RQ signal, especially at higher ethanol concentrations when the CHx signal is used. However, in this work the main purpose was not to perform disturbance rejection but rather track steady-states. Therefore, the ethanol signal was chosen as input for the dilution rate controller.

4.4.2 Performance of dilution rate controllers

The selection of dilution rate controller was a trade-off between high gain, fast response time and no overshoot on one side and a high standard deviation of the actuator signal (D) on the other side. It was therefore important to include noise in the simulations to monitor the standard deviation of the actuator signal. Since it was desired to track oxido-reductive steady-states and determine the corresponding dilution rate, a low standard deviation on the dilution rate was of great importance. Thus, the dilution rate controller gains were chosen to be rather low resulting in longer response times.

The output of a controller is usually given in deviation variables around an operating point. However, the desired operating point during setpoint tracking was unknown since the corresponding dilution rate was not known. The dilution rate controller should therefore be incremental where the operating point was continuously updated. The nonlinear controller was made incremental by updating D_{ref} continuously to eliminate off-set (equation (4.15)). The LQ controller was made incremental by using Δu instead of u in the objective function as suggested by Andersen *et al.* (1997).

The nonlinear controller was selected for use since it showed slightly better performance than the incremental PI controller due to the inclusion of the β parameter. It is possible that inclusion of a β parameter in

the incremental PI controller would have lead to a similar result, however since the nonlinear controller was found to work nicely, this was not pursued. Although the LQ controller showed better performance than both PI controllers, the nonlinear PI controller was preferred due to its simplicity which made it easier to implement in the fermenter control system (Labview).

The tuning of the dilution rate controllers can be quite tedious if a process model is not available. To overcome this obstacle Møller (1993) and Andersen *et al.* (1997) have applied an adaptive LQ controller where the tuning of the LQ controller was based on a 3rd order ARX model. The controller worked nicely at low ethanol concentrations, but failed at higher ethanol concentrations. As shown in table 4.6, the process dynamics becomes much slower at higher ethanol concentrations and the failure of the adaptive LQ controller might have been caused by an erroneous modelled dynamics at higher ethanol concentrations. In the current work, tuning of the PI controllers was based on model simulations. It was found that the controller parameters needed to be changed significantly in order to obtain acceptable tracking performance; e.g. the integration time needed to be increased at higher ethanol concentrations as a consequence of the slower process dynamics.

An interesting aspect of the applied dilution rate controllers was that the gain of the controllers needed to be positive although the steady-state process gain was negative (in the region with unstable steady-states). This apparent contradiction is, however, due to the fact that the high frequency gain of the process still is positive in the region of unstable steady-states, and the controller gain should be determined from the high frequency gain rather than the low frequency (steady-state) gain.

It can be concluded from the model simulations that a relatively simple (and easy to implement) controller can be used for setpoint tracking of oxido-reductive steady-states when proper controller parameters are used.

4.4.3 Performance of yeast model

Both the application areas and the limitations of the yeast model (Lei *et al.*, 2001) were illustrated by comparing model simulations and experimental data during dynamic conditions with closed loop control of the dilution rate. The model was found to be very applicable for describing growth on glucose at low ethanol concentrations where repression of the respiratory system, monitored by q_{O_2}, was not too strong. The model could therefore be used for tuning the nonlinear PI controller which proved capable of tracking ethanol concentrations up to 6 g/l.

The description of diauxic growth and ethanol consumption by the yeast model, however, did not correspond to the experimental results. The diauxic shift happened too fast in the model whereas the maximal ethanol consumption rate during growth on a mixture on glucose and ethanol was

lower than experimentally observed. The modelling of the compartment responsible for the dynamics during growth on ethanol (X_{Acdh}) should therefore be improved. Inclusion of an experimental determined time constant for generation of enzymes involved in ethanol consumption has been proposed by Sweere *et al.* (1988) to enable the bottleneck model (Sonnleitner and Käppeli, 1986) to describe the diauxic shift.

Although the yeast model (Lei *et al.*, 2001) contains glucose inhibition of oxidative dissimilation of pyruvate (r_2), the inhibition constant (K_{2i}) was estimated to a very large value such that practically no inhibition of r_2 takes place during growth on glucose in a continuous cultivation (Lei and Jørgensen, 2001). Therefore, neither glucose inhibition nor repression of the respiratory system was modelled and q_{O_2} is approximately constant during oxido-reductive growth. Since the cultivated strain showed a decrease in q_{O_2} at higher ethanol concentrations, the model failed to describe growth at ethanol concentrations above 6 g/l. The decrease in q_{O_2} at higher ethanol concentrations was most probably due to glucose repression of the respiratory system and not due to ethanol inhibition (Lei, 2001, chap.7). Due to the model deficiency in describing glucose repression, dilution rate controllers, tuned through model simulations to work at high ethanol concentrations, failed to track the desired steady-states and instead wash-out like scenarios were seen.

4.4.4 Accelero-productostat

Since it was not possible to track steady-state ethanol concentrations above 6 g/l by increasing the ethanol concentration stepwise, pseudo steady-states at high ethanol concentrations were obtained by increasing the ethanol setpoint continuously as a ramp. This operation mode, which we have chosen to denote accelero-productostat, enabled tracking of oxido-reductive pseudo steady-states at high ethanol concentrations. In the design of accelero-productostat experiments, in addition to the controller parameters, the slope of the setpoint ramp needs to be specified. Since only pseudo steady-states are obtained in an accelero-productostat, the slope of the setpoint ramp imposes a limit for the dynamics which can be identified, i.e. the time constants of the observed physiological events cannot exceed an upper limit. On the other hand, the accelero-productostat enables a quick determination of the (pseudo) steady-state profile for varying dilution rates in the oxido-reductive region compared to chemostat or productostat operation.

4.5 Conclusions

It was shown that it is possible to obtain oxido-reductive steady-states by operating a continuous cultivation as a productostat, where the dilution rate is manipulated based on an ethanol related measurement. Further-

more, the productostat was shown to be superior to the chemostat with respect to the response time when tracking oxido-reductive steady-states.

Based on model simulations, the ethanol concentration was found to be more promising for tracking oxido-reductive steady-states at low ethanol concentrations than the RQ measurement, whereas both measurements can be applied at higher ethanol concentrations. However, investigations of a linearised yeast model indicated that problems might occur when using ethanol as measurement at high ethanol concentration. If the controller is tuned too fast due to a RHP-zero approaching the imaginary axis and hence limiting the bandwidth of the controller.

A simple nonlinear PI controller was found to capable of tracking the desired setpoints with satisfactory performance and was therefore preferred over a LQ controller due to its simplicity.

Experimental work confirmed that the ethanol related measurements were well suited as input for a dilution rate controller and the model based tuning of the dilution rate controller worked well for ethanol concentrations from 0.1 to 6 g/l ethanol. At higher ethanol concentrations, setpoint tracking failed when the ethanol setpoint was increased stepwise as a consequence of erroneous control design since repression of the respiratory system was not included in the model upon which the controller was designed. Still, pseudo steady-states were obtained from 4.9 to 9 g/l ethanol by operating the continuous cultivation as an accelero-productostat where the ethanol setpoint was increased as a ramp over 90 h. The accelero-productostat provides a strong alternative to the accelerostat (Paalme and Vilu, 1992) for investigating the oxido-reductive growth regime in continuous yeast cultivations.

List of symbols

CER	carbon dioxide evolution rate [mmole CO_2/h]
CHx	measurement of CHx content in outlet gas from gas analyser [V]
D	dilution rate [h^{-1}]
D_{crit}	critical dilution rate in chemostat (onset of alcoholic fermentation) [h^{-1}]
D_{max}	upper limit for dilution rate controller [h^{-1}]
D_{min}	lower limit for dilution rate controller [h^{-1}]
$e(t)$	error term in dilution rate controller
Et	ethanol concentration [g/l]
G_p	process transfer function []
J	objective function for LQ controller []
K_c	controller gain []
OUR	oxygen uptake rate [mmole O_2/h]
Q	heat evolution rate [W/l]
Q_u	weight matrix on actuator movements in LQ controller []
Q_y	weight matrix on states in LQ controller []
q_{O_2}	specific oxygen uptake rate [mmole O_2/g bio/h]
RQ	respiratory quotient (q_{CO_2}/q_{O_2}) []
p_c	exponent in dilution rate controller []
t	time [h]
T_i	integration time in the dilution rate controller [h]
T_s	sample time time [h]
x	dry weight biomass concentration [g/l]
$y(t)$	measurement to dilution rate controller [V]
y_{ref}	setpoint in dilution rate controller [V]
$Y(t)$	Laplace transform of $y(t)$ []
$Y_{ref}(t)$	Laplace transform of $y_{ref}(t)$ []
z	zero in transfer function [h^{-1}]
β	parameter in dilution rate controller []
Δu	deviation in actuator variable [h^{-1}]
ΔD_{max}	maximal change of D during one sample period [h^{-1}]
τ_j	process time constant [h]

References

Andersen, M. (1990). *Multivariable identification for control of a continuous yeast cultivation*. Ph.D. thesis, KT, Technical University of Denmark.

Andersen, M.; Pedersen, N.; Brabrand, H.; Hallager, L. and Jørgensen, S. (1997). Regulation of a continuous yeast bioreactor near the critical dilution rate using a productostat. *J. Biotechnol.*, **54**, 1–14.

Axelsson, J. (1988). Experimental techniques and data treatment for

studying the dynamics of ethanol production/consumption in baker's yeast. *Anal. Chim. Acta*, **213**, 151–163.

Axelsson, J.; Münch, T. and Sonnleitner, B. (1992). Multiple steady-states in continuous cultivation of yeast. *IFAC Modelling and Control of Biotechnical Processes, Colorado, USA*, **10**, 383–386.

Creutzburg, K. (2001). *Optimization of metabolic networks for metabolite overproduction*. Ph.D. thesis, KT, Technical University of Denmark.

Duboc, P.; Cascão-Pereira, L. and von Stockar, U. (1998). Identification and control of oxidative metabolism in *Saccharomyces cerevisiae* during transient growth using calorimetric measurements. *Biotechnol. Bioeng.*, **57**, 610–619.

Lei, F. (2001). *Dynamics and nonlinear phenomena in continuous cultivations of* Saccharomyces cerevisiae. Ph.D. thesis, KT, Technical University of Denmark.

Lei, F. and Jørgensen, S. (2001). Estimation of kinetic parameters in a structured yeast model using regularisation. *Accepted for publication in J. Biotechnol.*.

Lei, F.; Rotbøll, M. and Jørgensen, S. (2001). A biochemically structured model for *Saccharomyces cerevisiae*. *Accepted for publication in J. Biotechnol.*.

Meyer, C. and Beyeler, W. (1984). Control strategies for continuous bioprocesses based on biological activites. *Biotechnol. Bioeng.*, **16**, 916–925.

Møller, H. (1993). *Modelling, identification and control of a continuous fermentation with* Saccharomyces cerevisiae. Ph.D. thesis, KT, Technical University of Denmark.

Møller, H. and Jørgensen, S. (1997). Continuous cultivation start-up control - an experimental investigation. *J. Biotechnol.*, **53**, 55–66.

Nayfeh, A. and Balachandran, B. (1995). *Applied nonlinear dynamics*. John Wiley & Sons, New York.

Paalme, T. and Vilu, R. (1992). *A new method of continuous cultivation with computer-controlled change of dilution rate*, pages 229–301. Pergamon Press, Oxford, UK. In Karim, M.N. and Stephanopoulos, G.(ed.): Modelling and control of biotechnical processes.

Skogestad, S. and Postlehwaite, I. (1996). *Multivariable feedback control*. Wiley.

Sonnleitner, B. and Käppeli, O. (1986). Growth of *Saccharomyces cerevisiae* is controlled by its limited respiratory capacity: Formulation and verification of a hypothesis. *Biotechnol. Bioeng.*, **28**, 927–937.

Sweere, A.; Giesselbach, J.; Barendse, R.; de Krieger, R.; Honderd, G. and Luyben, K. C. A. M. (1988). Modelling the dynamic behaviour of *Saccharomyces cerevisiae and its application in control experiments. Appl. Microbiol. Biotechnol.*, **28**, 116–127.

van Urk, H.; Mak, P.; Scheffers, W. and van Dijken, J. (1988). Metabolic responses of *Saccharomyces cerevisiae* CBS8066 and *Candida utilis* CBS 621 upon transition from glucose limitation to glucose excess. *Yeast*, **4**, 283–291.

5

Multiple steady-states in aerobic continuous cultivations of *S. cerevisiae* around the critical dilution rate

The steady-state behaviour of a continuous cultivation of Saccharomyces cerevisiae *CEN.PK113-7D around the critical dilution rate revealed that multiple steady-states exist in a region of dilution rates just below the critical dilution rate. Oxido-reductive steady-states were obtained at dilution rates up to 0.09 h^{-1} lower than the critical dilution rate by operating the bioreactor as a productostat, where the dilution rate was controlled based on an ethanol measurement. The existence of multiple steady-states were attributed to two distinct physiological effects occurring when growth changed from oxidative to oxido-reductive: i) A decrease in the efficiency of ATP production and utilisation (at ethanol concentrations below 3 g/l) and ii) Repression of the respiratory system (at higher ethanol concentrations). Both these effects could be interpreted as product inhibition of growth which, from a modelling point of view, was a key factor for obtaining multiple steady-states in a mathematical model of* S. cerevisiae.

5.1 Introduction

An increasing number of pharmaceutical products are being produced by the use of genetically engineered microorganisms and during cultivation of these microorganisms an important goal is to maximise the productivity of the desired protein. To fulfil this goal it is essential to understand the physiology of the microorganisms near the optimal operating conditions. One of the most commonly used eukaroytic microorganisms for genetic engineering is *Saccharomyces cerevisiae* (Zimmermann and Entian, 1997) and its growth in the close vicinity of the operating point for maximal biomass productivity during continuous cultivation is the topic of this paper.

In a glucose limited continuous cultivation *S. cerevisiae* exhibits two distinct growth regimes under aerobic conditions. At low dilution rates, the growth is purely oxidative and biomass and carbon dioxide are produced as main products. When the dilution rate is increased above a certain value, the critical dilution rate (D_{crit}), the growth changes to oxido-reductive growth and significant amounts of ethanol are formed. This phenomenon is usually referred to as the Crabtree effect (Crabtree, 1929; de Deken, 1966; Fiecther *et al.*, 1994) and has been defined as *the occurrence of alcoholic fermentation in spite of aerobic conditions* (van Dijken and Scheffers, 1986). It was originally thought to be caused by glucose repression of components of the respiratory chain (Beck and von Meyenburg, 1968) and of several enzymes in the tricarboxylic acid cycle (Polakis *et al.*, 1965). However, it is now generally accepted that, although repression does occur, ethanol production occurs as a consequence of a limited capacity in the respiratory system (Sonnleitner and Käppeli, 1986; Alexander and Jeffries, 1990).

In order to maximise the biomass productivity in a chemostat, the cultivation must be operated close to D_{crit}. This is of great industrial interest in heterologous protein production where recombinant *S. cerevisiae* is used as host organism. The productivity of the desired protein is most often closely related to the biomass productivity and robust operation as close to D_{crit} as possible is therefore important.

It has been reported (Rieger *et al.*, 1983) that the onset of oxido-reductive growth in *S. cerevisiae* depends on how fast the dilution rate is increased from an oxidative state. If too large steps were made, the growth became oxido-reductive at a lower dilution rate than when small steps were taken. This phenomenon has been found to be more pronounced at higher substrate concentrations (Rieger *et al.*, 1983), initially leading to the erroneous conclusion that D_{crit} decreases with increasing substrate concentration (Karrer, 1978).

The operational difficulties around D_{crit} has lead to speculations on whether multiple steady-states exist in a region just below D_{crit} such that for these dilution rates it is possible to obtain an oxidative as well as an oxido-reductive steady-state, depending on the history of the culture. Wenger and Dunlop (1994) have investigated the steady-state behaviour around D_{crit}. First the dilution rate have been increased, starting from an oxidative steady-state, and then decreased, starting from an oxido-reductive steady-state. It has been observed that the shift between oxidative and oxido-reductive growth (D_{crit}) occurred at a higher dilution rate when increasing the dilution rate than when decreasing the dilution rate, resulting in a range of dilution rates with multiple steady-states. Axelsson *et al.* (1992) has shown experimentally that it was possible to obtain two different steady-states for a dilution rate just below D_{crit}. By increasing the dilution rate from 0.22 to 0.40 h^{-1} for one hour and then returning to 0.22 h^{-1}, the cultivation changed from oxidative to oxido-reductive growth.

More evidence of multiple steady-states has been presented by Jørgensen *et al.* (1992). In their investigations of a productostat using an adaptive controller around D_{crit}, it has been found that the dilution rate initially decreased as the ethanol setpoint was increased. However, due to a high control gain which lead to a large standard deviation of the dilution rate at the obtained steady-states, the results were not conclusive whether or not multiple steady-states did exist.

Theoretical understanding of multiple steady-states has emerged through mathematical modelling that support the experimental indications. Axelsson *et al.* (1992) have shown that by including a term for inhibition of the oxidative capacity by ethanol in the model proposed by Sonnleitner and Käppeli (1986), multiple steady-states emerged at dilution rates just below D_{crit}. Wenger and Dunlop (1994) have described the growth around D_{crit} as a sum of two growth regimes (resembling oxidative and oxido-reductive growth, respectively). Each regime has been modelled with different μ_{max} and affinity constants. In a certain substrate interval (corresponding to the region around D_{crit}) both regimes are active resulting in multiple steady-states.

A structured model describing the aerobic growth of *S. cerevisiae* (Lei *et al.*, 2001) also exhibited multiple steady-states around D_{crit}. In this model, multiple steady-states occurred as a consequence of a change in the flux distribution between catabolism and anabolism when the growth changed from oxidative to oxido-reductive. In the presence of a compound related to acetaldehyde a new catabolic glucose uptake system is activated and relatively more of the glucose consumed is converted catabolically. This positive feedback regulation by acetaldehyde caused the model to exhibit multiple steady-states (Lei *et al.*, 2001).

In view of the relatively few reported studies on multiple steady-states in continuous yeast cultivations and the existence of different hypotheses regarding the physiological mechanisms leading to multiplicity, the purpose of this work is to answer the following two questions:

- Can multiple steady-states be experimentally demonstrated in continuous cultivations of *S. cerevisiae* around D_{crit}?
- What are the possible physiological mechanisms that causes multiple steady-states to occur?

5.2 Theory

To be able to connect the physiological mechanisms observed in *S. cerevisiae* to the possible existence of multiple steady-states in a continuous cultivation, it is necessary to understand how physiological phenomena such as product (or substrate) inhibition, excess substrate uptake and excess product formation influence the existence of multiple steady-states. Xiu *et al.* (1998) have investigated general unstructured growth models

with respect to the existence of multiple steady-states. Their main results related to *S. cerevisiae* will be applied in the following to discuss possible physiological mechanisms leading to multiple steady-state in *S. cerevisiae*.

5.2.1 Modelling multiple steady-states

In this paper the following, rather narrow, definition of multiple steady-states was used: A continuous cultivation was considered to exhibit multiple steady-states if at least two distinct, non-washout steady-states can be obtained for a region of dilution rates. More specific, we only consider how the cultivation respond as the dilution rate is changed and all other external parameters such as temperature, stirrer speed, substrate feed concentration, dissolved oxygen tension etc. are kept constant.

In a mathematical sense, multiple steady-states occur as a consequence of a fold bifurcation (Nayfeh and Balachandran, 1995). The term *bifurcation* is used to indicate a qualitative change in the features of a system such as the number and type of solutions, e.g. when a system changes from having one to several non-trivial steady-state solutions as one parameter is varied, a static bifurcation has occurred. Thus, by using a bifurcation analysis on mathematical models describing the growth of *S. cerevisiae*, mechanisms (kinetic expressions) leading to multiple steady-states can be identified.

Xiu *et al.* (1998) have performed a bifurcation analysis of growth kinetics for microorganisms leading to multiplicity in continuous cultures based on the following unstructured kinetic model:

$$\begin{aligned} &\text{Substrate:} && \frac{ds}{dt} = q_s\, x + D\,(S_f - s) \\ &\text{Biomass:} && \frac{dx}{dt} = (\mu - D)\, x \\ &\text{Product:} && \frac{dp}{dt} = q_p\, x - D\, p \end{aligned} \tag{5.1}$$

The specific growth rate was modelled using Monod kinetics extended with substrate and product inhibition:

$$\mu = \mu_{max} \frac{s}{s + K_s} \left(1 - \frac{s}{K_{si}}\right) \left(1 - \frac{p}{K_{pi}}\right) \tag{5.2}$$

where μ_{max} is the maximum specific growth rate, K_s is the affinity constant; K_{si} and K_{pi} are the critical concentrations of substrate and product above which growth stops. To account for the effect of metabolic overflow, the substrate consumption and product formation has been modelled as:

$$\begin{aligned} q_s &= m_s + \frac{\mu}{Y_s^m} + \Delta q_s^m \frac{s}{s + K_s^*} \\ q_p &= m_p + Y_p^m \mu + \Delta q_p^m \frac{s}{s + K_p^*} \end{aligned} \tag{5.3}$$

where m_s and m_p are maintenance terms while Y_s^m and Y_p^m are yield coefficients. The last term in both equations represent the increase in substrate consumption/product formation due to metabolic overflow.

Since μ_{max} can be obtained in a batch cultivation on glucose for *S. cerevisiae*, substrate inhibition of growth is not present during a growth of *S. cerevisiae* on glucose. With no substrate inhibition, Xiu *et al.* (1998) found that *product inhibition of growth* and *excess product formation* were necessary requirements for multiplicity. However, to be able to explain the biomass vs dilution rate profile as observed experimentally for *S. cerevisiae* (figure 5.5) *excess substrate uptake* should be included in the model. In *S. cerevisiae* both excess substrate uptake and product (ethanol) formation occurs when the growth shifts from oxidative to oxido-reductive (Meyenburg, 1969), thus the key issue regarding the existence of multiple steady-states in mathematical models of *S. cerevisiae* is whether or not product inhibition of growth is included in the model. The above observations are summarised in theorem 5.1.

Theorem 5.1 *For a mathematical model, describing growth of* S. cerevisiae *in a continuous cultivation, to exhibit multiple steady-states as observed experimentally in this paper, three mechanisms need to be included: Product inhibition of growth, excess substrate uptake and excess product formation.*

Although the models presented in literature exhibiting multiplicity do not fit directly into the general unstructured model presented in equation (5.1), it is possible to translate the mechanisms leading to multiplicity for these models into the general form. Axelsson *et al.* (1992) has included ethanol inhibition of the maximal oxidative capacity in the bottleneck model proposed by Sonnleitner and Käppeli (1986). This extended model exhibits excess substrate uptake and excess product formation when ethanol is formed. Moreover, ethanol inhibition of the maximal oxidative capacity can be translated into product inhibition of growth since addition of ethanol will lead to a decrease in the rate of oxidative catabolism and hence a decrease in biomass productivity.

In the model proposed by Lei *et al.* (2001) accumulation of acetaldehyde activates an extra catabolic substrate uptake system. In this model acetaldehyde is the product that inhibits growth since the enhanced substrate uptake leads to a relatively higher flux through the catabolism, thus the anabolic flux, and thereby growth, decreases.

It is important to stress that product inhibition of growth should be modelled as a feedback mechanism in order to obtain multiple steady-states. In the model from Sonnleitner and Käppeli (1986) excess substrate uptake and product formation occur along with a shift to a less energy efficient pathway at the critical dilution rate. However, the model does not exhibit multiple steady-states since there is no feedback mechanism (such

as product inhibition or activation of a new uptake system) modelled.

5.3 Materials and methods

5.3.1 Strain and medium

The yeast *Saccharomyces cerevisiae* CEN.PK113-7D was cultivated. The mineral medium contained per litre: 15 g $(NH_4)_2SO_4$, 3 g KH_2PO_4, 1.5 g $MgSO_4 \cdot 7H_2O$, 45 mg EDTA, 13.5 mg $ZnSO_4 \cdot 7H_2O$, 2.52 mg $MnCl_2 \cdot 2H_2O$, 0.9 mg $CoCl_2 \cdot 6H_2O$, 0.9 mg $CuSO_4 \cdot 5H_2O$, 1.2 mg $Na_2MoO_4 \cdot 2H_2O$, 13.5 mg $CaCl_2 \cdot 2H_2O$, 9 mg $FeSO_4 \cdot 7H_2O$, 3 mg H_3BO_3, 0.3 mg KI, 0.1 μl antifoam (Sigma A5551). After heat sterilisation of the medium, glucose (sterilised separately) was added (final concentration: 30 g/l) along with filter-sterilised vitamins. The final concentration of vitamins per litre was: 0.15 mg biotin, 3 mg calcium pantothenate, 3 mg nicotinic acid, 75 mg myo-inositol, 3 mg thiamine HCl, 3 mg pyridoxine HCl and 0.6 mg p-aminobenzoic acid.

5.3.2 Preparation of inoculum

S. cerevisiae strain CEN.PK113-7D was taken from -80°C and plated onto YPD agar plates and stored at 30°C. After three days a single culture was transferred to a shake-flask containing mineral medium with the following composition per litre: 7.5 g $(NH_4)_2SO_4$, 14.4 g KH_2PO_4, 0.5 g $MgSO_4 \cdot 7H_2O$, 30 mg EDTA, 9 mg $ZnSO_4 \cdot 7H_2O$, 1.68 mg $MnCl_2 \cdot 2H_2O$, 0.6 mg $CoCl_2 \cdot 6H_2O$, 0.6 mg $CuSO_4 \cdot 5H_2O$, 0.8 mg $Na_2MoO_4 \cdot 2H_2O$, 9 mg $CaCl_2 \cdot 2H_2O$, 6 mg $FeSO_4 \cdot 7H_2O$, 2 mg H_3BO_3, 0.2 mg KI, 50 μl antifoam (Sigma A5551). The initial pH of the mineral medium was adjusted to 6.5 by 2 M NaOH. Glucose was autoclaved separately and added (10 g/l) along with filter-sterilised vitamins. The final concentrations of vitamins per litre: 0.05 mg biotin, 1 mg calcium pantothenate, 1 mg nicotinic acid, 25 mg myo-inositol, 1 mg thiamine HCl, 1 mg pyridoxine HCl and 0.2 mg p-aminobenzoic acid. Cells, growing exponentially on glucose, were used as inoculum for the fermenter.

5.3.3 Equipment

The cultivations were carried out in a Braun M fermenter with a working volume of 1.0 l. The temperature setpoint was maintained at 30.0°C while pH was controlled at 5.0 by addition of 2 M NaOH. The base addition was monitored gravimetrically and used for on-line estimation of the biomass concentration (Lei, 2001, chap.6). The airflow was controlled by a mass flow controller (Bronkhorst HiTec F201C, setpoint 1.50 vvm) and the stirring speed was 1200 rpm. The dissolved oxygen tension was

measured by a oxygen electrode (Ingold electrode, type 322 756702) and remained above 40% during all experiments.

5.3.4 Analytical methods

5.3.4.1 Analysis of substrate and products

Culture dry weight samples (4-5 ml depending on biomass concentration) were taken from the fermenter outflow (no deviation compared to sampling directly from the fermenter was observed) and filtered over dried (10 min at 150 W), preweighed nitrocellulose filters (0.45 μm pore size; Gelman Pall Gelman Sciences, Ann Arbor, USA). Filters were washed with demineralised water, dried in a microwave oven (15 min at 150 W), stored in a desiccator for 15 min and weighed. Triplicate determinations were made and the maximal deviation between samples was 3%.

Cell suspension samples were withdrawn directly from the fermenter and filtered rapidly (0.45 μm, Sartorius AG, Göttingen, Germany) into cooled Eppendorf tubes (1.5 ml, 0°C). Ethanol (for concentrations up to 2 g/l, Boehringer Mannheim (BM) kit no. 176290), residual glucose (Unimate 5 GLUC, HK Roché) and acetate (BM kit no. 716251) were determined enzymatically using an automated analysis robot (Cobas Mira, Roché Diagnostic systems). Acetaldehyde was also determined enzymatically (BM kit no. 668613). Concentrations of glucose, succinate, glycerol, ethanol, acetate and pyruvate were measured by HPLC using an Aminex HPX-87H column (Bio-Rad) for separation. The column was kept at 65^{circ}C and eluted at 0.6 ml/min with 5 mM H_2SO_4. Pyruvate and acetate were detected by UV-spectrometry (Waters 486 Turnable Absorbance Detector at 210 nm). Glucose, succinate, glycerol and ethanol were detected refractometrically (Waters 410 Differential Refractometer).

5.3.4.2 Analysis of off-gas

The CO_2, O_2 and CHx content in the outlet gas was analysed with a Bruel & Kjær Innova Industrial Emissions Monitor 1311. The carbon dioxide production rate and oxygen uptake rate were calculated according to van Urk *et al.* (1988). The content of reducing gases in the outlet gas was determined using a Figaro TGS 822 sensor (Hammer electronic, Elsinore, Denmark). The Figaro and CHx signals were correlated to the extracellular ethanol concentration by the following relations: Figaro: $EtOH[g/l] = (Fig[V] - 0.21)/13.97$ and CHx: $EtOH[g/l] = 1.40 \cdot (CHx[V] + 0.01)$. These correlations were found valid in the range 0.5-10 V for the Figaro sensor and in the range 0.5-4.5 V for the CHx sensor, respectively (see figure 5.1). The sensitivity of the CHx signal was three times higher in experiments C4 and C6 (0–0.5% on the gas analyser) compared with C7 (0–1.5% on the gas analyser), however the above stated relationship relates to the CHx sensitivity from C7.

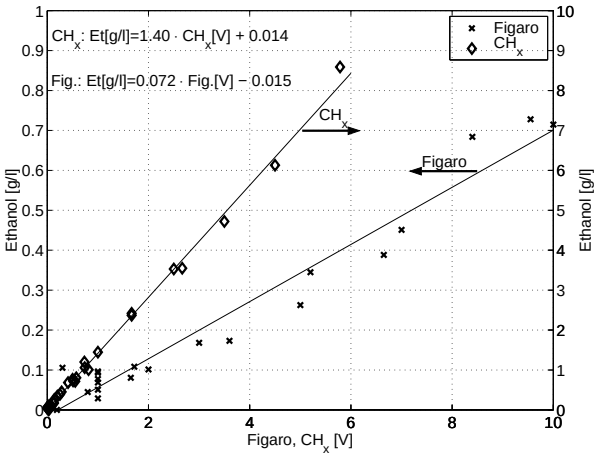

Figure 5.1. Relationship between the on-line ethanol related signals, Figaro and CH_x, and the ethanol concentration in the fermenter.

5.3.5 Cultivation conditions

The data presented in this paper were obtained from three independent continuous cultivations referred to as C4, C6 and C7.

5.3.5.1 Start-up procedure

The batch phase was started by injecting 5 ml inoculum cells into the reactor, the initial dry weight biomass concentration in the reactor was approximately 10 mg/l. Continuous cultivation was initiated when glucose was depleted (monitored by the CO_2 signal). C4 was run as a chemostat and the dilution rate was set to 0.20 h^{-1} when glucose was exhausted until a steady-state was obtained. For C6 and C7 the fermenter was operated as a productostat (Andersen *et al.*, 1997), where a dilution rate controller was manipulated to obtain steady-states at fixed ethanol concentrations.

5.3.5.2 Dilution rate calculations

The dilution rate was calculated from the substrate and base balances as the total liquid flow into the fermenter (substrate + base). Control of the flow rate was performed by manipulating the substrate feed pump based on the readings from the substrate and base balances. The base flow constituted between 2-5 % of the total inflow depending on the biomass concentration. The fermenter was placed on a balance and the working volume was kept constant by controlling the outflow via the outflow pump.

5.3.5.3 Productostat operation

To pursue the aim of investigating the behaviour of continuous cultivations of *S. cerevisiae* around D_{crit} the fermenter was operated as a productostat (Andersen *et al.*, 1997). In contrast to traditional chemostat operation

where the dilution rate is fixed in each operating point, the dilution rate is not specified in a productostat. Instead, a given product concentration is fixed and the dilution rate is manipulated, through a dilution rate controller, in order to obtain a steady-state corresponding to the product concentration.

To operate a productostat an essential requirement is a fast on-line measurement that can be related to the product concentration. In this work two ethanol-related measurements were available from the outlet gas: A Figaro sensor measuring the content of reducing gases and a CH_x measurement from the gas analyser. Ethanol was therefore chosen as the product which concentration was kept constant, thus the fermenter was operated as an ethanolostat. In this paper, the term *closed loop* operation was used to refer to the ethanolstat whereas *open loop* operation refers to a traditional chemostat.

If multiple steady-states do exist, at least one of the steady-states will be unstable (at least one eigenvalue is greater than zero, Nayfeh and Balachandran (1995)) and can therefore not be reached through open loop operation. This is illustrated in figure 5.2, where the steady-state solution for a biochemically structured yeast model is shown (Lei *et al.*, 2001). The model predicts three steady-states for a given dilution rate in a region of dilution rates below D_{crit}. Two of the steady-states are stable and should be obtainable in open loop, however, the unstable steady-state can only be obtained by specifying the ethanol (or biomass) concentration and using closed loop control of the dilution rate, e.g in a productostat.

The experimental strategy of the closed loop operations was to initially specify a very low ethanol concentration (approximately 0.1 g/l) as controller setpoint to obtain a steady-state in the vicinity of the onset of alcoholic fermentation. This steady-state will be referred to as D_{crit} since it corresponds to the dilution rate which will be found as D_{crit} in traditional chemostat experiments provided the dilution rate is increased slowly enough.

From D_{crit} small increments in the ethanol setpoint were made with the aim to follow the S-shaped ethanol concentration curve shown in figure 5.2.

5.3.5.4 Dilution rate controller

To operate in closed loop mode a dilution rate controller which can stabilise the cultivation at the desired product concentration was developed. The dilution rate controller was basically a PI controller, however with a nonlinear error term to account for the nonlinear behaviour of the ethanol concentration around the critical dilution rate.

The controller output, D, was calculated as:

$$e(t) = 2\frac{y_{ref}^{\beta p_c}}{y_{ref}^{\beta p_c} + y^{p_c}(t)} - 1 \tag{5.4}$$

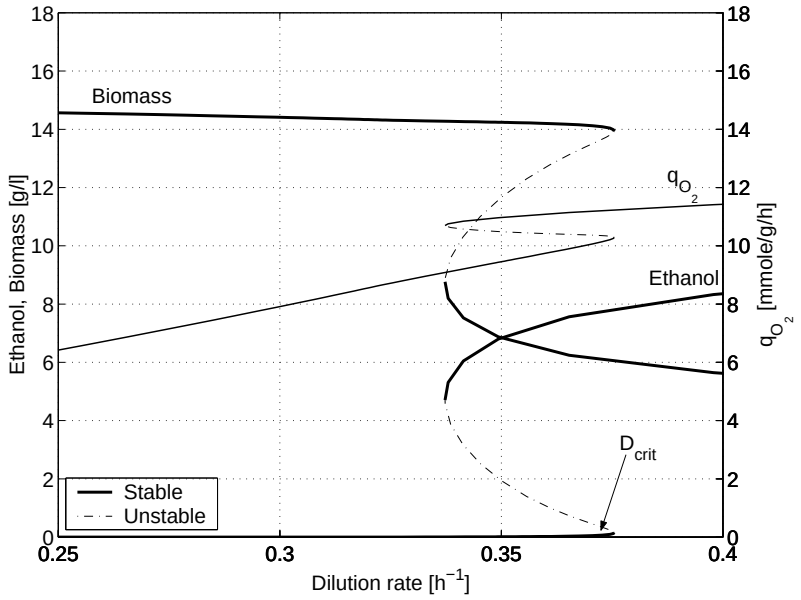

Figure 5.2. Steady-state model predictions of biomass, ethanol and the specific oxygen capacity, q_{O_2}, around D_{crit} for a feed concentration of 30 g/l glucose (Lei *et al.*, 2001). The simulations show that three distinct steady-states exist for a given dilution rate in a region around D_{crit}. The upper and lower steady-states are stable, however the dashed steady-state solution is unstable and can only be determined using closed loop control of the dilution rate.

$$D(t) = K_c\, e(t) + \frac{K_c}{T_i} \int_0^t \left(2 \frac{y_{ref}^{p_c}}{y_{ref}^{p_c} + y^{p_c}(t)} - 1 \right) d\tau \tag{5.5}$$

where $y(t)$ is the ethanol measurement (either the Figaro signal or the CH_x signal from the gas analyser) and $y_{ref}(t)$ is the current setpoint. The controller contains four parameters: K_c, T_i, β and p_c. K_c and T_i are the controller gain and integration time, respectively, β is a parameter included to improve the controller performance during a setpoint change since adjusting β moves the controller zero (Lei, 2001, chap.4) and p_c determines the nonlinearity of the controller. If p_c is 1 the controller is linear. The sampling time used was 1 minute.

The control parameters were tuned based on dynamic simulations of the planned experiment (Lei, 2001, chap.4) with the yeast model proposed by Lei *et al.* (2001). The exponential factor p_c was set to 3 throughout the experiment whereas K_c, T_i and β varied depending on the setpoint in each experiment (see table 5.2).

5.3.5.5 Steady-state condition

The criterion for a steady-state was defined to be achieved when the standard deviation of the CO_2 and O_2 signals did not exceed 3% during 20 h. In order to obtain such a steady-state during closed loop operation the culture was cultivated between 60 and 90 h (20-30 residence times) at a

certain setpoint.

For closed loop experiments C6 and C7, the steady-state corresponding to D_{crit} was established initially and as the last steady-state to check whether D_{crit} had changed during the course of the experiment. This was not the case since D_{crit} was reproduced within 0.01 h^{-1} in each experiment.

5.3.6 Computational methods

5.3.6.1 Data reconciliation

The quality of the obtained steady-state data were checked for gross measurement errors using a statistical test function, h (Nielsen and Villadsen, 1994), by assuming a relative error of 5% on all measurements. Since the degree of freedom is 2, the threshold value for rejecting data with 95 % confidence, is 5.99 (χ^2-distribution, Nielsen and Villadsen (1994)). The data were reconciled according to Heijden *et al.* (1994) before applied in the metabolic flux model.

5.3.6.2 Metabolic flux analysis

To further elucidate on the shift between oxidative and oxido-reductive growth a simple metabolic flux model was set-up. Previous experimental studies of multiple steady-states in *S. cerevisiae* have only considered metabolite and biomass concentrations from the extracellular medium, which are indicative of the existence of multiple steady-states, but not very informative regarding what physiological mechanisms that causes this phenomenon. By calculating the intrinsic fluxes based on a metabolic flux model it was possible to apply internal constraints such as ATP and redox balances to gain more information regarding the shift between oxidative and oxido-reductive growth (Verduyn, 1992).

The structure of the simple metabolic flux model is illustrated in figure 5.3 and model equations, stoichiometry and parameters are given in table 5.1.

Model assumptions

The stoichiometry for the model reactions, shown in table 5.1, was calculated from carbon and redox balances. For the catabolic reactions this is straight forward since the pathways for the reactions are simple. For the anabolic reaction, however, the whole anabolic machinery was lumped into one reaction and the stoichiometric coefficients for NADH (Y_{xNADH}) and CO_2 (α) needed to be determined from experimental data. The two coefficients are not independent but connected by a redox balance over the anabolic reaction: $\alpha = (\kappa + 2\mathrm{Y}_{xNADH})/4 - 1$. Thus either Y_{xNADH} or α needs to be determined.

The NADH produced in the anabolic reactions can be estimated from anaerobic data, since NADH needs to be regenerated by glycerol produc-

Table 5.1. Stoichiometric coefficients and equations for the metabolic flux model.

Stoichiometry		
Anabolism:	q_{ana}:	$CH_{1.82}O_{0.485}N_{0.16} + \alpha\ CO_2 - Y_{xATP}\ ATP + Y_{xNADH}\ NADH - (1+\alpha)\ CH_2O = 0$
Catabolism:	q_{glyol}:	$CH_{\frac{8}{3}}O - \frac{1}{3}\ ATP - \frac{1}{3}\ NADH - CH_2O = 0$
	q_{gly}:	$CH_{\frac{4}{3}}O + \frac{1}{3}\ ATP + \frac{1}{3}\ NADH - CH_2O = 0$
	q_{PDC}:	$\frac{2}{3}\ CH_2O_{0.5} + \frac{1}{3}\ CO_2 - CH_{\frac{4}{3}}O = 0$
	q_{EtOH}:	$CH_3O_{0.5} - \frac{1}{2}\ NADH - CH_2O_{0.5} = 0$
	q_{HAc}:	$CH_2O + \frac{1}{2}\ NADH - CH_2O_{0.5} = 0$
	$q_{cat,ox}$:	$CO_2 + \frac{4}{3}\ NADH + \frac{1}{3}\ FADH - CH_{\frac{4}{3}}O = 0$
	$q_{ox.phos}$:	$P/O\ ATP - NADH - \frac{1}{2}\ O_2 = 0$
	q_{Redox}	$NADH - FADH_2 = 0$
Equations		
Branchpoint:	glc	$-q_{glc} = (1+\alpha)\ q_{ana} + q_{gly} + q_{glyol}$
	CO_2	$q_{CO_2} = \frac{1}{3}\ q_{PDC} + q_{cat,ox} + \alpha\ q_{ana}$
	$acetald$	$q_{PDC} = \frac{3}{2}\ (q_{EtOH} + q_{HAc})$
	$ox.phos$	$q_{ox.phos} = 2\ q_{O_2}$
Constraints:	ATP	$0 = P/O\ q_{ox.phos} - \frac{1}{3}\ q_{glyol} + \frac{1}{3}\ q_{gly} - Y^{true}_{xATP}\ q_{ana}$
	$NADH$	$0 = -\ q_{ox.phos} + \frac{5}{3}\ q_{cat,ox} - \frac{1}{3}\ q_{glyol} + \frac{1}{3}\ q_{gly} + Y_{xNADH}\ q_{ana} - \frac{1}{2}\ q_{EtOH} + \frac{1}{2}\ q_{HAc}$
Parameters	Y_{xNADH}	0.23 (Verduyn *et al.*, 1990; Duboc *et al.*, 1998)
	α	0.21 (stoichiometric coefficient for CO_2, see text)
	P/O	1.20 (van Gulik and Heijnen, 1995)
	Y_{xATP}	calculated from ATP balance

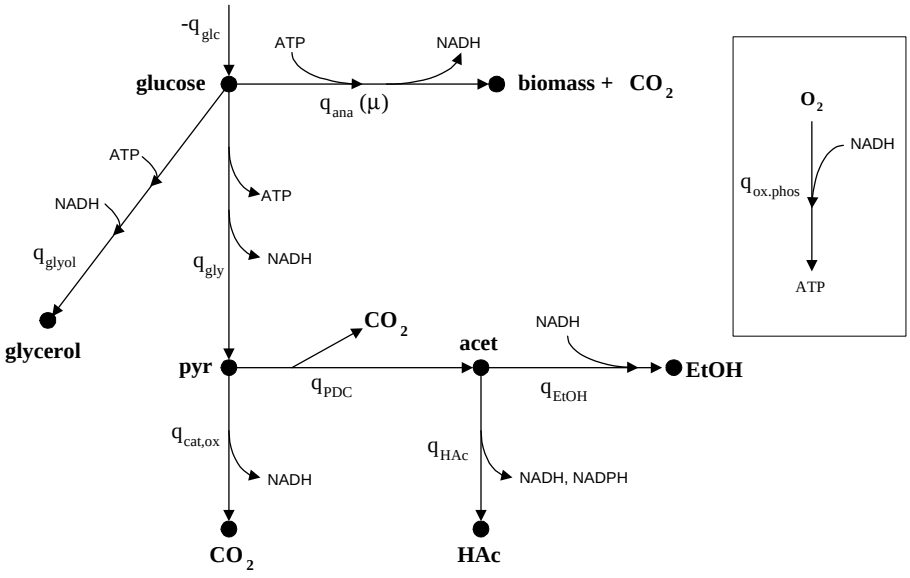

Figure 5.3. Simple MFA model used for calculation of intrinsic rates.

tion (Duboc *et al.*, 1998). The NADH amount produced in the anabolism is closely linked to the protein content of the cell (Verduyn *et al.*, 1990) which does not change significantly from anaerobic (55% at D=0.30 h^{-1}, Schulze (1995)) to aerobic (50% at D=0.30 h^{-1}, Verduyn (1992)) growth. In the anaerobic case a NADH balance yields: $Y_{xNADH} = \frac{1}{3} Y^{ana}_{xglyol}$. Duboc *et al.* (1998) used anaerobic data from Verduyn *et al.* (1990) to calculate Y_{xNADH} and found a value of 0.23 [mol/C-mol], which also was used in this work. Assuming a constant composition of biomass ($CH_{1.82}O_{0.485}N_{0.16}$, Herwig *et al.* (2001)), the stoichiometric coefficient for carbon dioxide (α) yields 0.21 [C-mol/C-mol].

For the conversion of acetaldehyde to acetate two isoenzymes of acetaldehyde dehydrogenase exist (a NADH and a NADPH dependent form), however since only NADH is included in the model it was necessary to assume that only NADH is formed by acetaldehyde dehydrogenase to obtain a redox balanced reaction.

During aerobic growth the biomass yield depends on the efficiency of the oxidative phosphorylation (the P/O ratio - moles of ATP produced per mole O_2 consumed) and the Y_{xATP} (moles ATP consumed per biomass produced). However, since it is virtually impossible to measure the *in-vivo* ATP production rate experimentally, the P/O ratio and Y_{xATP} cannot be determined independently from aerobic growth data. Instead, anaerobic growth data are often used for calculating Y_{xATP} since all ATP is produced by substrate phosphorylation under these conditions. By assuming that the anaerobic determined Y_{xATP} is valid for aerobic growth, the P/O

ratio can be estimated (Dekkers *et al.*, 1981; Verduyn, 1992). However, neither Y_{xATP} nor the P/O ratio are constant as the specific growth rate change. Y_{xATP} is closely linked to the biosynthesis of cell components and is therefore a function of cell composition (e.g. Y_{xATP} increases with increasing protein content, Verduyn *et al.* (1991)). Furthermore non-growth associated maintenance processes such as futile cycles, turnover of macromolecules and maintaining gradients will affect Y_{xATP} (Nielsen and Villadsen, 1994). A decline in the P/O ratio at increasing dilution rates at oxido-reductive growth has been contributed to the existence of an alternative, energetically unfavorable, cyanide-insensitive respiratory pathway (Alexander and Jeffries, 1990).

For the current metabolic flux analysis there is only one degree of freedom for calculation the P/O ratio and Y_{xATP}. Thus either the P/O ratio or Y_{xATP} needs to be fixed. This dilemma has been discussed by Verduyn (1992) where both methods (either fixing the P/O ratio or Y_{xATP}) were applied in a metabolic flux analysis of a continuous cultivation of *S. cerevisiae*. It was concluded that the uncertainty in assuming Y_{xATP} constant was greater than fixing the P/O ratio due to Y_{xATP}'s dependency on cell composition and byproducts.

Therefore, in the simple metabolic flux model presented here, it was decided to fix the P/O ratio and use Y_{xATP} as an indication of the combined efficiency of the oxidative phosphorylation and the biosynthesis. No growth independent maintenance term was included in the model since previous work have shown that this effect is negligible at high growth rates (Verduyn *et al.*, 1991). The P/O ratio in the model was assumed to have a constant value of 1.20 (van Gulik and Heijnen, 1995). The calculated value of Y_{xATP} naturally depends strongly on the fixed value of the P/O ratio, however the quantitative change in Y_{xATP} from one steady-state to another steady-state was found to be rather insensitive to the absolute value of the fixed P/O ratio.

5.4 Results

First, data illustrating how the critical dilution rate was determined using closed loop control are shown. Secondly, steady-state data are presented showing multiple steady-states and, finally, energetic aspects of the shift between oxidative and oxido-reductive growth are investigated by applying metabolic flux analysis on the steady-state data.

The experimental steady-state results were compared with simulations of the yeast model proposed by Lei *et al.* (2001) to elucidate the trend of the multiple steady-states observed experimentally. Since the model was developed for a different *S. cerevisiae* strain (CBS8066) with a higher D_{crit}, the dilution rate in the steady-state model simulations was decreased with 0.065 h^{-1} such that D_{crit} of the model corresponded to the experimentally observed D_{crit} (0.31 h^{-1}, for *S. cerevisiae* CEN.PK113-7D).

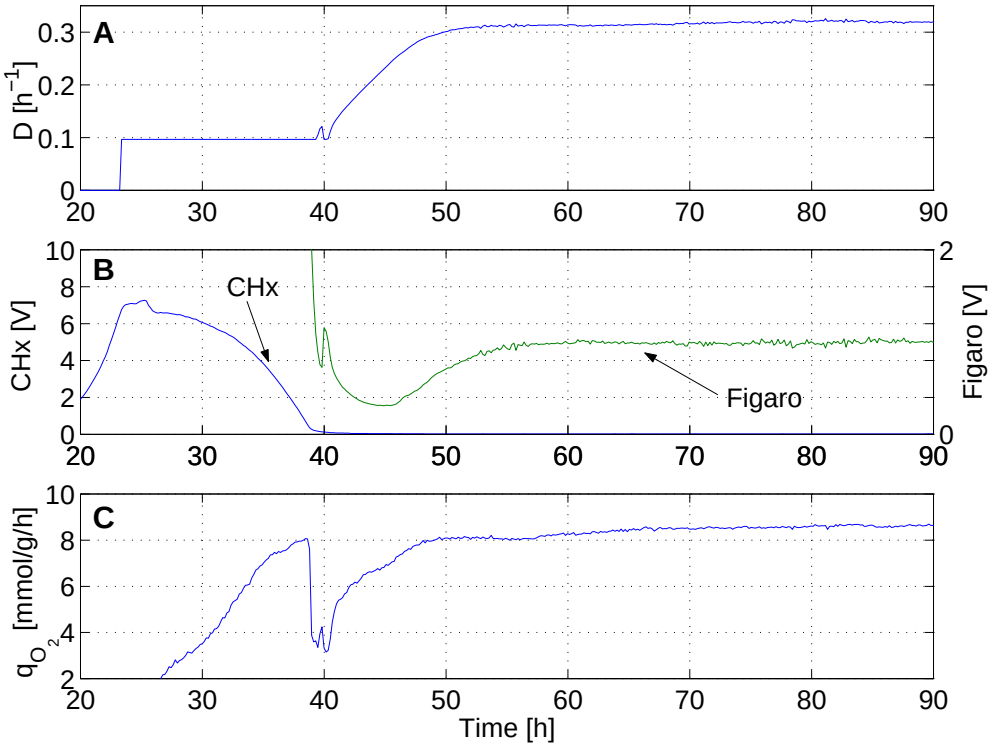

Figure 5.4. Determination of D_{crit} using closed loop control (cultivation C7). The dilution rate (A), the ethanol signals (B) and the specific oxygen uptake rate (C) are shown as function of time. The bioreactor was inoculated at time 0 hr and kept in batch mode until 23 h where continuous operation was initiated. The ethanol produced during the batch phase was exhausted at 40 h whereafter the Figaro measurement was controlled at 1.0 V (50 mg/l ethanol). A steady-state (C7.1) was obtained at 90 h corresponding to a dilution rate of 0.314 h^{-1}. The specific oxygen uptake rate, q_{O_2}, increased during consumption of ethanol from 23 to 40 h and again from 40 to 70 h.

All steady-states were named according to their cultivation and order. E.g. (C7.2) is the second steady-state obtained in cultivation C7. Values for steady-state data can be found in table 5.2.

5.4.1 Determination of the critical dilution rate

The start-up of a continuous cultivation operated as a productostat is illustrated in figure 5.4. The dilution rate controller was turned on when continuous operation was initiated at 23 h. The setpoint used corresponded to an extracellular ethanol concentration of 50 mg/l. However, the Figaro measurement was saturated such that the dilution rate was kept constant at its lower limit until almost all ethanol had been re-consumed (figure 5.4B). From 40 to 80 h, the dilution rate increased until a steady-state was achieved (figure 5.4A). The specific oxygen uptake rate, q_{O_2}, was calculated based on the oxygen uptake rate, OUR, and the biomass con-

centration which was estimated from the base signal (Lei, 2001, chap.6). q_{O_2} was at a low level (1.0 mmol/g/h) at the end of the batch phase as glucose was exhausted, however q_{O_2} increased to 8.0 mmole/g/h during consumption of ethanol from 23 to 40 h. When almost all ethanol was consumed at 38 h, q_{O_2} dropped to 3.8 mmole/g/h before increasing to 8.5 mmole/g/h from from 40 to 70 h (figure 5.4C). The response of q_{O_2} from 40 to 60 h is not caused by an increase in the maximal oxidative capacity but is due to the slow transient in the dilution rate caused by the low controller gain.

For the start-up of a continuous cultivation illustrated in figure 5.4, the value of the critical dilution rate for *S. cerevisiae* CEN.PK113-7D was found to be 0.314 h^{-1}.

5.4.2 Steady-state data

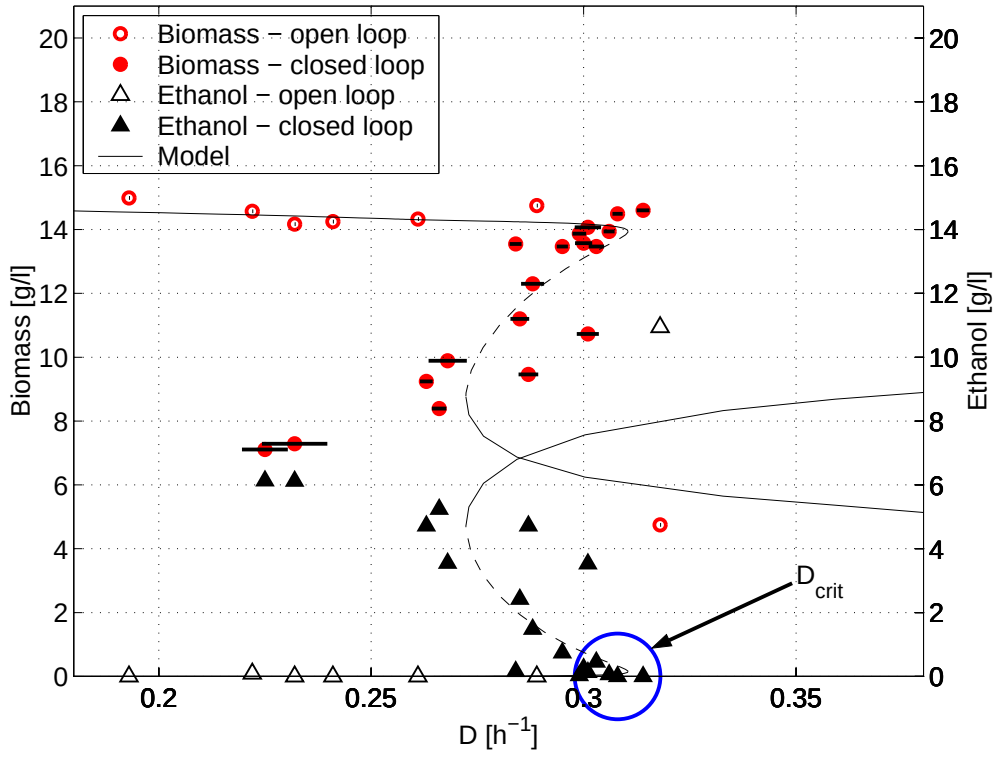

Figure 5.5. Steady-state concentrations for *S. cerevisiae* CEN.PK113-7D of biomass and ethanol using a glucose feed concentration of 30 g/l. All oxido-reductive steady-states except for D=0.318 h^{-1} (C7.6) were obtained using closed loop control (standard deviation of the dilution rate is shown with a horizontal line on the biomass data). The experimental data are compared to model simulations of the yeast model from Lei *et al.* (2001). The model simulations were based on *S. cerevisiae* CBS 8066 with D_{crit}=0.375 h^{-1}. The dilution rate of the simulated data were therefore decreased by 0.065 h^{-1} to fit the experimental data.

Table 5.2. Steady-state data given in chronological order. A dilution rate controller based on the RQ signal was used for two steady-states (C6.10 and C6.11). The sensitivity of the CHx signal was three times higher in experiments C4 and C6 compared with C7. The relationship between the CHx signal and the ethanol concentration described in section 5.3.4 relates to the CHx sensitivity from C7.

Steady-state	D [h^{-1}]	Controller parameters [K_c;T_i;β; setpoint[a]]	Ethanol [g/l]	Biomass [g/l]	q_{CO_2} [mmol/g/h]	q_{O_2}	Acetate [g/l]	Glucose [mg/l]	Pyruvate [mg/l]	Glycerol [g/l]	Acetald. [mg/l]
C4.1	0.193	open loop	0.00	14.99	5.50	5.09	0.00	14	0	0.00	*n.m.*[b]
C4.2	0.222	open loop	0.09	14.57	6.55	6.06	0.01	6	0	0.00	*n.m.*
C4.3	0.232	open loop	0.00	14.17	7.10	6.64	0.00	7	0	0.00	*n.m.*
C4.4	0.241	open loop	0.00	14.25	7.29	6.71	0.00	12	0	0.00	*n.m.*
C4.5	0.261	open loop	0.00	14.33	7.71	7.02	0.01	9	0	0.00	*n.m.*
C6.1	0.299	0.03;2;1;FS-1.0	0.03	13.87	9.40	8.71	0.06	21	10	0.01	*n.d.*[c]
C6.2	0.284	0.05;2;1;FS-3.0	0.16	13.55	9.22	8.41	0.11	27	8	0.09	*n.d.*
C6.3	0.306	0.05;2;1;FS-1.0	0.06	13.94	9.08	8.33	0.10	22	9	0.12	*n.d.*
C6.4	0.300	0.08;2;1;FS-5.0	0.25	13.57	9.22	8.33	0.21	22	5	0.49	*n.d.*
C6.5	0.303	0.10;2;1;FS-7.0	0.45	13.47	9.35	8.27	0.19	22	5	1.06	8
C6.6	0.295	0.06;2;1;CHxS-1.5	0.74	13.47	9.39	8.48	0.11	21	6	0.22	6
C6.7	0.288	0.08;2;1;CHxS-3.0	1.48	12.30	9.95	8.49	0.09	25	6	0.32	13
C6.8	0.285	0.08;4;1;CHxS-5.0	2.42	11.20	10.52	7.92	0.09	29	6	0.19	25
C6.9	0.268	0.10;2;1;CHxS-8.0	3.55	9.89	11.24	8.18	0.12	41	6	0.62	57
C6.10	0.266	0.08;4;1;RQ1.6	5.24	8.39	12.67	7.78	0.19	65	11	0.56	111
C6.11	0.232	0.20;4;1;RQ2.0	6.12	7.04	12.70	6.17	*n.m.*	*n.m.*	*n.m.*	*n.m.*	*n.m.*
C6.12	0.301	0.05;2;1;FS-1.0	0.13	14.07	9.26	8.63	0.08	16	6	0.51	*n.d.*
C7.1	0.314	0.05;2;1;FS-1.0	0.05	14.60	8.96	8.34	0.07	18	0	0.05	*n.d.*
C7.2	0.301	0.23;4;0.6;CHxS-2.5	3.53	10.73	11.30	8.18	0.24	40	10	0.01	42
C7.3	0.263	0.3;4;0.85;CHxS-3.5	4.72	9.24	11.43	7.00	0.26	47	10	0.04	102
C7.4	0.225	0.3;4;0.85;CHxS-4.5	6.13	7.11	12.11	6.03	0.38	115	30	0.47	184
C7.5	0.308	0.05;1;1;FS-1.0	0.10	14.49	9.04	8.08	0.08	20	0	0.01	*n.d.*
C7.6	0.318	open loop	10.94	4.75	21.06	2.25	0.29	193	110	0.51	68
C7.7	0.289	open loop	0.00	*n.m.*	7.62	6.99	0.00	*n.m.*	0	0.00	*n.m.*

[a] Measurement for dilution rate controller: FS: Figaro sensor, CS: CHx signal from gas analyser, RQ: Respiratory quotient.

[b] *n.m.*: Not measured.

[c] *n.d.*: Not detected.

Steady-states data presented in this work (table 5.2) were achieved in an experimental operating window corresponding to dilution rates from 0.19 to 0.32 h^{-1}. The steady-states clearly showed that multiple steady-states for a given dilution rate can be obtained in a dilution rate region below D_{crit}. (figure 5.5). Thus, for a dilution rate of 0.26 h^{-1} an oxidative steady-state without ethanol formation as well as an oxido-reductive steady-state were obtained. Thus, the data confirms previous indications of multiple steady-states in a continuous cultivation of *S. cerevisiae* (Axelsson *et al.*, 1992; Jørgensen *et al.*, 1992; Wenger and Dunlop, 1994).

The average D_{crit} found using closed loop control was determined to 0.31 h^{-1} for *S. cerevisiae* CEN.PK 113-7D (figure 5.5). This is slightly higher than what has been found previously during open loop operation (0.30 h^{-1}, van Hoek *et al.* (1998)).

The dilution rate for steady-state C7.2 was higher compared to other steady-states from C6 obtained at an ethanol concentration above 2 g/l. This might be due to that steady-state C7.2 was obtained after an increase in the ethanol setpoint from 0.1 to 3.5 g/l, whereas the steady-states obtained in C6 were reached after much smaller increments in the ethanol setpoint.

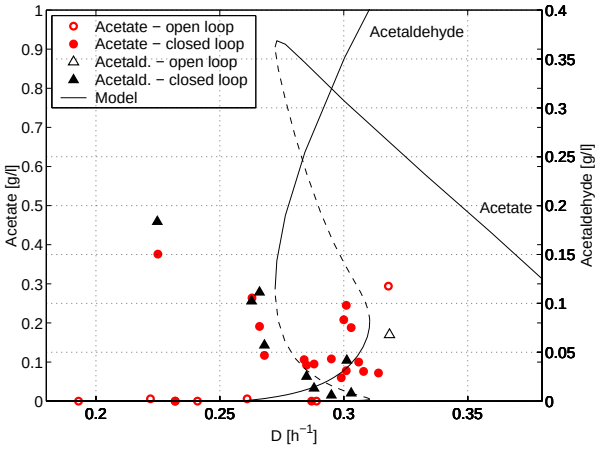

Figure 5.6. Steady-state acetate and acetaldehyde concentrations. The maximum acetaldehyde and acetate concentrations were found using closed loop operation at 0.23 h^{-1}. Model predictions (Lei *et al.*, 2001) for acetate and acetaldehyde using a substrate concentration of 30 g/l are shown as lines. The dilution rate has been rescaled to fit D_{crit} for the cultivated strain.

During oxido-reductive growth acetate, acetaldehyde, pyruvate and glycerol were detected. The experimentally obtained acetaldehyde profile (figure 5.6) showed an interesting pattern. The acetaldehyde concentration increased along with the ethanol concentration for all steady-states obtained in closed loop, however the acetaldehyde concentration for the open loop steady-state at D=0.318 h^{-1} (C7.6) was significantly lower (68 mg/l) than the maximum levels obtained in closed loop (180 mg/l). The acetate concentrations determined experimentally did not show any clear trend,

and it did not exceed 0.4 g/l even at an ethanol concentration above 10 g/l. The steady-state pyruvate concentrations increased with the ethanol concentration, but were less than 150 mg/l for all steady-states. As for acetate and acetaldehyde, no general relation between glycerol and ethanol concentrations could be found (table 5.2).

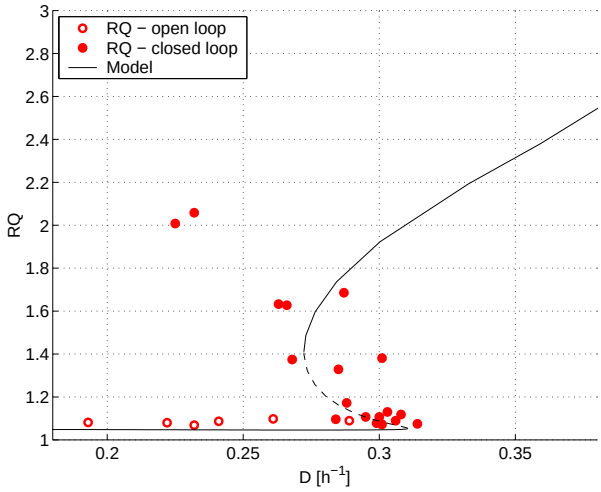

Figure 5.7. Experimental data for the respiratory quotient (RQ). The data point for 0.318 h^{-1}, steady-state C7.6, cannot be seen since its RQ (9.4) is out of range on the figure.

The respiratory quotient depicted in figure 5.7 showed that the cultivation indeed changed from oxidative (with a RQ around 1.07) to oxido-reductive growth. For the steady-state obtained in open loop at D=0.318 h^{-1}, the RQ was as high as 9.4 (not shown in figure 5.7) indicating a relatively low activity of the oxidative phosphorylation compared with substrate phosphorylation through ethanol production.

The specific oxygen uptake rate, q_{O_2}, shown in figure 5.8 exhibited an interesting pattern. In line with earlier work (Meyenburg, 1969; Postma *et al.*, 1989; van Hoek *et al.*, 1998), q_{O_2} increased linearly with the dilution rate during oxidative growth (open loop) until D_{crit} was reached. During closed loop operation, q_{O_2} remained constant at its maximum level (8.4 mmole/g/h) at steady-states corresponding to an ethanol concentration between 0 and 3.5 g/l, but at larger ethanol concentrations q_{O_2} decreased. A decrease of q_{O_2} with increasing ethanol concentrations has also been observed in a chemostat by van Hoek *et al.* (1998) for the same yeast strain as cultivated in this work.

In this work, it was not possible to obtain closed loop steady-states corresponding to an ethanol concentration larger than 6.1 g/l by increasing the ethanol setpoint stepwise. The dilution rate controller applied for closed loop operation was designed based on the Lei model (Lei, 2001, chap.4), however the very low oxidative capacity at high ethanol concentrations is not included in this model. Therefore, the controller used was designed too

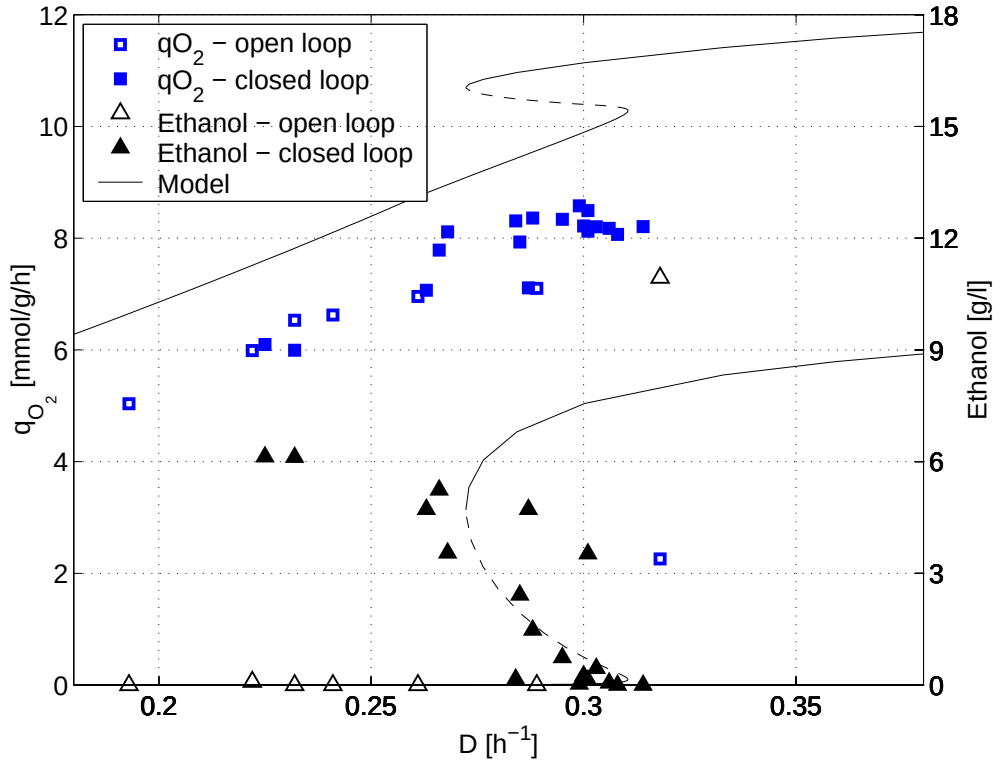

Figure 5.8. Steady-state values for the specific oxygen uptake rate, q_{O_2} compared with model simulations. The ethanol concentrations are shown to elucidate the position of the oxido-reductive q_{O_2} steady-states. The closed loop values should be compared to the dotted line of the model simulation. Note the very low q_{O_2} for the steady-state at D=0.318 h^{-1} (C7.6).

aggressively (a too high controller gain). As a result, washout of biomass at dilution rates well below μ_{max} (0.40 h^{-1}) occurred when the controller attempted to increase the ethanol concentration by increasing the dilution rate.

Furthermore, it was not possible to obtain oxido-reductive steady-states in open loop below 0.29 h^{-1} starting from an oxido-reductive steady-state and decreasing the dilution rate. When the dilution rate was decreased from 0.318 to 0.289 h^{-1} (steady-state C7.6 to steady-state C7.7) the ethanol concentration decreased to zero over a period of 100 h, indicating that oxido-reductive steady-states below D_{crit} cannot easily be obtained in open loop.

A metabolic flux analysis of the steady-state data was carried out using the simple metabolic flux model described in section 5.3.6.2 for investigating the energetics during the shift from oxidative to oxido-reductive growth. Since the current data does not allow the metabolic flux model to distinguish between the efficiency of the oxidative phosphorylation (P/O ratio) and ATP utilisation during biomass production (Y_{xATP}), the P/O ratio was fixed in the model and the calculated Y_{xATP} should therefore be

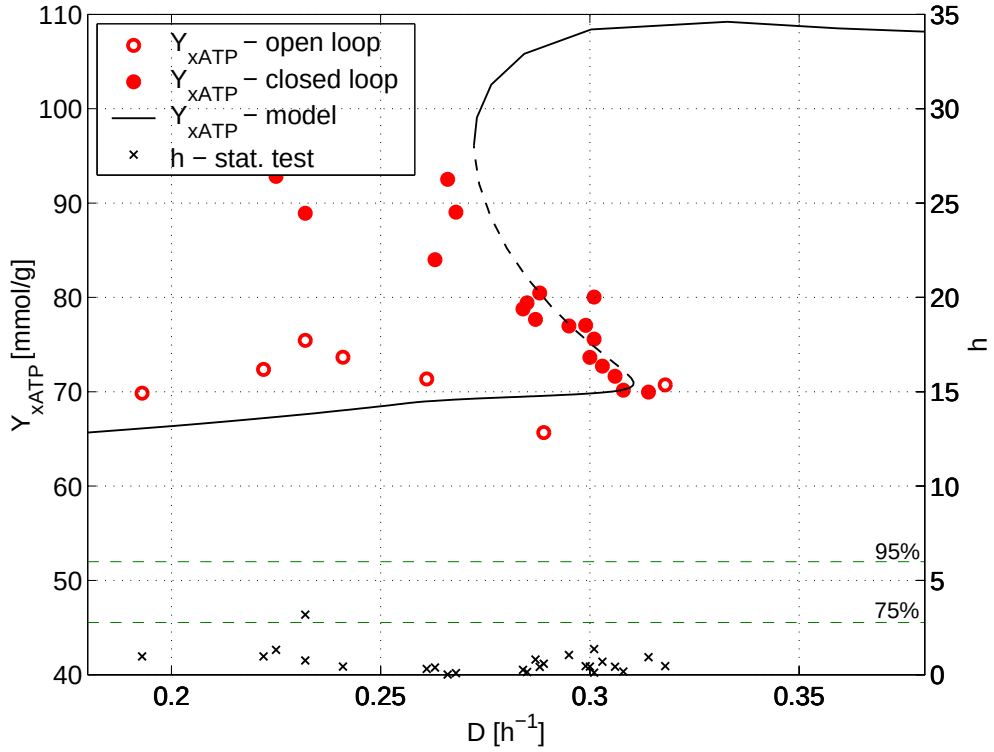

Figure 5.9. Experimental values of Y_{xATP} compared with model simulations. The closed loop data (full circles) should be compared to the dotted line of the model simulation. Note the low Y_{xATP} for the open loop steady-state at 0.318 h^{-1} (C7.6). A statistical test function, h, was calculated for all steady-states to check data quality (see section 5.3). The threshold values for h for rejecting data with 95% and 75% confidence are shown.

interpreted as the combined efficiency of ATP production in the oxidative phosphorylation and ATP utilisation in the anabolism.

Y_{xATP} was found to be approximately constant during oxidative growth, but increased significantly during oxido-reductive growth indicating a less efficient ATP utilisation (figure 5.9). This trend fitted well with model predictions of Y_{xATP} during oxido-reductive growth and also with previous findings by Verduyn *et al.* (1992) that have showed Y_{xATP} increased during oxido-reductive growth with increasing ethanol concentration. Interestingly, the oxido-reductive steady-state obtained in open loop at a dilution rate of 0.318 h^{-1} (steady-state C7.6) had a Y_{xATP} comparable with what was found during oxidative growth even though the steady-state is very much oxido-reductive with an ethanol concentration of almost 11 g/l and a RQ of 9.4.

5.5 Discussion

The discussion is initiated with a comparison of the application of the productostat to a traditional chemostat. Secondly, the physiology of *S. cerevisiae* in the region of multiple steady-states is investigated whereafter modelling aspects of multiple steady-states are discussed based on the experimental data.

5.5.1 Productostat vs chemostat

The productostat applied in this work, where the ethanol concentration was maintained at a fixed level using closed loop control of the dilution rate, represents a quick and accurate cultivation method for determining D_{crit}. Traditionally, determination of D_{crit} for yeast strains in a chemostat is time consuming since a whole series of steady-states need to be established in order to locate at which dilution rate the shift between oxidative and oxido-reductive metabolism occur. If the dilution rate increments are too large oxido-reductive growth might be triggered earlier compared to when smaller steps are taken (Rieger *et al.*, 1983). Instead the dilution rate might be increased slowly as a ramp until ethanol formation is observed (accelerostat, e.g. van Dijken *et al.* (2000)). This approach is naturally much quicker, however no real steady-states are obtained. Here, closed loop operation at a fixed low ethanol concentration is suggested as a quick and reliable method to determine D_{crit} in yeasts.

Closed loop control at D_{crit} can be used as a tool for strain characterisation since a high D_{crit} is an important parameter when selecting a recombinant yeast strain for producing a biomass related product. In addition, by investigating the possible candidates using closed loop operation, optimisation of the medium can take place at conditions corresponding to a maximal productivity of the desired product.

The slow adaptation of D_{crit} found using closed loop control (figure 5.4A) suggests that it might be possible to increase the critical dilution rate by prolonged operation at the same ethanol concentration in a productostat, whereas this is obviously not the case during traditional open loop operation in a chemostat. The slow increase in D_{crit} from 60 to 70 h might be linked to a corresponding increase in the specific oxygen uptake rate, q_{O_2} (figure 5.4C) observed in the same interval. If the maximal oxidative capacity, (q_{O_2} at D_{crit}) determines D_{crit} as it was proposed by Sonnleitner and Käppeli (1986), an increase in q_{O_2} would lead to a higher critical dilution rate. A similar dependency of D_{crit} on the cultivation time was also found by Møller and Jørgensen (1997) in their investigations of using closed loop control in start-up of a continuous cultivation.

Although the increase in the dilution rate from 60 to 70 h is less than the standard deviation of D_{crit} between different steady-states (C6.1, C6.3, C6.12, C7.1 and C7.5), the slow increase in the dilution rate when operating at D_{crit} was reproduced several times. Additionally, the fact that

D_{crit} for *S. cerevisiae* CEN.PK113-7D found in this work using closed loop control is higher than D_{crit} found by van Hoek *et al.* (1998) in a chemostat further supports the hypothesis that closed loop operation leads to a higher D_{crit}.

In the case, that the productivity of the desired product is biomass related, closed loop operation at a fixed low ethanol concentration not only prevents a sudden shift in metabolism (which might lead to high ethanol concentrations and lower productivity), but it also may increase in the oxidative capacity and thereby the biomass productivity ($D_{crit} \cdot x$).

5.5.2 Multiple steady-states

The experimental data presented in this work unquestionably confirms the existence of multiple steady-states in aerobic continuous cultivations of *S. cerevisiae*. However, multiple steady-states might not be an inherent property of aerobic continuous cultivations on glucose. Recent work by van Hoek *et al.* (2000) on the steady-state behaviour of *S. cerevisiae* CEN.PK 113-7D has shown no sign of multiple steady-states around D_{crit}, when a substrate feed concentration of 7.5 g/l glucose has been used. In the current work a substrate feed concentration of 31 g/l glucose was used. Thus, it seems as if the multiple steady-state phenomenon is more pronounced at higher substrate feed concentration as predicted in the model work by Lei *et al.* (2001).

The existence of multiple steady-states posed the obvious question: What are the physiological mechanisms causing this behaviour? The presented results confirmed that inhibition (or more likely repression) of the oxidative capacity does play a role in the existence of multiple steady-states as it has been proposed by Axelsson *et al.* (1992), since q_{O_2} decreased at high ethanol concentrations (figure 5.8).

Repression of q_{O_2} during oxido-reductive growth seems to be very strong in the cultivated strain and thereby increasing the region of multiple steady-states compared to strains where virtually no repression of the oxidative capacity occurs (Barford *et al.*, 1981; Rieger *et al.*, 1983). For the cultivated strain even small steps in the dilution rate (0.308 to 0.318 h^{-1}, C7.5 to C7.6) led to a significant decrease in q_{O_2} and no sign of derepression (increase in q_{O_2}) could be seen even after 100 h of cultivation. Thus, for the cultivated strain, q_{O_2} at oxido-reductive growth was not constant as observed by Barford *et al.* (1981); Rieger *et al.* (1983) for a different yeast strain. A decrease in q_{O_2} with increasing ethanol concentration has also been observed by van Hoek *et al.* (1998) confirming the presented results.

Although the ethanol concentration *per se* does neither repress (nor inhibit) the oxidative capacity (during a 10 g/l ethanol pulse experiment no decrease in q_{O_2} was observed, data not shown) a relationship between increasing ethanol concentration and decreasing q_{O_2} is evident from fig-

ure 5.8.

Repression of the oxidative capacity was, however, not the only effect causing multiple steady-states. Closed loop steady-states at low ethanol concentrations showed no sign of a decrease in q_{O_2} and still the dilution rate decreased as the ethanol setpoint was increased, thus another multiplicity causing mechanism must be present. The metabolic flux analysis provided a possible explanation by considering growth energetics (Y_{xATP}). It was observed that the efficiency of ATP production and utilisation decreased during oxido-reductive growth (figure 5.9). This observation fitted well with previous finding by Verduyn *et al.* (1992), that Y_{xATP} increased during oxido-reductive growth with increasing ethanol concentration. The cause for this decrease has not been fully resolved, although numerous suggestions have been proposed: Effects on Y_{xATP} by ethanol (at the level of the plasma membrane), inhibition of growth by the presence of acetaldehyde and uncoupling effects by acetate have been discussed by Verduyn *et al.* (1992), while Alexander and Jeffries (1990) have proposed that the P/O ratio decreases (which will give an increase in Y_{xATP} in the simple metabolic flux model) at oxido-reductive growth due to the presence of an alternative, less energy efficient, respiratory system.

The data presented here indicate a possible link between the presence of acetaldehyde and the increase in Y_{xATP} during oxido-reductive growth. It was observed (figures 5.6 and 5.9) that acetaldehyde as well as Y_{xATP} increased with the ethanol setpoint in closed loop operation, however for the steady-state at 0.318 h^{-1} in open loop (C7.6) both acetaldehyde and Y_{xATP} had a surprisingly low level compared to the other oxido-reductive steady-states. Thus, the presented results suggest that the efficiency of ATP production/utilisation might be negatively influenced by high acetaldehyde concentrations.

However, irrespective of the cause for the increasing Y_{xATP} during oxido-reductive growth, the increase in Y_{xATP} can from a modelling point of view explain why multiple steady-states are observed even when the oxidative capacity does not decrease since the increase in Y_{xATP} also can be interpreted as inhibition of growth by product formation (ethanol) which is a requirement for multiple steady-states (theorem 5.1).

5.5.3 Modelling multiple steady-states

According to theorem 5.1, at least three mechanisms need to be modelled to describe multiple steady-states as observed in this work. Since modelling of excess product (ethanol) formation and excess substrate uptake is necessary for any model that should describe the biomass and ethanol profiles around D_{crit}, modelling of product inhibition of growth is the key component for obtaining multiple steady-states in a mathematical model. In the previous section, two growth inhibiting phenomena were observed when the growth shifted from oxidative to oxido-reductive: i)

Repression of the oxidative metabolism and ii) less efficient ATP production/utilisation.

Axelsson *et al.* (1992) have showed that by including ethanol inhibition of the maximal oxidative capacity, the bottleneck model (Sonnleitner and Käppeli, 1986) would exhibit multiple steady-states near D_{crit}. Although this model might describe the steady-state behaviour around D_{crit} nicely, the modelled mechanism (ethanol inhibition of the oxidative metabolism) does not seem physiological plausible for the relatively low ethanol concentrations (0.1–10 g/l) observed in this work.

The yeast model proposed by Lei *et al.* (2001) does also exhibit multiple steady-states, however, not as a consequence of inhibition (or repression) of the oxidative metabolism. This is seen in figure 5.8 where the q_{O_2} predicted by the model was approximately constant above D_{crit}. However, the model showed a decreased ATP utilisation efficiency (increasing Y_{xATP} with increasing ethanol concentration), a phenomenon which also was observed experimentally and can cause multiple steady-states. In the model an increasing Y_{xATP} during oxido-reductive growth is not modelled directly, but is a consequence of the activation of an extra catabolic glucose uptake system during oxido-reductive growth. The extra catabolic glucose uptake system was modelled empirically to fit the experimentally observed behaviour during the shift from oxidative to oxido-reductive growth (Lei *et al.*, 2001) and the kinetic expression for this uptake system is therefore not based on any specific physiological observed mechanism.

The region of multiplicity for the Lei *et al.* (2001) model depicted along with the experimental results was smaller than experimentally observed. This discrepancy is, however, due to the fact that repression of the oxidative metabolism was not included in the model. If repression of the oxidative metabolism is included in the model, a larger multiplicity region would be obtained (Axelsson *et al.*, 1992).

5.5.4 Repression of q_{O_2} is a dynamic phenomenon

The fact that the cultivation changed back to purely oxidative growth when the dilution rate in open loop operation was decreased from 0.318 to 0.289 h^{-1} (C7.6 to C7.7) contradicts the steady-state solution for ethanol and biomass shown in figure 5.2. The model predicted that the growth would remain oxido-reductive until the dilution rate was decreased to a value where no multiple steady-states exist (below 0.33 h^{-1} for the model and below at least 0.23 h^{-1} according to experimental data). However, since the cultivation changed back to oxidative growth already at 0.289 h^{-1}, the model cannot account for the fact that an oxido-reductive steady-state can be achieved at 0.23 h^{-1} in closed loop and not in open loop.

Thus, in order to fully understand the steady-state results presented in this paper, it is necessary to study the transients leading to the steady-states. In this respect, the dynamics of repression and derepression of the

oxidative phosphorylation seems to play a key role regarding the width of the multiple steady-state region.

5.6 Conclusions

In this work, multiple steady-states around the critical dilution rate (D_{crit}) in aerobic glucose-limited continuous cultivations of *S. cerevisiae* CEN.PK113-7D was shown experimentally.

The existence of multiple steady-states were attributed to two distinct physiological effects occurring when growth changed from oxidative to oxido-reductive: i) A decrease in the efficiency of ATP production and utilisation and ii) Repression of the respiratory system. The latter effect was most pronounced at high ethanol concentrations whereas the first effect also increased with the ethanol concentration for closed-loop oxido-reductive steady-states, but was not observed during open-loop oxido-reductive steady-states. Through closed loop operation of the bioreactor, oxido-reductive steady-states at dilution rates up to 0.09 h^{-1} lower than the critical dilution rate were obtained.

From a modelling point of view, the observation of multiple steady-states sets an additional constraint on mathematical models describing the growth of *S. cerevisiae*; they should exhibit these types of multiple steady-states.

Currently, only few mathematical models exist which describe multiple steady-states around the critical dilution rate. The physiological mechanisms causing these models to exhibit multiple steady-states are questionable. The presented results suggested that at least two mechanisms should be included when modelling the shift between oxidative and oxido-reductive growth in *S. cerevisiae*: i) A decrease in the combined efficiency of the oxidative phosphorylation and ATP utilisation during oxido-reductive growth, and ii) Repression of the oxidative metabolism.

It does not seem likely that the ethanol concentration *per se* is the actual trigger of any of the two mechanisms and additional (especially dynamic) experimental investigations are needed to model the observed effects in a more physiologically reasonable manner. Especially, the dynamics of the repression and derepression of the oxidative metabolism should be studied since the dilution rate region where multiple steady-states occur seems to be strongly depended on the degree of repression of the oxidative metabolism.

The advantages of closed loop control of the dilution rate (productostat) were illustrated in the determination of D_{crit}. This productostat method is much quicker than using a traditional chemostat where the dilution rate is increased in small steps every time a steady-state has been obtained and also more accurate than running a continuous cultivation as an accelerostat.

The existence of multiple steady-states should be considered not only

when modelling *S. cerevisiae* but also during cultivation of the microorganism. If the critical dilution rate is approached too rapidly, the maximal growth rate without ethanol formation might be lower than what can be obtained if the dilution rate is increased at a slower rate. Closed loop control of the dilution rate should therefore be applied if it is desired to operate in the vicinity of the critical dilution rate. This might be the case in industry during biomass or heterologous protein production.

List of symbols

CER	carbon dioxide evolution rate [mmole CO_2/h]
CH_x	measurement of CH_x content in outlet gas from gas analyser [V]
D	dilution rate [h^{-1}]
D_{crit}	critical dilution rate in chemostat (onset of alcoholic fermentation) [h^{-1}]
$D_{washout}$	dilution rate in chemostat at which washout occurs [h^{-1}]
$e(t)$	error term in dilution rate controller
$EtOH$	ethanol concentration [g/l]
h	statistical test for quality of steady-state data[]
K_c	controller gain []
K_s	affinity constant [g/l]
K_{si}	substrate inhibition constant[g/l]
K_{pi}	production inhibition constant[g/l]
K_{si}	inhibition constant for reaction j [l/g-substrate]
m_s	substrate maintenance coefficient [g/g/h]
m_p	product maintenance coefficient [g/g/h]
OUR	oxygen uptake rate [mmole O_2/h]
q_{O_2}	specific oxygen uptake rate [mmole O_2/g bio/h]
q_{CO_2}	specific oxygen uptake rate [mmole CO_2/g bio/h]
q_i	specific production rate of component i [g/g/h] or [C-mol/C-mol/h]
r_i	reaction rate for reaction i [h^{-1}]
RQ	respiratory quotient (q_{CO_2}/q_{O_2}) []
p	product concentration [g/l]
p_c	exponent in dilution rate controller []
P/O	moles ATP produced in the oxidative phosphorylation divided by moles oxygen consumed [mol/mol]
s	substrate concentration [g/l]
S_f	inlet concentration of substrate [g/l]
t	time [h]
T_i	integration time in the dilution rate controller [h]
x	dry weight biomass concentration [g/l]
$y(t)$	measurement to dilution rate controller [V]
y_{ref}	setpoint in dilution rate controller [V]
Y	yield coefficients [g/g] or [C-mol/C-mol]
α	stoichiometric coefficient for CO_2 production in anabolic reaction [C-mol/C-mol]
β	parameter in dilution rate controller []
Δq_s^m	excess substrate consumption rate [g/g/h]
Δq_p^m	excess production production rate [g/g/h]
κ	degree of reduction for biomass []
μ	specific growth rate [h^{-1}]
μ_{max}	rate constant [h^{-1}]

References

Alexander, M. and Jeffries, T. (1990). Respiratory efficiency and metabolite partitioning as regulatory phenomena in yeasts. *Enzyme Microb. Technol.*, **12**, 2–19.

Andersen, M.; Pedersen, N.; Brabrand, H.; Hallager, L. and Jørgensen, S. (1997). Regulation of a continuous yeast bioreactor near the critical dilution rate using a productostat. *J. Biotechnol.*, **54**, 1–14.

Axelsson, J.; Münch, T. and Sonnleitner, B. (1992). Multiple steady-states in continuous cultivation of yeast. *IFAC Modelling and Control of Biotechnical Processes, Colorado, USA*, **10**, 383–386.

Barford, J.; Jeffery, P. and Hall, R. (1981). The Crabtree effect in *Saccharomyces cerevisiae* - primary control mechanism of transient? *Adv. Biotechnol.*, **1**, 255–260.

Beck, C. and von Meyenburg, H. (1968). Enzyme pattern and aerobic growth of *Saccharomyces cerevisiae* under various degrees of glucose limitation. *J. Bacteriol.*, **96**, 479–486.

Crabtree, H. (1929). Observations on the carbohydrate metabolism of tumours. *Biochem. J.*, **21**, 536–545.

de Deken, R. (1966). The Crabtree effect: A regulatory system in yeast. *J. Gen. Microbiol.*, **44**, 149.

Dekkers, J.; de Kok, H. and Roels, J. (1981). Energetics of *Saccharomyces cerevisiae* CBS 426: Comparison of anaerobic and aerobic glucose limitation. *Biotechnol. Bioeng.*, **23**, 1023–1035.

Duboc, P.; Stockar, U. v. and Villadsen, J. (1998). Simple generic model for dynamic experiments with *Saccharomyces cerevisiae* in continuous culture: Decoupling between anabolism and catabolism. *Biotechnol. Bioeng.*, **60**, 180–189.

Fiecther, A.; Fuhrmann, G. and Käppeli, O. (1994). Regulation of glucose metabolism in growing yeast cells. *Adv. Microb. Physiol.*, **36**, 145–180.

Heijden, R. v. d.; Romein, B.; Heijnen, J.; Hellinga, C. and Luyben, K. (1994). Linear constraint relations in biochemical reaction systems: I, Classification of the calculability and the balanceability of conversion rates. *Biotechnol. Bioeng.*, **43**, 3–10.

Herwig, C.; Marison, I. and von Stockar, U. (2001). On-line stoichiometry and identification of metabolic state under dynamic process conditions. *Biotechnol. Bioeng.*, page accepted for publication.

Jørgensen, S.; Møller, H. and Andersen, M. (1992). Adaptive control of continuous yeast fermentation. *Proc. 9th Int. Biotechnol. Symposium*, pages 364–369.

Karrer, D. (1978). *Der totale gefüllte Bioreaktor*. Ph.D. thesis, ETH, Zürich.

Lei, F. (2001). *Dynamics and nonlinear phenomena in continuous cultivations of* Saccharomyces cerevisiae. Ph.D. thesis, KT, Technical University of Denmark.

Lei, F.; Rotbøll, M. and Jørgensen, S. (2001). A biochemically structured model for *Saccharomyces cerevisiae*. *Accepted for publication in J. Biotechnol.*.

Meyenburg, K. v. (1969). *Katabolit-Repression und der Sprossungszyklus von Saccharomyces cerevisiae*. Ph.D. thesis, ETH Zürich.

Møller, H. and Jørgensen, S. (1997). Continuous cultivation start-up control - an experimental investigation. *J. Biotechnol.*, **53**, 55–66.

Nayfeh, A. and Balachandran, B. (1995). *Applied nonlinear dynamics*. John Wiley & Sons, New York.

Nielsen, J. and Villadsen, J. (1994). *Bioreaction Engineering Principles*. Plenum Press.

Polakis, E.; Bartley, W. and Meek, J. (1965). Changes in the activities of respiratory enzymes during the aerobic growth on yeast on different carbon sources. *Biochemical J.*, **97**, 298–302.

Postma, E.; Verduyn, C.; Scheffers, A. and van Dijken, J. (1989). Enzymic analysis of the Crabtree effect in glucose-limited chemostat cultures of *Saccharomyces cerevisiae*. *Appl. Env. Microbiol.*, **55**, 468–477.

Rieger, M.; Käppeli, O. and Fiechter, A. (1983). The role of a limited respiration in the complete oxidation of glucose by *Saccharomyces cerevisiae*. *J. Gen. Microbiol.*, **129**, 653–661.

Schulze, U. (1995). *Anaerobic physiology of Saccharomyces cerevisiae*. Ph.D. thesis, IBT, Technical University of Denmark.

Sonnleitner, B. and Käppeli, O. (1986). Growth of *Saccharomyces cerevisiae* is controlled by its limited respiratory capacity: Formulation and verification of a hypothesis. *Biotechnol. Bioeng.*, **28**, 927–937.

van Dijken, J. and Scheffers, W. (1986). Redox balances in the metabolism of sugars by yeasts. *FEMS Microbiol. Rev.*, **32**, 199–224.

van Dijken, J.; Bauer, J.; Brambilla, L.; Duboc, P.; Francois, J.; Gancedo, C.; Giuseppin, M.; Heijnen, J.; Hoare, M.; Lange, H.; Madden, E.; Niederberger, P.; Nielsen, J.; Parrou, J.; Petit, T.; Porro, D.; Reuss, M.; van Riel, N.; Rizzi, M.; Steensma, H.; Verrips, C.; Vindeloev, J. and Pronk, J. (2000). An interlaboratory comparison of physiological and genetic properties of four Saccharomyces cerevisiae strains. *Enzyme and Microbial Technology*, **26**(9-10), 706–714.

van Gulik, W. and Heijnen, J. (1995). A metabolic network stoichiometry analysis of microbial growth and product formation. *Biotechnol. Bioeng.*, **48**, 681–698.

van Hoek, P.; Flikweert, M.; van der Aart, Q.; Steensma, H.; van Dijken, J. and Pronk, J. (1998). Effects of pyruvate decarboxylase overproduction on flux distribution at the pyruvate branch point in *Saccharomyces cerevisiae*. *Appl. Env. Microbiol.*, **64**, 2133–2140.

van Hoek, P.; van Dijken, J. and Pronk, J. (2000). Regulation of fermentative capacity and levels of glycolytic enzymes in chemostat cultures of *Saccharomyces cerevisiae*. *Enzyme Microb. Technol.*, **26**, 724–736.

van Urk, H.; Mak, P.; Scheffers, W. and van Dijken, J. (1988). Metabolic responses of *Saccharomyces cerevisiae* CBS8066 and *Candida utilis* CBS 621 upon transition from glucose limitation to glucose excess. *Yeast*, **4**, 283–291.

Verduyn, C. (1992). *Energetic aspects of metabolic fluxes in yeasts*. Ph.D. thesis, Department of Biochemical Engineering, Delft University of Technology.

Verduyn, C.; Postma, E.; Scheffers, W. and van Dijken, J. (1990). Physiology of *Saccharomyces cerevisiae* in anaerobic glucose-limited chemostat cultures. *J. Gen. Microbiol.*, **136**, 395–403.

Verduyn, C.; Stouthammer, A.; Scheffers, W. and van Dijken, J. (1991). A theoretical evaluation of growth yields of yeasts. *Ant. van Leeuwenhoek Intl. J. Gen. and Mol. Microbiol.*, **59**, 49–63.

Verduyn, C.; Postma, E.; Scheffers, W. and van Dijken, J. (1992). Effect of benzoic acid on metabolic fluxes in yeasts: A continuous culture study on the regulation of respiration and alcoholic fermentation. *Yeast*, **8**, 501–517.

Wenger, K. and Dunlop, E. (1994). Coupling of micromixing, macromixing and the glucose effect in continuous culture of Saccharomyces cerevisiae. *AIChE Symp.Ser.*, **90**, 166–174.

Xiu, Z.; Zeng, A. and Deckwer, W.-D. (1998). Multiplicity and stability analysis of microorganisms in continuous culture: Effects of metabolic overflow and growth inhibition. *Biotechnol. Bioeng.*, **57**, 251–261.

Zimmermann, F. and Entian, K. (1997). *Yeast Sugar Metabolism*. Technomic Publishing Company, Inc.

6

Biomass estimation in batch and continuous cultures of *S. cerevisiae*

Two biomass estimation methods were investigated: A commercial probe measuring optical density (Wedgewood 653) and a software sensor estimating the dry weight biomass concentration based on the alkali addition rate. The optical density measurement could not describe the dry weight biomass concentration quantitatively in neither batch nor continuous cultivations. In contrast, the software sensor, which used a mass balance over the proton production and consumption in the medium, was able to estimate the dry weight biomass concentration within 5% during transient experiments in aerobic batch and continuous cultivations of Saccharomyces cerevisiae *CEN.PK113-7D when the production of organic acids were negligible. Inclusion of off-line acetate measurements was able to further improve the alkali based biomass estimate.*

6.1 Introduction

During cultivation of microorganisms in a bioreactor, regardless of the desired product, a key process variable is the amount of biocatalyst in the reactor, i.e. the biomass concentration. In physiological studies or during control and optimisation of a fermentation process, fluxes in and out of the cells are usually quantified as specific rates, i.e. relative to the biomass concentration. Thus, quantification of the biomass concentration is a prerequisite for studying the fermentation process in a quantitative manner.

Numerous methods have been proposed for on-line measurements of biomass, including *in-situ* sensors based on optical density (Junker *et al.*, 1994; Hatch and Veilleux, 1995), culture fluorescence (Lindemann *et al.*, 1999), and dielectric permittivity (Harris *et al.*, 1987; Davey, 1993; November and van Impe, 2000). Furthermore, software sensors (in which the biomass concentration is estimated on-line from other measured culture variables) have been proposed based on thermodynamics (Birou *et al.*,

1987; Boe and Loverien, 1990), carbon dioxide and oxygen conversion rates (Petkov and Davis, 1996) or pH control (San and Stephanopoulos, 1984; Vincente *et al.*, 1998). Recent reviews of on-line biomass monitoring have been presented by Olsson and Nielsen (1997) and Sonnleitner (1998).

The extensive list of proposed methods for on-line biomass estimation also reflects that no method for on-line biomass determination exist which is generally applicable in a process environment. Since biomass is a lumped variable consisting of DNA, RNA, proteins, macromolecules etc. no single method can monitor the development of all cellular components, which would be the optimal biomass measurement. Even off-line determination of cell dry weight measures both viable and dead cells, thus the dry weight biomass concentration might not always reflect the accumulated activity of the cells in a reactor, which most often is the desired biomass measurement. It is therefore not straight forward to compare different biomass estimation methods since no true reference exist, however, despite the drawback of the dry weight measurement, this method is often used as reference (Olsson and Nielsen, 1997).

In this study, two on-line biomass measurements were investigated, a software sensor based on the alkali addition rate to the culture and a commercial sensor (Wedgewood 653 absorbance monitor) measuring optical density. Biomass estimation based on the alkali addition rate during aerobic chemostat (San and Stephanopoulos, 1984) and batch (Vincente *et al.*, 1998) cultivations of *Saccharomyces cerevisiae* have found a linear relationship between the biomass production rate and the alkali addition rate provided that only small amounts of organic acids are formed. Theoretical works on the proton production and consumption pathways have appeared quite recently (Castrillo *et al.*, 1995; Siano, 1995) verifying the relationship between the alkali addition rate and biomass production rate.

In this study, the biomass estimate based on the alkali addition rate was compared with a commercial optical density sensor and off-line biomass (dry weight) measurements. A primary objective of this work was to validate the two sensors during batch and continuous cultivations of *Saccharomyces cerevisiae* and determine under which conditions the sensors are sufficiently accurate to be applied in quantitative studies where the specific rates during transient conditions needs to be determined. In particular, transient experiments where ethanol production occurs in *S. cerevisiae*, i.e. oxido-reductive growth were investigated.

6.2 Materials and Methods

6.2.1 Determination of proton exchange rate

Contributions to the proton exchange rate can be divided into three groups (figure 6.1). Firstly, during an aerobic yeast cultivation on mineral media, nitrogen is most often supplied as ammonium salts, resulting in a net

production of extracellular protons when ammonia is taken up by the cells. Secondly, the dissociation equilibria of products (e.g. acetate, carbon dioxide) or substrates will affect the extracellular proton concentration and thirdly, the buffering capacity of the media will affect the rate at which protons are being exchanged with the extracellular medium.

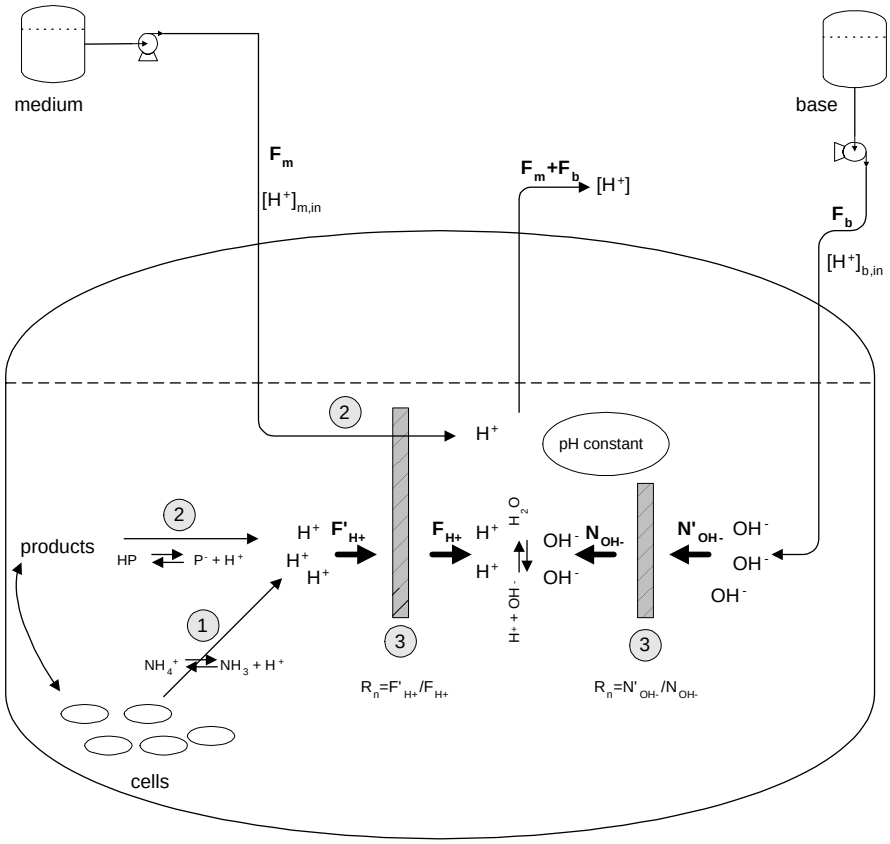

Figure 6.1. Schematic representation of factors influencing the extracellular proton concentration in a yeast fermentation when ammonium is used as nitrogen source. The proton concentration is affected by: 1) uptake of ammonia, 2) dissociation equilibrium of added substrates or products, and 3) the buffering capacity of the medium (symbolised by the gray walls on the figure). The rate of protons produced due to metabolic activity, F'_{H^+}, and addition rate of hydroxyl ions, N'_{OH^-}, were modulated by the same buffering capacity (Castrillo *et al.*, 1995). The figure was adapted and modified from Castrillo *et al.* (1995).

A proton concentration, $[H^+]$, mass balance over the buffered extracellular bioreactor medium yields

$$V\frac{d[H^+]}{dt} = F_m[H^+]_{m,in} + F_b[H^+]_{b,in} - (F_m + F_b)[H^+] + F_{H^+} - N_{OH^-}, \quad (6.1)$$

where V is the working volume of the bioreactor, F_m is the feed flow rate, $[H^+]_{m,in}$ is the proton concentration in the influent medium, F_b is the alkali

addition rate, $[H^+]_{b,in}$ is the proton concentration in the base solution, F_{H^+} is the net rate of proton production/consumption in the medium due to metabolic activity and N_{OH^-} is the rate of $[H^+]$-equivalents appearing in the medium due to pH control.

Under fermentation conditions where pH is kept constant, any variation in the proton concentration will be compensated by addition of base or acid. Thus, the effect of the buffering capacity can be neglected since the proton concentration in the extracellular medium is constant ($F'_{H^+}/F_{H^+} = N'_{OH^-}/N_{OH^-} = R_n$). Furthermore, as $[H^+]_{b,in} << [H^+]$ and $F_b << F_m$, the term $F_b[H^+]_{b,in}$ can be neglected in (6.1) and the outflow term can be simplified to $F_m[H^+]$. Thus, during constant pH conditions equation (6.1) reduces to

$$\begin{aligned} 0 &= F_m([H^+]_{m,in} - [H^+]) + F_{H^+} - N_{OH^-} \\ &\Updownarrow \\ 0 &= F_m \cdot q_{med,H^+} + F_{H^+} - N_{OH^-}, \end{aligned} \tag{6.2}$$

where q_{med,H^+} is the number of proton equivalents required for changing pH of the feed medium to pH of the culture. q_{med,H^+} is equal zero if the pH of the medium has been adjusted to the same pH as in the bioreactor (Castrillo *et al.*, 1995; Pham *et al.*, 1999). [1]

Neglecting the effect from q_{med,H^+}, the mass balance for the proton concentration in the extracellular medium can be expressed in terms of the net rate of protons produced due to cellular activity, F'_{H^+}, and the rate of $[H^+]$-equivalents added due to pH control, N'_{OH^-}:

$$0 = F_{H^+} - N_{OH^-} \Leftrightarrow 0 = F'_{H^+} - N'_{OH^-}. \tag{6.3}$$

The rate of $[H^+]$-equivalents added due to pH control, N'_{OH^-}, was monitored gravimetrically and the net rate of proton production, r_{H^+}, was calculated as

$$r_{H^+} = \frac{F'_{H^+}}{V} = \frac{N'_{OH^-}}{V}. \tag{6.4}$$

For an aerobic yeast cultivation on mineral medium, contributions to the net proton production rate due to metabolic activity were considered from three sources: 1) Uptake of ammonia, 2) production or consumption of organic acids or 3) acidification of the medium due to carbon dioxide production and subsequently dissociation of carbonic acid to carbonate. The latter effect can, however, be disregarded during growth at pH less than 7.0, since the consumption of hydroxide ions by carbonate has been found to be insignificant during these conditions (Noorman, 1989).

[1] However, in this work, the pH or the medium was 4.65 while the pH of the bioreactor was controlled at 5.00. The amount of proton equivalents required for increasing the pH of the medium to 5.00 was determined experimentally to $q_{med,H^+} = 0.515$ mM H^+ eq/l which corresponded to less than 1% of the total amount of base added during the continuous cultivations conducted in this work. The term was therefore neglected in further calculations.

During aerobic growth on glucose, the main products of yeast are biomass and carbon dioxide whereas insignificant amounts of organic acids are produced. In this case, the effect of organic acids can be disregarded as well, and the net proton production rate can be attributed to ammonia uptake by the cells. A 1:1 ratio has been observed between r_{H^+} and the uptake rate of ammonia, $r_{NH_3,uptake}$, when using $(NH_4)_2SO_4$ as N-source (Castrillo *et al.*, 1995). If ammonium is the only nitrogen source and no N-containing compounds are excreted, the biomass production rate is proportional to the proton production rate assuming that the nitrogen content in the biomass composition of the cells is constant. The volumetric biomass production rate, $r_x^{H^+}$ can then be calculated from the base addition rate

$$r_x^{H^+} = \frac{M_{DW} \cdot r_{H^+}}{Y_{xH}} = \frac{M_{DW} N'_{OH^-}}{Y_{xH} V} = [gDW/l/h], \tag{6.5}$$

where M_{DW} is the molar weight of dry weight biomass and Y_{xH} is the yield coefficient of mole protons produced per mole biomass. Y_{xH} equals the molar content of nitrogen in biomass constrained by the overall growth stoichiometry (Y_{xH}=d=z):

$$C_6H_{12}O_6 + b\,NH4^+ + c\,O_2 \rightarrow CH_xO_yN_z + d\,H^+ + e\,CO_2 + f\,H_2O \tag{6.6}$$

During oxido-reductive growth, in addition to biomass and carbon dioxide, ethanol and organic acids are produced by yeast. In such cases, the net proton production rate due to the presence of organic acids in the medium needs to be quantified in order to estimated the biomass production rate. During oxido-reductive growth on glucose, yeast produces e.g. acetic and pyruvic acid which dissociate in the medium producing protons. The contribution to the proton production rate from production or consumption of an organic acid can be quantified as:

$$r_{H^+,HA} = \frac{n \cdot r_{HA}}{1 + 10^{-(pH - pK_A)}}, \tag{6.7}$$

where r_{HA} is the production rate of the organic acid and n is the number of dissociated H^+.[2] Since the degree of dissociation decreases with pH, the effect of production or consumption of organic acid on the net proton production rate can be diminished by running a cultivation at a lower pH. E.g. the degree of dissociation of acetic acid in water (pK_{HAc}=4.76) is 0.635 at pH=5 but only 0.148 at pH=4.

If the production rates of organic acids, $r_{HA,i}$, are known, the net proton production rate due to growth can be determined as

$$r_{H^+,growth} = r_{H^+,total} - \sum_i r_{H^+,HA,i}, \tag{6.8}$$

[2]The degree of dissociation is also depends (weakly) on the ionic strength of the medium (Siano, 1995), however this effect was not considered in this work.

and the biomass production rate taking formation or consumption of organic acids, yields

$$r_x^{H^+} = \frac{M_{DW}}{Y_{xH}} \left(\frac{N'_{OH^-}}{V} - \sum_i \frac{n_i \cdot r_{HA,i}}{1 + 10^{-(pH - pK_{A,i})}} \right). \tag{6.9}$$

6.2.2 Estimation of biomass concentration

A dynamic mass balance for biomass

$$\frac{dx}{dt} = r_x - Dx \tag{6.10}$$

was solved to obtain an estimate of the biomass concentration for any given time during batch and continuous cultivations. The biomass concentration was estimated based on the previous biomass estimate, x_0, the estimated biomass production rate, $r_x^{H^+}$ and the dilution rate. The dynamic mass balance was solved at discrete steps assuming constant dilution (D_0) and biomass production ($r_{x0}^{H^+}$) rates within each interval

$$x_1 = x_0 \cdot \exp\left(\frac{r_{x0}^{H^+}}{x_0} - D_0)(t_1 - t_0) \right). \tag{6.11}$$

N'_{OH^-} (and thus $r_x^{H^+}$) was calculated as an average over a 10 min period while the calculation interval $(t_1 - t_0)$ in (6.11) was 1 min.

6.2.3 Strain and medium

The yeast *S. cerevisiae* CEN.PK113-7D was cultivated in an aerobic continuous culture. The substrate (glucose) concentration was 30 g/l and a defined medium was used (Lei, 2001, chap.5).

6.2.4 Preparation of inoculum

S. cerevisiae strain CEN.PK113-7D was taken from storage -80°C, plated onto YPD agar plates and incubated at 30°C. After three days, a single culture was transferred to a shake-flask containing mineral medium (Lei, 2001, chap.5), at an initial pH of 6.5 and containing 1% (w/v) glucose. Cells, growing exponentially on glucose, were used as inoculum for the fermenter.

6.2.5 Equipment and analytical methods

The fermentation set-ups have previously been described in Lei (2001, chap.5) (set-up 1) and in Lei (2001, chap.7) (set-up 2). Additionally, an absorbance monitor (also referred to as an OD-sensor) (Wedgewood 653 Absorbance monitor) kindly provided by Contech Instrumentering,

Charlottenlund, Denmark, was used as an on-line optical density measurement (950-1100 nm) in set-up 1. The monitor measures the forward light scatter with a path length of 0.5 cm. Furthermore, the input signal is filtering to decrease the effects of aeration and agitation. For all experiments the absorbance range on the OD-sensor was set to A_{range}=2. An analog output signal (4-20 mA) from the instrument was converted into a biomass estimate by the following linear relation: OD_{sensor}[g/l] = $A_{range} \cdot 0.5 \cdot (\mathrm{OD}_{sensor}$[mA]-4) to obtain a reading in the range 0-16 g/l. The biomass estimate from the OD-sensor was not calibrated with respect to experimental data.

6.2.6 Cultivation conditions

The data presented in this paper were obtained from six independent continuous cultivations. Five cultivations were carried out using set-up 1 (C4, C6, C7, C8 and B5) and one cultivation was carried out using set-up 2 (E3). The dynamic results presented in this paper are summarised in table 6.1

Table 6.1. Overview of the conducted dynamic experiments.

Experiment	Cultivation	Mode	Figure
EtOH: 0.1 → 3.6 g/l	C8	P	6.3
EtOH: 5.0 → 0.1 g/l	C8	P	6.4
D: 0.085 → 0.285 → 0.265 h^{-1}	E3	C	6.5
Batch on glucose (30 g/l)	B5	B	6.6

The table states for each experiment, the corresponding cultivation, operation mode (C: chemostat, P: productostat, B: batch) and the number of the figure in which the experiment is presented.

6.3 Results

6.3.1 Determination of the proportionality factor M_{DW}/Y_{xH}

The proportionality factor between the proton exchange rate used for growth ($r_{H^+,growth}$) and the estimated biomass production rate ($r_x^{H^+}$), M_{DW}/Y_{xH} needed to be determined in order to use the alkali addition rate for biomass estimation. A theoretical value for the proportionality factor can be calculated if the N-content in biomass and the molar weight of biomass are known. Since neither the elementary composition nor the ash content was determined in this work, values from literature were used.

The N-content (z) in biomass for the cultivated strain (*S. cerevisiae*, CEN.PK113-7D) has been found to be a function of the dilution rate

during chemostat operation where z=0.14+0.07 μ (Herwig *et al.*, 2001). Since most of the experiments performed in this work were carried out around the critical dilution rate (D_{crit}=0.31 h^{-1}) a constant N-content of z=0.16 N-mol/C-mol was assumed. The molar weight of dried biomass for *S. cerevisiae* CEN.PK113-7D has been determined by Herwig *et al.* (2001) to M_{DW}=25.65 g DW/C-mol (taking an ash content of 7% into account). Since d=b=z=Y_{xH} according to (6.6), a theoretical value for the proportionality factor was calculated as: M_{DW}/Y_{xH} = 25.65/0.16 = 160 g DW/mol H^+.

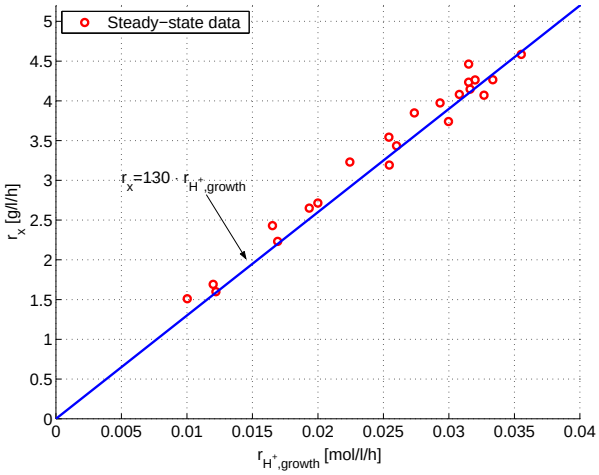

Figure 6.2. Experimental determination of M_{DW}/Y_{xH}. A linear relationship between the proton exchange rate used for growth $r_{H^+,growth}$ (6.8) and the biomass production rate r_x was observed for steady-state chemostat data taken from (Lei, 2001, chap.5).

The experimental value of M_{DW}/Y_{xH} was determined from continuous cultivations at steady-state in the dilution rate range from 0.22 to 0.32 h^{-1} (set-up 1). In figure 6.2, a linear relationship between the proton exchange rate used for growth $r_{H^+,growth}$ (6.8) and the experimental determined biomass production rate r_x based on dry weight measurements can be observed. The experimental proportionality factor was determined to 130 g DW/mol H^+ taking the acetate production into account. The contribution to $r_{H^+,growth}$ from acetate constituted less than 10% for all steady-states and less than 3% for most steady-states. The experimental proportionality factor was 19% lower than the theoretically calculated value. Thus, the experimentally observed base addition rate was larger than the theoretically estimated rate. Still, a linear relationship between $r_{H^+,growth}$ and r_x was observed for all steady-states and the experimentally determined M_{DW}/Y_{xH} was used for biomass estimation in the following dynamic experiments.

6.3.2 Biomass estimation during transients in continuous cultivations

The performance of the two biomass estimates (alkali addition rate and Wedgewood absorbance monitor) were investigated during transient conditions. In figures 6.3-6.4, two experiments within the oxido-reductive region are presented. The ethanol concentration was increased from 0.1 to 3.6 g/l in figure 6.3 and decreased from 5.0 to 0.1 g/l in figure 6.4. The off-line determined dry weight biomass samples are compared with the two on-line biomass estimates.

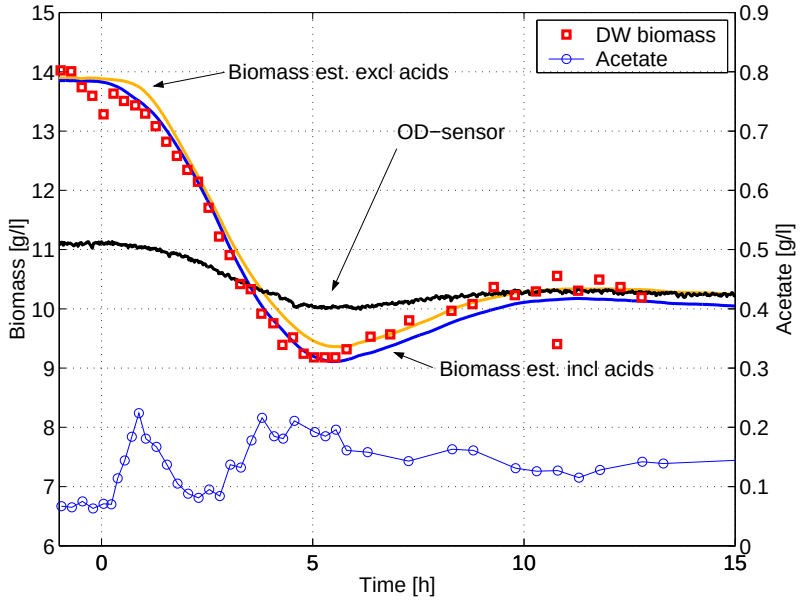

Figure 6.3. Biomass concentration and estimates during an increase in ethanol concentration from 0.1 to 3.6 g/l (productostat). Off-line dry weight samples are compared with an estimate from the alkali addition rate (with and without taking production and consumption of acetate into account) and with the reading of the Wedgewood absorbance monitor (OD-sensor).

The absorbance monitor (OD-sensor) measures the absorbance in the near infrared (NIR) region (from 950-1100 nm). By measuring in the NIR region, the saturation limit of the measurement with respect to high biomass concentrations has been increased compared to measuring in the visible range. From figures 6.3–6.4, it is evident that the OD-sensor was able to qualitatively describe the dynamics of the biomass concentration during the experiments, however the sensor reading cannot be correlated to the biomass concentration through a linear relationship.

In contrast, the biomass estimate based on the alkali addition rate describes the biomass dry weight concentration quantitatively very accurately. The effect of acetate production and consumption on the proton exchange rate from the cells to the medium is illustrated by showing the biomass estimate with and without including the effect of organic acids

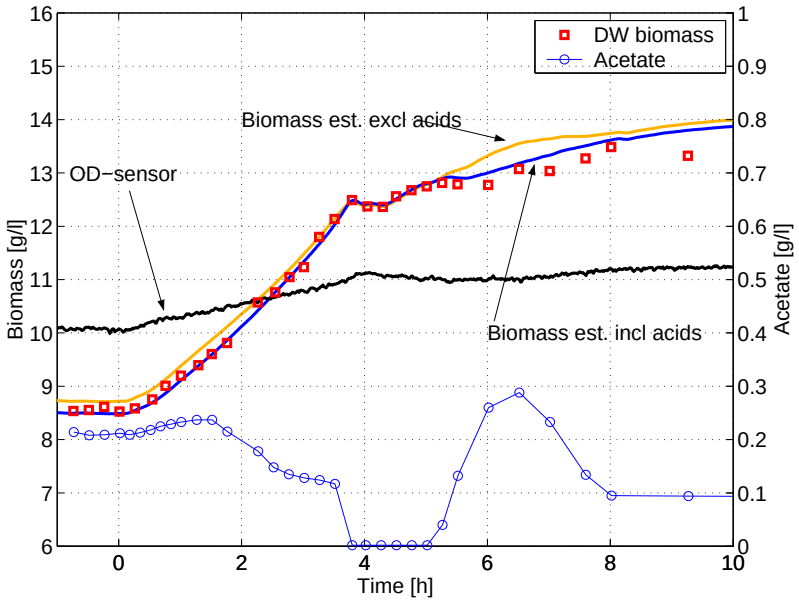

Figure 6.4. Biomass concentration and estimates during a decrease in ethanol concentration from 5.0 to 0.1 g/l (productostat). Off-line dry weight (DW) samples are compared with an estimate from the alkali addition rate (with and without taking production and consumption of acetate into account) and with the reading of the Wedgewood absorbance monitor (OD-sensor).

(only acetate was considered). The results show that when rapid changes in the acetate concentration occurred (e.g. between 0 and 1 h in figure 6.3 or between 5 and 6 h in figure 6.4), a better biomass estimate was obtained by including the effect of acetate production. However, due to the rather low acetate concentrations throughout the experiments, the biomass estimate, where the effect of organic acids has been disregarded, was also quite acceptable (within 5% of the off-line dry weight measurements).

Acetate formation could, however, not be neglected in the alkali based biomass estimate during a dilution rate shift-up from D=0.085 to 0.285 h^{-1} (figure 6.5). During this experiment, the acetate concentration increased to 1 g/l during the first 2 h, whereafter it began to decrease. Consequently, it was observed that acetate production had a significant effect on the biomass estimate during the first 5 h, where omission of acetate production led to a too high estimate of the specific growth rate, resulting in a biomass estimate 1.5 g/l too high (at 3 h). Including the effect of acetate production led to a lower biomass estimate, however it was still 0.5 g/l too high (at 3 h) compared to off-line dry weight measurements. However, since only the effect of acetate was considered, production of other organic acids such as succinate or pyruvate (which would results in an increased r_{H^+}) might account for this discrepancy.

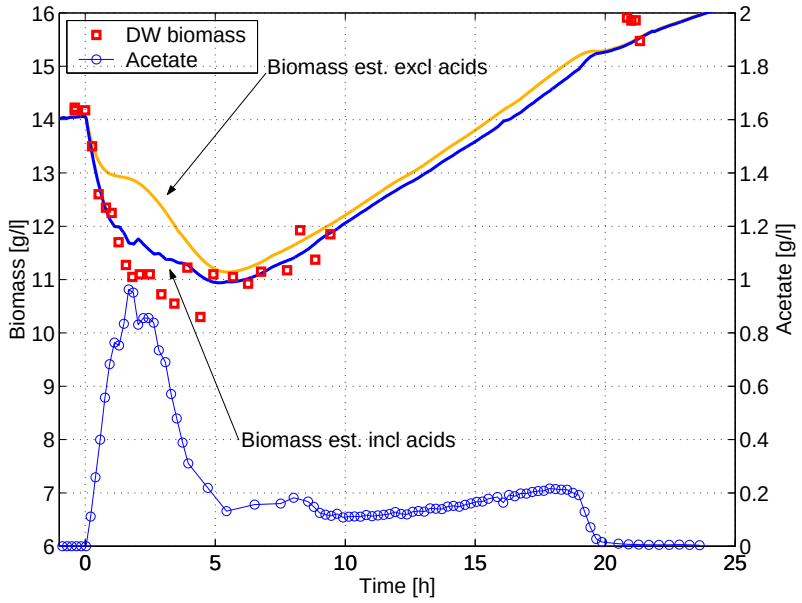

Figure 6.5. Biomass concentration and estimates during a dilution rate shift-up/down. At 0 h, D was increased from 0.08 to 0.285 h^{-1} and then decreased to 0.265 h^{-1} at 3.5 h. Off-line dry weight (DW) samples are compared with an estimate from the alkali addition rate (with and without taking production and consumption of acetate into account). This experiment was carried out using set-up 2 (see Materials and Methods) where the OD-sensor was not installed. Furthermore, the experimental value of the proportionality constant, M_{DW}/Y_{xH}, for set-up 2 was determined to 118 from steady-state experiments, a value which was used in figure 6.5.

6.3.3 Biomass estimation during a batch cultivation

A batch cultivation was carried out with an initial glucose concentration of 30 g/l to investigate how the two biomass estimates performed when glucose is depleted and subsequently pyruvate, acetate and ethanol are used as substrates (figure 6.6).

The OD-sensor exhibited a quite peculiar pattern. During growth on glucose the OD-sensor showed an approximately exponential increase, however when glucose was depleted at 21.5 h, an overshoot was observed and the OD signal decreased from 22.5 to 24 h. From 24 h, the OD signal began to increase exponentially again, however at 30 h, the increase was more linear than exponential and distinctly different from the increase in the dry weight biomass concentration.

The biomass concentration calculated from the base addition rate was found to describe the off-line dry weight concentrations within 5% during growth on glucose (13-21 h) and during growth on ethanol (31-38 h). However, in the intervening period, the biomass estimate yielded a too large value. Including the effects of acetate and pyruvate on the proton exchange rate did not improve the estimate significantly compared with

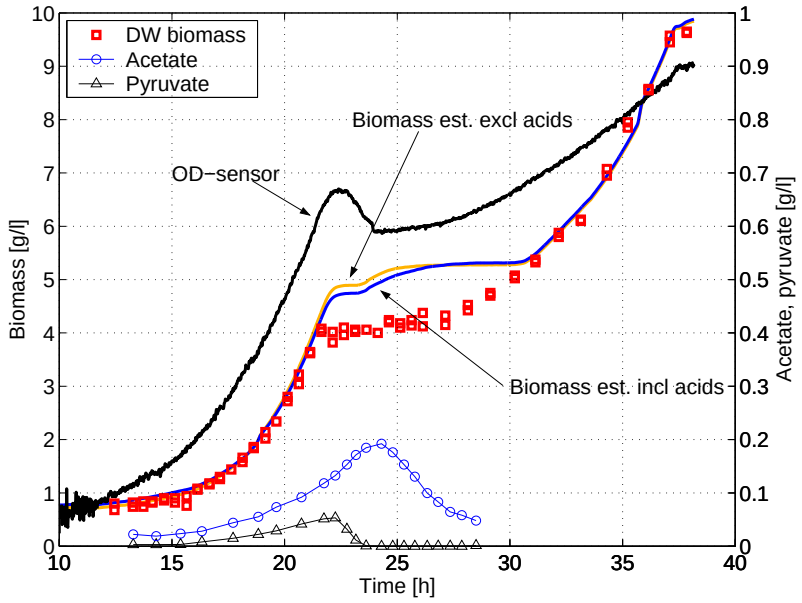

Figure 6.6. Biomass concentration and estimates during a batch cultivation. The initial glucose concentration was 30 g/l. Off-line dry weight (DW) samples are compared with an estimate from the alkali addition rate (with and without taking production and consumption or acetate and pyruvate into account) and with the reading of the Wedgewood absorbance monitor (OD-sensor).

the dry weight determined values.

In order to keep pH constant at 5.00, acid addition (2 M HCl) was necessary between 27.5 to 30 h. The effect of acid addition was not included in the biomass estimates since only 2.6 mmol H^+ was added during the whole experiment. When considering the whole course of the batch experiment, addition of 2.6 mmol H^+ required an extra 2.6 mmol OH^- to be added and the final biomass concentration was therefore estimated too high by $2.6 \cdot 0.130 = 0.34$ g biomass.

6.4 Discussion

6.4.1 Determination of M_{DW}/Y_{xH}

The proportionality constant M_{DW}/Y_{xH} determined during steady-state conditions for set up 1 was found to be valid throughout both batch and continuous cultivations using this set-up. However, the experimental determined M_{DW}/Y_{xH} was 19% lower than the theoretical value. This discrepancy between the theoretical and experimental proportionality constant was not observed by Vincente *et al.* (1998) where the mean value of the ratio $q_{H+}/q_{biomass}$ was equal to the N-content in biomass (0.15)[3] fitting

[3] q_{H+} and $q_{biomass}$ were both expressed in [mol eq/g/h]

well with experimental values of the nitrogen content in biomass (Oura, 1972; Sonnleitner and Käppeli, 1986).

The discrepancy between the experimental and theoretical proportionality constants might be attributed to: 1) A too high M_{DW} or a too low N-content used in the calculations of the theoretical value, 2) Erroneous determination of either the experimental alkali addition or biomass production rates, 3) significant proton production by other factors than ammonia uptake and acetate production, 4) an increase in the $r_{H^+}/r_{NH_3,uptake}$ ratio, or 5) excretion of nitrogen containing compounds in the media.

Ad 1) The molar weight of dry weight biomass and nitrogen content in biomass was taken from Herwig *et al.* (2001) and are similar to what have been reported from other authors (Oura, 1972; Sonnleitner and Käppeli, 1986). The experimentally determined M_{DW}/Y_{xH} corresponds to a N-content of 0.20 assuming the molar weight of biomass to be correct. It is therefore unlikely that the discrepancy is due to erroneous values of M_{DW} and N-content.

Ad 2) The concentration of the base was determined by titration with sulphuric acid and the standard deviation of the base concentration was less than 2%. Furthermore, elementary balances were fulfilled verifying the correctness of the dry weight biomass measurements.

Ad 3) Other factors which so far have been neglected but might affect the proton production rate could be e.g. uptake of inorganic phosphate (DNA synthesis and transcription requires phosphate and produces H^+, Siano (1995)), maintenance of intracellular pH (K^+ – H^+ exchange carrier), carbonate formations due to CO_2 production (discussed earlier) and production of other organic acids. The latter effect can be disregarded since the experimental M_{DW}/Y_{xH} was found to be constant during both oxidative and oxido-reductive growth (thus with and without production of organic acids due to metabolic overflow). The three other effects have been discussed by Siano (1995) where the influence of these factors on the proton production rate during growth at pH=5 and on mineral medium was concluded to be negligible.

Ad 4) The stoichiometry of one net proton produced per molecule of ammonium sulfate consumed have been reported by three different authors (Roos and Luckner, 1984; Huth *et al.*, 1990; Castrillo *et al.*, 1995) and is therefore not likely to be the cause for the observed discrepancy.

Ad 5) If nitrogen containing compounds are excreted from the cells into the medium without proton consumption, then the stoichiometric coefficients for ammonia uptake, b (=Y_{xH}, see (6.6)) would be larger than nitrogen content in biomass (z). Thus, the assumption of Y_{xH}=z used in the calculation of the theoretical value of M_{DW}/Y_{xH} would be invalid. Whether, excretion of nitrogen containing compounds during aerobic growth of *S. cerevisiae* on defined media occurs was not investigated in this work, however it seems unlikely that the cells would excrete approximately 19% of the nitrogen taken up during all growth conditions.

In conclusion, no satisfactory explanation can be provided to account for the discrepancy between the theoretical and the experimental M_{DW}/Y_{xH}. It was, furthermore, found that the experimental M_{DW}/Y_{xH} for set-up 2, was slightly lower than for set-up 1 (118 vs. 130), an observation which could not be accounted for as well.

However, the M_{DW}/Y_{xH} was constant during all operational modes for each set-up and the alkali addition rate could therefore be applied as an on-line estimate of the dry weight biomass concentration.

6.4.2 Biomass estimation using the alkali addition rate

It has been reported that respirofermentative carbon metabolism (consumption and production of ethanol) has a negligible effect on the proton production rate during batch and continuous steady-state cultivations of *S. cerevisiae*, enabling estimation of the biomass concentration based on the alkali addition rate (Vincente *et al.*, 1998). In this work, biomass estimation during transient conditions in continuous cultivations and during a batch cultivation were studied to elaborate on the possibilities and limitations of biomass estimation based on the alkali addition rate in these cases.

It has been shown that during transient experiments in a continuous cultivation within the oxido-reductive region the effect of production and consumption of organic acids is negligible, in line with the findings by Vincente *et al.* (1998). However, during a dilution rate shift-up from the oxidative region into the oxido-reductive region, large amounts of acetate were formed and needed to be included in the biomass estimation to obtain an acceptable estimate of the dry weight biomass concentration.

After glucose depletion in a batch experiment the biomass estimate was too high compared to dry weight measurements until acetate had been consumed (22–30 h in figure 6.6). Inclusion of pyruvate and acetate measurements did not improve the biomass estimate significantly, thus other factors increasing the proton production rate must be present. Since the biomass estimate was able to recapture the dry weight measurements during growth on ethanol (at 30 h), it is possible that the too high biomass estimate was caused by excretion of other organic acids or compounds. These compounds caused an accumulated increase in the proton production rate until they were reconsumed at 30 h (such that the accumulated effect on the proton production balance was zero) enabling the biomass estimate to match the dry weight measurements after 30 h.

6.4.3 OD sensor performance

The Wedgewood 653 absorbance monitor was able to qualitatively describe changes during glucose limited growth in continuous cultivations. However, during batch growth where the substrate changed from glucose over pyruvate and acetate to ethanol, the sensor overshot immediately

after glucose depletion and was not even able to describe the dry weight biomass concentration qualitatively. A comparison between the OD-signal during the batch cultivation and the ethanol setpoint decrease experiment in figure 6.4 reveals that the OD-sensor reading might vary for a given biomass concentration. Just before the batch experiment was terminated (37 h), the biomass concentration was 9 g/l and the OD-signal was translated into a biomass concentration of 8.5 g/l. However, during the ethanol shift-down experiment, the OD-sensor read 10.3 g/l when the dry weight biomass concentration was 9 g/l. Thus, the OD-sensor gave a higher reading for a given biomass concentration during growth on glucose compared to growth on ethanol. This might be due to the fact that the shape and volume of the yeast cells depend on the substrate, resulting in a lower optical density for a given dry weight biomass concentration during growth on ethanol compared to growth on glucose.

The OD-sensor was quite sensitive towards changes in the agitation speed (results not shown) which therefore needed to be kept constant during operation.

6.4.4 Application areas of the two biomass estimates

The investigation of this particular OD-sensor showed that the sensor cannot be used as a quantitative measurement of the dry weight biomass concentration. However, the sensor might be calibrated with dry weight measurements to be valid under very specific conditions where it could be applied quantitatively.

The investigated OD sensor (and other optical density measurements) might be used in industrial production as a supplementary measurement in the monitoring of microbial growth processes. It is, however, not recommendable to use only the OD-sensor for control of a microbial growth process due to the very nonlinear relationship with the dry weight biomass concentration and the sensitivity of the sensor towards changes in substrate and agitation speed.

In contrast, the dry weight biomass estimate based on the alkali addition rate (software sensor) can be applied as an on-line, quantitative measurement of the dry weight biomass concentration during most cultivation conditions. If large amounts of organic acids are produced, the effect of organic acid production needs to be included in the software sensor for suitable estimation of the dry weight biomass concentration. In the present study only ammonium was considered as nitrogen source since it is the uptake of ammonia which caused the proton production used for biomass estimation. If instead urea was used as nitrogen source, no net production of protons would occur as a consequence of nitrogen assimilation (Castrillo *et al.*, 1995) and the alkali addition rate cannot be used for biomass estimation. Furthermore, if complex media is used (which is often the case in industrial processes) with several nitrogen sources, biomass es-

timation based on the alkali addition rate might not be applicable as well.

However, for physiological studies in lab-scale on defined medium, the software sensor based on the alkali addition rate provides an on-line alternative to the dry weight biomass measurement. Thus, during dynamic conditions the biomass production rate can be determined with a higher accuracy using the software sensor compared to conducting dry weight measurements with a sample frequency of 15 or 30 min (Lei, 2001, chap.7).

6.5 Conclusions

Two biomass estimation measurements were investigated. A commercial absorbance probe (Wedgewood 653 - absorbance monitor) measuring optical density and a software sensor calculating the biomass concentration from the alkali addition rate.

The investigated OD-sensor was not able to describe the dry weight biomass concentration quantitatively neither in a batch nor in a continuous cultivation. The sensor reading differed nearly 20% for a given dry weight biomass concentration depending on what substrate was used (glucose or ethanol) and also on the agitation speed.

A software sensor based on the alkali addition rate was found to be very capable of describing both the dynamics as well as the concentration of dry weight biomass during transient experiments in batch and continuous cultivations. The software sensor had only one parameter which needs to be determined: The proportionality factor between alkali addition rate and biomass production rate, M_{DW}/Y_{xH}. This factor can be determined from steady-state experiments and was found to be constant for various operation modes for a given fermentation set-up. During transients where large amounts of organic acids were formed, the increase in the proton production rate due to organic acid production needed to be included in the biomass estimator, however during growth within the oxido-reductive region in continuous cultivations, the effect of organic acids were negligible. Estimation of dry weight biomass concentration based on the alkali addition rate provides an on-line measurement of the biomass production rate and serves as a less laborious alternative to off-line dry weight measurements in physiological studies when defined medium is used.

List of symbols

b	stoichiometric coefficient for ammonium on biomass [mol/C-mol]
c	stoichiometric coefficient for oxygen on biomass [mol/C-mol]
d	stoichiometric coefficient for [H^+] on biomass [mol/C-mol]
e	stoichiometric coefficient for CO_2 on biomass [mol/C-mol]
f	stoichiometric coefficient for H_2O on biomass [mol/C-mol]
CH_x	measurement of CH_x content in outlet gas from gas analyser [V]
D	dilution rate [h^{-1}]
D_{crit}	critical dilution rate in chemostat (onset of alcoholic fermentation) [h^{-1}]
DW	dry weight []
$EtOH$	ethanol concentration [g/l]
F_b	feed flow rate of base [l/h]
F_{H+}	net rate of proton production/consumption appearing in the medium due to metabolic acitivity [mol/h]
F'_{H+}	net rate of proton production/consumption due to metabolic acitivity [mol/h]
F_m	feed flow rate of medium [l/h]
$[H^+]$	concentration of protons [mol/l]
n	number of dissociated protons from an organic acid HA []
N_{OH^-}	rate of [H^+] equivalents appearing in the medium due to pH control [mol/h]
N'_{OH^-}	rate of [H^+] equivalents added to the medium due to pH control [mol/h]
M_{DW}	molar weight of dry weight biomass [g/C-mol]
$q_{biomass}$	specific growth rate [mol eq/g/h]
q_{H+}	specific production rate of [H^+] [mol/g/h]
$q_{med,H+}$	amount of proton equivalents required for changing pH of the feed medium to pH of the culture [mol/l]
R_n	buffering capacity []
r_{H+}	volumetric production rate of [H^+] [mol/l/h]
r_{HA}	volumetric production rate of HA (an organic acid) [mol/l/h]
$r_{H^+,HA}$	volumetric production rate of [H^+] due to dissociation of HA [mol/l/h]
$r_x^{H^+}$	volumetric production rate of biomass determined from the proton mass balance[g/l/h]
x	dry weight biomass concentration [g/l]
t	time [h]
V	volume [l]
Y_{xH}	yield coefficient of protons produced per biomass [mol H^+/C-mol]
z	nitrogen content in biomass [mol/C-mol]
μ	specific growth rate [h^{-1}]

References

Birou, B.; Marison, I. and von Stockar, U. (1987). Calorimetric investigation of aerobic fermentations. *Biotechnol. Bioeng.*, **30**, 650–660.

Boe, I. and Loverien, R. (1990). Cell counting and carbon utilization velocities via microbial calorimetry. *Biotechnol. Bioeng.*, **35**, 1–7.

Castrillo, J.; de Miguel, I. and Ugalde, U. (1995). Proton production

and consumption pathways in yeast metabolism. A chemostat culture analysis. *Yeast*, **11**, 1353–1365.

Davey, C. (1993). *The biomass monitor source book. A detailed user guide.* Aber instrumetns Ltd., UK, Aberystwyth, Wales.

Harris, C.; Todd, R.; Bungard, S.; Lovitt, R.; Morris, J. and Kell, D. (1987). Dielectric permittivity of microbial suspensions at radio frequencies: A novel method for the real-time estimation of microbial biomass. *Enz. Microb. Technol.*, **9**, 181–186.

Hatch, R. and Veilleux, B. (1995). Monitoring of Saccharomyces cerevisiae in Commercial Bakers' Yeast Fermentation. *Biotechnol. Bioeng.*, **46**(4), 371–374.

Herwig, C.; Marison, I. and von Stockar, U. (2001). On-line stoichiometry and identification of metabolic state under dynamic process conditions. *Biotechnol. Bioeng.*, page accepted for publication.

Huth, J.; Werner, S. and Mueller, H. (1990). The proton extrusion of growing yeast cultures as an on-line parameter in fermentation processes: Ammonia assimilation and proton extrusion are correlated by an 1:1 stoichiometry in nitrogen limited fed-batch fermentations. *J. Basic Microbiol.*, **30**, 561–567.

Junker, B.; Reddy, J.; Gbewonyo, K. and Greasham, R. (1994). On-line and in-situ monitoring technology for cell density measurement in microbial and animal cell cultures. *Bioprocess Eng.*, **10**(5-6), 195–208.

Lei, F. (2001). *Dynamics and nonlinear phenomena in continuous cultivations of* Saccharomyces cerevisiae. Ph.D. thesis, KT, Technical University of Denmark.

Lindemann, C.; Marose, S.; Scheper, T.; Nielsen, H.; Hitzmann, B. and Belgardt, K.-H. (1999). Two-dimensional fluorescence spectroscopy for application in biotechnology. *Proceedings of SPIE - The International Society for Optical Engineering*, **3534**, 83–91.

Noorman, H. (1989). *Methodology on monitoring and modelling of microbial metabolism.* Ph.D. thesis, Department of Biochemical Engineering, Delft University of Technology.

November, E. and van Impe, J. (2000). Evaluation of on-line viable biomass measurements during fermentations of *Candida utilis*. *Bioprocess Eng.*, **23**, 473–477.

Olsson, L. and Nielsen, J. (1997). On-line and *in-situ* monitoring of biomass in submerged cultivations. *Tibtech*, **15**, 517–522.

Oura, E. (1972). *The effect of aeration on the growth energetics and biochemical composition of baker's yeast*. Ph.D. thesis, University of Helsinki, Finland.

Petkov, S. and Davis, R. (1996). On-line biomass estimation using a modified oxygen utilization rate. *Bioprocess Eng.*, **15**(1), 43–46.

Pham, H.; Larsson, G. and Enfors, S.-O. (1999). Modelling of aerobic growth of *Saccharomyces cerevisiae*. *Bioprocess Eng.*, **20**, 537–544.

Roos, W. and Luckner, M. (1984). Relation between proton extrusion and fluxes of ammonium ions and organic acids in *Penicillium cyclopium*. *J. Gen. Microbiol.*, **130**, 1007–1014.

San, K.-Y. and Stephanopoulos, G. (1984). Utilization of pH measurements for product estimation. *Biotechnol. Bioeng.*, **26**, 1209–1218.

Siano, S. (1995). On the use of the pH control reagent addition rate for fermentation monitoring. *Biotechnol. Bioeng.*, **47**, 651–665.

Sonnleitner, B. (1998). *Bioprocess Engineering Course, Supetar, Croatia*, pages 370–399. National institute of chemistry, Slovenia. Ed. M. Berovic.

Sonnleitner, B. and Käppeli, O. (1986). Growth of *Saccharomyces cerevisiae* is controlled by its limited respiratory capacity: Formulation and verification of a hypothesis. *Biotechnol. Bioeng.*, **28**, 927–937.

Vincente, A.; Castrillo, J.; Teixeira, J. and Ugalde, U. (1998). On-line estimation of biomass through pH control analysis in aerobic yeast fermentation systems. *Biotechnol. Bioeng.*, **8**, 501–517.

7

Dynamics of the repression and derepression of the respiratory system in *S. cerevisiae*

Regulation of the respiratory system in Saccharomyces cerevisiae *upon changes in the feed rate and during pulse experiments to chemostat cultures was studied. The steady-state behaviour around the critical dilution rate in aerobic glucose-limited continuous cultivations was found to be strongly dependent on the degree of repression of the respiratory system, which could be manipulated depending on how the cultivation was operated. By applying closed loop control of the ethanol concentration using the dilution rate as manipulated variable, it was possible to obtain oxido-reductive steady-states below the critical dilution rate, due to a strong repression the respiratory system. These steady-states could not be achieved through traditional chemostat operation, since the repression of the respiratory system was alleviated when the dilution rate was decreased from oxido-reductive steady-states. Thus, the degree of repression of the respiratory system at steady-state is not only a function of the dilution rate, but also of the history of the culture.*

7.1 Introduction

Saccharomyces cerevisiae is an important microorganism widely used in industry for production of baker's yeast and heterologous proteins. *S. cerevisiae* also serves as an eukaryotic model organism for physiological studies, which has made it the most studied eukaryotic microorganism in academia.

In a glucose limited continuous cultivation, *S. cerevisiae* exhibits two distinct growth regimes under aerobic conditions. At low dilution rates, the growth is purely oxidative and biomass and carbon dioxide are produced as main products. When the dilution rate is increased above a certain value, i.e. the critical dilution rate (D_{crit}), the growth changes to oxido-reductive growth and ethanol is formed. This phenomenon is usually referred to as the Crabtree effect (Crabtree, 1929; de Deken, 1966; Fiecther *et al.*, 1994) and has been defined as *the occurrence of alcoholic fermentation in spite*

of aerobic conditions (van Dijken and Scheffers, 1986).

As a consequence of the Crabtree effect, a continuous cultivation must be operated close to D_{crit} in order to maximise the productivity of biomass or a biomass related product. Operation of a continuous cultivation in the vicinity of D_{crit} is, however, not straight forward. Recent experimental results show that multiple steady-states can be achieved for dilution rates below D_{crit} by operating a continuous cultivation as a productostat (Lei, 2001, chap.5), where the dilution rate was controlled based on the ethanol concentration. The existence of multiple steady-states complicate the chemostat operation of a continuous cultivation just below D_{crit}, since a sudden disturbance might trigger ethanol production and cause the cultivation to become oxido-reductive leading to a decreased biomass productivity.

Lei (2001, chap.5) has also showed that when a continuous cultivation was operated as a chemostat, oxido-reductive steady-states below D_{crit} could *not* be obtained by decreasing the dilution rate from an oxido-reductive steady-state above D_{crit}. Thus, the existence of multiple steady-states seems to be depended on the operation mode.

The occurrence of multiple steady-states have been attributed to changes in two parameters (Lei, 2001, chap.5) as the growth changed from oxidative to oxido-reductive: The specific oxygen uptake rate, q_{O_2} and the yield coefficient for ATP production per biomass, Y_{xATP}. Multiple steady-states can be caused by either a decrease in q_{O_2} or an increase in Y_{xATP} during oxido-reductive growth.

To explain the earlier observed dependence of the operation mode (chemostat vs. productostat) on the obtained steady-states (Lei, 2001, chap.5), the dynamics of q_{O_2} and Y_{xATP} were in this work investigated through various dynamic experiments where a continuous cultivation was operated both as a chemostat and as a productostat. Dynamic investigations of aerobic growth of *S. cerevisiae* have previously been conducted through sudden increases in the dilution rate (shift-ups, Sonnleitner and Hahnemann (1994); Duboc (1997)) or glucose pulses (van Urk *et al.*, 1988) to a continuous chemostat cultivation at steady-state. However, until now no physiological studies of *S. cerevisiae* have been carried out by operating a continuous cultivation as a productostat.

Recently, Herwig *et al.* (2001b) have observed that changes in the glycolytic flux were related to the repression of the respiratory system (monitored as q_{O_2}) during oxido-reductive growth on glucose. It has been suggested that an increase in the specific glycolytic flux during oxido-reductive growth might have a repressing effect on the respiratory system, while derepression was associated with a decrease in the glycolytic flux.

To perform a quantitative analysis of transient responses in continuous cultures, reliable data which fulfil carbon and redox balances are crucial such that gross measurement errors are avoided (Wang and Stephanopoulos, 1983; Herwig *et al.*, 2001a)). By considering the specific external fluxes

combined with a metabolic flux model valuable information regarding the dynamics of the intrinsic fluxes can be obtainedHerwig *et al.* (2001b).

The aim of this work was to address the following questions:

- How is the respiratory system repressed and derepressed during transient conditions?
- How does the efficiency of the ATP production/utilisation (Y_{xATP}) depend on the growth conditions and the degree of repression of the respiratory system?
- How does the history of the feed rate leading to a steady-state affect the oxido-reductive steady-states obtained in a continuous cultivation?

In the investigations of the dynamic experiments, the specific external fluxes were calculated from the raw data and reconciled reaction rates were obtained based on the redundancy in the measured rates. Intrinsic specific rates were calculated using a simple metabolic flux model to enable a more consistent interpretation of the dynamic results.

7.2 Materials and methods

7.2.1 Strain and medium

The yeast *S. cerevisiae* CEN.PK113-7D was cultivated in an aerobic continuous culture. The substrate (glucose) concentration was 30 g/l and a defined medium was used (Lei, 2001, chap.5).

7.2.2 Preparation of inoculum

S. cerevisiae strain CEN.PK113-7D was taken from storage at -80°C and plated onto YPD agar plates and incubated at 30°C. After three days a single culture was transferred to a shake-flask containing mineral medium (Lei, 2001, chap.5), at an initial pH of 6.5 and containing 1% (w/v) glucose. Cells, growing exponentially on glucose, were used as inoculum for the fermenter.

7.2.3 Equipment

Two different set-ups were used: Set-up 1 (experiments carried out at DTU, Denmark) and set-up 2 (experiments carried out at EPFL, Switzerland).

7.2.4 Set-up 1 at DTU, Denmark

Described in Lei (2001, chap.5).

7.2.5 Set-up 2 at EPFL, Switzerland

The cultivations were carried out in a bioreactor (Bioengineering, Wald, Switzerland) with a working volume of 2.0 l. The temperature was kept at 30±0.1°C while pH was controlled at 5.0 by addition of 8 M NaOH. The airflow was monitored by a mass flow meter (Brooks 5850E, Krämer AG, Unterägeri, Switzerland) and set to 1.5 vvm while the stirring speed was 1200 rpm. The dissolved oxygen tension was measured by an oxygen electrode (Mettler Toledo, Switzerland) and remained above 40% during all experiments.

7.2.5.1 On-line monitoring

For on-line analysis of the liquid broth, cell-free permeate was withdrawn from the reactor through a 0.2 μm propylene membrane via a cross-flow filter candle (PP19, ABC, Puchheim, Germany) with a velocity of 20 ml/h. The dead volume was displaced before each analysis as suggested by Christensen *et al.* (1996).

Ammonium and glucose were determined using a flow injection analysis system (Herwig *et al.*, 2001a), whereas ethanol and acetate were quantified using on-line gas chromatography (Herwig *et al.*, 2001a).

The outlet gas from the bioreactor was passed through a condenser and cooled to 12°C. Subsequently, the air was heated to avoid condensation before entering the gasanalyser. The oxygen and carbon dioxide content in the outlet gas was analysed with paramagnetic (Servomex, Crowborough, UK) and infrared (Servomex, Crowborough, UK) analysers, respectively. The water content in the outlet air was found to be constant and was taken into account in the calculation of molar gas rates. The total content of reducing gases in the outlet gas was determined using a Figaro TGS 822 sensor (Hammer Electronic, Elsinore, Denmark).

The substrate feed flow and the base addition was monitored gravimetrically and a PID controller adjusted the pump speed of the substrate feed to ensure a constant substrate feed flow. The base flowrate was automatically varied to maintain a constant pH. The working volume was kept constant by controlling (PID) the outflow pump using the fermenter balance.

7.2.5.2 Off-line samples

Culture dry weight samples (4-5 ml depending on biomass concentration) were taken from the fermenter outflow (no deviation compared to sampling directly from the fermenter was observed) and filtered over preweighed nitrocellulose filters (0.45 μm pore size; Gelman Pall Gelman Sciences, Ann Arbor, USA). After removal of medium, filters were washed with demineralised water, dried in a microwave oven (15 min at 150 W), stored in a desiccator for 15 min and weighed. Duplicate determinations were

made and the maximal deviation between samples was 5%.

For verification of the on-line ethanol and acetate measurements, cell suspension samples were withdrawn via the FIA sampling system and filtered rapidly (0.45 μm, Sartorius AG, Göttingen, Germany) into cooled Eppendorf tubes (1.5 ml, 0°C). Ethanol and acetate were quantified by enzymatic assay kits (acetate, BM no. 148261 and ethanol, BM no. 176290) using a Cobas Mira robot (Roché Diagnostic systems). Glucose feed concentration was determined enzymatically (Unimate 5 GLUC, HK Roché) also using the Cobas Mira system.

7.2.6 Cultivation conditions

The data presented in this paper were obtained from two different experimental set-ups. An overview over all presented experiments is given in table 7.1 where a name has been assigned to each experiment. Experiments with the prefix **C** were carried out using set-up 1 at DTU, whereas experiments with prefix **E** were conducted as EPFL, Switzerland. Experiments were conducted under two types of operation mode: Chemostat and productostat. In the first case the dilution rate was only changed during dilution rate shift-ups or downs, whereas the dilution rate was controlled based on the ethanol concentration in the latter case (Lei, 2001, chap.5). Chemostat operation is also referred to as *open loop* operation of a continuous cultivation, whereas the productostat also is denoted *closed loop* operation of a continuous cultivation.

7.2.6.1 Start-up

The batch phase was started by injecting 5 ml of inoculum culture into the reactor (initial biomass concentration in the fermenter was approximately 1.5 mg/l). The initial glucose concentration in the batch cultivation was 30 g/l. Continuous cultivation was initiated when glucose was depleted and the fermenter was operated as a productostat at an ethanol concentration of 0.1 g/l to determine D_{crit} (Lei, 2001, chap.5).

7.2.7 Computational methods

7.2.7.1 Data reconciliation

The quality of the obtained data were checked using a statistical test function, h (Nielsen and Villadsen, 1994), by assuming a relative error of 5% on all measurements. For all experiments where either biomass or ethanol were estimated the degree of freedom was 1, thus the threshold value for rejecting data with 95 % confidence, is 3.84 (χ^2-distribution, Nielsen and Villadsen (1994)). When neither the biomass nor ethanol were estimated (the biomass concentration was calculated from the base signal (Lei, 2001, chap.6), while the ethanol concentration was measured

Table 7.1. Overview of the presented experiments.

Label	Experiment	Cultivation	Mode	Figures	Bio.	EtOH
E3a	D: 0.085 → 0.31 h^{-1}	E3	C	7.1-7.2	+	+
E3b	D: 0.085 → 0.285 → 0.265 h^{-1}	E3	C	7.3-7.4	+	+
C7a	D: 0.308 → 0.318 → 0.289 h^{-1}	C7	C	7.5-7.6	+	-
E1a	Glucose pulse (D=0.24 h^{-1})	E1	C	7.7-7.8	-	+
E1b	Ethanol pulse (D=0.24 h^{-1})	E1	C	7.9	-	+
E1c	Acetate pulse (D=0.24 h^{-1})	E1	C	7.10-7.11	-	+
C7b	EtOH: 0.1 → 3.6 g/l	C7	P	7.12-7.13	+	+
C7c	EtOH: 3.6 → 4.9 g/l	C7	P	7.14-7.15	+	+
C7d	EtOH: 4.9 → 6.1 g/l	C7	P	not shown	+	+
C8c	EtOH: 4.9 → 0.1 g/l	C8	P	7.18-7.19	+	+
C8d	EtOH ramp: 4.9 → 10 g/l	C8	P	7.20-7.22	+	-

The table states the label of each experiment, the corresponding cultivation, operation mode (C: chemostat, P: productostat) and the number of the figures in which the experiment are presented. Furthermore, it is stated whether or not (+/-) the biomass (Bio) and ethanol (EtOH) were used in data reconciliation. The biomass estimate was obtained from the base signal Lei (2001, chap.6) whereas the ethanol measurement was obtained from the CHx signal (gas analyser).

by GC (set-up 2) or calculated from the CHx signal (set-up 1), thus the degree of freedom was 2. In this case, the threshold value for rejecting data with 95 % confidence, is 5.99 (χ^2-distribution, Nielsen and Villadsen (1994)). Whether biomass or ethanol concentrations were measured or estimated is stated in table 7.1.

Based on the raw data, conversion rates were calculated from all measured states using the window cumulation method proposed by Herwig *et al.* (2001a). Since a window size of 30 min (from t_1-15 min to t_1+15 min) was used process dynamics with a faster time constant cannot be identified from the calculated rates. E.g. the initial jump in q_{O_2} immediately after a dilution rate shift-up (Duboc *et al.*, 1998) appears to be a ramp over 30 min rather than a jump when looking at the presented data. The calculated conversion rates were reconciled according to Heijden *et al.* (1994).

7.2.7.2 Metabolic flux analysis

The metabolic flux model presented in Lei (2001, chap.5) was used for calculation of intrinsic rates and Y_{xATP}.

7.3 Results

The dynamics of an aerobic glucose-limited culture was investigated through three types of experiments: 1) Dilution rate shift-up/down, 2) pulse experiments, and 3) productostat experiments where the ethanol setpoint was changed. An overview over the presented experiments can be found in table 7.1. Two different set-ups were used (see section 7.2). For both set-ups the critical dilution rate was determined using closed-loop control of the dilution rate according to Lei (2001, chap.5). For set-up 1, D_{crit} was determined to 0.31 h^{-1}, while a value of 0.27 h^{-1} was found for set-up 2. A similar difference was found between the maximal growth rates for the two set-ups. For set-up 1, μ_{max} was found to be 0.39 h^{-1} during batch growth (calculated from the CO_2 signal), while μ_{max} for set-up 2 was 0.35 h^{-1} (also calculated from the CO_2 signal). The cause for this difference in growth rates between the two set-ups was not resolved.

The presentation and discussion of the results will focus on the the dynamic behaviour of the respiratory system (oxidative catabolism) and the efficiency of the ATP production/utilisation. The specific oxygen uptake rate, q_{O_2}, was used as a measure of the activity of the respiratory system, while Y_{xATP} calculated from a metabolic flux model was used to interpret the efficiency of the ATP turnover. A statistical test, h, was applied on all experiments to assure that the data fulfilled elementary balances (see section 7.2).

7.3.1 Dilution rate shift-up/down experiments

A dilution rate shift-up from oxidative to oxido-reductive growth was obtained by increasing the dilution rate from 0.085 to 0.31 h^{-1} (figures 7.1-7.2). An initial glucose accumulation was observed and the glucose concentration peaked (at 0.4 g/l), 0.5 h after the shift-up. The glucose profile showed a characteristic tail from 1 to 3 h as the glucose concentration decreased from 180 to 100 mg/l. A similar glucose response has also been observed by Rothen *et al.* (1996).

Acetate and ethanol formation occurred almost instantly after the shift-up. The acetate concentration reached its maximum value (1.0 g/l) 2.5 h after the shift-up whereafter it decreased to 0.2 g/l, whereas the ethanol concentration kept on increasing during the first 15 h after the dilution rate shift-up (figure 7.1). A negative acetate flux was observed between 3 and 5 h showing that the produced acetate was reconsumed by the cells and not washed out.

The response of the biomass/ATP yield coefficient, Y_{xATP} increased from 80 to 120 mmol/g immediately after the dilution rate was increased, however after 2 h it had dropped to 55 mmol/g, indicating a better ATP production/utilisation efficiency during oxido-reductive growth at D=0.31 h^{-1} compared to oxidative growth at D=0.085 h^{-1} (figure 7.2).

In the experiment shown in figures 7.3-7.4, the dilution rate was initially

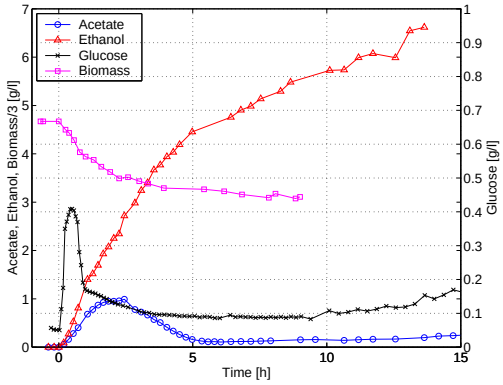

Figure 7.1. Experiment E3a: Dilution rate shift-up from oxidative to oxido-reductive growth in an aerobic glucose limited culture: At time 0 h, the dilution rate was increased from 0.085 to 0.31 h^{-1}. On-line measurements of ethanol, acetate and glucose are plotted along with off-line measurements of biomass as a function of time.

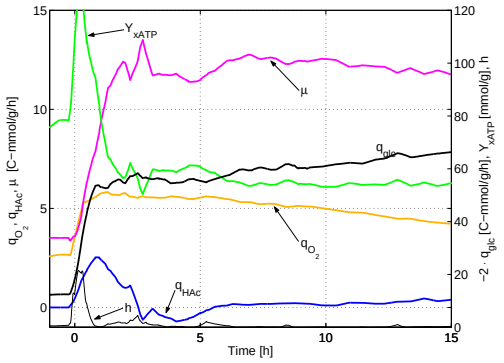

Figure 7.2. Specific rates for growth (μ), oxygen uptake (q_{O_2}), acetate production (q_{HAc}) and the glucose uptake rate (-q_{glc}) are shown together with the biomass/ATP yield coefficient (Y_{xATP}) and a statistical test (h) for the same experiment as shown in figure 7.1.

increased from 0.085 to 0.285 h^{-1} (to a dilution rate above D_{crit}=0.27 h^{-1}). However, to study the effect of a dilution rate shift-down from oxido-reductive growth, the dilution rate was decreased to 0.265 h^{-1} after 3.5 h.

The observed response during the first 3.5 h was very similar to the shift-up into the oxido-reductive regime shown in figures 7.1-7.2. However, the dilution rate shift-down at 3.5 h led to a continued increase of q_{O_2} (accompanied by a decrease in the glucose uptake rate) until ethanol exhaustion at 19 h. Although the ethanol concentration started to decrease after 5 h, ethanol formation (q_{Et}) did not stop until 15 h (figure 7.4). Ethanol was only consumed between 17 and 19 h. After ethanol exhaustion q_{O_2} dropped from 8.1 to 7.3 mmol/g/h.

In contrast to the catabolism, the anabolism (μ) was only affected slightly by the dilution rate shift-down since it had already reached its final level before the shift-down (after 2.5 h).

Another dilution rate shift-up and subsequently shift-down is illustrated in figures 7.5-7.6. As opposed to the previously presented experiments, this experiment was carried out in set-up 2, where D_{crit}=0.31 h^{-1}. The culture was operated in closed-loop at a steady-state corresponding to an ethanol concentration of 0.1 g/l and the dilution rate was 0.308 h^{-1}. The dilution rate was increased to 0.318 h^{-1} at time 0 h.

As a consequence of the dilution rate increase at time 0 h, the biomass concentration decreased and the ethanol concentration increased since the

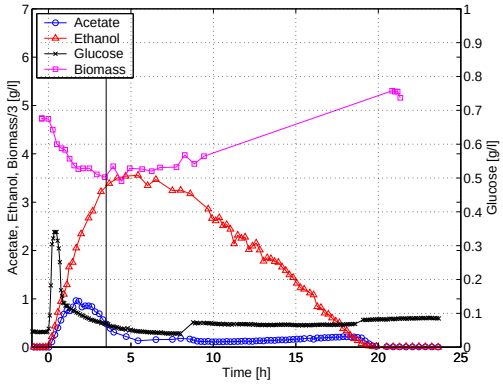

Figure 7.3. Experiment E3b: Dilution rate shift-up/down experiment in an aerobic glucose limited culture: At time 0 h, the dilution rate was increased from 0.085 to 0.285 h^{-1} whereafter it was decreased to 0.265 h^{-1} at 3.5 h (indicated with a vertical line). On-line measurements of ethanol, acetate and glucose are plotted along with off-line measurements of biomass as a function of time.

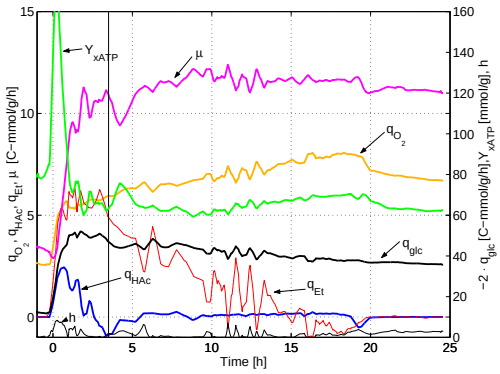

Figure 7.4. Specific rates for growth (μ), oxygen uptake (q_{O_2}), ethanol production (q_{Et}), acetate production (q_{HAc}) and glucose uptake (-q_{glc}) are shown together with the biomass/ATP yield coefficient (Y_{xATP}) and a statistical test (h) for the same experiment as shown in figure 7.3.

oxidative capacity of the cells was saturated.[1] q_{O_2} did not increase after the shift-up as observed during shift-ups from oxidative growth (figures 7.2 and 7.4), instead q_{O_2} decreased from 8.1 to 2.3 mmole/g/h over 70 h indicating an increasing repression of the respiratory system. After the dilution rate shift-down at 107 h, q_{O_2} increased until ethanol exhaustion. q_{O_2} reached a level of 9.1 mmole/g/h just before ethanol exhaustion which corresponds to a higher flux through the oxidative catabolism than what was obtained at any steady-state (Lei, 2001, chap.5).

After the dilution rate shift-up, -q_{glc} continued to increase until the shift-down to 0.289 h^{-1} at 107 h. As a consequence of the dilution rate shift-down the glucose uptake rate dropped immediately from 68 to 62 C-mmol/g/h, whereafter it continued to decrease until all ethanol was exhausted.

The Y_{xATP} showed an interesting peak 50 h after the shift-up, which corresponded to an oxido-reductive state with significant ethanol production (6 g/l) but with only a minor degree of q_{O_2} repression. As q_{O_2} was repressed further, Y_{xATP} decreased indicating a higher ATP production/utilisation efficiency. Following the dilution rate shift-down, Y_{xATP} reached its maximal value just before ethanol exhaustion (similar to q_{O_2}).

[1] The biomass concentration was calculated as in Lei (2001, chap.6)) while ethanol was monitored from the CHx signal (Ethanol-CHx) and calculated from the elementary balances (Ethanol-recon.)

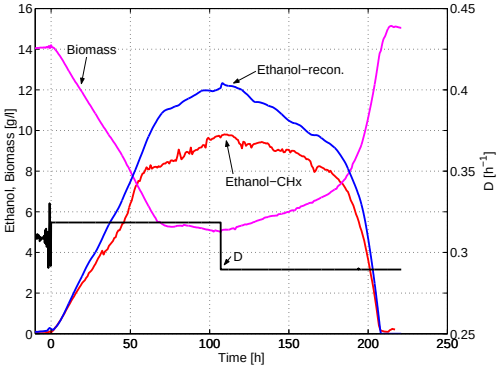

Figure 7.5. Experiment C7a: Dilution rate shift-up/down within the oxido-reductive region in an aerobic glucose limited culture: Before time 0 h, the culture was operated in closed loop at a steady-state corresponding to D=0.308 h^{-1}. At time 0 h, the dilution rate was increased to 0.318 h^{-1}. At 107 h the dilution rate was decreased to 0.289 h^{-1}. On-line estimates of ethanol and biomass are plotted along with the dilution rate as a function of time.

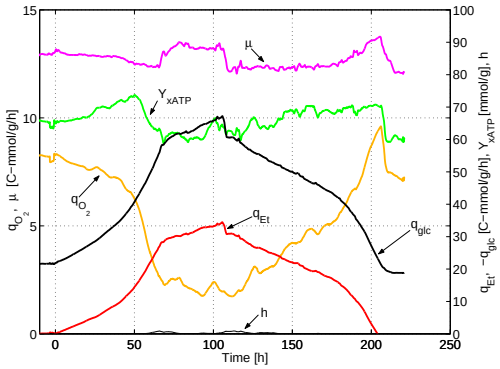

Figure 7.6. Specific rates for growth (μ), oxygen uptake (q_{O_2}), ethanol production (q_{Et}) and glucose uptake (-q_{glc}) are shown together with the biomass/ATP yield coefficient (Y_{xATP}) and a statistical test (h) for the same experiment as shown in figure 7.5.

7.3.2 Substrate pulses to an oxidative steady-state culture close to D_{crit}

When a 30 g/l glucose pulse was added to a steady-state culture at D=0.24 h^{-1} the glucose was consumed over a period of 2 h (figure 7.7). No significant increase in the biomass concentration could be observed, thus the glucose was mainly converted into CO_2, ethanol and acetate. Acetate and ethanol both reached their maximum concentrations as the glucose pulse was exhausted (1.0 and 9.0 g/l, respectively). A slight decrease in q_{O_2} was observed until 2.5 h where the glucose pulse was exhausted whereafter q_{O_2} increased back to its original level before the pulse.

The long term response of the glucose pulse showed that the cultivation did not return to an oxidative steady-state within the first 50 h after the pulse (figure 7.8). An apparent oxido-reductive steady-state seemed to be reached after 35 h where the ethanol concentration (and gas signals) remained constant for 10 h. However, at 48 h the ethanol concentration began to decrease along with a slow increase in q_{O_2} suggesting that the culture eventually would return to a oxidative steady-state and that the apparent oxido-reductive steady-state at D=0.24 h^{-1} was unstable.

No inhibitory effect of ethanol on the respiratory system was observed when a 8 g/l ethanol pulse was added to a steady-state cultivation at D=0.24 h^{-1} since q_{O_2} actually increased (figure 7.9). The cells were only

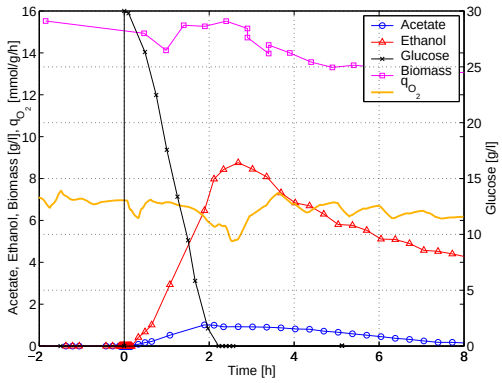

Figure 7.7. Experiment E1a: A glucose pulse of 30 g/l was added to a steady-state culture at D=0.24 h^{-1}. The specific oxygen uptake rate, q_{O_2}, is shown along with the glucose, ethanol, acetate and biomass concentrations as function of time.

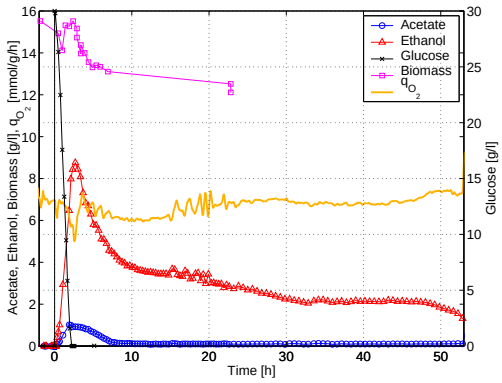

Figure 7.8. Long term response of the 30 g/l glucose pulse experiment shown in figure 7.7. Apparently an oxido-reductive steady-state was reached at 35 h, however this state was not stable since the ethanol concentration began to decrease at 48 h.

able to metabolise a small amount of ethanol (the ethanol uptake rate was around 1 C-mmol/g/h) and most of the ethanol was washed out. The ethanol pulse was followed by acetate formation and a maximal concentration of 0.47 g/l was observed 1.8 h after the pulse.

A 4 g/l acetate pulse showed an inhibitory effect on cell growth and on the respiratory system (figures 7.10-7.11). Immediately after the pulse, pH dropped to 3.3, but was restored within 10 min, q_{O_2} dropped from 6.1 to 2.3 mmol/g/h showing that the respiratory system was inhibited by either acetate or a low pH value. Since the RQ profile in figure 7.10 increased to 2.5, indicating oxido-reductive growth, the glucose uptake system was

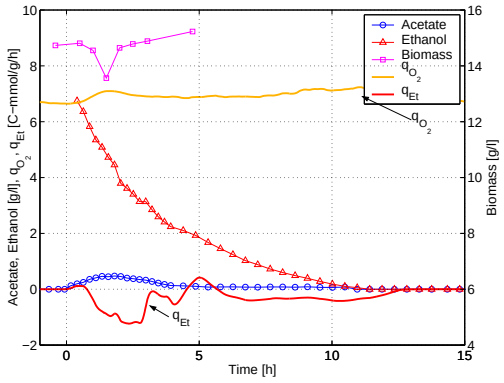

Figure 7.9. Experiment E1b: An ethanol pulse of 8 g/l was added to a steady-state culture at D=0.24 h^{-1} at time 0 h. Specific rates of oxygen uptake and ethanol production are shown along with ethanol, acetate and biomass concentrations as function of time.

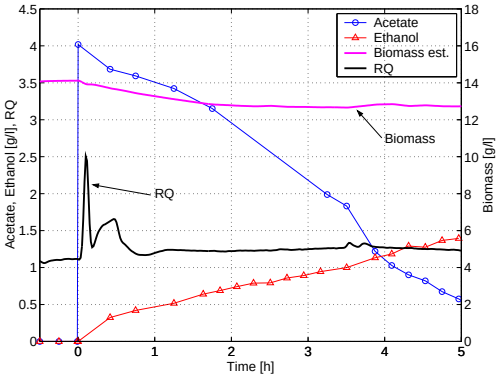

Figure 7.10. Experiment E1c: An acetate pulse of 4 g/l was added to a steady-state culture at D=0.24 h^{-1}. Ethanol and acetate concentrations are shown along with a biomass estimate based on the elementary balances and the respiratory quotient (RQ) as function of time.

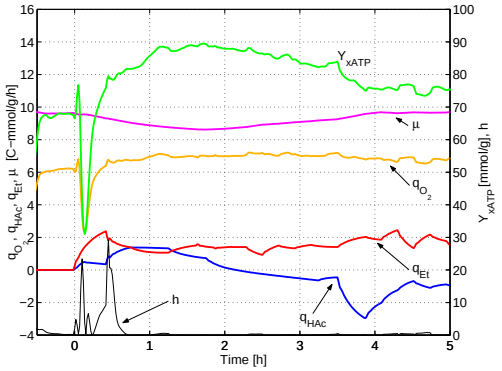

Figure 7.11. Specific rates for growth (μ), oxygen uptake (q_{O_2}) and ethanol production (q_{Et}) are shown together with the biomass/ATP yield coefficient (Y_{xATP}) and a statistical test (h) for the same experiment as shown in figure 7.10.

either not inhibited or inhibited less than the respiratory system during the experiment. Consequently, overflow occurred at the pyruvate branchpoint resulting in ethanol, and most interestingly, acetate production. From 0.15 h, q_{O_2} increased to 7.0 mmol/g/h which was a higher level than before the pulse, however ethanol production continued. The Y_{xATP} level increased from 68 to 90 mmol/g the first 2 h after the pulse, whereafter Y_{xATP} decreased to 75 mmol/g after 5 h (figure 7.11).

7.3.3 Closed loop operation in the oxido-reductive region

By operating continuous cultivations in closed loop, the dilution rate was manipulated in order to track different ethanol setpoints.

7.3.3.1 Shift-up in ethanol setpoint

The response of a continuous culture to an increase in the ethanol setpoint from 0.1 to 3.7 g/l is shown in figures 7.12-7.13. The desired ethanol concentration was obtained using a dilution rate controller. The controller initially increased the dilution rate in order to increase the ethanol concentration. After 2 h the controller began to decrease the dilution rate and eventually a steady-state was obtained at the desired ethanol concentration.

The first 20 minutes after the setpoint change, q_{O_2} increased with the dilution rate, whereafter q_{O_2} decreased until 2.5 h. From 2.5 h, q_{O_2} increased

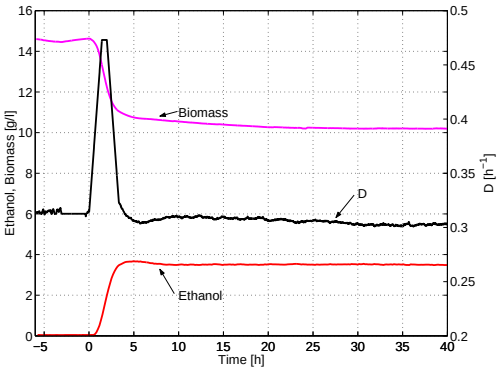

Figure 7.12. Experiment C7b: The ethanol setpoint was increased from 0.1 g/l to 3.6 g/l at time 0 h. The dilution rate was controlled in closed loop based on an ethanol measurement in order to track the desired ethanol setpoint. The biomass concentration was estimated from the base signal.

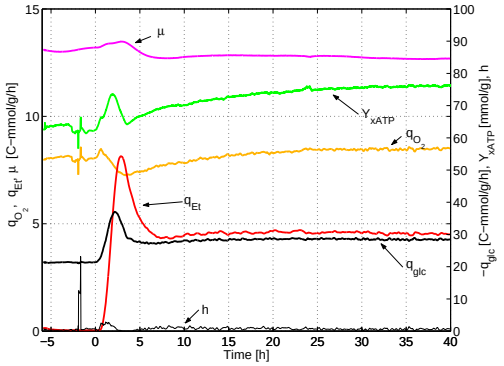

Figure 7.13. Specific rates for growth (μ), oxygen uptake (q_{O_2}), ethanol formation (q_{Et}) and glucose uptake (-q_{glc}) for the setpoint change shown in figure 7.12.

slowly until a steady-state was reached after 40 h. The q_{O_2} obtained at the new steady-state was slightly larger than before the setpoint change.

The dilution rate corresponding to the new steady-state was lower that the steady-state dilution rate before the setpoint change. This multiplicity was not caused by a decrease in q_{O_2}, but was instead due to the decreasing efficiency of ATP production/utilisation illustrated by the increasing Y_{xATP} in figure 7.13.

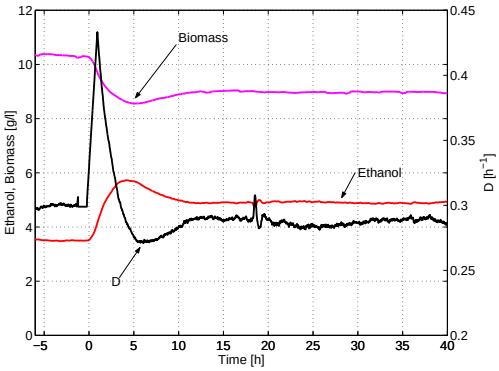

Figure 7.14. Experiment C7c: The ethanol setpoint was increased from 3.6 g/l to 4.9 g/l at time 0 h. The dilution rate controller was tuned rather aggressively resulting in an overshoot of the ethanol concentration.

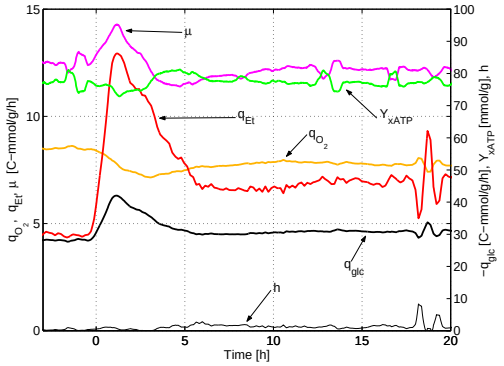

Figure 7.15. Specific rates for growth (μ), oxygen uptake (q_{O_2}), ethanol formation (q_{Et}) and glucose uptake (-q_{glc}) for the setpoint change shown in figure 7.14.

In a setpoint tracking experiment where the ethanol concentration was increased from 3.6 to 4.9 g/l (figures 7.14-7.15), the q_{O_2} decreased from 8.18 to 7.15 mmol/g/h as the dilution rate was increased to 0.43 h^{-1} during the first 3 h. Although q_{O_2} increased when the dilution rate was decreased after 3 h, q_{O_2} only reached a level of 7.71 mmol/g/h after 20 h and did not return to its initial value as observed during the ethanol setpoint change from 0.1 to 3.6 g/l (figure 7.13).

7.3.3.2 Relations between the oxidative phosphorylation and glucose uptake rate/glycolytic flux

The relation between q_{O_2} and -q_{glc} is illustrated in figure 7.16 where the specific oxygen uptake rate is plotted vs. the glucose uptake rate for three experiments where the ethanol setpoint was increased (C7b, C7c, C7d). Furthermore, the results from the dilution rate shift-up/down experiment shown in figures 7.5-7.6 are included in the figure (C7a). From this experiment, only the data between 40 and 180 h were plotted to obtain less confusing figures. In figure 7.17 the glycolytic flux (q_{gly}) is compared with q_{O_2}.

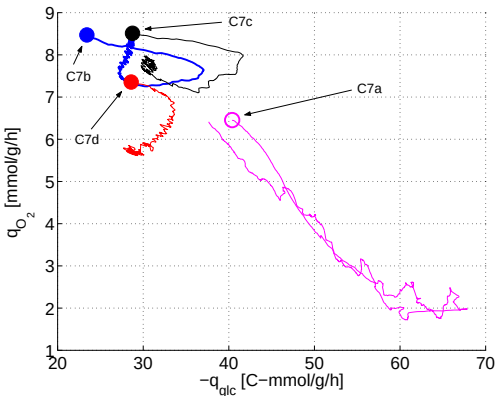

Figure 7.16. Phase plot of the relationship between the specific oxygen uptake rate (q_{O_2}) and the glucose uptake rate (-q_{glc}). In C7b-d the ethanol setpoint was increased (C7b: 0.1 to 3.6 g/l, C7c: 3.6 to 4.9 g/l and C7d: 4.9 to 6.1 g/l), while C7a is the same experiment as shown in figure 7.5 (from 40 to 180 h). A circle indicates the start of each experiment; open circle - open loop and full circle - closed loop.

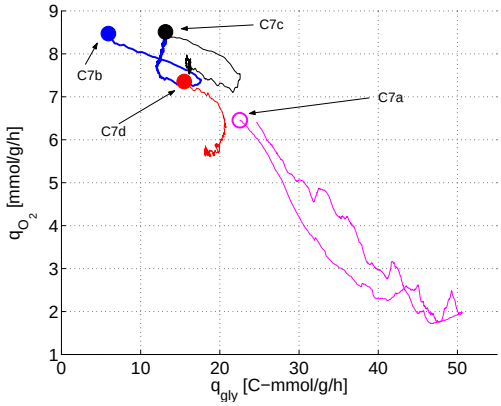

Figure 7.17. Relationship between the specific oxygen uptake rate (q_{O_2}) and the glycolytic flux (q_{gly}) calculated from a metabolic flux model for the same four experiments as shown in figure 7.16.

The comparison between the four experiments show an interesting pattern with respect to the repression and derepression of q_{O_2}. In the C7a

and C7b, the respiratory system became fully derepressed and q_{O_2} reached back to its original level. In C7c, q_{O_2} began to increase as -q_{glc} and q_{gly} decreased, however q_{O_2} did not increase to its original level indicating that a full derepression did not occur. In C7d, q_{O_2} did not increase at all throughout the experiment even when -q_{glc} (and q_{gly}) decreased.

7.3.3.3 Shift-down in ethanol setpoint

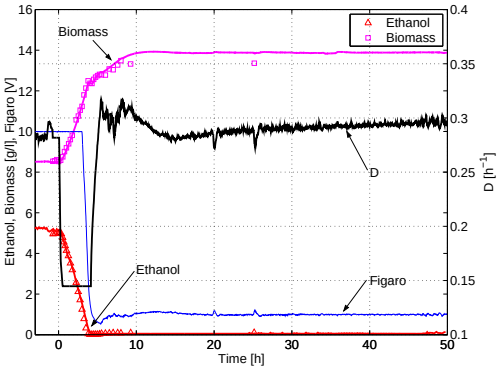

Figure 7.18. Experiment C8c: The ethanol setpoint was decreased from 4.9 g/l to 0.1 g/l at time 0 h. The new ethanol setpoint corresponded to 1.0 V on the reducing gas sensor (Figaro)

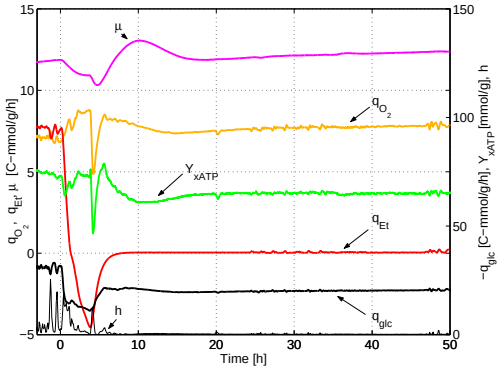

Figure 7.19. Specific rates for growth (μ), oxygen uptake (q_{O_2}), ethanol formation (q_{Et}) and glucose uptake (-q_{glc}) for the setpoint change shown in figure 7.18.

The dynamics of derepression of the respiratory system was studied by performing a shift-down in the ethanol setpoint from 4.9 to 0.1 g/l (figures 7.18-7.19). Immediately after the setpoint change, the dilution rate controller decreased the dilution rate to the lower allowed limit of 0.14 h^{-1} until almost all ethanol was exhausted. A depression of the respiratory system was observed as q_{O_2} increased from 7.1 to 8.8 mmol/g/h as the ethanol concentration decreased. When the controller increased the dilution rate to track the desired ethanol setpoint (0.1 g/l, Figaro 1 V) from 6 to 12 h, q_{O_2} decreased slightly (from 8.2 to 7.4 mmol/g/h). However, after 12 h it increased slowly to 8.0 mmol/g/h at 50 h. The slow increase in q_{O_2} from 12 to 50 h was accompanied by an increase in the dilution rate (0.284 to 0.300 h^{-1}). A similar increase in q_{O_2} (and D) was also observed in (Lei, 2001, chap.5) during determination of the critical dilution rate.

Y_{xATP} decreased from 75 to 65 mmol/g during the setpoint change indicating that the ATP production/utilisation efficiency in the cells were higher at the new growth conditions. This corresponds well with the results obtained during an ethanol setpoint increase from 0.1 to 3.6 g/l (figure 7.13) where Y_{xATP} increased as well.

7.3.3.4 Accelero-productostat

In the investigation of multiple steady-states in (Lei, 2001, chap.5) no steady-states have been obtained in closed loop at ethanol concentrations above 6.1 g/l. To study the steady-state behaviour at high ethanol concentrations the bioreactor was operated in closed loop and the ethanol setpoint was increased as ramp from 4.9 to 10 g/l over 90 h (figures 7.20-7.21). This operation mode, also referred to as an accelero-productostat, was chosen to avoid wash-out scenarios which were observed when the ethanol setpoint was increased stepwise from a steady-state with an ethanol concentration above 5 g/l Lei (2001, chap.5).

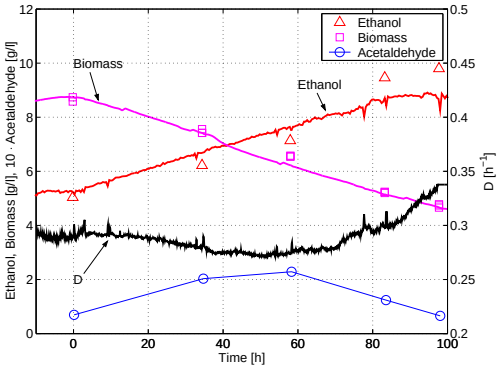

Figure 7.20. Experiment C8d: The ethanol setpoint was increased as a ramp from 4.9 to 10 g/l over 90 h. Off-line measurements of ethanol (△), biomass (□) and acetaldehyde (○) are shown as symbols, whereas full lines for biomass and ethanol are estimates (base and CHx signals).

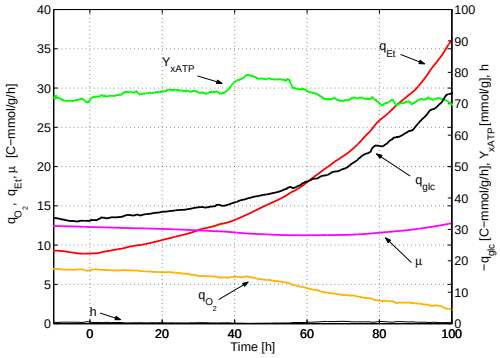

Figure 7.21. Specific rates for growth (μ), oxygen uptake (q_{O_2}), ethanol formation (q_{Et}) and glucose uptake (-q_{glc}) for the setpoint change shown in figure 7.20.

As the ethanol setpoint was increased, the dilution rate initially decreased from 0.293 to 0.271 h^{-1}, however after 50 h the dilution rate began to increase. At 90 h the controller was not able to track the ethanol concentration and the dilution rate increased to the upper limit of the controller: 0.338 h^{-1}. The q_{O_2} decreased throughout the experiment and, as observed in other setpoint change experiments, the decrease in q_{O_2} was accompanied by an increase in the specific glucose uptake rate (-q_{glc}).

The Y_{xATP} increased from 70 to 79 mmol/g during the first 50 h, whereafter it decreased back to 70 mmol/g. Interestingly, the acetaldehyde concentration exhibited a similar pattern reaching its maximal concentration (220 mg/l) after 60 h. Furthermore, the two effects causing the multiplicity (repression of the respiratory system and a decreasing efficiency of the ATP production/utilisation) were also observed during the ramp experiment (figure 7.21).

To illustrate that multiple quasi-steady-states for a region of dilution

rates were obtained during the ramp experiment the biomass and ethanol profiles from figure 7.20 are plotted versus the dilution rate in figure 7.22. Although the figure does not show *true* steady-states as defined in (Lei, 2001, chap.5), the result fits well with the steady-state results from (Lei, 2001, chap.5).

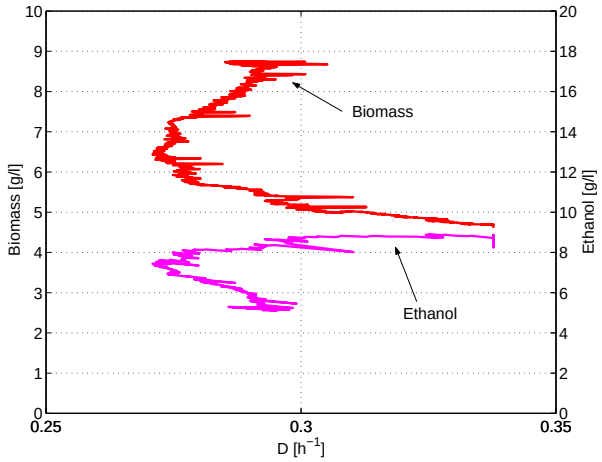

Figure 7.22. Experiment C8d: The biomass and ethanol concentrations from the accelero-productostat experiment (figure 7.20) are shown as function of the dilution rate to illustrate that multiple quasi steady-states were obtained for a region of dilution rates during the ramp.

7.4 Discussion

In this paper, the regulation of the respiratory system (q_{O_2}) and the efficiency of the ATP production/utilisation (Y_{xATP}) were studied during dynamic conditions. The discussion is structured in the following manner: First the regulation of the respiratory system is discussed by considering the dynamics of its repression and derepression. Secondly, the response of Y_{xATP} during the various dynamic experiments will be discussed. Finally, the steady-state results from Lei (2001, chap.5) showing multiplicity are re-evaluated by taking the the history of the culture into account.

7.4.1 Dynamics for regulation of the respiratory system

The response of q_{O_2} to a sudden increase in dilution rate (shift-up) in continuous cultivations of *S. cerevisiae* has been studied extensively by Duboc (1997). An immediate increase in the catabolic activity has been observed (as a jump in q_{O_2} and q_{CO_2}) when the dilution rate was increased from an oxidative steady-state. Subsequently, q_{O_2} increased further over a period of 4-6 h. In this work, however, during a shift-up from oxidative

growth to a dilution rate within the oxido-reductive region, it was observed that q_{O_2} did not stay at its maximal level but began to decrease (figure 7.2) indicating an increased repression of the respiratory system. Repression of the respiratory system was also observed when the dilution rate was increased from an oxido-reductuve steady-state both in open loop (when D was increased at 0 h in figure 7.6) and in closed loop (during the first 3 h as D was increased in figures 7.13 and 7.15) experiments.

Derepression of the respiratory system was obtained during dilution rate shift-down experiments (figures 7.4, 7.6 and 7.19), where a prolonged increase in q_{O_2} was observed until ethanol was exhausted.

It has been suggested that the *HAP4* gene is involved in the regulation of the respiratory system (Blom *et al.*, 2000), where Hap4p is a subunit of the Hap2/3/4/5 complex which acts as a mitochondrial promoter activator. The expression of *HAP4* has been found to be repressed by Snf1p which is a key regulatory gene in the signalling pathway of glucose repression (Johnston, 1999). Thus, it might be that the repression of the respiratory system is related to glucose repression, although unknown factors can be involved in the repression of the respiratory system.

The mechanisms of glucose sensing and how an intracellular signal for the glucose repression pathway is generated are still being studied, however it is now generally accepted that phosphorylation of glucose by either hexokinases or glucokinases is required for glucose repression (Scheffler *et al.*, 1998). The presented results of the relationship between q_{O_2} and -q_{glc} (figures 7.16) showed that the repression of the respiratory system was related to the glucose uptake rate and thereby the phosphorylation rate of intracellular glucose. Hence, it might be speculated that the repression of the respiratory system is mediated through the glucose repression pathway via Reg1p, Snf1p and the Hap2/3/4/5 complex originating from the phosphorylation of intracellular glucose. The derepression mechanism of the respiratory system seemed to be even more complex since it was observed that a derepression might occur when -q_{glc} (and q_{gly}) was decreased (C7a and C7b), however a fully derepression did not occur at higher ethanol concentrations (C7c and C7d).

It has been proposed by Herwig *et al.* (2001b) that the specific glycolytic flux has an repressing effect on the respiratory system. The relationship between q_{O_2} and q_{gly} can also be identified in figure 7.17, however from the presented results, i.e. the similarities between figures 7.17 and 7.16, it is not possible to draw any definite conclusion on whether repression of the respiratory system is more dependent on the glycolytic flux than the specific glucose uptake rate.

7.4.1.1 Derepression of the respiratory system: Effect of operation mode

The difference between open and closed loop operation with respect to derepression of the respiratory system can also be elucidated by consider-

ing the phase plots of q_{O_2} against -q_{glc} or q_{gly} (figures 7.16-7.17).

In the closed loop experiments C7c and C7d, q_{O_2} decreased as the ethanol setpoint was increased, however q_{O_2} did not increase back to its original level at steady-state as opposed to experiment C7b. To explain these observations, a hypothesis is proposed: *For a derepression of the respiratory system to occur a certain decrease in the glycolytic flux is required at high glycolytic fluxes (i.e. high ethanol concentrations).* During closed loop operation the glycolytic flux is tightly controlled (the glycolytic flux is closely related to the ethanol concentration) and the decrease in the glycolytic flux required for derepression is therefore not always obtained during an ethanol setpoint increase in closed loop operation. Therefore derepression of the respiratory system will not occur at high glycolytic fluxes (and ethanol concentrations) in closed loop operation mode. This hypothesis can explain the observed behaviour in experiments C7b-C7d. In experiment C7b, the glycolytic flux (and ethanol concentration) were apparently sufficiently low such that a derepression could occur without a decrease in the glycolytic flux (figure 7.17), whereas this was not the case in experiments C7c and C7d.

The above hypothesis also explains the behaviour observed in experiment C7a when a derepression of the respiratory system occurred as a dilution rate shift-down was performed (figure 7.6). When the dilution rate was decreased at 107 h, the glycolytic flux (experiment C7a in figure 7.17) decreased sufficiently to enable a derepression of the respiratory system and thereby an increase in q_{O_2}. Since the cultivation was operated in open loop, the increased q_{O_2} led to a decrease in ethanol concentration. Subsequently, the biomass concentration increased leading to a even lower q_{gly} and further derepression. Since there was no control of the glycolytic flux during the experiment, q_{gly} therefore continued to decrease upon the dilution rate shift-down until all ethanol was consumed (see figure 7.6). Thus, closed loop operation indirectly controls the glycolytic flux such that a full derepression of the respiratory system cannot be obtained at high values of the ethanol concentration and the glycolytic flux whereas this is possible during open loop operation. It is important to stress that it is *a negative change* in the glycolytic flux that is required for derepression of the respiratory system. Derepression might therefore occur at high glycolytic fluxes (e.g. C7a) and not at lower glycolytic fluxes (e.g. C7d) depending on how the glycolytic flux is changed.

Consequently, the degree of repression of the respiratory system at a given oxido-reductive steady-state does not only depend on the current steady-state values of all metabolites and fluxes, but is also a function of the operation mode and thereby the history of the culture. Since the ethanol concentration for a fixed dilution rate depends heavily on the value of q_{O_2}, the high sensitivity of q_{O_2} towards the operation mode and history of the culture makes it very difficult to obtain reproducible oxido-reductive steady-states both in open and closed loop.

7.4.2 Y_{xATP}

It was observed that Y_{xATP} was larger than its initial value during the first 1.5 h following the dilution rate shift-ups from oxidative growth (figures 7.2 and 7.4). A similar response has also been observed by van Urk *et al.* (1988) when a glucose pulse was added to an oxidative continuous cultivation at D=0.1 and 0.2 h^{-1}. van Urk *et al.* have compared the total ATP production from catabolism with the ATP needed for growth and it has been observed that during the first 30 min after the pulse much more ATP was produced that was needed for growth, corresponding to an increase in Y_{xATP}. The increase in Y_{xATP} is also be related to the decoupling between anabolism and catabolism which has been described by Duboc *et al.* (1998). This decoupling occurs since the cells cannot increase the anabolic machinery (ATP utilisation) as quickly as the catabolic machinery (ATP production).

It has been found that Y_{xATP} was approximately constant at oxidative growth, whereas Y_{xATP} increased for the steady-states obtained in closed loop with an ethanol concentration between 0.1 and 6 g/l (Lei, 2001, chap.5). However, at an ethanol concentration of 11 g/l, Y_{xATP} had the same lower level as during oxidative growth. The same trend was observed repeatedly in this study and is best illustrated in figures 7.13, 7.19 and 7.21. In figure 7.13, a clear increase in Y_{xATP} was observed as the ethanol concentration increased, whereas Y_{xATP} decreased with the decreasing ethanol concentration in figure 7.19. The dynamics of Y_{xATP} during these two experiments was similar to the dynamics of q_{O_2}, where Y_{xATP} increased along with q_{O_2}. During the ethanol setpoint ramp (figure 7.21), however, Y_{xATP} showed a significantly different dynamics than q_{O_2}. Y_{xATP} reached its maximal value at an ethanol concentration of 7 g/l whereafter it decreased. Interestingly, the acetaldehyde concentration peaked at the same time as Y_{xATP}, a relationship which also was observed by Lei (2001, chap.5). It has previously been observed that acetaldehyde inhibits growth (Stanley *et al.*, 1993) and the current results suggests that acetaldehyde acts as an inhibitor on cell growth by decreasing the efficiency of either ATP production (P/O ratio) or ATP utilisation.

Whether the strong decrease in q_{O_2} immediately after the acetate pulse was due to an inhibitory effect on the oxidative phosphorylation by acetate or caused by a drop in pH to 3.3 for 10 min remains unclear. However, after 0.5 h, when the cultivation was back to the same q_{O_2} level as before the pulse, Y_{xATP} was much higher than before the pulse, indicating a decreased ATP production/utilisation efficiency. Even though q_{O_2} increased further, ethanol production continued. Probably the acetate pulse causes an uncoupling effect at the plasma membrane (Verduyn *et al.*, 1992) resulting in a drain of ATP for maintaining the intracellular pH (protons need to be pumped out of the cell by plasma membrane ATPase) and thereby a less efficient ATP utilisation for growth.

It is interesting to note that during derepression of the respiratory sys-

tem (figures 7.4, 7.6 and 7.19), Y_{xATP} increased and the cells obtained a less efficient ATP production/utilisation. This observation might provide a possible explanation of why glucose repression of the respiratory system takes place in *S. cerevisiae*: The low ATP production/utilisation efficiency of a derepressed oxido-reductive state is not desirable for the cells, which therefore represses the respiratory system in order to operate more efficiently. However, why a derepression of the respiratory system leads to a higher Y_{xATP} remains to be established.

7.4.3 Multiple steady-states

The region of dilution rates where multiple steady-states exist in a continuous cultivation of *S. cerevisiae* can be investigated in several ways: By operating a continuous cultivation as a chemostat (open loop), as a productostat (closed loop) or as an accelero-productostat, where the ethanol setpoint is changed as a ramp.

If the region around D_{crit} is investigated in open loop, first by increasing D and subsequently decreasing D to check whether multiple steady-states exist, the range of dilution rates where multiplicity occurs will be rather small. If only fully derepressed steady-states are obtained below D_{crit} as D is decreased, the multiplicity will only be caused by an increase in Y_{xATP} with increasing ethanol concentrations as observed in figures 7.12-7.13. Closed loop operation, on the contrary, where the ethanol setpoint is increased stepwise will result in oxido-reductive steady-states far below D_{crit} (Lei, 2001, chap.5). It can therefore be concluded that oxido-reductive steady-states far below D_{crit} only can be obtained through closed loop operation where the derepression of the respiratory system is avoided by controlling the glycolytic flux. However, by investigating the multiple steady-state region in an accelero-productostat, both the derepression effect observed during dilution rate shift-downs in a chemostat and the repression effect by sudden increases in dilution rate during a setpoint change in a productostat, can be diminished.

It was shown that it is possible to obtain oxido-reductive growth for a prolonged period below D_{crit} in open loop operation. When a glucose pulse was added to an oxidative growing culture, ethanol production continued in more than 50 h (figure 7.8). Axelsson *et al.* (1992) has also shown that by increasing the dilution rate from just below D_{crit} to a high value (D=0.4 h^{-1}) for one hour and then back to its original value, oxido-reductive growth continued for 65 h, where an oxido-reductive steady-state was assumed.

In order to develop a mathematical model exhibiting multiple steady-states for a continuous yeast cultivation, Axelsson *et al.* (1992) have included inhibition of the respiratory system by ethanol. However, in this work an ethanol concentration less than 8 g/l did neither repress nor inhibit the respiratory system (figure 7.9), indicating that the ethanol con-

centration does not seem to play a role in the repression of the respiratory system observed in this work.

7.5 Conclusions

The flux through the oxidative phosphorylation in *S. cerevisiae* was found to decrease upon an increase in the dilution rate within the oxido-reductive growth regime due to repression of the respiratory system. It was possible to the alleviate the repression through a dilution rate shift-down which resulted in an increasing specific oxygen uptake rate, q_{O_2}. When a dilution rate shift-down was performed to a dilution rate below D_{crit}, q_{O_2} kept on increasing until ethanol was exhausted.

The repression and derepression of the respiratory system was strongly related to changes in the glycolytic flux. It was found that an increasing glycolytic flux was required for repression of the respiratory system, whereas a derepression could occur without a decrease in the glycolytic flux at conditions with a low glycolytic flux and a low ethanol concentration.

It was shown that the ethanol concentration is not uniquely defined by the dilution rate at an oxido-reductive steady-state but also is a function of the degree of repression of the respiratory system. Through closed loop control of the dilution rate, it was possible to obtain oxido-reductive steady-states at dilution rates far below D_{crit} due to a strong repression of the respiratory system. These steady-states could, however, not be obtained in open loop, since a dilution rate shift-down from an oxido-reductive steady-state led to a derepression of the respiratory system. It can therefore be concluded that the range of dilution rates where multiple steady-states can be obtained differs depending on the operation mode and that this multiplicity dilution rate range is larger for closed loop than open loop operation.

It should still be possible to obtain oxido-reductive steady-states below D_{crit} through open loop operation due to the increase in Y_{xATP} at oxido-reductive growth. However, the effect of Y_{xATP} on multiple steady-states seemed to be much less pronounced than the effect of repression of the respiratory system and is therefore difficult to decouple from the repression. The effect of Y_{xATP} should therefore be studied in *S. cerevisiae* strains where the repression of the respiratory system is less pronounced than for the strain used in this work and through experiments where sudden changes in the dilution rate, which causes repression, are avoided. The latter requirement can be satisfied in an accelero-productostat, where the setpoint of the dilution rate controller is changed as a ramp. Thus, the accelero-productostat represents a promising tool for further investigations of multiple steady-state in continuous yeast cultivations.

Although, it might be difficult to obtain oxido-reductive steady-states below D_{crit} in open loop, transients with ethanol formation below D_{crit}

can easily be triggered by sudden increases in the glucose feed. It was observed that more than 50 h of cultivation could be required before ethanol had disappeared from a culture when exposed to a glucose pulse. This behaviour is highly undesirable from a production point of view, since ethanol formation equals decreasing biomass productivity. However, by using closed loop control of the dilution rate such scenarios can be avoided.

List of symbols

CH_x	measurement of CH_x content in outlet gas from gas analyser [V]
D	dilution rate [h^{-1}]
D_{crit}	critical dilution rate [h^{-1}]
$EtOH$	ethanol concentration [g/l]
h	statistical test for data quality []
q_{CO_2}	specific carbon dioxide production rate [mmol/g/h]
q_{Et}	specific ethanol production rate [C-mmol/g/h]
$-q_{glc}$	specific glucose uptake rate [C-mmol/g/h]
q_{gly}	glycolytic flux [C-mmol/g/h]
q_{HAc}	specific acetate production rate [C-mmol/g/h]
q_{O_2}	specific oxygen uptake rate [mmol/g/h]
μ	specific growth rate [C-mmol/g/h]
μ_{max}	maximum specific growth rate [h^{-1}]
RQ	respiratory quotient (q_{CO_2}/q_{O_2}) []
Y_{xATP}	yield coefficient: ATP per dry weight biomass [mmol/g]

References

Axelsson, J.; Münch, T. and Sonnleitner, B. (1992). Multiple steady-states in continuous cultivation of yeast. *IFAC Modelling and Control of Biotechnical Processes, Colorado, USA*, **10**, 383–386.

Blom, J.; de Mattos, M. and Grivell, L. (2000). Redirection of the respiro-fermentative flux distribution in *Saccharomyces cerevisiae* by overexpression of the transcription factor Hap4p. *Appl Environ Microbiol*, **66**, 1970–1973.

Christensen, L.; Marcher, J.; Schulze, U.; Carlsen, M.; Min, R. and Villadsen, J. (1996). Semi-on-line analysis for fast and precise monitoring of bioreaction processes. *Biotechnol. Bioeng.*, **52**, 237–247.

Crabtree, H. (1929). Observations on the carbohydrate metabolism of tumours. *Biochem. J.*, **21**, 536–545.

de Deken, R. (1966). The Crabtree effect: A regulatory system in yeast. *J. Gen. Microbiol.*, **44**, 149.

Duboc, P. (1997). *Transient growth of Saccharomyces cerevisiae, a quantitative approach*. Ph.D. thesis, Swiss Federal Institute of Technology, Lausanne, Switzerland.

Duboc, P.; Stockar, U. v. and Villadsen, J. (1998). Simple generic model for dynamic experiments with *Saccharomyces cerevisiae* in continuous culture: Decoupling between anabolism and catabolism. *Biotechnol. Bioeng.*, **60**, 180–189.

Fiecther, A.; Fuhrmann, G. and Käppeli, O. (1994). Regulation of glucose metabolism in growing yeast cells. *Adv. Microb. Physiol.*, **36**, 145–180.

Heijden, R. v. d.; Romein, B.; Heijnen, J.; Hellinga, C. and Luyben, K. (1994). Linear constraint relations in biochemical reaction systems: I, Classification of the calculability and the balanceability of conversion rates. *Biotechnol. Bioeng.*, **43**, 3–10.

Herwig, C.; Marison, I. and von Stockar, U. (2001a). On-line stoichiometry and identification of metabolic state under dynamic process conditions. *Biotechnol. Bioeng.*, page accepted for publication.

Herwig, C.; Marison, I. and von Stockar, U. (2001b). The role of acetate and repression of the oxidative phosphorylation by the glycolytic flux during transient conditions. *Biotechnol. Bioeng.*, **??**, not even submitted.

Johnston, M. (1999). Feasing, fasting and fermenting, glucose sensing in yeast and other cells. *TIG*, **15**, 29–33.

Käppeli, O.; Lorencez-Gonzales, I.; Kuhne, I. and Sonnleitner, B. (1988). Title not known. *8th Int. Biotechnology Symposium*, pages 467–478.

Lei, F. (2001). *Dynamics and nonlinear phenomena in continuous cultivations of* Saccharomyces cerevisiae. Ph.D. thesis, KT, Technical University of Denmark.

Lei, F.; Rotbøll, M. and Jørgensen, S. (2001). A biochemically structured model for *Saccharomyces cerevisiae*. *Accepted for publication in J. Biotechnol.*.

Nielsen, J. and Villadsen, J. (1994). *Bioreaction Engineering Principles*. Plenum Press.

Pham, H.; Larsson, G. and Enfors, S.-O. (1998). Growth and energy metabolism in aerobic fed-batch cultures of *Saccharomyces cerevisiae*: Simulation and model verification. *Biotechnol. Bioeng.*, **60**, 474–482.

Postma, E.; Verduyn, C.; Scheffers, A. and van Dijken, J. (1989). Enzymic analysis of the Crabtree effect in glucose-limited chemostat cultures of *Saccharomyces cerevisiae*. *Appl. Env. Microbiol.*, **55**, 468–477.

Rothen, S.; Saner, M.; Meenakshisundaram, S.; Sonnleitner, B. and Fiechter, A. (1996). Glucose uptake kinetics of *Saccharomyces cerevisiae* monitored with a newly developed FIA. *J. Biotechnol.*, **50**, 1–12.

Scheffler, I.; de la Cruz, B. and Prieto, S. (1998). Control of mRNA turnover as a mechanism of glucose repression in *Saccharomyces cerevisiae*. *Int. J. Biochem. Cell Biol.*, **30**, 1175–1193.

Sonnleitner, B. and Hahnemann, U. (1994). Dynamics of the respiratory bottleneck of Saccharomyces cerevisiae. *J. Biotechnol.*, **38**, 63–79.

Stanley, G. A.; Douglas, N. G.; Every, E. J.; Tzanatos, T. and Pamment, N. B. (1993). Inhibition and stimulation of yeast growth by acetaldehyde. *Biotech Letters*, **15**(12), 1199.

van Dijken, J. and Scheffers, W. (1986). Redox balances in the metabolism of sugars by yeasts. *FEMS Microbiol. Rev.*, **32**, 199–224.

van Urk, H.; Mak, P.; Scheffers, W. and van Dijken, J. (1988). Metabolic responses of *Saccharomyces cerevisiae* CBS8066 and *Candida utilis* CBS 621 upon transition from glucose limitation to glucose excess. *Yeast*, **4**, 283–291.

Verduyn, C.; Postma, E.; Scheffers, W. and van Dijken, J. (1992). Effect of benzoic acid on metabolic fluxes in yeasts: A continuous culture study on the regulation of respiration and alcoholic fermentation. *Yeast*, **8**, 501–517.

Wang, N. and Stephanopoulos, G. (1983). Application of macroscopic balances to the identification of gross measurement errors. *Biotechnol. Bioeng.*, **25**, 2177–2208.

8

Acetate production in *S. cerevisiae* during growth on glucose

Acetate production in S. cerevisiae *was studied during aerobic growth on glucose through dynamic experiments in continuous cultivations. The amount of acetate formed during a dilution rate shift-up was dependent on the initial dilution rate before the shift-up; a shift-up from a low dilution rate (D=0.085 to 0.31 h^{-1}), yielded the largest acetate accumulation (1.0 g/l). The maximal acetate production rate was observed approximately 1 h after the dilution rate was increased in all experiments. The dynamics of acetate production was shown neither to be controlled by the enzyme activities of acetaldehyde dehydrogenase (ACDH) and acetyl-CoA synthetase (ACS), nor acetaldehyde inhibition of ACDH. Instead, it was proposed that the mitochondrial NAD^+ concentration is involved in the control of the acetate production during an increase in dilution rate.*

8.1 Introduction

Acetate is excreted as a by-product during alcoholic fermentation by *Saccharomyces cerevisiae*. In beer and vine production, the acetate concentration should be kept below a threshold value (0.4 g/l in beer and 0.8 g/l in wine) to comply with product quality requirements (Hough *et al.*, 1982; Fleet and Heard, 1992). During aerobic growth in baker's yeast and heterologous protein production, acetate and ethanol are undesirable by-products. Whereas ethanol formation in *S. cerevisiae* has been studied extensively during both aerobic (Meyenburg, 1969; Rieger *et al.*, 1983; Pham *et al.*, 1998) and anaerobic conditions (Verduyn *et al.*, 1990; Nissen *et al.*, 1997) and is quite well understood, several questions are still unanswered regarding the mechanisms leading to acetate production in *S. cerevisiae*.

The aim of this work was to obtain an increased understanding of how acetate production in *S. cerevisiae* is controlled. During growth of *S. cerevisiae* on glucose, acetate is formed via the pyruvate dehydrogenase (PDH)

bypass when the PDH complex is saturated due to a limited capacity of the oxidative metabolism. The PDH-bypass involves three reactions converting pyruvate to acetyl-CoA: Pyruvate decarboxylase (PDC; EC 4.1.1.1), acetaldehyde dehydrogenase (ACDH; EC 1.2.1.5 and EC 1.2.1.4), and acetyl-CoA synthetase (ACS, EC 6.2.1.1) (figure 8.1). Acetyl-CoA is also produced from pyruvate by the pyruvate dehydrogenase complex (PDH; EC 1.2.4.1), a large mitochondrially located multienzyme complex. However, due to the inability of *S. cerevisiae* to transport acetyl-CoA from mitochodria to the cytosol, acetyl-CoA formed through the PDH bypass plays an essential role providing cytosolic acetyl-CoA, in particular for lipid synthesis (Flikweert *et al.*, 1996).

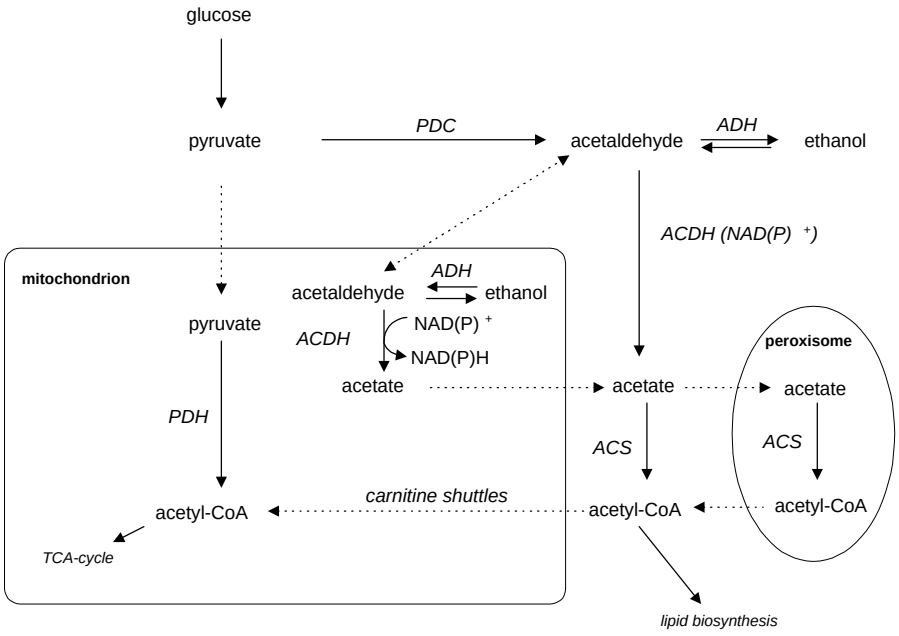

Figure 8.1. Schematic representation of the compartmentation of enzymes involved in the pyruvate metabolism: PDH (pyruvate dehydrogenase), PDC (pyruvate decarboxylase), ADH (alcohol dehydrogenase), ACDH (acetaldehyde dehydrogenase), and ACS (acetyl-CoA synthetase).

Six PDC genes, involved in the decarboxylation of pyruvate into acetaldehyde, have been described in literature. *PDC1*, *PDC5*, and *PDC6*, have been found to encode for structural genes whereas the gene products from *PDC2*, *PDC3*, and *PDC4*, are believed to be involved in the control of the expression of the structural genes (Hohmann, 1997). Recently, it has been observed that the amount of acetate formed by a *pdc*1Δ mutant during alcoholic fermentation on glucose (batch experiment) was similar to its wild-type, although the PDC activity was 4-fold lower in the mutant (Remize *et al.*, 2000). In contrast, a glucose pulse to a *pdc*2Δ mutant

growing oxidatively at D=0.1 h^{-1} resulted in an approximately two-fold lower acetate production (Flikweert *et al.*, 1999). The PDC activity of the *pdc*2Δ mutant was decreased 3-fold compared to the wild-type.

The oxidation of acetaldehyde to acetate is the second step in the PDH bypass and is carried out by two isoenzymes using either NAD^+ or $NADP^+$ as co-factor. A cytosolic and a mitochondrial enzyme have been isolated from *S. cerevisiae*. The cytosolic isoenzyme is Mg^{2+}-activated and $NADP^+$-specific, whereas the K^+-stimulated mitochondrial enzyme has a higher affinity for NAD^+, but also accepts $NADP^+$ (Jacobson and Bernofsky, 1974). The nomenclature for designating the genes responsible for ACDH activity has been rather confusing, but has recently been clarified (Navarro-Avino *et al.*, 1999). Three genes encode for the cytosolic isoenzyme: *ALD2*, *ALD3*, and *ALD6*, whereas *ALD4* and *ALD5* correspond to the mitochondrial enzyme. It has been proposed that the cytosolic $NADP^+$-dependent enzyme is responsible for acetate production during growth on glucose whereas the mitochondrial enzyme is more active during growth on ethanol (Llorente and de Castro, 1977). The *ALD6* gene encodes for the cytosolic, Mg^{2+}-activated acetaldehyde dehydrogenase (Meaden *et al.*, 1997) and its gene product Ald6p plays an important role in the control of acetate production on glucose, although it is not solely responsible for production of cytosolic acetyl-CoA. Deletion of *ALD6* resulted in a 30-60 % reduced NADP-dependent ACDH activity and a proportionally decrease in the acetate production without impairing the growth rate (batch experiments, Remize *et al.* (2000)). Furthermore, overexpression of *ALD6* led to an increase in the acetate production as well as the activity level of NADP-dependent ACDH suggesting that the level of Ald6p is involved in the control of acetate formation during growth on glucose (Remize *et al.*, 2000).

The last step in the PDH bypass is the conversion of acetate to acetyl-CoA mediated by ACS. Two structural genes encoding ACS, *ACS1* and *ACS2* have been described. Both genes are extramitochondrial and located in the cytosol (*ACS2*) and in the peroxisomal membrane (*ACS1*) (de Jong-Gubbels, 1998, chap.6). The transcription of *ACS1* is repressed by glucose (at concentrations above 100 mg/l) and to a lesser extent by ethanol (van den Berg *et al.*, 1996). Furthermore, its gene product, Acs1p, is subject to glucose catabolite inactivation (de Jong-Gubbels *et al.*, 1997). *ACS2*, on the other hand, is expressed constitutively and an *acs*2Δ mutant could not grow at high glucose concentrations in batch experiments (van den Berg *et al.*, 1996). ACS does not seem to be involved in the control of the acetate production. Overexpression of either *ACS1* or *ACS2* did not decrease the acetate production during exposure to excess glucose during oxidative growth in continuous cultivation at D=0.1 h^{-1}, although the ACS activity was increased 3-6 fold. Instead, overexpression of *ACS1* resulted in a two-fold increase in the acetate production (de Jong-Gubbels *et al.*, 1998). Remize *et al.* (2000) have also observed that overexpression

of *ACS2* did not have a significant effect on the acetate production during alcoholic batch fermentations.

It has been suggested that acetate production during transient aerobic growth on glucose might be partly controlled by the available capacity of the oxidative phosphorylation (Herwig and von Stockar, 2001). Consequently, large amounts of acetate can only be produced during conditions when overflow occurs at the pyruvate branchpoint and the reoxidation of NADH in the oxidative phosphorylation is *not* a limiting step in the metabolism (Herwig and von Stockar, 2001). Such conditions has been obtained through sudden increases in the dilution rate where it has been observed that the rate of dissimilation of pyruvate through the TCA cycle increase slower than the rate of NADH reoxidation in the oxidative phosphorylation (Herwig and von Stockar, 2001). As a result, significant amounts of acetate, but no ethanol, was formed during the first 3 h after the increase in dilution rate.

Although numerous mathematical models describing aerobic growth of *S. cerevisiae* have appeared during the last 15 years (Sonnleitner and Käppeli, 1986; Barford, 1990; Steinmeyer and Shuler, 1989; Villadsen and Nielsen, 1990; Sonnleitner and Hahnemann, 1994; Pham *et al.*, 1998; Lei *et al.*, 2001), a description of the acetate concentration has most often not been included. In the model proposed by Lei *et al.* (2001), acetate is included, however the acetate profiles predicted by the model did not fit very well with experimental data during neither dilution rate shift-up nor batch experiments and it was concluded that the acetate production during dynamic conditions could not be described properly in the proposed model (Lei *et al.*, 2001).

In the present work the role of acetate formation during dynamic conditions for aerobic growth of *S. cerevisiae* and the mechanisms involved the regulation of acetate production was studied based on dynamic experiments in continuous cultivations. *In-vitro* enzyme activity measurements were performed of ACDH and ACS in order to monitor the regulation of the maximal possible fluxes through the reactions in the PDH bypass. The experimental observations were compared with previous studies reported in literature and mathematical modelling of acetate production in *S. cerevisiae* during aerobic conditions was discussed.

8.2 Materials and methods

8.2.1 Strain and medium

The yeast *S. cerevisiae* CEN.PK113-7D was cultivated in an aerobic continuous culture. The substrate (glucose) concentration was 30 g/l and a defined medium was used (Lei, 2001, chap.5).

8.2.2 Preparation of inoculum

S. cerevisiae strain CEN.PK113-7D was taken from storage at -80°C and plated onto YPD agar plates and incubated at 30°C. After three days, a single culture was transferred to a shake-flask containing mineral medium (Lei, 2001, chap.5), at an initial pH of 6.5 and containing 1% (w/v) glucose. Cells, growing exponentially on glucose, were used as inoculum for the fermenter.

8.2.3 Equipment and analytical methods

The equipment and analytical methods (except for enzyme activity measurements) have been described previously in Lei (2001, chap.5) (set-up 1) and in Lei (2001, chap.7) (set-up 2).

8.2.3.1 Preparation of cell free extract

For preparation of cell free extracts, 4 ml culture samples were harvested by centrifugation (5000 rpm/5') and washed twice with 4 ml 10 mM potassium phosphate buffer (pH 7.5, containing 2 mM EDTA) before stored at -20°C. Before assaying, the samples were thawed at room temperature, washed and resuspended in a sonication buffer (100 mM potassium phosphate, pH 7.5, 2mM $MgCl_2$) whereafter 2 mM 1,4-dithiothreitol (DTT) was added. Extracts were prepared in a FastPrep instrument (FP120 FastPrep cell disruptor, Savent Instruments, NY, USA) using 0.2-0.5 mm diameter glass beads at 0°C ($2 \cdot 20$ sec). Unbroken cells, glass beads and debris were removed by centrifugation at 4°C (20 min at 19,000 g) and the clear supernatant was used as cell-free extract.

8.2.3.2 Enzyme activities

ACDH and ACS activities were assayed at 30°C immediately after preparation of the cell free extracts. The reaction rates were monitored by measurement of the production rate of NAD(P)H at 340 nm. The reaction rates were proportional with the amount of extract added. The protein content of the cell free extracts were determined by the Lowry method using bovine serum albumin as standard (Lowry *et al.*, 1951). The enzyme activities are given in U/mg protein, where U is μmol substrate/min.

Acetaldehyde dehydrogenases (NAD^+ and $NADP^+$): The assay mixture contained 100 mM potassium phosphate buffer (pH 8.0), 15 mM pyrazole, 0.4 mM dithiothreitol, 10 mM KCl and 0.4 mM NAD^+ or $NADP^+$. The reaction was started with 0.1 mM acetaldehyde (Postma *et al.*, 1989).

Acetyl-CoA synthetase: The assay mixture contained 100 mM Tris-HCl, 10 mM L-malate, 0.2 mM CoA, 8 mM ATP, 1 mM NAD, 10 mM $MgCl_2$, 18 U L-malate dehydrogenase and 3.3 U citrate synthase. The

reaction was started with 100 mM potassium acetate (van den Berg *et al.*, 1996).

8.2.4 Cultivation conditions

The data presented in this paper were obtained from two different experimental set-ups. An overview over all presented experiments is given in table 8.1 where a name has been assigned to each experiment. Experiments with the prefix **C** were carried out using set-up 1 at DTU, whereas experiments with prefix **E** were conducted as EPFL, Switzerland. The critical dilution rate for set-up 1 was determined to 0.31 h^{-1} while D_{crit}=0.27 h^{-1} for set-up 2. The experiments were conducted under two types of operation mode: Chemostat and productostat. In the first mode the dilution rate was only changed during dilution rate shift-ups or downs, whereas the dilution rate was controlled based on the ethanol concentration in the latter case (Lei, 2001, chap.5). The presented experiments are summarised in table 8.1.

Table 8.1. Overview of the conducted experiments.

Label	Experiment	Cultivation	Mode	Figures	Bio.
E2a	D: 0.15 $\rightarrow$ 0.25 h^{-1}	E2	C	8.2	+
E3a	D: 0.085 $\rightarrow$ 0.31 h^{-1}	E3	C	8.3,8.5	+
E3b	D: 0.085 $\rightarrow$ 0.285 $\rightarrow$ 0.265 h^{-1}	E3	C	8.4,8.6-8.8	+
C8a	EtOH: 0.1 $\rightarrow$ 3.6 g/l	C8	P	8.9	+
E1d	Pyruvate pulse (D=0.24 h^{-1})	E1	C	8.10	–

The table states the label of each experiment, the corresponding cultivation, operation mode (C: chemostat, P: productostat) and the number of the figures in which the experiment are presented. Furthermore, it is stated whether or not (+/–) the biomass (Bio) measurement was used in data reconciliation. The biomass measurement was obtained from the base signal Lei (2001, chap.6).

8.2.5 Computational methods

8.2.5.1 Data reconciliation

The quality of the obtained data were checked using a statistical test function, h, by assuming a relative error of 5% on all measurements (Lei, 2001, chap.7). Conversion rates were calculated using a window size of 30 min and subsequently reconciled according to Heijden *et al.* (1994).

8.2.5.2 Metabolic flux analysis

The metabolic flux model presented in Lei (2001, chap.5) was used for calculation of intrinsic rates.

8.3 Results

The dynamics of acetate production and consumption in aerobic, glucose limited continuous cultivations were investigated through variations in the feed rate and pulses.

8.3.1 Acetate formation during dilution rate shift-ups

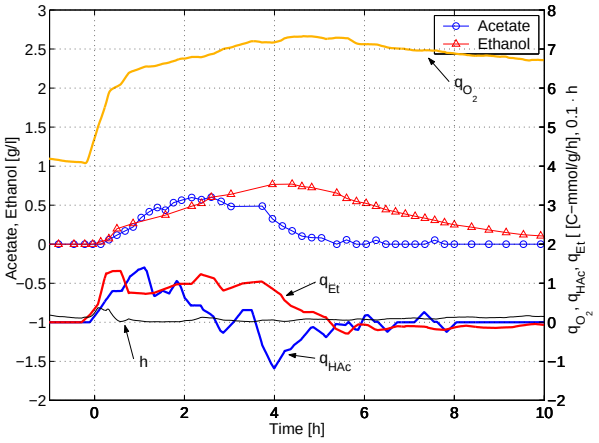

Figure 8.2. Experiment E2a: Dilution rate shift-up within the oxidative region in an aerobic glucose limited culture: At time 0 h, the dilution rate was increased from 0.15 to 0.25 h^{-1}. On-line measurements of ethanol, acetate are plotted along with specific rates for oxygen uptake (q_{O_2}), ethanol production (q_{Et}) and acetate production (q_{HAc}) as function of time after the shift-up. Furthermore, the statistical test, h, is shown.

Three dilution rate shift-up experiments were performed to monitor the dynamics of acetate formation and consumption (figures 8.2-8.4). The first experiment was a D-shift within the oxidative region (D=0.15 to 0.25 h^{-1}), whereas the second experiment was a D-shift into the oxido-reductive region (D=0.085 to 0.31 h^{-1}). The third experiment was also a D-shift into the oxido-reductive region (D=0.085 to 0.285 h^{-1}), however after 3.5 h, a D shift-down to 0.265 h^{-1} was performed to bring the culture back to oxidative growth (D_{crit}=0.27 h^{-1}). In all three experiments, the acetate concentration reached its maximal value approximately two hours after the increase in dilution rate. The maximal acetate production rates, however, already peaked one hour after the shift-up. The acetate response was clearly different from the ethanol concentration which, in all three experiments, continued to increase as the acetate concentration began to decrease after 2 h.

The maximal acetate concentration obtained during the experiments differed depending on the initial dilution rate. When D was increased from 0.15 to 0.25 h^{-1}, the maximal acetate concentration was 0.55 g/l (figure 8.2), whereas an acetate concentration of 1 g/l was obtained in

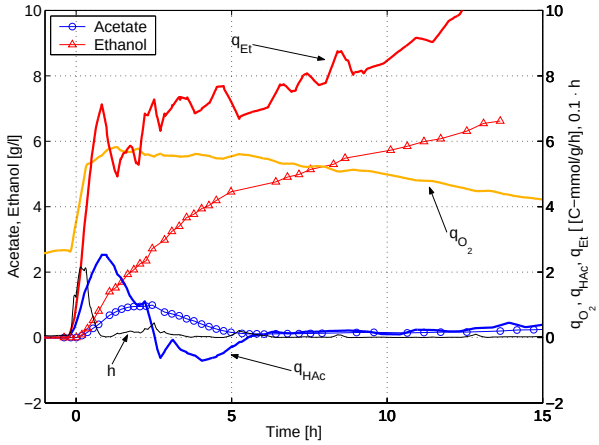

Figure 8.3. Experiment E3a: Dilution rate shift-up from oxidative to oxido-reductive growth in an aerobic glucose limited culture: At time 0 h, the dilution rate was increased from 0.085 to 0.31 h^{-1}. On-line measurements of ethanol, acetate are plotted along with specific rates for oxygen uptake (q_{O_2}), ethanol production (q_{Et}) and acetate production (q_{HAc}) as function of time after the shift-up. Furthermore, the statistical test, h, is shown.

the two shift-up experiments from 0.085 to respectively 0.31 and 0.285 h^{-1} (figures 8.3 and 8.4).

The dilution rate shift-down performed in experiment E3b after 3.5 h (figure 8.4) did not affect the acetate profile significantly and the acetate concentration continued to decrease as if no shift-down had occurred (compare figures 8.3 and 8.4). The ethanol concentration, on the other hand, was affected by the shift-down, illustrating a different regulation of ethanol and acetate formation.

Interestingly, the maximal acetate concentration obtained during transient conditions in a continuous cultivation (1 g/l) was significantly larger than the maximal acetate concentration obtained at any steady-state (0.38 g/l, steady-state C7.4, Lei (2001, chap.5)).

8.3.1.1 Enzyme activities

Measurements of the enzyme activities for ACDH (NAD and NADP-dependent) and ACS were performed during experiments E3a and E3b. The enzyme activity profiles during the first 10 h were very similar in the two experiments (figures 8.5-8.6). The activity of ACS decreased in both experiments from around 0.20 to 0.08 U/mg during the first two hours after the shift-up whereafter it increased back to its original level. NAD-dependent ACDH activity decreased throughout both experiments. From an initial level around 0.45 U/mg to 0.15 U/mg after 8 h. In the shift-up experiment to D=0.31 h^{-1} the NAD-dependent acetaldehyde dehydrogenase activity continued to decrease and a very low activity (0.018 U/mg) was measured after 24 h. The NADP-dependent ACDH activity

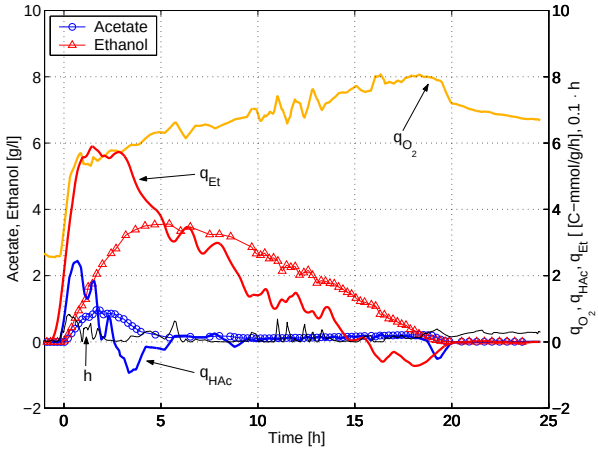

Figure 8.4. Experiment E3b: Dilution rate shift-up/down experiment in an aerobic glucose limited culture: At time 0 h, the dilution rate was increased from 0.085 to 0.285 h^{-1} whereafter it was decreased to 0.265 h^{-1} at 3.5 h. On-line measurements of ethanol, acetate are plotted along with specific rates for oxygen uptake (q_{O_2}), ethanol production (q_{Et}) and acetate production (q_{HAc}) as function of time after the shift-up. Furthermore, the statistical test, h, is shown.

decreased from 0.35 to 0.2 U/mg during the first 5 h after the shift-up in both experiments, whereafter it became constant (figure 8.6).

8.3.1.2 Intrinsic rates

Based on a metabolic flux model (Lei, 2001, chap.5), intrinsic rates were calculated for experiment E3b. The flux through the TCA cycle, $q_{cat,ox}$ and the flux through the oxidative phosphorylation, $q_{ox.phos}$ are shown together with the acetate production rate in figure 8.7. The initial increase in $q_{ox.phos}$ was larger than the increase in $q_{cat,ox}$ leading to a relative higher flux through the oxidative phosphorylation compared with the flux through the TCA cycle between 0.5 and 2 h. Thus, a decoupling between the oxidative catabolism and the oxidative phosphorylation as observed by Herwig and von Stockar (2001) was apparent.

8.3.1.3 *In-vivo* vs. *in-vitro* fluxes

To calculate the *in-vivo* flux distribution around the acetaldehyde branch-point in experiment E3b, it was assumed that acetyl-CoA produced from ACDH only was used in biosynthetic reactions and was not dissimilated to NADH and CO_2 in the TCA cycle. To avoid underestimation of the flux through ACDH, it was further assumed that acetyl-CoA produced by the PDH complex does not contribute with acetyl-CoA for biosynthesis, but is dissimilated to NADH and CO_2 in the TCA cycle. The acetyl-CoA requirement for biosynthesis has been estimated to 3.4 mmol/g biomass (Pronk *et al.*, 1994). This corresponds to a biosynthetic flux of

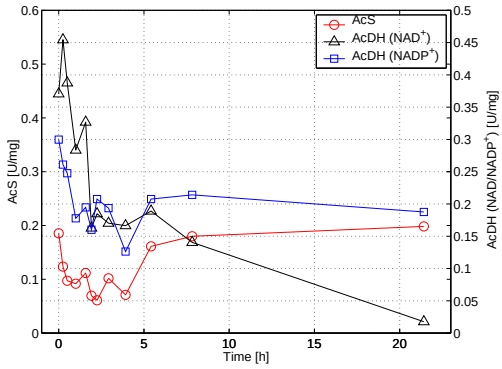

Figure 8.5. Experiment E3a: *In-vitro* determined activities of NAD and NADP-dependent acetaldehyde dehydrogenase and acetyl CoA synthetase during a dilution rate shift-up from 0.085 to 0.31 h^{-1}.

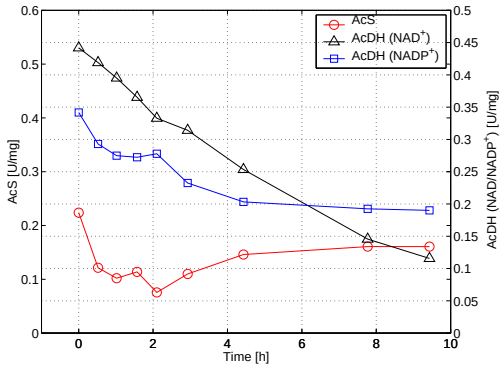

Figure 8.6. Experiment E3b: *In-vitro* determined activities of NAD and NADP-dependent acetaldehyde dehydrogenase and acetyl CoA synthetase. The dilution rate was increased from 0.085 to 0.285 h^{-1} at time 0 h and decreased to 0.265 h^{-1} at 3.5 h.

$q_{biosyn.} = 6.8 \cdot \mu$ C-mmol/g/h. Based on the above assumptions, the total flux through ACDH can then be calculated as: $q_{ACDH} = q_{HAc} + q_{biosyn.}$. The maximal flux through ACDH based on the *in-vitro* measured enzyme activities was calculated by assuming a constant soluble protein content of 40 % (g protein/g biomass) throughout the experiment. It was furthermore assumed that only the NADP-dependent form of ACDH was active in the conversion of acetaldehyde to acetate. For example, at time 0 h, the NADP-linked ACDH activity was 0.34 U/mg = 0.34 μmol acetate/mg

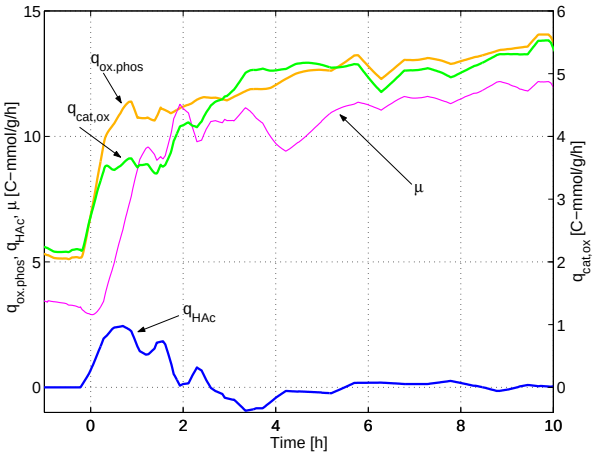

Figure 8.7. Experiment E3b: D was increased from 0.085 to 0.285 h^{-1} at 0 h and decreased to 0.265 h^{-1} at 3.5 h. Specific growth rate (μ), specific oxidative phosphorylation rate ($q_{ox.phos}$) and specific oxidative catabolism rate ($q_{cat,ox}$) are compared with the specific acetate production rate as function of time.

pro/min = 16.32 C-mmol acetate/g bio/h.

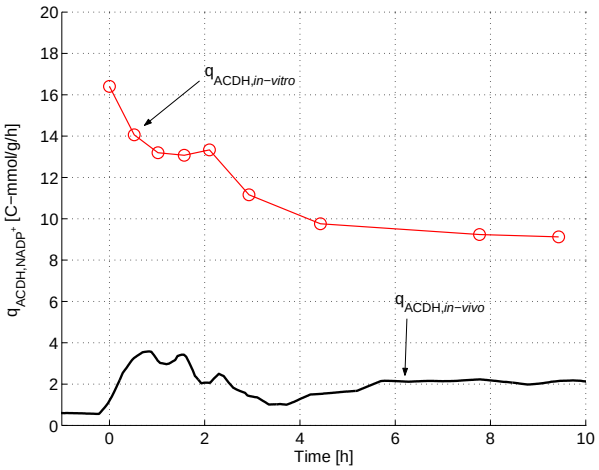

Figure 8.8. Experiment E3b: D was increased from 0.085 to 0.285 h^{-1} at 0 h and decreased to 0.265 h^{-1} at 3.5 h. Comparison between the *in-vivo* flux through ACDH calculated from the metabolic flux model described in Lei (2001, chap.5) and the maximal flux calculated from the *in-vitro* enzyme activities of NADP-dependent ACDH.

It is apparent that the calculated flux based on enzyme measurements were at least three times larger than the *in-vivo* calculated flux through ACDH throughout the experiment (figure 8.8).

8.3.1.4 Uptake of acetate used in biosynthesis

The maximal uptake rate of acetate during experiment E3b was 1.0 C-mmol/g/h at 3.5 h. The specific growth rate was 11 C-mmol/g/h = 0.28 h^{-1} and the biosynthetic requirement for acetyl-CoA can be calculated as $0.28 \cdot 6.8 = 1.9$ C-mmol/g/h. Thus, acetate taken up from the medium was probably used to supply acetyl-CoA to the biosynthesis.

8.3.2 Acetate production in a productostat

To investigate the dynamics of acetate production within the oxido-reductive region, an increase in the ethanol setpoint from 0.1 to 3.6 g/l was carried out by controlling the cultivation as a productostat (Lei, 2001, chap.5). The acetate profile exhibits an interesting pattern during the ethanol setpoint change (figure 8.9). The dilution rate was increased during the first 3 h, however, the acetate concentration increased only during the first 0.9 h from 0.06 to 0.23 g/l, whereafter it decreased to 0.08 g/l. When the dilution rate began to decrease after 3 h, the acetate concentration increased again to 0.2 g/l, whereafter it decreased slightly to a steady-state level of 0.15 g/l. The acetate concentration during the experiment was significantly lower than observed during dilution rate shift-ups from oxidative

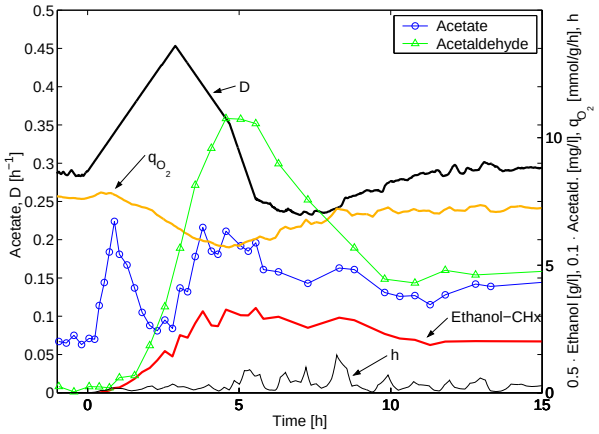

Figure 8.9. Experiment C8a: The ethanol setpoint was increased from 0.1 g/l to 3.6 g/l at time 0 h. The dilution rate was controlled based on an ethanol measurement in order to track the desired ethanol setpoint. Measurements of acetate, acetaldehyde and ethanol (CHx signal) are plotted along with specific oxygen uptake rate (q_{O_2}) and the dilution rate (D) as function of time after the shift-up. Furthermore, the statistical test, h, is shown.

steady-states (figures 8.2-8.4, 0.5 g/l – 1.0 g/l). However, similar to the previous experiments, the maximal acetate production rate was reached after 1 h (data not shown).

The dynamics of the acetaldehyde and ethanol concentration profiles were quite similar during the experiment. Both concentrations peaked at 5 h where the acetaldehyde concentration was 107 mg/l and the ethanol concentration was 5.0 g/l.

Enzyme activities were only measured at steady-state before and after the ethanol setpoint change. The activity of ACS was 0.12 U/mg before and 0.08 U/mg after the shift-up, while NAD-dependent ACDH activity decreased from 0.16 to 0.07 U/mg during the experiment. A similar decrease was observed for the NADP-dependent ACDH activity which dropped from 0.10 to 0.05 U/mg.

At the steady-state reached after the setpoint change, the maximal possible flux through NADP-dependent ACDH was calculated based on enzyme activity measurements. With a soluble protein content of 45 % (measured at for steady-state at D=0.31 h^{-1}), the measured activity of 0.05 U/mg corresponds to a flux of 2.7 C-mmol/g/h. The *in-vivo* calculated flux was: $q_{ACDH} = q_{HAc} + q_{biosyn.}$ = 0.15 C-mmol/g/h + 6.8 C-mmol/g · 0.30 h^{-1} = 2.19 C-mmol/g/h.

8.3.3 Pyruvate pulse

A 2 g/l pyruvate pulse added to a chemostat operating at a dilution rate slightly below D_{crit} (D=0.24 h^{-1}, D_{crit}=0.27 h^{-1}) showed that the cells were able to take up and metabolise pyruvate rapidly (figure 8.10). Interest-

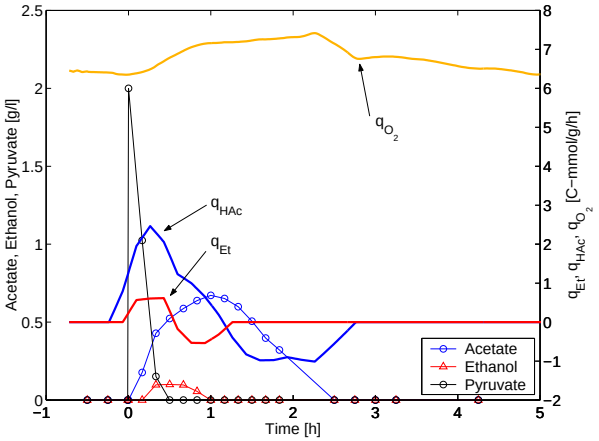

Figure 8.10. Experiment E1d: A pyruvate pulse of 2 g/l was added to a steady-state culture at D=0.24 h^{-1}. Pyruvate, ethanol, acetate concentrations are shown along with the specific rates of oxygen uptake (q_{O_2}), ethanol (q_{Et}) and acetate production (q_{HAc}) as function of time.

ingly, much more acetate than ethanol was produced. The acetate concentration increased to 0.65 g/l, whereas the ethanol concentration peaked at 0.1 g/l. The amount of acetate formed was similar to the amount observed in experiment E2a (figure 8.2), however much less ethanol was formed during the pyruvate pulse.

8.4 Discussion

In the following, the effects of enzyme activities, acetaldehyde concentration and the decoupling between $q_{cat,ox}$ and $q_{ox.phos}$ on the regulation of acetate production in *S. cerevisiae* will be discussed based on the presented results and previously reported work in literature. Furthermore, mathematical modelling of acetate production will be discussed.

8.4.1 Regulation of acetate production

8.4.1.1 Enzyme activities

The presented results indicate that the dynamics of the acetate production the first couple of hours following a dilution rate shift-up is not controlled by the *in-vitro* activities of acetaldehyde dehydrogenases or acetyl-CoA synthetase. During experiments where the dilution rate was increased (figures 8.2, 8.3, 8.4 and 8.9), it was observed that the acetate production rate peaked after approximately 1 h, whereafter it decreased. However, the *in-vitro* enzyme activities of ACDH (NAD and NADP-dependent) and ACS decreased during the first 2 h after the shift-up (figures 8.5-8.6). If the observed decrease in acetate production after 1 h only was due to an decrease in the ACDH activity, it would be expected that the

in-vivo calculated flux through ACDH would be in the same range as the flux through ACDH assuming the enzyme was operating at its maximal capacity. However, the *in-vitro* calculated flux through NADP-dependent ACDH was more than 3 times larger than in the *in-vivo* flux (figure 8.8).

If the flux through ACS is correlated with the ACS enzyme activity during a dilution rate shift-up, the observed decrease in the ACS enzyme activity (figures 8.5-8.6) would result in an increased acetate production provided the flux through ACDH is constant. However, whereas acetate production rate peaked 1 h after the dilution rate shift-up, the ACS activity continued to decreased until 2 h. Thus, the dynamics of the ACS enzyme activity and the acetate production rate did not correspond well enough to conclude that the *in-vitro* activity of ACS is involved in the control of acetate production during transient conditions. It has previously been reported that an increase in the ACS activity through overexpression of either *ACS1* or *ACS2* does not reduce acetate formation during exposure of excess glucose (de Jong-Gubbels, 1998), also suggesting that the enzyme activity of ACS does not control acetate production in *S. cerevisiae* during aerobic growth on glucose.

The amount of acetate produced after a dilution rate shift-up might be dependent on the initial enzyme activity of ACDH before the shift-up. During a D shift-up from a low dilution rate much more acetate was formed (1.0 g/l) compared with a D shift-up from oxido-reductive growth (0.2 g/l) (compare figures 8.3 and 8.9). Similarly, the enzyme activity of both NAD and NADP-dependent ACDH was higher at lower dilution rates.

The levels of NAD and NADP-dependent ACDH were very similar during the investigated experiments. However, 22 h after the dilution rate shift-up to 0.31 h^{-1} (figure 8.5), the activity of NADP-dependent ACDH was 10 times larger than the activity of NAD-dependent ACDH. This observation suggests that NADP-dependent ACDH is responsible for the main flux through ACDH after a prolonged period (20 h) of oxido-reductive growth.

8.4.1.2 Acetaldehyde concentration

The acetaldehyde concentration might be an important factor in the regulation of the acetate production since substrate inhibition of mitochondrial K^+-activated ACDH has been observed at acetaldehyde concentrations above 15 mg/l (Jacobson and Bernofsky, 1974). Jacobson and Bernofsky have observed that the *in-vitro* activity of mitochondrial K^+-activated ACDH decreased by 63 % at high acetaldehyde concentrations (220 mg/l) compared with the maximal ACDH activity obtained at 15 mg/l. In the presented results, the calculated *in-vivo* flux through ACDH (figure 8.8) increased during the first one hour, but then decreased from 3.7 to 1 C-mmol/g/h during the next 2.5 h (a 73% decrease). Therefore, a possible explanation for the decreasing acetate production rate after 1 h during

transient conditions could be that ACDH was inhibited by acetaldehyde. By using an enzymatic kit for acetaldehyde determination (set-up 1) where the detection limit is 1 mg/l, it was found that acetaldehyde concentration increased from 6 to 56 mg/l when the acetate decreased during an ethanol setpoint increase (between 1 and 3 h in figure 8.9). However, since the acetate concentration began to increase after 3 h, when the acetaldehyde concentration still was increasing, acetaldehyde inhibition of ACDH did not control the dynamics of acetate production.

8.4.1.3 Decoupling between $q_{cat,ox}$ and $q_{ox.phos}$

The decoupling of $q_{cat,ox}$ and $q_{ox.phos}$ (figure 8.7) seemed to be strongly correlated with the acetate production rate. This connection can be elucidated by considering the NADH balance. The intrinsic rates of $q_{ox.phos}$ and $q_{cat,ox}$ were calculated from a metabolic flux model with three NADH producing pathways: 1) Conversion of glucose to CO_2 ($q_{cat,ox}$) via the glycolysis and the TCA cycle, 2) The anabolic pathway from glucose to biomass (μ), and 3) Conversion of glucose to acetate (q_{HAc}). If the NADH balance closes, the sum of these three pathways is proportional to the rate of oxidative phosphorylation ($q_{ox.phos}$) since NADH is reoxidised by oxidative phosphorylation (no glycerol production was observed). It could be observed that the responses for $q_{cat,ox}$ and μ were almost proportional and the difference between $q_{cat,ox}$ and $q_{ox.phos}$ must therefore be related to the q_{HAc} profile (figure 8.7). Thus, the decoupling of $q_{cat,ox}$ and $q_{ox.phos}$ during acetate formation is primarily a consequence of the NADH balance.

The decoupling of $q_{cat,ox}$ and $q_{ox.phos}$ has also been observed during dilution rate shift-up experiments with two different *S. cerevisiae* strains (Herwig and von Stockar, 2001) and they have speculated that the dissimilation of pyruvate through the TCA cycle, in addition to the oxidative phosphorylation, is a bottleneck in the catabolism initially after a dilution rate shift-up. According to Herwig and von Stockar (2001), after a dilution rate shift-up, overflow at the pyruvate branchpoint occurs due to a limitation in the TCA cycle. Since the oxidative phosphorylation is not saturated at this point, acetate is produced instead of ethanol[1] since NADH produced can be reoxidised through the oxidative phosphorylation producing ATP. When the oxidative phosphorylation becomes limiting, the acetate production rate is down-regulated since NADH cannot be reoxidised and instead more ethanol is formed.

If acetate production is a consequence of the decoupling between $q_{cat,ox}$ and $q_{ox.phos}$, the available capacity of the oxidative phosphorylation must be quantified by the cell in terms of a concentration or signal. Otherwise, inhibition or activation of the enzymes involved in acetate production (ACDH) cannot be regulated by the decoupling between $q_{cat,ox}$ and

[1]From an energetical point of view, it is more preferable for the cell to produce acetate than ethanol since NADH is formed in the pathway from glucose to acetate, whereas ethanol formation is NADH neutral.

$q_{ox.phos}$. In this paper, we propose that the NAD^+ concentration within the mitochondria might be involved in the control of acetate production during dilution rate shift-ups on glucose limited media: When the oxidative phosphorylation becomes limiting, the concentration of NAD^+ in the mitochondria decreases as a consequence of a limitation of reoxidation of NADH. Since NAD^+ is the preferred co-substrate for mitochondrial K^+-activated ACDH (Jacobson and Bernofsky, 1974), the flux through ACDH is down-regulated as the oxidative phosphorylation saturates. According to this hypothesis, it is the K^+-activated NAD(P)-dependent ACDH located in the mitochondria (figure 8.1) and not the cytosolic NADP-dependent ACDH which is responsible for the acetate accumulation following a dilution rate shift-up on glucose.

Acetate production during the dilution rate shift-up experiment from D=0.08 to 0.31 h^{-1} in figure 8.3 can be explained by the hypothesis. During the first 1 h, the oxidative phosphorylation was not limiting (due to the decoupling between $q_{cat,ox}$ and $q_{ox.phos}$) and the acetate production rate increased. However, after 1 h, the oxidative phosphorylation became limiting resulting in a lower mitochondrial NAD^+ concentration and thus a lower flux through mitochondrial NAD-dependent ACDH. Thereby the acetate production rate decreased.

The proposed hypothesis also can explain the peculiar acetate response observed during an increase in ethanol setpoint in a productostat (figure 8.9). The acetate concentration increased until one hour after the setpoint change whereafter it began to decrease. The peak in acetate concentration after 1 h coincided with a small peak in the specific oxygen uptake rate (q_{O_2}) indicating saturation of the oxidative phosphorylation and thereby a decreasing NAD^+ concentration. Thus, acetate production was down-regulated. After 3 h, the decrease in dilution rate caused a derepression of the oxidative phosphorylation (Lei, 2001, chap.7) which resulted in an increase in the mitochondrial NAD^+ concentration and thereby an increased acetate concentration.

Since the pathway from glucose to acetate consumes more NAD^+ than the conversion of pyruvate to acetate, it was expected that a pulse of pyruvate would produce relatively more acetate than ethanol compared to a dilution rate shift-up where the glucose feed is increased. Indeed, the maximal acetate production rate during the pyruvate pulse experiment was twice as large as during the dilution rate shift-up experiment (2.5 vs. 1.4 C-mmol/g/h). In contrast, the maximal ethanol formation rate was twice as low during the pyruvate pulse experiment (0.6 vs. 1.3 C-mmol/g/h) compared to the dilution rate shift-up experiment (compare figures 8.2 and 8.10).

The amount of acetate formation during batch growth on glucose has been found to be dependent of the activity of cytosolic NADP-dependent ACDH and not on the activity of mitochondrial K^+-activated NAD(P)-dependent ACDH (Remize *et al.*, 2000). This observation is not in contrast

to the proposed hypothesis of K^+-activated NAD(P)-dependent ACDH being responsible for acetate accumulation during a dilution rate shift-up since the oxidative phosphorylation is saturated throughout batch growth on glucose as opposed oxidative growth in a continuous cultivation.

8.4.2 Modelling of acetate formation

In order to develop a proper model for describing acetate production it is necessary to be able to model the fluxes through both mitochondrial abnd cytosolic ACDH as well as cytosolic ACS. From the preceding discussions, it seems likely that it is the flux through ACDH which is responsible for acetate production whereas the flux through ACS changes with slower dynamics. A mathematical description of the flux through ACDH is therefore the main challenge for modelling the acetate production. According to the presented results, modelling of the NAD^+ concentration is essential, whereas substrate inhibition of ACDH by acetaldehyde (Jacobson and Bernofsky, 1974) only seemed to be of minor importance. Both NAD and NADP-dependent ACDH are repressed by glucose (Postma *et al.*, 1989). It might therefore be necessary to include a compartment describing the enzyme activity of NAD-dependent ACDH in a mathematical model in order to model the different amount of acetate formed during dilution rate shift-ups depending on the glycolytic flux which can be related to glucose repression (Lei, 2001, chap.7).

In the yeast model proposed by Lei *et al.* (2001) a description of the mitochondrial NAD^+ concentration was not included and neither was a constitutive flux through ACDH for production of cytosolic acetyl-CoA for biosynthesis during oxidative growth on glucose (Flikweert *et al.*, 1996). It is therefore not expected that the model is able to describe the observed acetate dynamics presented in this paper.

In some yeast strains, acetate excretion has been observed at specific growth rates where no ethanol was formed (Postma *et al.*, 1989). This observation was used in the model formulation of the yeast model (Lei *et al.*, 2001), and the model therefore predicts a steady-state acetate formation at a dilution rate below D_{crit} where ethanol formation sets in. However, for the strain cultivated in this work (*S. cerevisiae*, CEN.PK113-7D), no acetate was observed below D_{crit}, instead acetate and ethanol formation set in at the same dilution rate (Lei, 2001, chap.5). This observation should also be included in a mathematical model for aerobic growth on glucose of the investigated *S. cerevisiae* strain.

8.5 Conclusions

In this work, the role of acetate production in *S. cerevisiae* was studied during growth on glucose. The maximal acetate production rate during various dilution rate shift-up experiments was observed approximately 1 h

after the shift-up. The maximal acetate concentration during a D shift-up was a function of the initial dilution rate where D shift-ups from a low dilution rate yielded the largest acetate accumulation.

The dynamics of acetate production during D shift-ups was found to be distinctly different from the dynamics of the enzyme concentrations of acetaldehyde dehydrogenase (ACDH) or acetyl-CoA synthetase (ACS). Furthermore, it was shown that inhibition of ACDH by acetaldehyde did not control the dynamics of acetate production.

The decoupling between the rate of oxidative phosphorylation ($q_{ox.phos}$) and the flux through the PDH complex ($q_{cat,ox}$) was found to be correlated to the acetate production through the NADH balance. It was proposed that the dynamics of the acetate production following a dilution rate shift-up was regulated by the NAD^+ concentration in the mitochondria and the acetate production rate is thereby linked to the saturation of the oxidative phosphorylation.

Further investigations are needed to validate the proposed hypothesis. The effect of the NAD^+ concentration on the reaction rate of ACDH needs to be quantified. Furthermore, measurements of the NAD^+ concentration within the mitochondria as function of time during dilution rate shift-ups would aid further investigations of the role of acetate during transient conditions.

List of symbols

$ACDH$	acetaldehyde dehydrogenase []
ACS	acetyl-CoA synthetase []
PDC	pyruvate decarboxylase []
PDH	pyruvate dehydrogenase []
D	dilution rate [h^{-1}]
D_{crit}	critical dilution rate [h^{-1}]
$EtOH$	ethanol concentration [g/l]
h	statistical test for data quality []
q_{ACDH}	specific flux through acetaldehyde dehydrogenase [C-mmol/g/h]
q_{Et}	specific ethanol production rate [C-mmol/g/h]
q_{HAc}	specific acetate production rate [C-mmol/g/h]
q_{O_2}	specific oxygen uptake rate [mmol/g/h]
μ	specific growth rate [C-mmol/g/h]

References

Barford, J. (1990). A general model for aerobic yeast growth: Continuous culture. *Biotechnol. Bioeng.*, **35**, 921–927.

de Jong-Gubbels, P. (1998). *Metabolic fluxes at the interface of glycolysis and TCA cycle in Saccharomyces cerevisiae*. Ph.D. thesis, Kluyver Laboratory of Biotechnology, Delft University of Technology.

de Jong-Gubbels, P.; van den Berg, M. and Steensma, H. (1997). The *Saccharomyces cerevisiae* acetyl-coenzyme A synthetase encoded by the *ACS1* gene, but not the *ACS2*-encoded isoenzyme, is subject to glucose catabolite inactivation. *FEMS Microbiol. Lett.*, **153**, 75–81.

de Jong-Gubbels, P.; van den Berg, M.; Luttik, M.; Steensma, H.; van Dijken, J. and Pronk, J. (1998). Overproduction of acetyl-CoA synthetase isoenzymes in respiring cells of *Saccharomyces cerevisiae* does not reduce acetate production after exposure to excess glucose. *FEMS Microbiol. Lett.*, **165**, 15–20.

Fleet, H. and Heard, G. (1992). *Wine microbiology and biotechnology*, pages 27–54. Harwood Academic publishers, Chur, Switzerland.

Flikweert, M.; van der Zanden, L.; Janssen, W.; Steensma, H.; van Dijken, J. and Pronk, J. (1996). Pyruvate decarboxylase: An indispensable enzyme for growth of *Saccharomyces cerevisiae on glucose*. *Yeast*, **12**, 247–257.

Flikweert, M.; Kuyper, M.; van Maris, A.; Kötter, P.; van Dijken, J. and Pronk, J. (1999). Steady-state and transient-state analysis of growth and metabolite production in a *Saccharomyces cerevisiae* strain with

reduced pyruvate-decarboxylase activity. *Biotechnol. Bioeng.*, **66**, 42–50.

Heijden, R. v. d.; Romein, B.; Heijnen, J.; Hellinga, C. and Luyben, K. (1994). Linear constraint relations in biochemical reaction systems: I, Classification of the calculability and the balanceability of conversion rates. *Biotechnol. Bioeng.*, **43**, 3–10.

Herwig, C. and von Stockar, U. (2001). A small metabolic flux model to identify transient metabolic regulations in *S. cerevisiae*. *Bioprocess Biosystems Eng.*, **XX**, submitted.

Hohmann, S. (1997). *Pyruvate decarboxylases*, chapter 11, pages 187–211. Technomic Publishing Company, Inc. In Zimmermann, F.K. and Entian, K.D (ed.): Yeast sugar metabolism.

Hough, J.; Briggs, D.; Stevensand, R. and Young, T. (1982). *Beer flavour and beer quality*, volume II, pages 839–876. Chapman and Hall, London, United Kingdom.

Jacobson, M. and Bernofsky, C. (1974). Mitochondrial acetaldehyde dehydrogenase from *Saccharomyces cerevisiae*. *Biochim. et Biophys.*, **350**, 277–291.

Lei, F. (2001). *Dynamics and nonlinear phenomena in continuous cultivations of* Saccharomyces cerevisiae. Ph.D. thesis, KT, Technical University of Denmark.

Lei, F.; Rotbøll, M. and Jørgensen, S. (2001). A biochemically structured model for *Saccharomyces cerevisiae*. *Accepted for publication in J. Biotechnol.*.

Llorente, N. and de Castro, I. (1977). Physiological role of yeasts NAD(P)+ amd NADP+-linked aldehyde dehydrogenases. *Rev. Esp. Fisiol.*, **33**, 135–142.

Lowry, O.; Rosebrough, N.; Farr, A. and Randall, R. (1951). Protein measurement with the folin phenol reagent. *J. Biol. Chem.*, **193**, 265–275.

Meaden, P.; Dickinson, F.; Mifsud, A.; Tessier, W.; Westwater, J.; Bussey, H. and Midgley, M. (1997). The *ALD6* gene of *Saccharomyces cerevisiae* encodes a cytosolic, Mg^{2+}-activated acetaldehyde dehydrogenase. *Yeast*, **13**, 1319–1327.

Meyenburg, K. v. (1969). *Katabolit-Repression und der Sprossungszyklus von Saccharomyces cerevisiae*. Ph.D. thesis, ETH Zürich.

Navarro-Avino, J. P.; Prasad, R.; Miralles, V. J.; Benito, R. M. and Serrano, R. (1999). A Proposal for Nomenclature of Aldehyde Dehydrogenases in Saccharomyces cerevisiae and Characterization of the Stress-inducible ALD2 and ALD3 Genes. *Yeast*, **15**(10A), 829–842.

Nissen, T.; Schulze, U.; Nielsen, J. and Villadsen, J. (1997). Flux distributions in anaerobic, glucose-limited continuous cultures of *Saccharomyces cerevisiae*. *Microbiology - Reading*, **143**(1), 203–218.

Pham, H.; Larsson, G. and Enfors, S.-O. (1998). Growth and energy metabolism in aerobic fed-batch cultures of *Saccharomyces cerevisiae*: Simulation and model verification. *Biotechnol. Bioeng.*, **60**, 474–482.

Postma, E.; Verduyn, C.; Scheffers, A. and van Dijken, J. (1989). Enzymic analysis of the Crabtree effect in glucose-limited chemostat cultures of *Saccharomyces cerevisiae*. *Appl. Env. Microbiol.*, **55**, 468–477.

Pronk, J.; Wenzel, T.; Luttik, M.; Klassen, C.; Scheffers, W.; Steensma, H. and van Dijken, J. (1994). Energetic aspects of glucose metabolism in a pyruvate-dehydrogenase-negative mutant of *Saccharomyces cerevisiae*. *Microbiology*, **140**, 601–610.

Remize, F.; Andrieu, E. and Dequin, S. (2000). Engineering of the pyruvate dehydrogenase bypass in *Saccharomyces cerevisiae*: Role of the cytosolic Mg^{2+} and mitochondrial K^{+} acetaldehyde dehydrogenases Ald6p and Ald4p in acetate formation during alcoholic fermentation. *Appl. Env. Microbiol.*, **66**, 3151–3159.

Rieger, M.; Käppeli, O. and Fiechter, A. (1983). The role of a limited respiration in the complete oxidation of glucose by *Saccharomyces cerevisiae*. *J. Gen. Microbiol.*, **129**, 653–661.

Sonnleitner, B. and Hahnemann, U. (1994). Dynamics of the respiratory bottleneck of Saccharomyces cerevisiae. *J. Biotechnol.*, **38**, 63–79.

Sonnleitner, B. and Käppeli, O. (1986). Growth of *Saccharomyces cerevisiae* is controlled by its limited respiratory capacity: Formulation and verification of a hypothesis. *Biotechnol. Bioeng.*, **28**, 927–937.

Steinmeyer, D. and Shuler, M. (1989). Structured model for *Saccharomyces cerevisiae*. *Chem. Eng. Sci.*, **44**, 2017–2030.

van den Berg, M. A.; de Jong-Gubbels, P.; Kortland, C.; van Dijken, J.; Pronk, J. and Steensma, H. (1996). The two acetyl-coenzyme A synthetases of *Saccharomyces cerevisiae* differ with respect to kinetic properties and transcriptional regulation. *J. Biol. Chem.*, **271**, 28953–28953.

Verduyn, C.; Postma, E.; Scheffers, W. and van Dijken, J. (1990). Physiology of *Saccharomyces cerevisiae* in anaerobic glucose-limited chemostat cultures. *J. Gen. Microbiol.*, **136**, 395–403.

Villadsen, J. and Nielsen, J. (1990). Modelling of fermentation kinetics. *Proc. Eur. Congress Biotechnol.*, pages 259–266.

9

Conclusions and outlook

9.1 Multiple steady-states

In this Ph.D study the possible existence of multiple steady-states was investigated in aerobic glucose limited continuous cultivation of *S. cerevisiae*. In this work the *S. cerevisiae* strain CEN.PK113-7D was chosen as model organism for investigating the multiple steady-states phenomenon since this strain is widely used as a reference strain in the scientific yeast community (van Dijken *et al.*, 2000). It was shown that both an oxidative as well as an oxido-reductive steady-state could be obtained for the same dilution rate in an interval just below the critical dilution rate, thus multiple steady-states were identified.

It could be shown that the existence of multiple steady-states were attributed to two distinct physiological effects occurring when growth changed from oxidative to oxido-reductive: i) A decrease in the efficiency of ATP production and utilisation and ii) Repression of the respiratory system. The latter effect was most pronounced at high ethanol concentrations whereas the first effect also increased with the ethanol concentration for closed-loop oxido-reductive steady-states, but was not observed during open-loop oxido-reductive steady-states. Through closed loop operation of the bioreactor, oxido-reductive steady-states at dilution rates up to 0.09 h^{-1} lower than the critical dilution rate were obtained using a feed glucose concentration of 30 g/l.

However, it was further shown that oxido-reductive steady-states determined in a continuous culture are not uniquely defined by the dilution rate (in a chemostat) or the ethanol setpoint (in a productostat), but also is a function of the history of the culture. The oxido-reductive steady-states were found to be strongly dependent on the degree of repression of the respiratory system. Depending on how the cultivation was operated, different degrees of repression could be obtained at a given dilution rate (or ethanol setpoint).

The respiratory system of the investigated *S. cerevisiae* strain (CEN.PK113-7D) was observed to be very easily repressed during oxido-reductive growth resulting in a low specific oxygen uptake rate (q_{O_2}). Even after 100 h cultivation at oxido-reductive growth no derepression was observed. These observations are in contrast to previous reports for other *S. cerevisiae* strains where q_{O_2} stays at its maximum level during oxido-reductive growth (Bar-

ford and Hall, 1979; Rieger *et al.*, 1983). Since a strongly repressed respiratory system results in a large dilution rate interval of multiple steady-states, it might be speculated that the oxido-reductive steady-states obtained at dilution rate far below D_{crit} using the productostat only can be obtained using *S. cerevisiae* strains where the respiratory system is easily repressed. The strain used by Barford and Hall (1979) or Rieger *et al.* (1983) should therefore be investigated in a productostat to clarify this.

9.2 Productostat operation

It was shown that it is possible to obtain oxido-reductive steady-states by operating a continuous cultivation as a productostat, where the dilution rate is manipulated based on an ethanol related measurement.

The existence of multiple steady-states implies hysteresis. Consequently, a small increase in the dilution rate might result in a significantly decrease in biomass productivity when operating close to the maximal biomass productivity. The productostat is the obvious choice for operating in the vicinity of maximal biomass productivity in contrast to the chemostat, since the productostat is able to maintain the cultivation at the desired operating point even if a disturbance occurs. Furthermore, the productostat was shown to be superior to the chemostat with respect to the response time when tracking oxido-reductive steady-states.

The productostat operation principle also seems suitable to avoid sustained oscillations in continuous yeast cultivations. The sustained oscillations occur within a region of dilution rates below the critical dilution rate: If oscillations are observed in a chemostat, productostat operation should be initiated to maintain the measured state variable constant (e.g. the CO_2 content in the outlet gas). A properly tuned dilution rate controller should be able to dampen the oscillations and return the cultivation to a steady-state.

A limitation of the productostat is that it requires an on-line measurement which relates to the state of the cells in the cultivation. For *S. cerevisiae*, this requirement is fulfilled since existing on-line off-gas measurements can be related to the ethanol concentration. However, for other microorganisms productostat operation might not be possible since a suitable product related on-line measurement is not available.

The dependence of an oxido-reductive steady-state on the history of a cultivation implies that when comparing oxido-reductive steady-states for different strains of *S. cerevisiae*, it is crucial to operate the cultivation in an similar manner for each strain. For this purpose the accelero-productostat is a promising operation methodology since it avoids sudden increases in the dilution rate which was found to affect the degree of repression of the respiratory system and thereby the oxido-reductive steady-state. The accelero-productostat also enables a quick determination of the (pseudo) steady-state profile as function of the dilution rate in the oxido-reductive

region compared to chemostat and even productostat operation. Furthermore, multiple (pseudo) steady-states can be identified in an accelero-productostat as opposed to an accelerostat.

9.3 Biomass estimation in *S. cerevisiae* cultivations

A software sensor based on the alkali addition rate was developed and found capable of describing both the dynamics as well as the concentration of dry weight biomass during transient experiments in batch and continuous cultivations. The software sensor had only one parameter which has to be determined: The proportionality factor between alkali addition rate and biomass production rate, M_{DW}/Y_{xH}. This factor can be determined from steady-state experiments and was found to be constant for various operation modes for a given fermentation set-up. During transients where large amounts of organic acids were formed, the increase in the proton production rate due to organic acid production needed to be included in the biomass estimator, however during growth within the oxido-reductive region in continuous cultivations, the effect of organic acids were negligible. Estimation of dry weight biomass concentration based on the alkali addition rate provides an on-line measurement of the biomass production rate and serves as a less laborious alternative to off-line dry weight measurements in physiological studies of *S. cerevisiae* when defined medium is used.

9.4 Acetate formation in *S. cerevisiae*

In the investigation of acetate production in *S. cerevisiae* during dynamic conditions it was found that neither the enzyme concentrations of acetaldehyde dehydrogenase (ACDH) or acetyl-CoA synthetase (ACS) nor acetaldehyde inhibition of ACDH control the dynamics of acetate production following a dilution rate shift-up on glucose limited media. Instead, a hypothesis correlating the acetate production to the saturation of the respiratory system was formulated. It was proposed that the dynamics of the acetate production following a dilution rate shift-up is controlled by the NAD^+ concentration in the mitochondria. It was speculated that acetate accumulation during the first hour following a dilution rate shift-up is due to an increased flux through mitochondrial ACDH, however when the oxidative phosphorylation becomes limiting the availability of mitochondrial NAD^+ decreases since the rate of NADH reoxidation is limited. Consequently, the flux through mitochondrial ACDH and thereby acetate production decreases since mitochondrial NAD^+ is substrate for ACDH reaction.

9.5 Modelling of *S. cerevisiae*

The biochemically structured model presented in chapter 3 was found to be useful for designing dilution rate controllers for the productostat at low ethanol concentrations, however several model deficiencies were identified during the present study: The model was not able to describe neither the repression of the respiratory system nor acetate production properly. Furthermore, no experimental evidence was found to verify that acetaldehyde is the trigger compound for excess glucose uptake during oxido-reductive growth. The fundamental problem in the model is that neither redox balances nor the ATP balance are modelled and since these balances are involved in control of triggering oxido-reductive growth, repression of the respiratory system, and acetate production the model cannot describe these phenomena.

9.6 Outlook

The present study has focussed on the existence of multiple steady-states in *S. cerevisiae* CEN.PK113-7D, however this phenomenon might be present for a whole range of organisms exhibiting overflow metabolism. In future works it would be interesting to study other *S. cerevisiae* strains (with a lower degree of repression of the respiratory system) as well as other organisms exhibiting overflow metabolisms (e.g. *E. coli*) to see if multiple steady-states is an abundant phenomenon in continuous cultivations of microorganisms.

The accelero-productostat was proposed as an alternative method for quickly determining the oxido-reductive (pseudo) steady-state profile as function of the dilution rate. However, the design of such experiments need to be further investigated since this operation mode introduces yet another parameter compared to the productostat, namely the slope of the ethanol setpoint ramp.

Further investigations are needed to validate the proposed hypothesis on acetate formation during dilution rate shift-ups in aerobic glucose limited cultures of *S. cerevisiae*. The effect of the NAD^+ concentration on the reaction rate of ACDH needs to be quantified. In addition, measurements of the NAD^+ concentration within the mitochondria as function of time during dilution rate shift-ups would aid further investigations of the role of acetate during transient conditions. Finally, dilution rate shift-up experiments using a *S. cerevisiae* $\Delta ald4$ single deletion mutant could also be used for validating the hypothesis since a reduced acetate accumulation compared to the wild-type should be expected.

Based on the experimental results presented and hypotheses proposed in this work, an improved mathematical model describing the aerobic growth of *S. cerevisiae* on glucose or ethanol limited media can be developed. Repression of the respiratory system during oxido-reductive growth needs

to be included to elucidate its effect on the region of multiple steady-states. Repression of the respiratory system was experimentally observed to be related to either the glucose uptake rate or the glycolytic flux which could be used for modelling repression. However, for a more mechanistic description of the repression, signal transduction pathways for glucose repression in *S. cerevisiae* as well as regulation of the transcription of the repressed genes will have to be included. Furthermore, modelling of the mitochondrial NAD^+ concentration should be attempted in order to describe acetate accumulation during dilution rate shift-ups on glucose limited media.

References

Barford, J. and Hall, R. (1979). An examination of the Crabtree effect in *Saccharomyces cerevisiae*: The role of respiratory adaptation. *J. Gen. Microbiol.*, **114**, 267–275.

Rieger, M.; Käppeli, O. and Fiechter, A. (1983). The role of a limited respiration in the complete oxidation of glucose by *Saccharomyces cerevisiae*. *J. Gen. Microbiol.*, **129**, 653–661.

van Dijken, J.; Bauer, J.; Brambilla, L.; Duboc, P.; Francois, J.; Gancedo, C.; Giuseppin, M.; Heijnen, J.; Hoare, M.; Lange, H.; Madden, E.; Niederberger, P.; Nielsen, J.; Parrou, J.; Petit, T.; Porro, D.; Reuss, M.; van Riel, N.; Rizzi, M.; Steensma, H.; Verrips, C.; Vindeloev, J. and Pronk, J. (2000). An interlaboratory comparison of physiological and genetic properties of four Saccharomyces cerevisiae strains. *Enzyme and Microbial Technology*, **26**(9-10), 706–714.

Appendices

A

Estimation of kinetic parameters in a structured yeast model using regularisation

In this work a procedure for estimating kinetic parameters in biochemically structured models was developed. The approach is applicable when the structure of a kinetic model has been set up and the kinetic parameters should be estimated.

The procedure consists of five steps. First, initial values were found in or calculated from literature. Hereafter using sensitivity analysis the most sensitive parameters were identified. In the third step physiological knowledge was combined with the parameter sensitivities to manually tune the most sensitive parameters. In step four, a global optimisation routine was applied for simultaneous estimation of the most sensitive parameters identified during the sensitivity analysis. Regularisation was included in the simultaneous estimation to reduce the effect of insensitive parameters. Finally, confidence intervals for the estimated parameters were calculated.

This parameter estimation approach was demonstrated on a biochemically structured yeast model containing 11 reactions and 37 kinetic constants as a case study.

A.1 Introduction

The application of mathematical models in the field of biotechnology for describing growth of microorganisms is developing rapidly. In order for these models to describe and predict the dynamic changes taking place in the cell and its surrounding environment, it is necessary to model the reaction rates using kinetic expressions. Due to the great complexity of the cell, obviously, not all reactions can be modelled individually. In dynamic models, only the most important reactions or pathways are modelled using kinetic expressions. What reactions to include and the structure of the model is dependent on the purpose of the model. However, despite the differences in the model purpose and structure, the question of how to estimate and validate the kinetic parameters plays an important role in

mathematical modelling.

A.1.1 Estimation of kinetic parameters

Most often parameter estimation of kinetic parameters in simple unstructured biochemical models is carried out by either determining one parameter at a time from a specific experiment or by calculating all parameters simultaneously using a least square or maximum likelihood criterion. These procedures are possible because the number of parameters to be determined is limited (less than 10) and sufficient experimental data are available to perform a robust estimation of each parameter. However, in cases when the number of kinetic parameters is significantly larger and the experimental data are limited this approach is often not feasible and the parameter estimation is not as straight forward.

What are the challenges when estimating a large number of kinetic parameters?

Due to the nonlinearity of a kinetic model the estimation problem is inherently nonlinear and thus most likely contains multiple local minima. The solution of interest is the global minimum which hopefully also provides the biologically most reasonable parameters. However, due to the existence of multiple minima good initial estimates of the parameters are crucial to ensure that the obtained solution is close to a physiologically reasonable minimum. When a solution has been found for the estimation problem it should be checked how robust the minimum is by rerunning the estimation routine with the new set of parameters as initial guesses. Furthermore the robustness may be evaluated by starting from different but also physiologically reasonable initial values. A global minimum may be determined using an evolutionary algorithm for parameter estimation (Schmidt and Isaacs, 1995). However, correlation between model parameters also contribute an obstacle to determining a unique minimizing parameter set.

Large estimation problems are usually very stiff. This is caused by large variations in the parameter sensitivity, a problem which can be reduced by using Tikhonov regularisation (Hansen, 1996). By penalising the movement of a parameter from its initial value it is assured that the most insensitive parameters are bound to their initial values. The variances of the parameter estimates are hereby reduced at the expense of introducing model bias. However, for kinetic models it is usually not possible to obtain a perfect fit between dynamic experimental data and the model, thus the model bias introduced by regularisation is therefore negligible provided that the weight on the regularisation term is chosen wisely (the L-criterion Hansen (1996)).

Traditionally another obstacle in parameter estimation of kinetic models is the strong correlation between the rate constant and affinity constant in Monod type expressions (Holmberg, 1981). It has been shown that

the rate and affinity constants of the Monod model are not identifiable during a standard batch experiment (Nihtilä and Virkukunen, 1977) and much work has focused on design of experiments for optimal parameter estimation (Baltes *et al.*, 1994; Munack, 1988). It was beyond our scope to design optimal experiments for parameter estimation based on the model in question, however the choice of estimation data was governed by the motivation of using existing experimental data from various operation modes to reduce the number of insensitive model parameters.

In this work, a methodology for estimating kinetic parameters in structured growth models was developed. The methodology was illustrated in a case study where kinetic parameters in a two compartment biochemically structured model (Lei *et al.*, 2001) were estimated.

A.2 Methodology

This section describes a parameter estimation procedure in five steps which was developed in order to estimate kinetic parameters in structured models. First, initial guesses for the parameters were obtained either from literature or by performing simple model calculations using selected sets of experimental data. Secondly, a sensitivity analysis of the parameters was performed and thirdly the parameters were manually tuned based on physiological knowledge regarding metabolic fluxes and the metabolite concentrations combined with the results from the sensitivity analysis. In step four, a simultaneous parameter estimation was performed where a weighted least squares method was combined with regularisation. Finally, the obtained parameter estimates were validated by calculating confidence intervals and the covariance matrix for the estimates.

A.2.1 Step 1: Obtaining initial parameter values

A prerequisite for solving a mathematical model is that all model parameters are assigned. This is, however, not the case when the model structure including the kinetic expressions has been set up. Thus, initial values for kinetic parameters are required before any model solution can be obtained. A procedure for obtaining initial parameter values is outlined below:

1 Make a literature survey in order to find approximate values for the kinetic parameters. In this way values for most affinity constants in the catabolic reactions were obtained.

2 Calculate parameter values using experimental data and model equations. Most rate constants were estimated this way.

3 A rough initial guess for remaining parameters (including the inhibition constants) was made based on the model structure compared with experimental data.

A.2.2 Step 2: Parameter sensitivities

Before continuing to manually tune and eventually optimise the parameter values, a sensitivity analysis should be conducted to pinpoint the most sensitive parameters. This is important since only the most sensitive parameter should be tuned manually and the most insensitive parameters should be excluded from the simultaneous optimisation routine.

Based on the initial parameter values, it might not always be possible to solve the model. Therefore manual tuning of the parameters can be necessary before a sensitivity analysis can be carried out. Thus, Step 2 and 3 are not fully sequential, but usually performed simultaneously.

For an ODE system of the form

$$\frac{d\mathbf{y}}{dt} = \mathbf{f}(\mathbf{p}, \mathbf{y}, t) \tag{A.1}$$

the sensitivity coefficients, $\mathbf{u} = \frac{\partial \mathbf{y}}{\partial \mathbf{p}}$, can be calculated as the solution to the ODE system (Himmelblau, 1968):

$$\dot{\mathbf{u}} = \frac{\partial \mathbf{f}}{\partial \mathbf{y}}\mathbf{u} + \frac{\partial \mathbf{f}}{\partial \mathbf{p}} \tag{A.2}$$

The initial condition for (A.2) is $\mathbf{u}(0) = \mathbf{0}$ provided $\mathbf{y}(0)$ does not depend on the parameters, $\mathbf{p}$. If one or more of the initial states were to be estimated the corresponding initial sensitivities will clearly be nonzero, however the initial states were not estimated in this work. The *relative sensitivity*, $\delta_{y,p}(i,j)$, for the j'th parameter, p_j, towards a concentration, y_i, can then be calculated as:

$$\delta_{y,p}(i,j) = \frac{p_j}{y_i} \cdot \frac{\partial y_i}{\partial p_j} \tag{A.3}$$

This measure for sensitivity is often used, however, for y_i values close to zero a very large relative sensitivity may be obtained due to the division by y_i. Therefore, in the current work, for all state values (y_i) below 0.001 the relative sensitivity function was set to zero.

The relative sensitivity in (A.3) was calculated with respect to a single state in the model. A *datapoint sensitivity* for a given parameter can be obtained by adding up the relative sensitivities for all states. For chemostat operation this datapoint sensitivity is calculated at different operation points (dilution rates) and then averaged to yield one *overall experiment sensitivity* for the experiment for a given parameter. The overall experimental sensitivity function, $\Delta_p(j)$, can be expressed as:

$$\Delta_p(j) = \frac{1}{n}\sum_{k=1}^{n}\sum_{i=1}^{N} \frac{p_j}{y_i(k)} \cdot \left| \left. \frac{\partial y_i}{\partial p_j} \right|_{x=x(k)} \right| \tag{A.4}$$

where n is the number of data points and N is the number of states in the model.

A.2.3 Step 3: Manual tuning

When a kinetic model is as complex as the one treated in this note, optimisation routines for simultaneous estimation of parameters require good initial estimates to ensure convergence to a physiological reasonable minimum. Manual tuning based on a priori knowledge of the cell metabolism was therefore applied to obtain a physiological reasonable solution of the model before all parameters were estimated simultaneously.

During manual tuning of parameters physiological knowledge about the metabolism of the microorganism is combined with the parameter sensitivities. If a metabolic flux analysis has been carried out, tuning of the parameters can be conducted not only by comparing the concentrations of the metabolites (actual data points) but also by comparing the flux distributions between data and model simulations. However, even if a flux distribution is not available, physiological knowledge regarding the relative fluxes through the pathways can be used in the estimation of parameters.

A.2.4 Step 4: Final optimisation

In this step a simultaneous estimation of selected kinetic parameters was performed using an optimisation routine.

The objective function, F, which was minimised during the parameter optimisation contains two terms: A least square term and a regularisation term:

$$\min_{\theta} F = \sum_{l=1}^{L} W_l \sum_{i=1}^{I_l} w_i^2 \sum_{k=1}^{K_{li}} (z(t_{lik}) - \hat{z}(\hat{\theta}, t_{lik}))^2 + W_{reg} \sum_{j=1}^{J} \lambda_j \left(\frac{\theta^{in} - \hat{\theta}}{\theta^{in}} \right)^2 \tag{A.5}$$

L is the number of different experiments, I_l the number of different measurements in the l'th experiment and K_{li} is the number of data points for the i'th measurement in the l'th experiment. $z(t_{lik})$ are the experimental data points while $\hat{z}(\hat{\theta}, t_{lik})$ are the corresponding model prediction. J is the number of parameters, θ is the parameter vector and θ^{in} is the initial value of the parameter vector. W_l, w_i, W_{reg} and λ_j are weights.

A.2.5 Step 5: Quality of estimates

Based on the experimental data used for parameter estimation a confidence interval for the estimated parameters was calculated based on the covariance matrix and a F-test on whether the parameter is significant or not (Himmelblau, 1968).

A.3 Results

The model applied as case study in this note was a two compartment biochemically structured model describing aerobic growth of *Saccharomyces*

cerevisiae under ideal fermentation conditions (Lei *et al.*, 2001).

The kinetic model includes 18 stoichiometric coefficients and 37 kinetic constants. All the stoichiometric coefficients was found from standard text books on biochemistry (Roels, 1983; Stryer, 1995) by using carbon and redox balances and assuming the biomass composition to be known. The remaining 37 kinetic parameters had to be found either in literature or estimated from experimental data.

A.3.1 Estimation data

The estimation data were selected such that the kinetic parameters were estimated based on both static as well as dynamic data to reduce the number of insensitive parameters to be estimated compared with using only steady-state data. For the yeast model, it was decided to use experimental data from three different modes of operation. Thus, experimental data from continuous cultivations (steady-state chemostat and dilution rate shift-up) and a batch cultivation were used for parameter estimation.

The chemostat data were obtained from Postma *et al.* (1989b) and Frandsen (1993) and consists of 111 data points. The experimental data for a batch cultivation (128 data points) and a dilution rate shift-up experiments (126 data points) were also obtained from Frandsen (1993). Obviously, by using experimental data from various authors the data quality might be lower compared to using a single data source. However, since no such source was available in literature, data from various authors had to be used. All data used for parameter estimation are collected in A.5.1.

A.3.2 Step 1: Obtaining initial parameter values

The parameter values found in literature are given in table A.1. However, not all values given in the table can directly be used in the yeast model. The affinity constants K_{1h} and K_{1l} are valid for the glucose uptake system whereas model reaction (r_1) is a lumped reaction that includes the glycolytic pathway as well as the glucose uptake system. Therefore it was expected that these values would change significantly during the parameter estimation, however the ratio between K_{1l} and K_{1h} should be maintained. For K_2 and K_3 it should be kept on mind that the ratio intracellular/extracelullular concentration of pyruvate in *S. cerevisiae* is approximately 100:1 at pH=5 (which was the operating condition) so the extracellular affinity constant should be decreased by a factor of 100 since the literature value is based on an intracellular concentration. Furthermore, reaction (r_3) is based on Hills equation where the pyruvate concentration is raised to the fourth power, which implies a further modification of K_3.

If a parameter cannot be found in literature an initial estimate can be calculated by inserting experimental data in the model (Nikolajsen and Nielsen, 1989). A rough estimate of the parameter value can be calculated

Table A.1. Affinity constants from literature.

Parameter	Value	Unit	Ref.
K_{1l}	3.6-9.0	[g/l]	Bisson and Fraenkel (1983); Postma *et al.* (1989a)
K_{1h}	0.18-0.36	[g/l]	Postma *et al.* (1989a)
K_2	0.0114-0.0572	[g/l]	Kresze and Ronft (1981)
K_3	0.523	[g/l]	Postma *et al.* (1989b)
K_4	$2.64 \cdot 10^{-4}$	[g/l]	Postma *et al.* (1989b)
K_5	0.0102	[g/l]	Frenkel and Kitchens (1981)
K_6	0.034	[g/l]	Barman (1969)
K_{6e}	0.057	[g/g]	Barman (1969)

based on a few data points from a chemostat experiment. Especially for the most sensitive parameters in the model it was important to have good initial estimates in order to be able to solve the model equations numerically. An example of how k_7 and K_7 were calculated from chemostat data is given in A.5.2.

In-vitro enzyme activity measurements can also be applied for obtaining initial estimates of rate constants. This method can be applied only if the modelled reaction is not lumped and is illustrated in A.5.3. This approach led to initial estimates for k_2, k_3, k_4, k_5, k_{5e} and k_6. It should, however, be pointed out that the *in-vitro* capacity of a given enzyme was used in the calculations, whereas the reactions in the model mirror *in-vivo* reactions. Furthermore, the *in-vitro* enzyme activities vary when changing the operation conditions hence the initial parameter estimate calculated also depends on the operation conditions. Therefore, the results from this approach should be interpreted carefully before applied to the model. Nevertheless, a crude estimate of the rate constants can be obtained by this method. All calculated initial estimates can be seen in table A.2.

The inhibition constants in the model were initially assigned a value corresponding to the concentration range where it is assumed inhibition of the current reaction sets in. Initial values for the remaining kinetic parameters were found by manually fitting experimental data with model simulations.

A.3.3 Step 2: Parameter sensitivities

Overall experimental sensitivities were calculated for all parameters for each of the experiments used for parameter estimation (batch, steady-state chemostat and dilution rate shift-up). The most sensitive parameters with respect to the overall experimental sensitivity in each experiment are

Table A.2. Initial parameter estimates calculated from experimental data (see section A.5.2+A.5.3).

Parameter	Value	Unit	Ref.
k_{1h}	0.87	[g/g/h]	Frandsen (1993); Postma *et al.* (1989b)
k_2	0.198	[g/g/h]	Flikweert *et al.* (1997)
k_3	3.57	[g/g/h]	Postma *et al.* (1989b)
k_4	99.1	[g/g/h]	Postma *et al.* (1989b)
k_5	0.108	[g/g/h]	Postma *et al.* (1989b)
k_{5e}	0.60	[g/g/h]	Postma *et al.* (1989b)
k_6	3.9	[g/g/h]	Postma *et al.* (1989b)
k_7	1.14	[g/g/h]	Frandsen (1993)
K_7	0.0043	[g/l]	Frandsen (1993)
k_8	0.832	[g/g/h]	Livense (1984); Postma *et al.* (1989b)

given in table A.3.

Table A.3. Overall experiment sensitivities for the 10 most sensitive kinetic parameters in the yeast model evaluated during chemostat ($D = 0.08, 0.12, ..., 0.44\ h^{-1}$), batch and dilution rate shift-up simulations, respectively.

Parameter	Chemostat $\Delta_p(j)$	Parameter	Batch $\Delta_p(j)$	Parameter	Shift-up $\Delta_p(j)$
k_7	44.3	k_7	18.9	k_7	154.7
k_{10}	23.9	k_{10}	8.62	k_{10}	101.2
k_2	13.1	k_4	3.19	k_2	38.5
k_{1h}	12.1	k_{9e}	2.18	k_{1l}	37.5
K_7	7.30	k_6	1.82	k_4	8.83
K_{1h}	2.57	k_{1l}	1.70	k_{1l}	6.07
k_{1e}	1.80	k_{6r}	1.42	k_9	4.13
k_{1l}	1.72	k_{1e}	1.16	k_{1e}	3.30
K_{1l}	1.63	k_{9c}	1.14	k_{9c}	3.11
K_{10}	1.20				

The sensitivity analysis led to two main conclusions:

1) As expected, rate constants were the most sensitive parameters and should therefore be attempted estimated. Due to the strong correlation between affinity and rate constants, the affinity constants should be fixed during this estimation.

2) The result of the sensitivity analysis pinpoints the most sensitive parameters for the various experiments, however validation of the reliability

of a given parameter was not obtained. Therefore confidence intervals should be calculated for all parameters estimated (step 5).

A.3.4 Step 3: Manual tuning

In the current model, four branch points were present: Glucose, pyruvate, acetaldehyde and acetate. At the glucose branch point, k_{1h} and k_7 were manually tuned by considering the flux distribution of glucose between catabolism and anabolism during a continuous cultivation. The ratio between the two rate constants must correspond to the carbon distribution between anabolism and catabolism at low dilution rates. k_2 and k_3 were tuned by considering the flux distribution at the pyruvate node for various fluxes through the glycolysis (corresponding to different dilution rates in a continuous cultivation) and it was ensured that the overflow towards acetaldehyde took place at the correct dilution rate by adjusting k_2. Similar tuning was performed for k_4 and k_6 at the acetaldehyde branch point. k_5, k_{5e} and k_8 were fitted to model the acetate accumulation during chemostat and batch experiments. In this way the most sensitive extracellular rate constants were tuned.

During the manual tuning the inhibition constants as well as the intracellular parameters were tuned to fit the experimental data as well as possible. Moreover, a final tuning of some affinity constants were made to obtain the correct concentration level during chemostat experiments.

A.3.5 Step 4: Final optimisation

Due to the strong correlation between the rate and affinity constants in Monod-type expressions mentioned earlier, it was decided to omit the affinity constants from the final parameter estimation. The exclusion of affinity constants can be justified by the low sensitivity of most of these parameters found in step 2. It turned out that the affinity constants values found in literature could be applied without modifications (except for those mentioned during step 1) while the remaining affinity constants were determined through manual tuning in step 3.

A total of 22 parameters (18 rate and 4 inhibition constants) were estimated in gPROMS (Process Systems Enterprise Ltd.) using a weighted least square method with Tikhonov regularisation included.

The tuning of the objective function weights was performed with the purpose of obtaining an acceptable distribution between the contributions from the three experiments and the regularisation term to the objective function. The regularisation weights, λ_j, were all set to 1 since the contribution from each parameters already was normalised in the objective function (division by θ_j). The weights on the various experiments were set to 1 ($W_{l=chemostat}$, $W_{l=batch}$ and $W_{l=shift}$) while W_{reg} was set to 100. Values for the measurements weights can be found in table A.4.

Table A.4. Measurement weights, w_i, used during parameter estimation.

Measurement	Chemostat	Batch	Shift-up
q_{glu} (uptake)	1	-	-
glucose	5	1	7
pyruvate	40	50	40
acetaldehyde	6	-	-
acetate	10	10	5
ethanol	1.5	0.5	1
biomass (DW)	2	-	1
X_a	5	1.5	5
X_{Acdh}	60	-	-
OUR	0.7	-	-
CER	0.5	-	-

For the current model data were available for the glucose uptake rate for various dilution rate in a chemostat. These data were used as data points and compared with the total glucose conversion (r_1+r_7).

During the simultaneous estimation of parameters the parameter space was constrained by setting upper and lower limits for a given parameter value. These bound were set more or less empirically since most of the estimated parameters do not have a physiological reasonable upper and lower limit.

The final estimates of the model parameters are given in table A.5.

A.3.6 Step 5: Quality of estimates

The confidence intervals listed in table A.6 states the interval for which the estimated parameters with a probability of 95% will lie based on a F-test. The table shows confidence intervals for four cases: 1) When the parameters were estimated using only chemostat data, 2) using only batch data, 3) using chemostat and D-shift-up data and finally 4) using all three experiments simultaneously. It can be seen that the confidence intervals decrease as more experiments are included in the estimation procedure and for most of the estimated parameters an acceptable confidence level is obtained.

The correlation between the estimated parameters was calculated by computing the normalised covariance matrix. The matrix is presented in table A.7 and the most pronounced correlations between the parameters are shown in bold. A covariance of 1 means that two parameters are fully correlated whereas a value of zero indicates that the two parameters are not correlated.

Table A.5. Kinetic parameter values for the model. Parameter units are given in the list of symbols.

Parameter	Value	Parameter	Value	Parameter	Value
k_{1h}	0.584	k_4	4.80	K_7	0.0101
K_{1h}	0.0116	K_4	$2.64 \cdot 10^{-4}$	k_8	0.589
k_{1l}	1.43	k_5	0.0104	k_9	0.008
K_{1l}	0.94	K_5	0.0102	K_9	$1.0 \cdot 10^{-6}$
k_{1e}	47.1	k_{5e}	0.775	k_{9e}	0.0751
K_{1e}	0.12	K_{5e}	0.10	K_{9e}	13
K_{1i}	14.2	K_{5i}	440	K_{9i}	25
k_2	0.501	k_6	2.82	k_{9c}	$3.99 \cdot 10^{-3}$
K_2	$2.0 \cdot 10^{-5}$	K_6	0.034	k_{10}	0.392
K_{2i}	0.101	k_{6r}	0.0125	K_{10}	$2.3 \cdot 10^{-3}$
k_3	5.81	K_{6e}	0.057	k_{10e}	$3.39 \cdot 10^{-3}$
K_3	$5.0 \cdot 10^{-7}$	k_7	1.203	K_{10e}	$1.8 \cdot 10^{-3}$
				k_{11}	0.02

A.4 Discussion and Conclusions

The model performance with respect to limitations in the structure was evaluated in the model paper (Lei *et al.*, 2001), however the quality of the obtained parameter estimates and the estimation procedure will be discussed here.

The first step in the parameter estimation procedure was to obtain initial values for all parameters in the model in order to be able to solve the model. Literature data of enzyme kinetics and calculations based on model equations were used for obtaining a rough estimate of the parameters.

Manual tuning of some parameters was necessary in order to initially obtain a solution for the model. Although manual tuning of parameters is a very empirical method, it was shown how this method could be applied together with physiological knowledge to fit the overflow metabolism according to the model assumptions by adjusting the most sensitive parameters.

The results from the sensitivity analysis showed that the rate constants were much more sensitive that affinity constants. This supports the decision of not including affinity constants in the simultaneous estimation in step four. Two of the most sensitive parameters in the chemostat case were k_7 and K_7, however due to the strong correlation between them, it was not possible to obtain a robust estimate of both parameters from the experiment.

By including regularisation in the optimisation step a constraint was imposed on the insensitive parameters. This led to an easier optimisation

Table A.6. Confidence intervals (±) for the parameters estimated during the final optimisation step. The confidence intervals are based on the 95% significance level in a F-test, thus the parameters will lie within the estimated interval with a probability of 95%.

Parameter	Value	Only Chemostat	Only Batch	Chemostat and Shift-up	All
k_{1l}	1.430	±2.390	±1.588	±0.717	±0.302
k_{1h}	0.584	±0.190	±5.445	±0.076	±0.033
k_{1e}	47.100	±9.510	±39.392	±4.887	±3.684
K_{1i}	14.200	±7.365	±19.359	±3.414	±2.615
k_2	0.501	±0.097	±22.572	±0.056	±0.047
K_{2i}	0.101	±1.507	±9.914	±0.853	±0.415
k_3	5.810	±2.028	±2.483	±1.211	±0.419
k_4	4.800	±13.068	±13.565	±4.688	±2.987
k_5	0.010	±0.207	±1.892	±0.087	±0.051
K_{5i}	440.000	±40.755	±21.842	±22.632	±2.763
k_{5e}	0.775	±8.340	±6.229	±2.323	±0.889
k_6	2.820	±1.789	±5.125	±0.911	±0.561
k_{6r}	0.013	±0.014	±0.028	±0.007	±0.003
k_7	1.203	±0.229	±0.441	±0.105	±0.042
k_8	0.589	±4.628	±0.054	±1.435	±0.004
k_9	0.008	±0.100	±0.245	±0.029	±0.008
k_{9e}	0.075	±0.535	±0.475	±0.120	±0.056
K_{9i}	25.000	±41.398	±42.842	±22.272	±4.176
k_{9c}	0.004	±0.029	±0.141	±0.012	±0.008
k_{10}	0.392	±0.260	±0.327	±0.050	±0.028
k_{10e}	0.003	±0.277	±0.095	±0.055	±0.013
k_{11}	0.020	±1.161	±0.168	±0.172	±0.009

Table A.7. Normalised covariance matrix for the estimated parameters during the final optimisation. The numerically largest covariances between the parameters are shown in bold (threshold value: 0.650).

	k_{1l}	k_{1h}	k_{1e}	K_{1i}	k_2	K_{2i}	k_3	k_4	k_5	K_{5i}	k_{5e}	k_6	k_{6r}	k_7	k_8	k_9	k_{9e}	K_{9i}	k_{9c}	k_{10}	k_{10e}	k_{11}
k_{1l}	1.000																					
k_{1h}	**-0.673**	1.000																				
k_{1e}	0.217	-0.297	1.000																			
K_{1i}	0.215	-0.379	**0.685**	1.000																		
k_2	0.001	-0.093	0.015	0.077	1.000																	
K_{2i}	-0.212	-0.076	-0.082	0.187	0.042	1.000																
k_3	0.151	-0.082	0.422	0.205	-0.167	0.146	1.000															
k_4	-0.111	0.124	-0.351	-0.285	0.008	0.062	-0.053	1.000														
k_5	-0.031	0.294	-0.011	-0.111	**-0.788**	0.103	0.148	-0.191	1.000													
K_{5i}	-0.292	0.370	-0.382	-0.476	0.081	-0.390	-0.270	-0.293	-0.011	1.000												
k_{5e}	0.211	-0.276	-0.225	-0.125	0.295	0.043	-0.091	0.289	-0.525	-0.048	1.000											
k_6	0.090	0.089	-0.109	**-0.663**	0.005	-0.244	0.006	0.000	0.080	0.382	0.110	1.000										
k_{6r}	-0.011	0.207	-0.614	-0.730	-0.029	-0.039	-0.202	0.419	0.095	0.283	0.285	**0.690**	1.000									
k_7	-0.135	0.474	-0.351	-0.542	-0.229	-0.264	0.017	0.272	0.326	0.281	0.009	0.323	0.418	1.000								
k_8	0.417	-0.469	**0.820**	**0.693**	0.046	0.063	0.588	0.003	-0.169	-0.555	0.129	-0.185	-0.444	-0.341	1.000							
k_9	0.264	-0.363	0.092	0.158	0.432	0.008	-0.178	-0.345	-0.362	0.177	0.417	0.047	-0.208	-0.131	0.113	1.000						
k_{9e}	0.192	-0.153	0.183	0.027	0.119	-0.160	-0.161	**-0.671**	-0.018	0.377	0.283	0.252	-0.052	-0.003	-0.018	0.526	1.000					
K_{9i}	-0.171	0.264	**-0.774**	-0.632	-0.140	0.096	-0.389	-0.019	0.262	0.199	-0.122	0.103	0.378	0.239	**-0.868**	-0.174	-0.086	1.000				
k_{9c}	-0.062	0.313	0.012	-0.086	**-0.734**	0.063	0.214	-0.429	**0.878**	0.081	-0.509	0.066	0.048	0.227	-0.202	-0.454	0.116	0.316	1.000			
k_{10}	0.149	0.139	-0.234	-0.354	-0.052	-0.135	0.085	0.472	0.080	-0.115	0.277	0.197	0.331	**0.849**	-0.028	0.029	-0.110	0.081	-0.085	1.000		
k_{10e}	-0.592	0.605	-0.316	-0.438	0.019	-0.341	-0.265	-0.118	0.060	**0.831**	-0.268	0.282	0.228	0.349	-0.600	-0.101	0.150	0.191	0.111	-0.128	1.000	
k_{11}	-0.246	0.292	**-0.691**	-0.523	-0.124	0.437	-0.133	0.002	0.309	0.321	0.085	0.135	0.414	0.473	-0.607	0.032	0.057	0.646	0.314	0.356	0.146	1.000

problem by preventing these parameters from moving around randomly in the parameter space. Since it was found that the sensitivities of the estimated parameters differed significantly, it was justified to use Tikhonov regularisation during the optimisation step.

Due to the use of regularisation where the initial estimates are part of the objective function, a rerun of the estimation routine with the minimising parameter set as initial values did not give exactly the same estimates as the previous run since the objective function had been changed. It was therefore difficult to check whether a global minimum was reached. However it is believed that the proposed methodology, where much effort is placed on obtaining physiologically reasonable initial estimates, provides a parameter set corresponding to a physiologically reasonable local minimum.

The importance of using data from different operating conditions is evident from the calculated confidence intervals in table A.6. E.g. the parameter, k_8 (biomass formation from acetate), was only sensitive during batch growth. This fits well with the physiological assumption in the model that this reaction is repressed by glucose and therefore only active after glucose depletion in a batch cultivation. On the contrary, the rate constant for conversion of pyruvate in the TCA cycle, k_2, is very insensitive during a batch cultivation, and a chemostat experiment is needed for robust estimation of this parameter. These examples show the necessity of using both dynamic and steady-state data in the parameter estimation procedure.

Most of the estimated parameters in the final optimisation have a reasonable confidence interval indicating that the experiments chosen for parameter estimation were sufficient. However, for some parameters an acceptable estimate was not obtained which implies that either the parameter is insensitive towards all the experiments used or the model structure cannot describe all experimental data used for estimation. Since most of the parameters in question were shown to be sensitive during the sensitivity analysis in step 2, the reason for the large confidence interval must be due to an insufficient model structure. The largest deviations were:

- K_{2i}: The model does not account for the increase in OUR at D_{crit} due to an uncoupling effect (Postma *et al.*, 1989b).
- k_4 and k_{5e}: The model is generally not able to quantify the acetate profile satisfactorily as discussed in Lei *et al.* (2001).
- k_9 and k_{9c}: Discrepancies in the description of X_{Acdh} compartment.
- k_{10e}: Decay of X_a during growth on ethanol is not well described.

The first two cases have been dealt with in the model paper, however the large confidence intervals for k_9, k_{9c} and k_{10e} points to that the modelling of the compartments in the model does not fit the experimental data

very well. Thus more experimental data which can be related to the two compartments should be obtained to improve the modelling of the compartments.

The covariance matrix in table A.7 shows that although some parameters are quite correlated, most parameters estimated in the optimisation step are only weakly correlated and thereby suitable for being estimated simultaneously. The strongest correlations between parameters are found between rate constants in reactions leading to a metabolite or biomass and reactions involved in generation or degradation of a compartment. E.g. the covariance between k_7 (production of biomass) and k_{10} (degradation of active biomass compartment) is 0.849 and a perturbation in both rate constants will affect the biomass concentration strongly. Thus, for a structured model it is very difficult to estimate parameters involved in pathway reactions and parameters involved in cell compartmentation independently from each other.

After the simultaneous estimation of parameters in step four an evolutionary algorithm could be used for determining a parameter set corresponding to a more global minimum, however it was not attempted in this work.

List of symbols

CER	carbon dioxide evolution rate [mmole CO_2/h]
D	dilution rate [h^{-1}]
f_i	ith model equation
F	objective function
I_i	number of different measurements in the l'th experiment
k_i	rate constant for reaction i [g substrate /g X_a/h]
K_{li}	number of data points for the i'th measurement in the l'th experiment
K_i	affinity constant for reaction i [g-substrate/l]
K_{ji}	inhibition constant for reaction j [l/g-substrate]
K_M	affinity constant [g-substrate/l]
L	number of experiments
n	number of datapoints during sensitivity analysis
N	number of states in the model
OUR	oxygen uptake rate [mmole O_2/h]
p_j	jth kinetic parameter
q_{CO_2}	specific carbon dioxide evolution rate [mmole CO_2/g DW/h]
q_{O_2}	specific oxygen uptake rate [mmole O_2/g DW/h]
q_{glu}	glucose uptake rate [g glu/h]
r_i	reaction rate for reaction i [h^{-1}]
s_i	extracellular concentration of component i [g/l]
S_f	inlet concentration of glucose in chemostat [g/l]
S_i	intracellular concentration of component i
u	sensitivity coefficient
U	specific enzyme activity [g enzyme · mg protein/g bio]
v_{max}	rate constant [h^{-1}]
V	volume [l]
w_i	weight on measurement i
W_l	weight on experiment l
W_{reg}	weight on regularisation term
y_i	ith model state
x	biomass concentration [g/l]
X_i	Intracellular concentration of compartment i [no unit, between 0 and 1]
z_{lik}	experimental data point
$\hat{z_{lik}}$	estimated state in model
$\delta_{f,p}$	relative sensitivity of parameter p with respect to function f
Δ_p	overall experiment sensitivity of parameter p
θ	parameter vector
$\hat{\theta}$	estimated parameter vector
λ_j	weight on parameter j

References

Baltes, M.; Schneider, R.; Sturm, C. and Reuss, M. (1994). Optimal experimental design for parameter estimation in unstructured growth models. *Biotechnol. Prog.*, **10**, 480–488.

Barman, T. (1969). *Enzyme Handbook vol.1*. Springer-Verlag Heidelberg New York.

Bisson, L. and Fraenkel, D. (1983). Involvement of kinase in glucose and fructose uptake by *Saccharomyces cerevisiae*. *Proc. Natl. Acad. Sci.*, **80**, 1730–1734.

Flikweert, M.; van Dijken, J. and Pronk, J. (1997). Metabolic responses of pyruvate decarboxylase-negative *Saccharomyces cerevisiae* to glucose excess. *Appl Environ Microbiol*, **63**, 3399–3404.

Frandsen, S. (1993). *Dynamics of Saccharomyces cerevisiae in continuous culture*. Ph.D. thesis, IBT, Technical University of Denmark.

Frenkel, E. and Kitchens, R. (1981). Acetyl-CoA synthetase from baker's yeast (*Saccharomyces cerevisiae*). *Methods Enzymol.*, **71**, 317–324.

Hansen, P. (1996). *Rank-deficient and discrete ill-posed problems*. Polyteknisk Forlag. Doctoral thesis.

Himmelblau, D. (1968). *Process analysis by statistical methods*. John Wiley and Sons.

Holmberg, A. (1981). A systems engineering approach to biotechnical processes - Experiences of modelling, estimation and control methods. *Acta Polytech. Scand.*, **Ma 33**, 1–45.

Kresze, G.-B. and Ronft, H. (1981). Pyruvate dehydrogenase complex from baker's yeast. I. Purification and some kinetic and regulatory properties. *Eur. J. Biochem.*, **119**, 573–579.

Lei, F.; Rotbøll, M. and Jørgensen, S. (2001). A biochemically structured model for *Saccharomyces cerevisiae*. *Accepted for publication in J. Biotechnol.*.

Livense, J. (1984). *An investigation of the aerobic, glucose-limited growth and dynamics of* Saccharomyces cerevisiae. Ph.D. thesis, Purdue University, USA.

Munack, A. (1988). Optimal feeding strategy for identification of Monod-type models by fed batch experiments. *Reprints of the 4th International Congress on Computer Applications in Fermentation Technology*.

Nihtilä, M. and Virkukunen, J. (1977). Practical identifiability of growth and substrate consumption models. *Biotechnol. Bioeng.*, **19**, 1831–1850.

Nikolajsen, K. and Nielsen, J. (1989). *Structured models for microbial systems*. Ph.D. thesis, IBT, Technical University of Denmark.

Postma, E.; Scheffers, A. and van Dijken, J. (1989a). Kinetics of growth and glucose transport in glucose-limited chemostat cultures of *Saccharomyces cerevisiae* CBS 8066. *Yeast*, **5**, 159–165.

Postma, E.; Verduyn, C.; Scheffers, A. and van Dijken, J. (1989b). Enzymic analysis of the Crabtree effect in glucose-limited chemostat cultures of *Saccharomyces cerevisiae*. *Appl. Env. Microbiol.*, **55**, 468–477.

Roels, J. (1983). *Energetics and kinetics in biotechnology*. Elsevier Biomedical Press.

Schmidt, K. and Isaacs, S. (1995). An evolutionary algorithm for initial state and parameter estimation in complex biochemical models. *Preprints of the 6th Int. Conference on Computer Appl. in Biotech.*, pages 239–242.

Sebastian, J.; Mian, F. and Halvorson, H. (1973). Effect of the growth rate on the level of the DNA-dependent RNA polymerases in *Saccharomyces cerevisiae*. *Febs. Letters*, **34**, 159–162.

Stryer, L. (1995). *Biochemistry 4th edition*. W.H. Freeman and Company, New York.

A.5 Appendices

A.5.1 Parameter estimation data

A.5.1.1 Batch data

Table A.8. Batch data used for estimation of kinetic parameters. All data are from Frandsen (1993).

Time [h]	glu [g/l]	pyr [g/l]	acetate [g/l]	etoh [g/l]	4×RNA [g RNA/g DW]
0	14	0	0	0.13	-
1	14	0	0.015	0.12	-
2	14	0	0.01	0.125	0.04
3	14	0	0.02	0.11	0.064
4	14	0	0.025	0.112	0.24
5	14	0	0.005	0.11	0.16
6	14	0	0.04	0.14	0.26
7	14	0	0.03	0.15	0.136
8	14	0	0.03	0.16	0.12
9	14	0	0.025	0.22	0.172
10	14	0	0.025	0.235	0.16
11	14	0.002	0.03	0.3	0.1
12	13.2	0.002	0.035	0.4	0.228
13	13	0.005	0.04	0.45	0.268
14	12.5	0.01	0.05	1.4	0.3
15	10.8	0.013	0.1	1.75	0.464
16	9.6	0.016	0.12	2.75	0.428
17	8	0.02	0.115	4.15	0.44
18	4.9	0.018	0.175	4.75	0.4
19	0.7	0.017	0.21	6.2	0.372
20	0	0.002	0.25	5.85	0.36
21	0	0	0.275	5.8	0.352
22	0	0	0.285	5.75	0.352
23	0	0	0.175	5.5	0.32
24	0	0	0.08	5.25	-
25	0	0	0.02	5	0.32
26	0	0	0.04	4.5	0.332
27	0	0	0.04	3.8	0.24
28	0	0	0.07	3.1	0.208
29	0	0	0.06	2.1	0.152
30	0	0	0.02	0.8	0.168
31	0	0	0.015	0.08	0.16
32	0	0	0.015	0.05	0.16

A.5.1.2 Chemostat data

Table A.9. Chemostat data used for estimation of kinetic parameters. All data are from Postma *et al.* (1989b) except the RNA measurements and q_{glu} (the glucose uptake rate) which are from Frandsen (1993). During the parameter estimation the glucose uptake rate was compared with the sum of model reactions r_1+r_7 corresponding to the glucose converted in the model. Note that the RNA content given is four times the actual measured value in [g RNA/g DW]. This is due to the assumption that the active biomass compartment, X_a, is proportional to the RNA content of the cell and the proportionality factor is 4. (0*) indicates that no traces of the metabolite could be detected and a value of zero has been used during parameter estimation.

D [h^{-1}]	glu [g/l]	pyr [g/l]	acet [g/l]	acetate [g/l]	etoh [g/l]	biomass [g DW/l]	4× RNA [g RNA /g DW]	$A_{Acdh,NAD}$ [U/mg]	q_{O_2} [mmole /g DW/h]	q_{CO_2} [mmole /g DW/h]	q_{glu} [g glu /h]
0.10	0.008	-	-	-	-	7.5	0.204	0.0304	2.5	2.6	0.17
0.15	0.015	-	-	-	-	7.5	0.268	0.0328	4.1	4.2	0.33
0.20	0.0195	-	-	-	-	7.5	0.292	0.0232	5.3	5.5	0.38
0.25	0.026	-	-	-	-	7.5	-	0.0252	6.9	7.1	0.48
0.275	-	-	-	-	-	7.65	0.336	0.0152	6.9	7.5	0.52
0.30	-	0.0002	-	-	-	7.5	-	0.02	7.3	8.0	0.57
0.325	0.0305	-	0*	0.012	0*	7.5	0.38	0.0104	9.1	9.5	0.625
0.34	-	0.0016	0*	0.006	0*	7.275	-	-	9.9	10.2	-
0.365	0.0336	0.0045	0*	-	0*	7.05	0.412	-	9.8	10.1	0.70
0.38	0.0482	0.0078	0*	-	0.37	7.125	0.464	-	11.8	12.0	0.80
0.39	-	0.0104	0.051	0.096	1.06	3.6	-	-	11.5	18.0	-
0.40	0.1097	-	0.167	0.126	2.39	3.3	0.576	0.016	9.5	20.5	-
0.415	0.1074	0.024	0.180	0.168	3.22	3.03	0.516	-	9.6	23.0	1.5
0.43	0.121	-	0.172	0.18	3.55	2.7	0.556	0.004	9.8	25.0	1.65
0.45	0.1779	0.0365	0.129	0.18	3.50	2.475	0.528	-	10.3	30.0	1.95
0.47	-	-	-	0.15	2.95	2.55	-	0.004	10.4	29.0	-
0.48	-	0.0294	-	0.12	2.67	2.55	-	0.004	10.5	30.5	-

A.5.1.3 Dilution rate shift-up data

Table A.10. Dilution rate shift-up data used for estimation of kinetic parameters. All data are from Frandsen (1993). As in table A.9 the RNA content given is four times the actual measured value in [g RNA/g DW].

Time [h]	glu [g/l]	pyr [g/l]	acetate [g/l]	etoh [g/l]	biomass [g DW/l]	4×RNA [g RNA/g DW]
0.000	0.02	0.002	-	0	7.75	0.208
0.017	-	0.0018	-	0	-	-
0.033	0.05	0.003	-	0	-	-
0.050	-	0.0045	0.007	0	-	-
0.067	0.08	0.005	-	0.02	-	-
0.083	-	0.004	-	0.023	-	-
0.12	0.105	0.0035	0.018	0.04	-	-
0.15	0.125	0.004	0.015	0.06	7.02	-
0.18	0.14	0.0038	0.02	0.09	-	0.22
0.22	-	0.0046	0.019	0.11	6.81	-
0.25	-	0.0049	0.03	0.15	-	-
0.28	-	0.0055	0.034	0.16	-	-
0.32	0.11	0.0063	0.045	0.175	6.52	0.252
0.42	-	0.007	0.05	0.185	6.37	-
0.50	0.08	0.0075	0.06	0.24	-	0.256
0.67	0.065	0.0082	0.075	0.26	6.01	0.284
1.00	0.059	0.0095	0.08	0.28	5.90	0.308
1.33	0.05	0.011	0.08	0.29	5.94	-
1.67	0.045	0.01	0.075	0.3	5.86	0.32
2.00	0.04	0.0095	0.065	0.305	6.01	-
2.67	0.036	0.007	0.06	0.315	6.08	0.312
3.33	0.033	0.0062	0.055	0.28	6.15	0.328
3.67	0.03	0.006	0.053	0.23	-	0.328
4.00	0.028	0.0062	0.058	0.2	6.30	0.33
4.50	0.025	0.004	0.07	0.07	6.73	0.324
5.00	0.026	0.0045	-	0.01	6.95	0.328
5.50	0.024	0.0035	0.005	0.005	7.02	0.312
6.00	0.027	0.0036	0.003	0	6.95	0.316

A.5.2 Example 1

In this example it is shown how an initial guess for the kinetic parameters in reaction (r_7) was calculated based on experimental data. Consider the mass balance for biomass:

$$\frac{\mathrm{d}x}{\mathrm{dt}} = (0.732\, r_7 + 0.619\, r_8 - \mathrm{D}) \cdot x \qquad \text{(A2.1)}$$

Since it is assumed that reaction (r_8) is repressed by glucose, only reaction (r_7) is active during growth on glucose in a continuous culture. Considering steady-state yields:

$$0.732\, k_7 \cdot \frac{s_{glu}}{s_{glu} + K_7} \cdot X_a - \mathrm{D} = 0 \qquad \text{(A2.2)}$$

Now experimental data from Frandsen (1993) obtained for *S. cerevisiae*, CBS 8066 in a continuous culture with glucose as limiting substrate was used. Two data points were considered:

$D = 0.200\,\mathrm{h^{-1}}$, $s_{glu} = 19.5\,\mathrm{mg/l},$, Intra. RNA $= 7.3\%$ ($\Rightarrow X_a = 0.292$)
$D = 0.415\,\mathrm{h^{-1}}$, s_{glu}= 107.4 mg/l, Intra. RNA $= 12.9\%$ ($\Rightarrow X_a = 0.516$)

To quantify the amount of active biomass pool, X_a, it was assumed that X_a is proportional to the level of intracellular RNA, which is given as %RNA [100% · g RNA/ g biomass]. The proportionality factor was set to 0.04 [X_a/%RNA].

(A2.2) was then solved for k_7 and K_7:

$$k_7 = 1.14\, \frac{\mathrm{g\,glu}}{\mathrm{g}\, X_a/\mathrm{h}}; \qquad K_7 = 0.0043\ \mathrm{g\,glu/l} \qquad \text{(A2.3)}$$

To conclude, calculations of affinity constants based on parts of the model and chemostat data are very uncertain due to the strong correlation between the rate and affinity constant. The method is therefore of applicable for calculating good initial estimates for rate constants while one should be more reluctant to use the method for estimating affinity constants.

A.5.3 Example 2

In Michaelis-Menten kinetics, the rate constant can be interpreted as a maximum capacity for the reaction. Consider the reaction (r_3) from pyruvate to acetaldehyde which is catalysed by pyruvate decarboxylase(PDC). The experimental measured specific enzyme activity can be converted to a rate constant under the assumption that the enzyme activity is approximately constant during all growth conditions. Postma *et al.* (1989b) measured the specific activity of PDC *in vitro* during a chemostat experiment. Although the specific enzyme activity increased approximately 25%

at the critical dilution rate it can be considered constant for the purpose of calculating an initial estimate of k_3.

An average specific enzyme activity of 0.6 U/mg protein was used in these calculations. Furthermore it was assumed that the protein content in the cell is proportional to the active biomass compartment, X_a, using a proportionality factor of 3/2 (g protein/g X_a). The assumption of proportionality between protein content and X_a is quite valid since Sebastian *et al.* (1973) has showed that the protein content in yeast cells increased from 0.35 to 0.62 (g protein/g cell) from low to high dilution rates during a chemostat experiment which corresponds nicely with 4*RNA content of the cell (according to Frandsen (1993)). The specific enzyme activity can be converted to the same unit as k_3:

$$\begin{aligned} \mathrm{A_{PDC}} &= 0.60\,\mathrm{U/mg\ pro} \\ &= 0.60 \cdot 10^{-6} \frac{\text{mole pyr}}{\text{mg pro} \cdot \text{min}} \cdot 88.07 \frac{\text{g pyr}}{\text{mole pyr}} \cdot 1.5 \frac{\text{mg pro}}{\text{mg X}_\text{a}} \\ &\quad \cdot 60 \frac{\text{min}}{\text{h}} \cdot 1000 \frac{\text{mg}}{\text{g}} \\ &= 4.76 \frac{\text{g pyr}}{\text{g X}_\text{a} \cdot \text{h}} \end{aligned}$$

which then was used as an initial estimate for k_3.

B

Matlab files - documentation

B.1 Calculations performed on dynamic data

To perform a comprehensive interpretation of raw fermentation process data such as flow rates, metabolite and biomass concentrations, balance readings etc., the data should be expressed as reaction rates in order to quantify the fluxes into and out from the cell at any given time (Nielsen and Villadsen, 1994). The quality of the data should be checked to ensure that the elementary balances close and no gross measurement errors are present (Heijden *et al.*, 1994a). Only when these steps have been performed (and no significant measurement errors have been observed), the data can be used for metabolic flux analysis. Methods for transforming raw process data into reconciled reaction rates have been proposed by Wang and Stephanopoulos (1983); Heijden *et al.* (1994a) and recently Herwig *et al.* (2001) extended the methodology to be valid during dynamic conditions when the accumulation term cannot be neglected.

The conversion from raw process data into reconciled reaction rates requires several calculation steps. In this work, data obtained during dynamic conditions were converted into reconciled reaction rates through a number of calculation steps. All steps were carried out in Matlab through a series of Matlab functions which were written in order to automate the calculation procedure. The reconciled reaction rates were used as input to the metabolic flux model described in Lei (2001, chap.5). This model was also implemented as a Matlab function.

In this appendix, all Matlab functions used in data treatment are described. Furthermore, at the end of the appendix, an example of a main Matlab file, calling the described functions ,are given.

B.2 Structure of process data matrix

The raw process data are entered as a matrix where each row corresponds to a different time. The structure of the on-line process data matrix, `Mdata`, is given in table B.1.

Table B.1. Structure of on-line process data matrix, Mdata. These measurements were sampled with a one minute interval.

Column	DTU data	EPFL data
1	Time [h]	Time [h]
2	Substrate balance [g]	Substrate balance [g]
3	Dilution rate setpoint [h^{-1}]	Flow rate [g/s]
4	Fermenter balance [g]	Fermenter balance [g]
5	Base balance [g]	Base balance [g]
6	$\%O_2$ in outlet air	$\%O_2$ in outlet air
7	$\%CO_2$ in outlet air	$\%CO_2$ in outlet air
8	pO_2 [%]	pO_2 [%]
9	D_{ref} [h^{-1}]	pH
10	OD biomass sensor [g/l]	Temperature [°C]
11	CH_x signal [V]	Stirrer speed [rpm]
12	Figaro sensor [V]	Figaro sensor [V]
13	Airflow [l/min]	Airflow [l/min]

B.3 Flow rates (dilu.m)

```
[rOH,D,D2,F]=dilu(Mdata,Cbase,vol,Int1,Int2,Int3)
```

The function calculates base addition rate, `rOH` [M/h], substrate feed rate, `F` [1/h], and dilution rate, `D` [1/h], based on the base and substrate balances. The dilution rate is also obtained based on a pump speed estimate provided by the substrate pump, `D2` (for the EPFL data) or the setpoint to the dilution rate controller (DTU data). The advantage of `D2` compared with `D` calculation is that the pump speed output (EPFL) or the dilution rate setpoint (DTU) was kept constant when the feed bottle was refilled whereas the `D` calculation results in a discontinues estimate of the dilution rate during refilling of the feed bottle.

`Mdata` is the on-line process data matrix containing (given in table B.1). `Cbase` is the base concentration, `vol` is the working volume, `Int1` and `Int2` are the number of samples used for calculation of `D` and `rOH` and `Int3` is the number of samples over which the calculated `rOH` is averaged to obtain a more smooth estimate.

In the calculations, the density of the feed solution was set to 1.018 and the density of the base is set to 1.000 g/ml.

B.4 Molar gas rates (gasberegn.m)

```
[CER,OUR,RQ]=gasberegn(Mdata,co2_in,o2_in,vol,o2_wet)
```

This subroutine calculates the molar carbondioxide evolution rate, `CER`, and oxygen uptake rate, `OUR`. Additionally the respiratory quotient, `RQ`, is

calculated. The formula used is according to van Urk *et al.* (1988).

$$y_{H_2O} = \frac{y_{O_2,in} - y_{O_2,wet}}{y_{O_2,in}} \tag{B.1}$$

$$F_{g,out}\ [\text{l/min}] = F_{g,in} \cdot \frac{1 - y_{O_2,in} - y_{CO_2,in}}{1 - y_{O_2} - y_{CO_2} - y_{H_2O}} \tag{B.2}$$

$$CER\ [\text{mmole/l/h}] = 1000 \cdot 60 \cdot \frac{F_{g,out} \cdot y_{CO_2} - F_{g,in} \cdot y_{CO_2,in}}{V_m \cdot vol} \tag{B.3}$$

$$OUR\ [\text{mmole/l/h}] = 1000 \cdot 60 \cdot \frac{F_{g,in} \cdot y_{O_2,in} - F_{g,out} \cdot y_{O_2}}{V_m \cdot vol} \tag{B.4}$$

where $y_{O_2,wet}$ is the oxygen reading when there is no metabolic activity but only evaporation of water. It was assumed that this quantity remains constant throughout the experiment. V_m is the molar volume (24.4 mole/l was used) and F_g is the airflow.

B.5 Consumption rates (rM_calc.m)

```
[rM,M_int]=rM_calc(M,Mdata,Mw,M_feed,Int,Cbase)
```

The function calculates the rate of consumption, `rM`, for a given metabolite, M, based on the concentration of M using a dynamic mass balance. Since the sampling frequency of metabolites such as ethanol, glucose and acetate usually is larger than the sampling frequency for gas rates, the function initially carries out a linear interpolation (and extrapolation) between the measured data points to obtain a metabolite vector, `M_int`, of the same length as the time column in `Mdata`.

`M` is a matrix (two columns) consisting of a time column and a concentration column.

The metabolite consumption rate, `rM`, is subsequently calculated using a discrete version of the dynamic mass balance in a window of `Int` samples (This value was set to 1 to obtain instant rates, since the calculated gas rates from `gasberegn.m` were not averaged as well). Finally the consumption rate is converted to the unit [C-mole/l/h] by division of the molar weight, `Mw`.

In the case where the metabolite is presented in the feed, the metabolite feed concentration, `M_feed`, and the base concentration, `Cbase`, also need to be specified.

B.6 Smoothing of rates (rx_smooth.m)

```
r_smo=rx_smooth(rM,Int)
```

The function calculates a moving average of the reaction rate, `rM`, using `Int` samples. Thus, a less noisy signal is obtained on the expense of the fast dynamics. A value of 15 (minutes) was used for `Int`.

B.7 Estimation of reaction rates (r_est.m)

```
[r_est_Data,h,carbon,DR]=r_est(rData)
```

This function provides a least square estimate of all reaction rates, `r_est_Data`, based on the measured rates, `rData`, and elemental balances for C, H, O and N. Furthermore a statistical test, `stat_h`, is calculated to quantify the quality of the obtained estimate. Carbon and degree of reduction balances are calculated from the input reaction rates(`carbon` and `DR`).

Four different versions of `r_est` are available (`r_est1`, `r_est2`, `r_est3` and `r_est4`) each using different set of measurements. A comparison between the four different versions are given in table B.2

Table B.2. Overview of measured (m) and estimated (e) rates in each of the four reaction rates estimation functions.

Measurement	r_est1	r_est2	r_est3	r_est4
Glucose	m	m	m	m
O_2	m	m	m	m
CO_2	m	m	m	m
Acetate	m	m	m	m
Ethanol	e	m	m	m
Biomass	m	e	m	e
Glycerol	m	n.i[a]	m	n.i
Pyruvate	n.i	n.i	n.i	m
H_2O	e	e	e	e
NH_3	e	e	e	e
Degrees of redundancy	1	1	2	1

[a] Not included in estimation routine.

B.7.1 Theory

If the number of measurements is larger than the degree of freedom (F)[1] a system is said to be overdetermined. In this case, naturally, it is possible to calculate the missing rates. However, the overdetermined system further allows us to check the quality of the data as well as obtaining the estimate of all reaction rates (measured and calculated) which minimises the least square error of the elementary balances (Nielsen and Villadsen, 1994).

[1] The degree of freedom, F, is calculated as F=M+N+1-I, where M is the number of metabolic products, N is the number of substrates and I is the number of constraints. Possible metabolic products are CO_2, acetate, ethanol, glycerol, pyruvate and water while the number of substrates (three: Glucose, oxygen and ammonia) and constraints (four: carbon, hydrogen, oxygen and nitrogen balances) is fixed.

The following notation is taken from Nielsen and Villadsen (1994). Elementary balances for all components in the system can be written in matrix form as

$$E \cdot q = 0 \tag{B.5}$$

where E is an elementary matrix containing the stoichiometry for all components in the system (one column for each component and one row for each compound). q is a vector containing the conversion rates of each component. The conversion rates can be divided into measured, q_m, and non-measured rates, q_c.

$$E \cdot q = E_m q_m + E_c q_c = 0 \tag{B.6}$$

where E_c is the elementary matrix for the calculated rates and E_m is the elementary matrix for the measured rates. The non-measured rates might be calculated if the degree of freedom is less or equal to the number of measured rates. In the case when the degree of freedom is equal to the number of measured rates the system is said to be determined and the non-measured rates, q_c, can be calculated as:

$$q_c = -E_c^{-1} E_m q_m \tag{B.7}$$

However when the system is overdetermined (number of measured rates is larger than the degree of freedom), E_c is not quadratic and its inverse cannot be found. Instead q_c can be calculated as (Nielsen and Villadsen (1994)):

$$q_c = -(E_c^T E_c)^{-1} E_c^T E_m q_m \tag{B.8}$$

By combining (B.6) and (B.8), q_c can be eliminated

$$\begin{aligned} & E_m q_m + E_c q_c = 0 \\ & \Downarrow \\ & (E_m - (E_c^T E_c)^{-1} E_c^T E_m) q_m = 0 \end{aligned} \tag{B.9}$$

The redundancy matrix (Heijden *et al.* (1994a,b)), R, is defined as

$$R \cdot q_m = 0 \Leftrightarrow R = E_m - (E_c^T E_c)^{-1} E_c^T E_m \tag{B.10}$$

If the rank of the redundancy matrix is greater than 0, the system is overdetermined and each independent row in R gives a relation between the measured rates. The reduced form of R where all rows are independent is denoted R_r.

A minimum variance estimate of the reaction rates is obtained by calculating the solution to the minimum least squares problem. By assuming that the measurement errors are normally distributed, the optimal set of measured reaction rates are found to be (Nielsen and Villadsen (1994))

$$\hat{q}_m = (I - F R_r^T P^{-1} R_r) \overline{q}_m \tag{B.11}$$

where $\overline{q}_m$ are the measured rates and F is the variance-covariance matrix. If the measurements are uncorrelated (as assumed here) F is a diagonal matrix with the elements

$$F(i,i) = (var(i) \cdot \overline{q}_m(i))^2 \tag{B.12}$$

where $var(i)$ is the relative measurement error of the i'th reaction rate. P is computed as

$$P = R_r F R_r^T \tag{B.13}$$

The non-measured rates can now be calculated as

$$q_c = -(E_c^T E_c)^{-1} E_c^T E_m \hat{q}_m \tag{B.14}$$

To quantify the quality of the estimate of the reaction rates, a test function, h, is introduced. The test function is calculated as the sum of the weighted squares of the residuals, $\varepsilon = R_r \overline{q}_m$.

$$h = \varepsilon^T P^{-1} \varepsilon \tag{B.15}$$

It has been shown that the test function, h, is chi-square distributed (Heijden *et al.* (1994b)) with a degree of freedom of Rank(R). Thus by comparing the calculated test function with values of the χ^2-distribution, the obtained estimates can be evaluated.

In the case of `r_est1`, `r_est2` and `r_est4` the degree of redundancy is 1 (and thus the degree of freedom for the χ^2-distribution) which for a confidence level of 95% yield a χ^2 value of 3.84. Thus, if h is greater than 3.84, it can be concluded with 95% confidence that the estimated rates violate the elementary balances taking the measurement noise into account and the quality of the data is therefore very questionable. For `r_est1`, the degree of redundancy is 2, which yields a χ^2 value of 5.99.

Naturally the test function, h, is largely dependent on how the variance-covariance matrix is designed, which essentially is a question of how the measurement variance is chosen. The smaller the variance, the higher h value is obtained. In the current calculations a relative error of 5% is used for all measurements.

B.8 Estimation of biomass I (bioest.m)

```
[bio1,mu1,bio2,mu2]=bioest(Kbio,Mdata,bioini,Ts,rHAc,
Interval,phi)
```

The function calculates estimates of the specific growth rate and the biomass concentration based on the base signal (Lei, 2001, chap.6). Two methods were used.

1 Calculation of the specific growth rate assuming constant biomass composition and that the acidification of the broth solely is caused by the cells taking up ammonia, thus producing [H^+]. Due to pH control, the base addition rate base is then proportional to the uptake of ammonia from the broth. Since the biomass composition is constant, the ammonia uptake rate is proportional with the specific growth rate. The proportional factor between base addition rate [M/h] and specific growth rate [h^{-1}] is `Kbio`.

2 The method is identical to method 1, except the influence of acetate production and consumption is included in the estimates. The dissociation degree of acetate at pH=5 (0.635) was calculated for a pure mixture of acidic acid and water.

`bioini` is the initial biomass concentration, `Ts` is the sample time, `rHAc` is the acetate consumption rate, `Interval` is the number of samples over which the specific growth rate estimate is averaged to reduce the variance of the estimate and `phi` is the dilution rate of the cell-free permeate withdrawn from the reactor for on-line sampling using the GC or FIA (EPFL experiments).

`bio1` and `mu1` are the biomass concentration and the specific growth rate, respectively, obtained using method 1, whereas `bio2` and `mu2` are determined using method 2.

B.9 Estimation of biomass II (bioest_c.m)

```
[bio,mu]=bioest_c(rx,Mdata,bioini,Ts,Interval,phi)
```

The function calculates estimates of the specific growth rate, `mu`, and the biomass concentration, `bio`, based on the biomass production rate, `rx`, obtained from the `r_est`. Otherwise similar to `bioest.m`.

B.10 Metabolic flux analysis (mfa_model1.m)

```
[qgly,qPDC,qcat_ox,qox_phos,YxATP,NADH_sum]=mfa_model1(qglc,
qana,qEtOH,qHAc,qco2,qo2,qglyol,PO,0,YxNADH,alpha)
```

The function calculates the intrinsic rates in the metabolic flux model described in Lei (2001, chap.5).

B.11 Smooth plot (plotfilt.m)

```
qM=plotfilt(qM,sample_int);
```

The function calculates a moving average for the specific reaction rate, `qM`, using `sample_int` samples. The filter was applied to obtain a less noisy signal before plotting the calculated rates. The specific gas rates were not filtered since these signals were less noisy. As a consequence of `sample_int` being greater than 1, a time delay was introduced such that the dynamics of the filtered rates is slower than the dynamics of the gas rates. This can most clearly be seen right after a dilution rate shift-up. Thus, one should be careful when comparing the fast dynamics between the filtered and the not filtered rates. In these cases no filtering should be applied.

References

Heijden, R. v. d.; Romein, B.; Heijnen, J.; Hellinga, C. and Luyben, K. (1994a). Linear constraint relations in biochemical reaction systems: I, Classification of the calculability and the balanceability of conversion rates. *Biotechnol. Bioeng.*, **43**, 3–10.

Heijden, R. v. d.; Romein, B.; Heijnen, J.; Hellinga, C. and Luyben, K. (1994b). Linear constraint relations in biochemical reaction systems: II, Diagnosis and estimation of gross errors. *Biotechnol. Bioeng.*, **43**, 11–20.

Herwig, C.; Marison, I. and von Stockar, U. (2001). On-line stoichiometry and identification of metabolic state under dynamic process conditions. *Biotechnol. Bioeng.*, page accepted for publication.

Lei, F. (2001). *Dynamics and nonlinear phenomena in continuous cultivations of* Saccharomyces cerevisiae. Ph.D. thesis, KT, Technical University of Denmark.

Nielsen, J. and Villadsen, J. (1994). *Bioreaction Engineering Principles*. Plenum Press.

van Urk, H.; Mak, P.; Scheffers, W. and van Dijken, J. (1988). Metabolic responses of *Saccharomyces cerevisiae* CBS8066 and *Candida utilis* CBS 621 upon transition from glucose limitation to glucose excess. *Yeast*, **4**, 283–291.

Wang, N. and Stephanopoulos, G. (1983). Application of macroscopic balances to the identification of gross measurement errors. *Biotechnol. Bioeng.*, **25**, 2177–2208.

B.12 Main Matlab file: k8su1.m

```
%%%%%%5%%%%%%%%%%%%%%%%%%%%%%%%%%%%%%%%%%%%%%%%%%%%%%%%%%%%%%%%%%%%%%%%%%%%
%
% Main matlab file for calculating reaction rates and
% data reconciliation
%
% Experiment with CEN.PK 113-7D
%
% Productostat-KONT8-setpoint change: Figaro 1.0 V to CHx 2.5 V
%
% Experiment conducted at DTU 17/1-2001
%
% By Morten Skov Hansen and Frede Lei
%
% Created 26/2-2001 by Frede Lei
%
% Last updated: 24/4/01
%%%%%%%%%%%%%%%%%%%%%%%%%%%%%%%%%%%%%%%%%%%%%%%%%%%%%%%%%%%%%%%%%%%%%%%%%%%
% The first line of data file not included in data matrix
%%%%%%%%%%%%%%%%%%%%%%%%%%%%%%%%%%%%%%%%%%%%%%%%%%%%%%%%%%%%%%%%%%%%%%%%%%%

clear all
%External provided parameters
Shift_time=0; %[h]
vol=1.000; %[l] determined after experiment
phi_speed=0; %[ml/h]
phi=phi_speed/1000/vol; %[1/h]
Cbase=2; %[M]
Mw_Gly=30.7; %[g/C-mol]
Mw_HAc=30.03; %[g/C-mol]
Mw_Et=23.04; %[g/C-mol]
Mw_glc=30.03; %[g/C-mol]
Mw_bio=23.85; %[g DW/C-mol] C H(1.82) O(0.485) N(0.16), ash 7.0%
ash=0.07; Mw_DW=Mw_bio/(1-ash);
%Factor from Airflow [l/h]*EtOH [g/l] to qEt_strip[C-mmol/h]
K_et=0.00733;
S_f=30.2; %feed concentration of glucose [g/l]
co2_in=0.025; %[%]
o2_in=20.95; %[%]
o2_wet=20.9; %[%]
Ts=60/3600; %[h]
Kbio=130; %[g DW/mol OH-] for DTU experiments
bioini=14.0; %[g DW/h] experimental data
CHx_fac=1.5; %conversion factor from CHx to ethanol

%Calculation window (no. of samples/minutes)
Window=30; Windowbase=30; Plotwindow=1;
```

```
%Structure of data file:
T_string(1)={'Time'};
T_string(2)={'Feed Balance [g]'};
T_string(3)={'D_{set} [1/h]'};
T_string(4)={'Fermenter Balance [g]'};
T_string(5)={'Base Balance [g]'};
T_string(6)={'% O_2'};
T_string(7)={'% CO_2'};
T_string(8)={'pO_2'};
T_string(9)={'D_{ref} [1/h]'};
T_string(10)={'OD Biomass'};
T_string(11)={'CHx [V]'};
T_string(12)={'Figaro [V]'};
T_string(13)={'Airflow'};
T_string(14)={'r_{OH^-} [M/l/h]'};
T_string(15)={'D [1/h]'};
T_string(16)={'D2 [1/h]'};
T_string(17)={'CER [mmole/l/h]'};
T_string(18)={'OUR [mmole/l/h]'};
T_string(19)={'RQ'};
T_string(20)={'Biomass est[g DW/l]]'};
T_string(21)={'Biomass est incl. acetate [g DW/l]]'};
T_string(22)={'\mu (base est) [1/h]'};
T_string(23)={'Biomass est from carbon balance [g DW/l]]'};
T_string(24)={'\mu (carbon bal.) [1/h]'};
T_string(25)={'q_{O_2} [mmole O_2/g DW/h]'};
T_string(26)={'q_{CO_2} [mmole CO_2/g DW/h]'};

%Loading of online data
file1='su1_online.txt';
Mdata1 = dlmread(file1,'\t',1,0); %read data from the second line
a=size(Mdata1,2);
Mtext1=textread(file1,'%q',a); %read text from the first line

%Only need part of data file
Mdata=Mdata1(1:2000,:);
Mdata(:,1)=Mdata(:,1)-ones(size(Mdata,1),1)*Shift_time;

%loading of HPLC and DW data
file2='su1_hplc.txt';
file3='su1_dw.txt';
file4='su1_glu.txt';
file5='su1_acet.txt'; %acetaldehyde
hplcdata = dlmread(file2,'\t',1,0); %read data from the second line
dwdata = dlmread(file3,'\t',1,0); %read data from the second line
gludata = dlmread(file4,'\t',1,0); %read data from the second line
acetdata = dlmread(file5,'\t',1,0); %read data from the second line
```

```
%convert CHx signal to ethanol conc.
et=[Mdata(10:10:1600,1) 1.50*Mdata(10:10:1600,11)];

%General names
pyr=hplcdata(:,[1 2]);
hac=hplcdata(:,[1 3]);
et_raw=hplcdata(:,[1 4]);
gly=hplcdata(:,[1 5]);
suc=hplcdata(:,[1 6]);
acetald=acetdata;
dw=dwdata;
glc=[gludata(:,1) gludata(:,2)/1000]; %conversion [mg/l] to [g/l]

%%%%%%%%%%%%%%%%%%%%%%%%%%%%%%%%%%%%%%%%%%%%%%%%%%%%%%%%%%%%%%%%%%%%%%%%%%%
% Calculations
%%%%%%%%%%%%%%%%%%%%%%%%%%%%%%%%%%%%%%%%%%%%%%%%%%%%%%%%%%%%%%%%%%%%%%%%%%%
%Flow rates
[rOH,D,D2,F]=dilu_dtu(Mdata,Cbase,vol); %rOH[M/l/h], D[1/h]
Mdata=[Mdata rOH D D2];

%molar gases rate
[CER,OUR,RQ]=gasberegn(Mdata,co2_in,o2_in,vol,o2_wet);%CER/OUR[mmol/l/h]
Mdata=[Mdata CER OUR RQ];

%Metabolite production/consumption rates
Inta=1;%for ethanol and acetate, no average is taken
Intet=1;

[rAc_r,hac_int]=rM_calc(hac,Mdata,Mw_HAc,0,Inta); %Acetate  [C-mol/l/h]
[rGly_r,gly_int]=rM_calc(gly,Mdata,Mw_Gly,0,Inta); %Glycerol[C-mol/l/h]

%Ethanol including evaporation of ethanol
[rEt_r,Et_int]=rM_calc_etoh(et,Mdata,Mw_Et,0,Intet,[],K_et);[C-mol/l/h]
%Glucose
[rglc_r,glc_int]=rM_calc(glc,Mdata,Mw_glc,S_f,Inta,Cbase); [C-mol/l/h]


Intb=Window;%SMOOTHENING FACTOR FOR RATES
CER=rx_smooth(Mdata(:,17),Intb); OUR=rx_smooth(Mdata(:,18),Intb);
rAc=rx_smooth(rAc_r,Intb); rGly=rx_smooth(rGly_r,Intb);
rEt=rx_smooth(rEt_r,Intb); rglc=rx_smooth(rglc_r,Intb);
OUR_old=OUR; CER_old=CER;

%Biomass estimate from base signal
Intc=Windowbase;
[bio1,mu1,bio2,mu2]=bioest(Kbio,Mdata,bioini,Ts,rAc,Intc,phi);%[g/l]
rx_base=mu2.*bio2; %biomass productivity from base signal [Cmmol/l/h]
```

```
rx_r=rx_base./Mw_DW*1000; %[g/l/h]

%Reconciliation of data, statistical test, h,
%carbon and degree of reduction balances
rData=[rglc*1000 OUR CER rAc*1000 rEt*1000 rGly*1000 rx_r];%[Cmmole/l/h]
[r_est_Data,stat_h,car,DR]=r_est3(rData); %use etoh and biomass

%Unpacking
%biotrue=r_est_Data(:,7)./Mdata(:,1)*Mw_DW/1000; %[1/h]
rglc=r_est_Data(:,1)/1000; OUR=r_est_Data(:,2);
CER=r_est_Data(:,3); rAc=r_est_Data(:,4)/1000;
rEt=r_est_Data(:,5)/1000; rGly=r_est_Data(:,6)/1000;
rx=r_est_Data(:,7)/1000*Mw_DW;

%Biomass estimate from elementar balances
[bio_c,mu_c]=bioest_c(rx,Mdata,bioini,Ts,1,phi);
Mdata=[Mdata bio1 bio2 mu2 bio_c mu_c]; biotrue=bio2; mutrue=mu2;

%specific rates [mC-mole/g DW/h]
qo2=OUR./biotrue; qco2=CER./biotrue; Mdata=[Mdata qo2 qco2];
qHAc=rAc./biotrue*1000; qEtOH=rEt./biotrue*1000;
qglc=rglc./biotrue*1000; qmu=mutrue/Mw_bio*1000;
qGly=rGly./biotrue;

%yields on glucose
Ysx_b=-rx_base./Mw_bio./rglc;
Ysx_c=-rx./Mw_bio./rglc;
YsEtOH=-rEt./rglc;
YsHAc=-rAc./rglc;
Ysco2=-Mdata(:,17)./rglc/1000;
Yso2=Mdata(:,18)./rglc/1000;%negative yield since O2 is consumed
Ysx=Ysx_b; % base estimate is used..

%%%%%%%%%%%%%%%%%%%%%%%%%%%%%%%%%%%%%%%%%%%%%%%%%%%%%%%%%%%%%%%%%%%%%%%%%%%
% MFA model with fixed P/O ratio
%%%%%%%%%%%%%%%%%%%%%%%%%%%%%%%%%%%%%%%%%%%%%%%%%%%%%%%%%%%%%%%%%%%%%%%%%%%
%Metabolic flux model using reconciled data
%Metabolic flux model parameters
alpha=0.2075;
qana=qmu; %change name
qglyol=qGly; %change name
YxNADH=0.23; %fixed from data reconcilation and redox balance
PO=1.2; %fixed P/O ratio

[qgly,qPDCx,qcat_oxx,qox_phos,YxATP,NADH_sum]=
mfa_model1(qglc,qana,qEtOH,qHAc,qco2,qo2,qglyol,PO,0,YxNADH,alpha);
%unit [mC-mol/g DW/h]
```

```
%convert YxATP from [mole ATP/C-mole bio] to [mmole ATP/g DW]
YxATPx=YxATPx/Mw_DW*1000;

%Filtering for plotting purposes
sample_int=Plotwindow;
qHAc=plotfilt(qHAc,sample_int);
qmu=plotfilt(qmu,sample_int);
mu_c=plotfilt(mu_c,sample_int);
qgly=plotfilt(qgly,sample_int);
qPDC=plotfilt(qPDC,sample_int);
qcat_ox=plotfilt(qcat_ox,sample_int);
qEtOH=plotfilt(qEtOH,sample_int);
YxATP=plotfilt(YxATP,sample_int);
qox_phos=plotfilt(qox_phos,sample_int);

%Set axis properties for figures
xmin=-1; %x-axis for all figures
xmax=15;
y1_1=[0.2 0.50]; %figure1, 1st y-axis
y1_2=[0 0.05]; %figure1, 2nd y-axis
y2_1=[40 200];
y2_2=[1 3];
y3_1=[0 10];
y3_2=[17 22];
y4_1=[6 15];
y4_2=[0 0.9];
y5_1=[0.2 0.4];
y6_1=[0 15];
y6_2=[0 0.6];
y7_1=[-0.5 1];
y7_2=[0 90];
y8_1=[-1.5 15];
y8_2=[-2.1 21];
y9_1=[-1 20];
y9_2=[-1.5 30];
y10_1=[0 15];
y10_2=[0 100];

%Calling plot routine
plt_fig_k8su1
```

C

Experiments and steady-state results

C.1 Conducted experiments

In tables C.1-C.2 an overview is given of the cultivations conducted at DTU and EPFL from which results have been presented in this thesis. All steady-state results obtained from the cultivations C4-C8 are presented in figures C.1-C.7.

Table C.1. Description of each cultivation with *S. cerevisiae* CEN.PK113-7D conducted at DTU wherefrom results have been presented in this thesis. The corresponding steady-state values can be found on the next pages.

Cultivation	Steady-states	Description
C4	C4.1-C4.8	Chemostat steady-states for dilution rates from 0.2 1/h to the critical dilution rate and productostat experiments (setpoint tracking of ethanol). The experiment ran for 770 h before liquid saturated an outlet air filter causing high pressure in the fermenter and consequently a trashed pH-meter.
C5	C5.1-C5.8	Productostat experiments using the ethanol concentration. Cultivation stopped according to schedule after 660 h.
C6	C6.1-C6.12	Productostat experiments using either the ethanol concentration or RQ. Cultivation stopped after 1000 h.
C7	C7.1-C7.8	Chemostat and productostat (using the ethanol concentration) experiments. Cultivation stopped after 860 h.
C8	C8.1-C8.11	Chemostat, productostat and accelero-productostat (ethanol concentration as measurement) experiments. Cultivation stopped after 840 h.
B1	–	Batch cultivation of 30 g/l glucose.

Table C.2. Description of each cultivation with *S. cerevisiae* CEN.PK113-7D conducted at EPFL wherefrom results have been presented in this thesis. For each cultivation, the names of the dynamical experiments presented in the thesis are stated.

Cultivation	Experiment	Description
E1	E1a–E1d	Pulse experiments to an oxidative culture in steady-state at D=0.24 h^{-1}. Glucose (E1a), ethanol (E1b), acetate (E1c) and pyruvate (E1d) pulses where made.
E2	E2a	Dilution rate shift-up from 0.15 to 0.25 h^{-1}.
E3	E3a–E3b	Dilution rate shift-ups from 0.08 to respectively 0.31 and 0.265 h^{-1}.

C4 - STEADY-STATE RESULTS

Label	Time [h]	D [1/h]	D (std)	F [1/h]	Kc/Dref/Setpoint	Interval	EtOH [g/l]
C4.1a	99.83	0.193	0.0000	0.184	no control	29 h	0.00
C4.1b	150.35	0.193	0.0000	0.184	no control	25 h	0.00
C4.2	221.56	0.222	0.0000	0.210	no control	20 h	0.09
C4.3	269.45	0.232	0.0000	0.219	no control	28 h	0.00
C4.4	313.08	0.241	0.0000	0.228	no control	27 h	0.00
C4.5	361.53	0.261	0.0000	0.246	no control	31 h	0.00
C4.6	677.67	0.323	0.0020	0.307	0.05/0.32/Fig6.0	17 h	0.35
C4.7	725.90	0.320	0.0021	0.305	0.05/0.34/Fig8.0	42 h	0.68
C4.8	760.00	0.320	0.0132	0.305	0.05/0.34/CHx 2.0	30 h	1.20

Label	D	Biomass	DW est.	qCO2	qO2	RQ	CER	OUR	Glucose	Acetald.	Pyruvate	Glycerol	Acetate
	[1/h]	[g DW/l]	[g DW/l]	[mmole/g DW/h]	[mmole/g DW/h]		[mmole/h]	[mmole/h]	[mg/l]	[mg/l]	[mg/l]	[g/l]	[g/l]
C4.1a	0.193	14.76	11.90	5.54	5.20	1.07	81.73	76.68	0.0	not meas	0.0	0.000	0.000
C4.1b	0.193	14.99	12.08	5.50	5.09	1.08	82.52	76.32	14.5	not meas	0.0	0.000	0.000
C4.2	0.222	14.57	13.75	6.55	6.06	1.08	95.39	88.32	6.3	not meas	0.0	0.000	0.006
C4.3	0.232	14.17	13.72	7.10	6.64	1.07	100.62	94.14	7.2	not meas	0.0	0.000	0.000
C4.4	0.241	14.25	14.15	7.29	6.71	1.09	103.85	95.55	11.8	not meas	0.0	0.000	0.000
C4.5	0.261	14.33	14.46	7.71	7.02	1.10	110.50	100.62	8.7	not meas	0.0	0.000	0.006
C4.6	0.323	13.30	13.00	10.83	9.95	1.09	144.08	132.31	16.9	not meas	3.4	0.033	0.129
C4.7	0.320	12.81	12.77	11.24	10.19	1.10	143.91	130.49	17.5	not meas	6.5	0.458	0.126
C4.8	0.320	not meas	12.21	11.58	10.20	1.13	141.43	124.62	not meas	not meas	not meas	not meas	not meas

CARBON BALANCE

Label	IN	OUT	OUT	OUT	OUT	Sf	% error
	glucose	biomass	CO2	Met. (aq)	EtOH (g)	[g/l]	
C4.1a	0.190	0.111	0.082	0.000	0.000	31.00	**-1.404**
C4.1b	0.190	0.113	0.083	0.000	0.000	31.00	**-2.869**
C4.2	0.217	0.126	0.095	0.001	0.000	31.00	**-2.551**
C4.3	0.226	0.128	0.101	0.000	0.000	31.00	**-0.978**
C4.4	0.235	0.134	0.104	0.000	0.000	31.00	**-1.055**
C4.5	0.254	0.146	0.111	0.000	0.000	31.00	**-0.894**
C4.6	0.317	0.168	0.144	0.007	0.001	31.00	**-0.646**
C4.7	0.314	0.160	0.144	0.016	0.001	31.00	**-2.031**
C4.8	0.315	0.152	0.141	0.017	0.002	31.00	**0.787**

DEGREE OF REDUCTION BALANCE

Label	IN	IN	OUT	OUT	% deviation
	glucose	O2	biomass	met.	
C4.1a	0.760	-0.307	0.485	0.000	**-4.15**
C4.1b	0.760	-0.305	0.493	0.000	**-5.05**
C4.2	0.868	-0.353	0.551	0.007	**-5.02**
C4.3	0.906	-0.377	0.559	0.000	**-3.32**
C4.4	0.942	-0.382	0.586	0.000	**-2.75**
C4.5	1.016	-0.402	0.636	0.000	**-2.29**
C4.6	1.268	-0.529	0.733	0.049	**-3.34**
C4.7	1.258	-0.522	0.699	0.113	**-6.05**
C4.8	1.259	-0.498	0.666	0.136	**-3.28**

Figure C.1. Steady-state data obtained from C4.

C4 - STEADY-STATE RESULTS

ENZYME ACTIVITIES

Label	Protein content	Pdc	Acs	AlDH (NAD+)	AlDH (NADP+)	ADH
	% [g/g DW]	[U/mg prot]	[U/mg prot]	[U/mg prot]	[U/mg prot]	[U/mg prot]
C4.1a	not meas	not meas	not meas	not meas	not meas	not meas
C4.1b	45.4	0.25	0.11	0.32	0.21	2.06
C4.2	43.6	0.24	0.19	0.90	0.36	2.02
C4.3	47.6	0.11	0.12	0.44	0.26	2.62
C4.4	49.0	not meas	not meas	not meas	not meas	not meas
C4.5	49.3	0.18	0.14	0.36	0.33	2.54
C4.6	47.6	0.21	0.12	0.07	0.06	0.61
C4.7	49.2	not meas	not meas	not meas	not meas	not meas
C4.8	not meas	not meas	not meas	not meas	not meas	not meas

Figure C.2. Enzymatic measurements for the steady-states in C4.

C5 - STEADY-STATE RESULTS

Label	Time [h]	D [1/h]	D (std)	F [1/h]	Kc/Ti[h]/Setpoint	Interval	EtOH [g/l]
C5.1a	96.76	0.283	0.0024	0.269	0.1/0.25/Figaro2.0	17 h	0.11
C5.1b	100.67	0.283	0.0023	0.269	0.1/0.25/Figaro2.0	20 h	0.12
C5.2	212.88	0.266	0.0014	0.253	0.05/0.27/Figaro6.0	30 h	0.44
C5.3b	245.08	0.278	0.0023	0.264	0.05/0.27/CHx 1.5	15 h	0.72
C5.3c	260.84	0.279	0.0020	0.265	0.05/0.27/CHx 1.5	12 h	0.76
C5.3d	280.36	0.275	0.0037	0.261	0.05/0.27/CHx 1.5	32 h	0.80
C5.4a	332.63	0.290	0.0015	0.276	0.05/0.27/CHx 2.5	12 h	1.16
C5.4b	353.44	0.284	0.0015	0.270	0.05/0.27/CHx 2.5	17 h	1.08
C5.5	424.36	0.282	0.0000	0.266	Open loop	14 h	0.14
C5.6	500.91	0.301	0.0035	0.285	0.05/0.27/Figaro1.0	20 h	0.08
C5.7	553.17	0.291	0.0047	0.275	0.05/0.29/Figaro1.5	27 h	0.14
C5.8	630.00	0.290	0.0024	0.275	0.06/0.27/Figaro4.0	30 h	0.20

Label	D	Biomass	DW est.	qCO2	qO2	RQ	CER	OUR	Glucose	Acetald.	Pyruvate	Glycerol	Acetate
	[1/h]	[g DW/l]	[g DW/l]	[mmole/g DW/h]	[mmole/g DW/h]		[mmole/h]	[mmole/h]	[mg/l]	[mg/l]	[mg/l]	[g/l]	[g/l]
C5.1a	0.283	12.09	13.14	10.36	9.81	1.06	125.26	118.59	27.2	0.00	6.5	0.090	0.095
C5.1b	0.283		13.13	9.55	9.03	1.06	125.35	118.59	27.2	0.00	4.9	0.190	0.092
C5.2	0.266	12.99	13.25	9.07	8.45	1.07	117.87	109.79	28.1	0.00	10.6	0.168	0.236
C5.3b	0.278		12.94	9.29	8.27	1.12	120.15	107.02	24.3	0.00	4.3	0.198	0.111
C5.3c	0.279	12.81	12.80	9.28	8.39	1.11	118.92	107.43	25.2	0.00	7.3	0.075	0.155
C5.3d	0.275	12.81	12.69	9.25	8.29	1.12	118.48	106.25	28.2	0.00	5.8	0.079	0.136
C5.4a	0.290		12.30	10.26	9.15	1.12	126.20	112.56	30.6	0.00	8.6	0.053	0.206
C5.4b	0.284	12.39	12.38	9.85	8.94	1.10	122.00	110.76	41.5	0.00	9.2	0.080	0.141
C5.5	0.282	14.81	14.73	7.73	7.07	1.09	114.45	104.76	16.8	0.00	9.3	0.145	0.094
C5.6	0.301	14.07	14.23	9.09	8.28	1.10	127.93	116.51	15.9	0.00	5.8	0.096	0.055
C5.7	0.291	13.32	13.99	9.39	8.45	1.11	125.01	112.61	14.7	0.00	6.8	0.141	0.106
C5.8	0.290	13.51	13.98	9.32	8.32	1.12	125.87	112.39	13.3	0.00	10.2	0.076	0.210

CARBON BALANCE

Label	IN	OUT	OUT	OUT	OUT	SI	% error
	glucose	biomass	CO2	Met. (aq)	EtOH (g)	[g/l]	
C5.1a	0.278	0.134	0.125	0.004	0.000	31.00	**5.294**
C5.1b	0.277	0.145	0.125	0.004	0.000	31.00	**0.945**
C5.2	0.261	0.135	0.118	0.009	0.001	31.00	**-0.521**
C5.3b	0.272	0.140	0.120	0.012	0.001	31.00	**-0.226**
C5.3c	0.273	0.139	0.119	0.012	0.001	31.00	**1.009**
C5.3d	0.270	0.137	0.118	0.013	0.001	31.00	**-0.030**
C5.4a	0.285	0.139	0.126	0.018	0.002	31.00	**0.288**
C5.4b	0.279	0.137	0.122	0.016	0.001	31.00	**0.891**
C5.5	0.275	0.162	0.114	0.004	0.000	31.00	**-2.240**
C5.6	0.294	0.167	0.128	0.003	0.000	31.00	**-1.394**
C5.7	0.284	0.159	0.125	0.004	0.000	31.00	**-1.431**
C5.8	0.284	0.158	0.126	0.006	0.000	31.00	**-2.216**

DEGREE OF REDUCTION BALANCE

IN	IN	OUT	OUT	% deviation
glucose	O2	biomass	met.	
1.110	-0.474	0.583	0.018	**3.11**
1.110	-0.474	0.633	0.020	**-1.60**
1.044	-0.439	0.590	0.042	**-2.60**
1.089	-0.428	0.612	0.065	**-1.48**
1.093	-0.430	0.608	0.064	**-0.74**
1.079	-0.425	0.599	0.073	**-1.77**
1.140	-0.450	0.607	0.098	**-1.31**
1.115	-0.443	0.599	0.089	**-1.44**
1.098	-0.419	0.708	0.017	**-4.12**
1.175	-0.466	0.730	0.013	**-2.87**
1.137	-0.450	0.694	0.020	**-2.46**
1.135	-0.450	0.692	0.023	**-2.63**

Figure C.3. Steady-state data obtained from C5.

C6 - STEADY-STATE RESULTS

Label	Time [h]	D [1/h]	D (std)	F [1/h]	Kc/Ti[h]/Setpoint	Interval	EtOH [g/l]
C6.1	102.17	0.299	0.0016	0.283	0.03/2/Fig.1.0	10 h	0.03
C6.2	223.95	0.284	0.0014	0.270	0.05/2/Fig.3.0	20 h	0.16
C6.3a	268.45	0.308	0.0028	0.292	0.05/2/Fig.1.0	15 h	0.07
C6.3b	288.13	0.306	0.0013	0.289	0.05/2/Fig.1.0	20 h	0.06
C6.4	362.83	0.300	0.0020	0.283	0.08/2/Fig.5.0	40 h	0.25
C6.5	437.60	0.303	0.0018	0.287	0.10/2/Fig.7.0	40 h	0.45
C6.6	504.00	0.295	0.0013	0.280	0.06/2/CHx1.5	35 h	0.74
C6.7	579.00	0.288	0.0027	0.275	0.08/2/CHx3.0	44 h	1.48
C6.8a	620.00	0.292	0.0018	0.279	0.08/4/CHx5.0	30 h	2.37(est)
C6.8b	649.00	0.285	0.0022	0.272	0.08/4/CHx5.0	15 h	2.42
C6.9	720.00	0.268	0.0045	0.258	0.10/2/CHx8.0	40 h	3.55
C6.10	795.00	0.266	0.0017	0.257	0.08/4/RQ1.6	25 h	5.24
C6.11	911.00	0.232	0.0077	0.226	0.20/2/RQ2.0	40 h	6.12(est)
C6.12	985.00	0.301	0.0031	0.285	0.05/2/Fig1.0	35 h	0.13

Label	D	Biomass	DW est.	qCO2	qO2	RQ	CER	OUR	Glucose	Acetald.	Pyruvate	Glycerol	Acetate
	[1/h]	[g DW/l]	[g DW/l]	[mmole/g DW/h]	[mmole/g DW/h]		[mmole/h]	[mmole/h]	[mg/l]	[mg/l]	[mg/l]	[g/l]	[g/l]
C6.1	0.310	13.87	13.67	9.40	8.71	1.08	130.36	120.90	21.0	not detect.	9.6	0.008	0.060
C6.2	0.295	13.55	13.26	9.22	8.41	1.10	124.93	113.97	27.3	not detect.	7.6	0.095	0.106
C6.3a	0.319	14.30	14.01	8.90	8.06	1.10	127.26	115.24	22.3	not meas.	3.6	0.097	0.116
C6.3b	0.317	13.94	14.04	9.08	8.33	1.09	126.56	116.14	21.9	not detect.	9.5	0.120	0.100
C6.4	0.310	13.57	14.07	9.22	8.33	1.11	125.11	113.01	22.0	not detect.	5.0	0.491	0.208
C6.5	0.314	13.47	13.85	9.35	8.27	1.13	125.93	111.40	22.0	8.10	4.7	1.063	0.188
C6.6	0.306	13.47	12.87	9.39	8.48	1.11	126.50	114.26	21.4	6.01	6.4	0.220	0.108
C6.7	0.299	12.30	12.27	9.95	8.49	1.17	122.43	104.44	25.0	13.20	5.9	0.319	0.095
C6.8a	0.302	not meas.	11.38	10.64	8.38	1.27	120.81	95.08	not meas.	not meas.	not meas.	not meas.	not meas.
C6.8b	0.295	11.20	11.46	10.52	7.92	1.33	117.84	88.69	29.3	25.20	5.7	0.185	0.092
C6.9	0.278	9.89	9.99	11.24	8.18	1.37	111.14	80.85	41.1	57.17	5.7	0.620	0.117
C6.10	0.275	8.39	8.69	12.67	7.78	1.63	106.33	65.34	64.9	111.33	10.8	0.555	0.191
C6.11	0.241	not meas.	7.02	12.70	6.17	2.06	88.90	43.19	not meas.	not meas.	not meas.	not meas.	not meas.
C6.12	0.312	14.07	14.04	9.26	8.63	1.07	130.20	121.42	16.0	not detect.	6.4	0.514	0.078

CARBON BALANCE

Label	IN	OUT	OUT	OUT	OUT	Sf	% error
	glucose	biomass	CO2	Met. (aq)	EtOH (g)	[g/l]	
C6.1	0.292	0.162	0.130	0.001	0.000	31.00	**-0.409**
C6.2	0.279	0.150	0.125	0.004	0.000	31.00	**-0.371**
C6.3a	0.301	0.172	0.127	0.003	0.000	31.00	**-0.516**
C6.3b	0.299	0.166	0.127	0.003	0.000	31.00	**0.802**
C6.4	0.292	0.159	0.125	0.010	0.000	31.00	**-0.650**
C6.5	0.296	0.159	0.126	0.019	0.001	31.00	**-2.784**
C6.6	0.289	0.155	0.126	0.013	0.001	31.00	**-2.048**
C6.7	0.284	0.138	0.122	0.023	0.002	31.00	**-0.640**
C6.8a	0.288	0.129	0.121	0.032	0.003	31.00	**1.068**
C6.8b	0.281	0.124	0.118	0.033	0.003	31.00	**0.962**
C6.9	0.266	0.103	0.111	0.048	0.005	31.00	**-0.465**
C6.10	0.265	0.087	0.106	0.068	0.007	31.00	**-1.058**
C6.11	0.233	0.063	0.089	0.068	0.008	31.00	**2.300**
C6.12	0.294	0.165	0.130	0.008	0.000	31.00	**-3.093**

IN	IN	OUT	OUT	% deviation
glucose	O2	biomass	met.	
1.169	-0.484	0.706	0.006	**-2.29**
1.114	-0.456	0.657	0.022	**-1.79**
1.204	-0.461	0.751	0.016	**-1.95**
1.195	-0.465	0.727	0.016	**-1.02**
1.170	-0.452	0.693	0.052	**-2.26**
1.184	-0.446	0.695	0.095	**-4.42**
1.157	-0.457	0.677	0.076	**-4.50**
1.134	-0.418	0.604	0.139	**-2.32**
1.152	-0.380	0.564	0.203	**0.38**
1.124	-0.355	0.543	0.203	**2.01**
1.065	-0.323	0.452	0.304	**-1.33**
1.060	-0.261	0.380	0.430	**-0.98**
0.934	-0.173	0.277	0.434	**5.35**
1.178	-0.486	0.723	0.038	**-5.83**

Figure C.4. Steady-state data obtained from C6.

C6 - STEADY-STATE RESULTS

ENZYME ACTIVITIES

Label	Protein content % [g/g DW]	Pdc [U/mg pro]	Acs [U/mg pro]	AlDH (NAD+) [U/mg pro]	AlDH (NADP+) [U/mg pro]	ADH [U/mg pro]
C6.1	49.4	0.60	0.12	0.16	0.10	0.81
C6.2	48.8	0.56	0.14	0.12	0.08	0.67
C6.3a	47.4	0.62	0.15	0.14	0.10	0.74
C6.3b	48.6	0.50	0.16	0.16	0.11	0.83
C6.4	50.4	0.58	0.13	0.11	0.09	0.99
C6.5	48.6	0.44	0.16	0.12	0.10	0.90
C6.6	48.0	0.52	0.15	0.13	0.10	0.73
C6.7	46.8	0.62	0.17	0.13	0.10	0.64
C6.8b	45.0	0.45	0.13	0.09	0.06	0.77
C6.9	45.4	not det.	0.08	0.07	0.05	0.55
C6.10	45.5	not det.	0.04	0.03	0.03	0.30
C6.12	37.2	0.43	0.21	0.10	0.11	1.06

Figure C.5. Enzymatic measurements for the steady-states in C6.

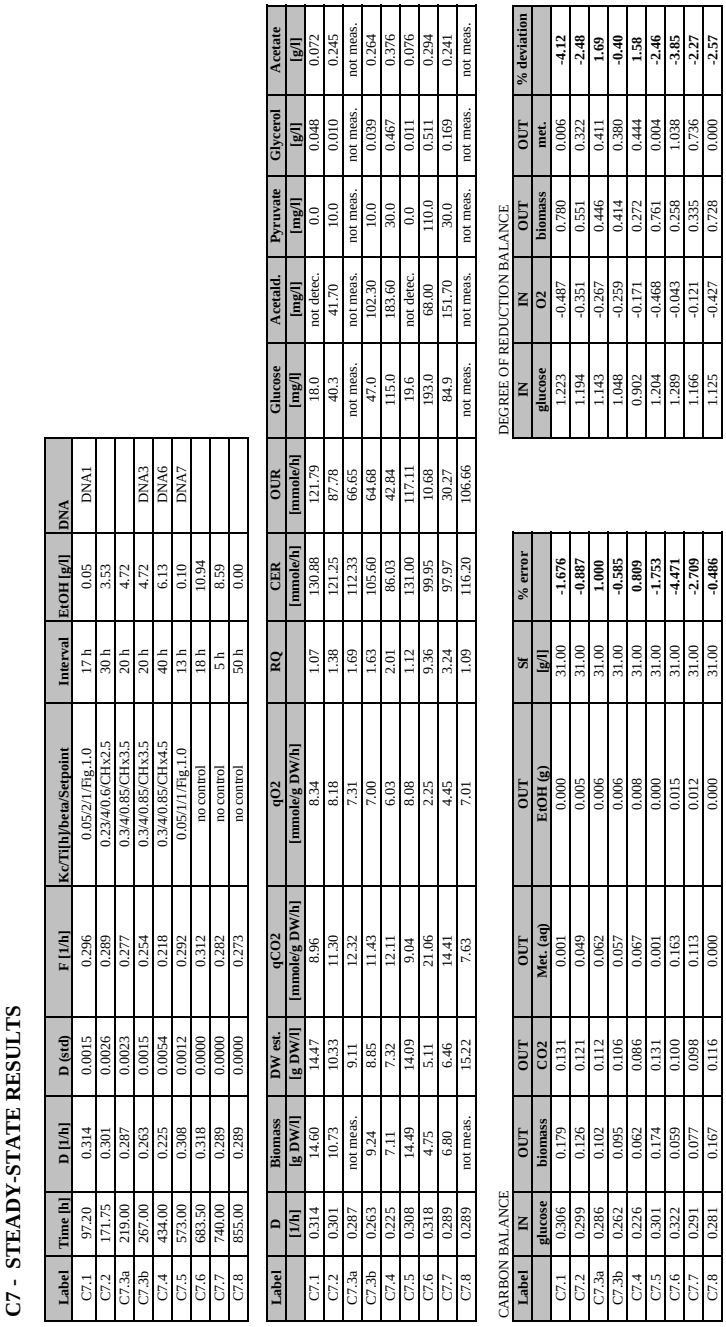

C7 - STEADY-STATE RESULTS

Label	Time [h]	D [1/h]	D (std)	F [1/h]	Kc/Ti[h]/beta/Setpoint	Interval	EtOH [g/l]	DNA
C7.1	97.20	0.314	0.0015	0.296	0.05/2/1/Fig.1.0	17 h	0.05	DNA1
C7.2	171.75	0.301	0.0026	0.289	0.23/40.6/CHx2.5	30 h	3.53	
C7.3a	219.00	0.287	0.0023	0.277	0.3/40.85/CHx3.5	20 h	4.72	
C7.3b	267.00	0.263	0.0015	0.254	0.3/40.85/CHx3.5	20 h	4.72	DNA3
C7.4	434.00	0.225	0.0054	0.218	0.3/40.85/CHx4.5	40 h	6.13	DNA6
C7.5	573.00	0.308	0.0012	0.292	0.05/1/1/Fig.1.0	13 h	0.10	DNA7
C7.6	683.50	0.318	0.0000	0.312	no control	18 h	10.94	
C7.7	740.00	0.289	0.0000	0.282	no control	5 h	8.59	
C7.8	855.00	0.289	0.0000	0.273	no control	50 h	0.00	

Label	D	Biomass	DW est.	qCO2	qO2	RQ	CER	OUR	Glucose	Acetald.	Pyruvate	Glycerol	Acetate
	[1/h]	[g DW/l]	[g DW/l]	[mmole/g DW/h]	[mmole/g DW/h]		[mmole/h]	[mmole/h]	[mg/l]	[mg/l]	[mg/l]	[g/l]	[g/l]
C7.1	0.314	14.60	14.47	8.96	8.34	1.07	130.88	121.79	18.0	not detec.	0.0	0.048	0.072
C7.2	0.301	10.73	10.33	11.30	8.18	1.38	121.25	87.78	40.3	41.70	10.0	0.010	0.245
C7.3a	0.287	not meas.	9.11	12.32	7.31	1.69	112.33	66.65	not meas.	not meas.	not meas.	not meas.	not meas.
C7.3b	0.263	9.24	8.85	11.43	7.00	1.63	105.60	64.68	47.0	102.30	10.0	0.039	0.264
C7.4	0.225	7.11	7.32	12.11	6.03	2.01	86.03	42.84	115.0	183.60	30.0	0.467	0.376
C7.5	0.308	14.49	14.09	9.04	8.08	1.12	131.00	117.11	19.6	not detec.	0.0	0.011	0.076
C7.6	0.318	4.75	5.11	21.06	2.25	9.36	99.95	10.68	193.0	68.00	110.0	0.511	0.294
C7.7	0.289	6.80	6.46	14.41	4.45	3.24	97.97	30.27	84.9	151.70	30.0	0.169	0.241
C7.8	0.289	not meas.	15.22	7.63	7.01	1.09	116.20	106.66	not meas.	not meas.	not meas.	not meas.	not meas.

CARBON BALANCE

Label	IN	OUT	OUT	OUT	Sf	% error
	glucose	biomass	CO2	Met. (aq)	EtOH (g)	[g/l]	
C7.1	0.306	0.179	0.131	0.001	0.000	31.00	**-1.676**
C7.2	0.299	0.126	0.121	0.049	0.005	31.00	**-0.887**
C7.3a	0.286	0.102	0.112	0.062	0.006	31.00	**1.000**
C7.3b	0.262	0.095	0.106	0.057	0.006	31.00	**-0.585**
C7.4	0.226	0.062	0.086	0.067	0.008	31.00	**0.809**
C7.5	0.301	0.174	0.131	0.001	0.000	31.00	**-1.753**
C7.6	0.322	0.059	0.100	0.163	0.015	31.00	**-4.471**
C7.7	0.291	0.077	0.098	0.113	0.012	31.00	**-2.709**
C7.8	0.281	0.167	0.116	0.000	0.000	31.00	**-0.486**

DEGREE OF REDUCTION BALANCE

IN	IN	OUT	OUT	% deviation
glucose	O2	biomass	met.	
1.223	-0.487	0.780	0.006	**-4.12**
1.194	-0.351	0.551	0.322	**-2.48**
1.143	-0.267	0.446	0.411	**1.69**
1.048	-0.259	0.414	0.380	**-0.40**
0.902	-0.171	0.272	0.444	**1.58**
1.204	-0.468	0.761	0.004	**-2.46**
1.289	-0.043	0.258	1.038	**-3.85**
1.166	-0.121	0.335	0.736	**-2.27**
1.125	-0.427	0.728	0.000	**-2.57**

Figure C.6. Steady-state data obtained from C7.

C8 - A1 STEADY-STATE RESULTS

Label	Time [h]	D [1/h]	D (std)	F [1/h]	Kc/Tiih/beta/Setpoint	Interval	EtOH [g/l]
C8.1a	98.35	0.290	0.0020	0.275	0.05/2/1.00/Fig.1.0	28 h	0.00
C8.1b	138.72	0.286	0.0011	0.271	0.05/2/1.00/Fig.1.0	18 h	0.00
C8.2a	233.22	0.290	0.0031	0.279	0.23/4/0.60/CHx2.5	53 h	3.75
C8.2b	306.22	0.292	0.0041	0.281	0.23/4/1.00/CHx2.5	16 h	3.75
C8.3	427.05	0.280	0.0024	0.271	0.30/4/0.85/CHx3.5	40 h	4.95
C8.4	501.30	0.304	0.0016	0.287	0.05/2/1.00/Fig.1.0	13 h	0.10
C8.5	598.39	0.328	0.0000	0.324	open loop	8 h	6.70
C8.6	690.14	0.293	0.0017	0.283	0.20/2/1.00/CHx3.5	8 h	5.04
C8.7	724.72	0.280	0.0017	0.272	CHx_ramp(CHx=4.47)	pseudo ss (1 h)	6.22
C8.8	748.30	0.274	0.0007	0.268	CHx_ramp(CHx=5.11)	pseudo ss (1 h)	7.14
C8.9	773.55	0.300	0.0011	0.294	CHx_ramp(CHx=5.78)	pseudo ss (1 h)	9.46
C8.10	788.05	0.335	0.0023	0.329	open loop (CHx=5.88)	pseudo ss (1 h)	9.80
C8.11	837.17	0.276	0.0028	0.269	0.20/2/1.00/CHx5.5	7 h	7.93

Label	D	Biomass	DW est.	qCO2	qO2	RQ	CER	OUR	Glucose	Acetald.	Pyruvate	Glycerol	Acetate
	[1/h]	[g DW/l]	[g DW/l]	[mmole/g DW/h]	[mmole/g DW/h]		[mmole/h]	[mmole/h]	[mg/l]	[mg/l]	[mg/l]	[g/l]	[g/l]
C8.1a	0.290	13.67	14.02	8.83	8.19	1.08	120.66	111.99	21.0	0.00	2.0	0.020	0.060
C8.1b	0.286	14.02	13.83	8.58	7.87	1.09	120.36	110.30	19.0	0.00	3.0	0.030	0.070
C8.2a	0.290	10.00	10.07	11.46	6.81	1.68	114.55	68.14	55.0	0.00	5.0	0.050	0.170
C8.2b	0.292	10.00	10.18	10.77	6.61	1.63	107.68	66.14	55.0	0.00	5.0	0.050	0.170
C8.3	0.280	8.54	8.81	12.60	6.96	1.81	107.58	59.44	78.0	115.14	7.0	0.060	0.210
C8.4	0.304	13.50	14.07	9.52	8.59	1.11	128.52	116.01	12.0	1.77	2.0	0.010	0.082
C8.5	0.328	2.60	2.84	25.29	0.89	28.34	65.75	2.32	10310.0	4.73	43.0	0.930	0.129
C8.6	0.293	8.63	8.97	12.96	7.24	1.79	111.85	62.52	29.5	69.35	4.7	0.007	0.158
C8.7	0.280	7.47	7.47	13.51	6.17	2.19	100.97	46.08	71.5	203.06	11.3	0.187	0.180
C8.8	0.274	6.56	6.34	14.91	4.89	3.05	94.52	31.01	54.5	228.65	21.6	0.285	0.214
C8.9	0.300	5.23	5.33	18.13	3.07	5.90	96.57	16.38	114.5	123.93	29.6	0.302	0.211
C8.10	0.335	4.73	4.83	21.46	2.30	9.34	103.57	11.09	275.7	65.55	42.5	0.341	0.235
C8.11	0.276	5.74	6.04	15.37	4.46	3.45	92.79	26.93	127.1	175.35	26.8	0.276	0.216

CARBON BALANCE

Label	IN	OUT	OUT	OUT	OUT	Sf	% error
	glucose	biomass	CO2	Met. (aq)	EtOH (g)	[g/l]	
C8.1a	0.276	0.155	0.121	0.001	0.000	30.20	**-0.048**
C8.1b	0.272	0.156	0.120	0.001	0.000	30.20	**-2.085**
C8.2a	0.281	0.113	0.115	0.050	0.005	30.20	**-0.738**
C8.2b	0.282	0.114	0.108	0.050	0.005	30.20	**1.944**
C8.3	0.272	0.093	0.108	0.063	0.007	30.20	**0.414**
C8.4	0.289	0.160	0.129	0.001	0.000	30.20	**-0.196**
C8.5	0.326	0.033	0.066	0.220	0.009	30.20	**-0.490**
C8.6	0.284	0.099	0.112	0.066	0.007	30.20	**0.402**
C8.7	0.274	0.082	0.101	0.080	0.008	30.20	**1.083**
C8.8	0.269	0.070	0.095	0.090	0.010	30.20	**1.708**
C8.9	0.296	0.061	0.097	0.130	0.013	30.20	**-1.576**
C8.10	0.331	0.062	0.104	0.153	0.013	30.20	**-0.106**
C8.11	0.271	0.062	0.093	0.101	0.011	30.20	**1.783**

DEGREE OF REDUCTION BALANCE

IN	IN	OUT	OUT	% deviation
glucose	O2	biomass	met.	
1.105	-0.448	0.677	0.001	**-1.82**
1.088	-0.441	0.683	0.001	**-3.40**
1.123	-0.273	0.495	0.316	**3.51**
1.130	-0.265	0.498	0.318	**4.37**
1.088	-0.238	0.407	0.403	**3.63**
1.156	-0.464	0.699	0.000	**-0.66**
0.855	-0.009	0.145	0.674	**3.05**
1.137	-0.250	0.431	0.420	**3.23**
1.095	-0.184	0.357	0.512	**3.80**
1.077	-0.124	0.307	0.580	**6.11**
1.183	-0.066	0.268	0.831	**1.61**
1.324	-0.044	0.270	0.954	**4.20**
1.083	-0.108	0.270	0.645	**5.58**

Figure C.7. Steady-state data obtained from C8.